UNIVERSIDAD DE CHILE
FACULTAD DE CIENCIAS FÍSICAS Y MATEMÁTICAS
DEPARTAMENTO DE GEOLOGÍA

SHALLOW RESERVOIR CONDITIONS IN THE FUI GROUP SMALL ERUPTIVE CENTRES IN THE SOUTHERN VOLCANIC ZONE (CHILEAN ANDES)

TESIS PARA OPTAR AL GRADO DE MAGISTER EN CIENCIAS, MENCIÓN GEOLOGÍA

MEMORIA PARA OPTAR AL TÍTULO DE GEÓLOGA

FRANCISCA CONSTANZA MALLEA LILLO

PROFESOR GUÍA:
MIGUEL ÁNGEL PARADA REYES

PROFESOR CO-GUÍA:
EDUARDO MORGADO BRAVO

MIEMBROS DE LA COMISIÓN:
PATRICIA LARREA MÁRQUEZ
ÁNGELO CASTRUCCIO ÁLVAREZ

SANTIAGO DE CHILE

2021

RESUMEN DE LA MEMORIA PARA OPTAR AL TÍTULO DE: Geóloga y grado de Magister en Ciencias, Mención Geología
POR: Francisca Constanza Mallea Lillo
FECHA: Agosto 2021
PROFESOR GUÍA: Miguel Ángel Parada Reyes

SHALLOW RESERVOIR CONDITIONS IN THE FUI GROUP SMALL ERUPTIVE CENTRES IN THE SOUTHERN VOLCANIC ZONE (CHILEAN ANDES)

El Grupo Fui es un conjunto de Centros Eruptivos Menores (CEM) holocenos ubicados al este y noreste del Complejo Volcánico Mocho-Choshuenco (CVMC), en el segmento Central de la Zona Volcánica Sur de Los Andes, segmento en el cual están ubicados los volcanes más peligrosos y de alto riesgo en Chile. Se definieron dos subgrupos para el Grupo Fui, en base a sus características composicionales y petrográficas: Fui Norte y Fui Sur, separados solo por ~2 km. Los productos volcánicos de Fui Norte son basaltos (49 – 52 wt% SiO_2) ricos en olivino, enriquecidos en elementos incompatibles, mientras que el material volcánico de Fui Sur es más diferenciado (andesitas basálticas a andesitas; 55 – 58 wt% SiO_2) con menos proporción de olivino y mayor plagioclasa y clinopiroxeno, y empobrecido en elementos incompatibles. Los cristales de olivino y plagioclasa de ambos subgrupos están caracterizados por dos zonas composicionales: Alta-Fo, Alta-An (Zona 1, Fo_{78-89} y An_{76-93}) y Baja-Fo, Baja-An (Zona 2, Fo_{60-78} y An_{57-73}). Los fenocristales y microfenocristales de olivino, plagioclasa y clinopiroxeno forman cúmulos cristalinos que son abundantes entre las muestras estudiadas. Mediante geotermobarometría y modelos realizados con el *freeware* rhyolite-MELTS v.1.0.2, se calcularon condiciones correspondientes a un reservorio cortical somero (hasta 7.6 km en Fui Norte y hasta 18.9 km en Fui Sur) para las composiciones de la Zona 2 (olivino Baja-Fo y plagioclasa de Baja-An) en equilibrio con un fundido equivalente a la composición de la masa fundamental de las muestras. Se determinó un contenido de agua entre 0.4 – 2 wt% y 0.9 – 3 wt% para las composiciones de la Zona 2 de los CEM Fui Norte y Fui Sur, respectivamente, bajo condiciones de oxidación de QFM-1, QFM y NNO. Por el contrario, las composiciones de la Zona 1 (Alta-Fo y Alta-An) se encuentran en desequilibrio con un fundido equivalente a la composición de la masa fundamental. Se propone que la Zona 1 se formó durante una etapa temprana de cristalización en una zona del reservorio con un enrejado cristalino denso (*mush zone*) para los dos subgrupos de CEM. Esto, debido a su composición más primitiva y su común ocurrencia formando parte de cúmulos cristalinos. A pesar de la cercanía entre los CEM de Fui Norte y Fui Sur, se infiere que sus orígenes e historias magmáticas son independientes entre sí, debido a las relevantes diferencias en sus signaturas geoquímicas y sus características petrográficas donde, además, se reconoce una relación genética entre los magmas de Fui Sur y los del CVMC.

"Lo que puede el sentimiento no lo ha podido el saber, ni el más claro proceder, ni el más ancho pensamiento"

Volver a los 17, Violeta Parra.

"Un cronopio encuentra una flor solitaria en medio de los campos. Primero la va a arrancar, pero piensa que es una crueldad inútil y se pone de rodillas a su lado y juega alegremente con la flor, a saber: le acaricia los pétalos, la sopla para que baile, zumba como una abeja, huele su perfume, y finalmente se acuesta debajo de la flor y se duerme envuelto en una gran paz. La flor piensa: Es como una flor."

Flor y Cronopio, Julio Cortázar.

A los detalles y al sentir, a la curiosidad y el descubrimiento, a la esencia de ser humana.

AGRADECIMIENTOS

En primera instancia, agradecer al proyecto CONICYT-FONDAP 15090013, Centro de Excelencia en Geotermia de los Andes (CEGA) y al Departamento de Geología de la Universidad de Chile por financiar el desarrollo de esta investigación. Al Departamento de Postgrado y Postítulo de la Vicerrectoría de Asuntos Académicos por su ayuda para una pasantía corta de investigación en la *University of Bristol*, UK.

Gracias a Miguel Ángel Parada, mi profesor guía, por confiar en mi trabajo y en mis capacidades, por permitir que desarrollara mi curiosidad en la petrología desde Fund. de Petro, y posteriormente con los Proyectos I y II, culminando con esta tesis en la cual pude explorar y explotar mis intereses y capacidades. Gracias a Eduardo Morgado, mi profesor co-guía, quien fue un excelente apoyo y mentor desde que comencé la tesis. También a Patricia Larrea y Ángelo Castruccio, gracias por sus correcciones y comentarios que permitieron mejorar este trabajo.

Gracias a mis hermanos, Javier y Nicolás, que día a día me inspiran a ser mejor hermana, mejor persona y me entregan el ánimo y las risas y esa complicidad de hermanos que ha sido tan necesaria para sacar la vida adelante. Gracias a mi mamá, mujer de fuego, quien me alienta y me acompaña siempre, me ayuda a tejer mis alas cada vez más grandes y me apoya en cada loca idea que se me cruza por la cabeza. Gracias a mi papá, por recordarme las cosas esenciales de la vida a través de sus frases cliché y mostrarme siempre la vida con humildad, simpleza y sencillez. Gracias a ambos, que a pesar de que son como el agua y el aceite logran el equilibrio perfecto entre mis ganas de volar y mantenerme en la tierra.

Gracias a mi alma gemela, mi mejor amiga, mi hermana. Gracias Kika por conectarnos siempre tan profundamente, por apañarme siempre en las buenas y en las malas, por estar cada milésima de segundo acompañándonos y creciendo juntas *since* 2000 en el kínder A. Gracias a mis amigues de la vida, de los colegios, por cada junta y carrete para compartir y actualizarnos de nuestras vidas fuera de lo académico. Cada une de ustedes ha sido muy importante en algunos momentos, más que nombrarlos en este texto los llevo siempre en mis pensamientos.

Agradezco profundamente a mis amigues del Plan Común, Catita, Santi, y especialmente a la Jazz, que nos apañamos en cada control, examen y exámenes de segunda de la tortura de los dos primeros años de u; fuiste un gran apoyo, una amiga, compañera y familia hasta el día de hoy. Gracias también a otros amigues con los que conectamos en esos años, el cariño sigue intacto. Agrego acá el agradecimiento a mi amigo de remo y de la vida; Dany, gracias por aparecer en mi camino y ayudarme con cada tarea, trabajo y estudio de física, matemática y programación hasta el día de hoy; tu guía y apoyo siempre ha sido muy importante para mí para lograr los desafíos académicos. Y obviamente, a todo el equipo de Remo UChile (qepd) gracias por cada momento en el remo, por las travesías en las lagunas, las chelas, las pizzas, chorrillanas, carretes, y los entrenamientos, obvio.

Mil gracias por existir en mi vida a mis amigas hermosas de geo, son las cabras más bacanas que pude conocer: Valy, Danisita, Fersita, Jazz (de nuevo), Arrocita, Cami (camala), Coty, Ale Cevo y un largo etc de compañeras y amigas bacanas que me regaló la vida. Gracias por la

confianza, por el aguante, por dar cara, y en general por todo. Agrego acá a otras mujeres bellísimas que conocí gracias a geología: Gene, Carli, Frani, Dani Parra, Tami, Giss, Sami etc. A todas las geomujeres puro amor y por sobretodo a Andinas Chile! La Red de Geocientíficas Chilenas que está rebalsando de amor y *power* femenino!

Gracias también a los cabros, Chaino, Richi, Negrito y en especial al Sebita y Navi, gracias por esas largas y profundas conversaciones y obvio también las copuchas infaltables. Gracias Claudito por ser el mejor vecino en la sala de postgrado.

Un millón de gracias a la Blanquis, la tía Mary, Rosita, Vero, Maritza, Don Carlos y a todos los funcionarios del Dpto de Geología, los he extrañado un montón en este tiempo de encierros y cuarentena; gracias a la tía Mary por esas conversaciones amorosas buena onda que te llenan de energía para comenzar el día; y a la Blanquis por toda su ayuda y disposición en cada mínimo trámite que hay que hacer para sobrevivir a la burocracia de la u.

A los amigos que hice gracias a la petro: Darío, Pelao, Chiri, Claudio, Mila. Mil gracias por ser una inspiración, un ejemplo a seguir, y estar siempre ahí respondiendo mis más mínimas dudas. Esta tesis no podría haber sido posible sin la guía de ustedes. Agrego acá las mil gracias a Claudio, Flo, Anto y Santi por recibirme y adoptarme por un mes en su hogar en Bristol, me siento demasiado afortunada de haber tenido la oportunidad de conocerlos y quererlos, y compartir con ustedes como parte de su familia en mi estadía por las Europas. Gracias a la Gilla por su tremendo apañe con la figura del modelo final, además de talentosa geóloga e ilustradora, calidad de persona y amiga. Gracias a toda la gente que me apañó en el terreno de esta tesis, en especial al Ale y Mendo por ser los mejores ayudantes. A la Fran y don Luis de Huilo Huilo, a Jorge del Fundo El Depósito y a Darío Salas de la RNMCH, por acompañarnos y guiarnos entre árboles y volcancitos.

Además, me gustaría agradecer la formación e integridad de varios profesores del Dpto de Geología, gracias por la eterna disposición, pasión por la enseñanza, y en especial, gracias a aquellas/os que se atreven a innovar y flexibilizar en docencia.

Miles de gracias a la gente que lucha, a la gente que marcha, a la gente que sueña. Gracias por el despertar colectivo del 18O, honores a quienes viven hoy con marcas del estallido, y por siempre honor a quienes perdieron la vida en la lucha. Gracias a todas y cada una de las personas que han aparecido en mi camino inspirándome y siendo grandes referentes. En especial, gracias a las mujeres, que juntas avanzamos hacía una nueva forma feminista de relacionarnos en sociedad.

Gracias a la madre naturaleza por estar dispuesta a ser estudiada, y deleitarnos con su magnífica belleza. Gracias a la vida, que me ha dado tanto.

TABLA DE CONTENIDO

ÍNDICE DE FIGURAS

ÍNDICE DE TABLAS

Capítulo 1: Introducción

1.1 Estructura de la tesis

Este trabajo se enfoca en el estudio petrológico y geoquímico de productos volcánicos holocenos de los centros eruptivos menores (CEM) del Grupo Fui, con atención particular en lavas e incluyendo comparaciones geoquímicas con muestras del Complejo Volcánico Mocho-Choshuenco (CVMC).

En el capítulo 1 se presenta la motivación y objetivos de este trabajo, el marco geológico de la zona de estudio, la descripción del área de trabajo y la campaña de terreno, además de las metodologías utilizadas.

El capítulo 2 consiste en un manuscrito que será sometido a la revista *Journal of Volcanology and Geothermal Research*. En este trabajo, se muestran los resultados obtenidos a partir de las muestras analizadas, incluyendo geoquímica de roca total y descripción petrográfica de las lavas, y un estudio detallado de la química mineral de los cristales de olivino, plagioclasa y clinopiroxeno. Además, se lleva a cabo la determinación de condiciones pre-eruptivas con herramientas termodinámicas, una discusión de los datos obtenidos y conclusiones alcanzadas en el trabajo realizado.

En el capítulo 3 se plasman las conclusiones globales del estudio y, por último, en la sección de Anexos se adjuntan tablas e información adicional obtenida en el desarrollo de este trabajo.

1.2 Objeto de estudio y motivación

El volcanismo monogenético o de CEM (recientes discusiones sobre el término “CEM” en Németh and Kereszturi, 2015; Cañón-Tapia, 2016; McGee and Smith, 2016) es el tipo de volcanismo más

abundante en el mundo y se presenta en diferentes configuraciones tectónicas (Németh, 2010; Cañón-Tapia, 2016). Este tipo de volcanismo está caracterizado por pequeños volúmenes de material emitido (<1 km^3; Németh & Kereszturi, 2015) durante un tiempo acotado desde días a algunos años (≤10 años; Németh & Kereszturi, 2015). Los productos volcánicos que forman este tipo de volcanismo no están restringidos en un rango composicional, sin embargo, generalmente corresponden a composiciones basálticas (Valentine and Gregg, 2008; Németh, 2010).

El volcanismo de los CEM es comúnmente considerado como simples pulsos magmáticos que ascienden directamente desde el manto con mínimas interacciones con la corteza (e.g., Walker, 1993; Valentine and Perry, 2007; Rasoazanamparany et al., 2015; McGee and Smith, 2016). Sin embargo, hay evidencias de que en los CEM ocurre cristalización polibárica en la corteza en diferentes configuraciones tectónicas (e.g., Johnson et al., 2008; Erlund et al., 2010; Gao et al., 2017; Morgado et al., 2017; Coote et al., 2018; Coote and Shane, 2018; Shane and Coote, 2018), incluyendo complejos *plumbing systems*, reservorios en niveles someros y medios de la corteza, y el desarrollo de reservorios con zonas de enrejados densos cristalinos (*crystal mush*). Debido a lo anterior, es que en este estudio se pretende caracterizar las condiciones pre-eruptivas de los CEM del Grupo Fui, para conocer el nivel de profundidad y complejidad de sus reservorios; así como la historia magmática pre-eruptiva a través del análisis de los cristales presentes en las muestras en estudio.

Los CEM del Grupo Fui se ubican entre 8 y 16 km al noreste del CVMC y al oeste de la Zona de Falla Liquiñe Ofqui (ZFLO; ver Fig. 1.1). En este estudio se considerarán los volcanes Chanchán como parte del Grupo Fui. La configuración espacial descrita para los CEM del Grupo Fui, el CVMC y la ZFLO no es única en la Zona Volcánica Sur (ZVS), otros trabajos han abordado el estudio de CEM al este y noreste de volcanes compuestos: Al norte del Grupo Fui, los CEM Caburgua-Huelemolle y volcán Villarrica (Morgado et al., 2015 y 2017; McGee et al., 2017) y el

volcán Huililco y volcán Quetrupillán (Brahm et al., 2018), mientras que al sur de la zona de estudio Bucchi et al. (2015) estudiaron el campo volcánico Carrán-Los Venados y complejo volcánico Puyehue-Cordón Caulle. Debido a esto, es que la importancia de caracterizar las condiciones magmáticas y procesos que dan origen a estos conos no solo repercutirá en presentar nuevos datos para la zona, sino que también permite comparar el sistema volcánico estudiado con otros aledaños, para comprender los mecanismos pre-eruptivos y el nivel de relación entre volcanes compuestos y CEM en la ZVS.

Además, debido a su distribución espacial y composición de los productos volcánicos emitidos, el Grupo Fui ha sido separado en dos subgrupos, los cuales en este estudio serán referidos como Fui Norte (cuatro CEM al norte del Río Fuy; polígonos de tonalidades rojas en la Fig. 1.1b) y Fui Sur (16 CEM al sur del Río Fuy; polígonos de tonalidades azules de la Fig. 1.1b). Este trabajo tendrá el objetivo de caracterizar y contrastar los procesos pre-eruptivos de ambos subgrupos.

En este estudio se incluyen análisis de geoquímica de roca total combinados con un detallado estudio microscópico textural y composicional de las fases minerales de lavas del Grupo Fui. La investigación estará enfocada en resolver interrogantes de carácter petrológico, presentando por primera vez estimaciones de condiciones físicas pre-eruptivas para los CEM del Grupo Fui, utilizando herramientas geoquímicas y termodinámicas, además de modelaciones termodinámicas con el *freeware* rhyolite-MELTS, contribuyendo así al entendimiento de los procesos magmáticos que dieron origen a los CEM en estudio. Además, se discute sobre las similitudes y diferencias entre los productos volcánicos de los dos subgrupos del Grupo Fui y su relación con los productos volcánicos del CVMC a través de nuevos datos de geoquímica de roca total presentados para este complejo volcánico.

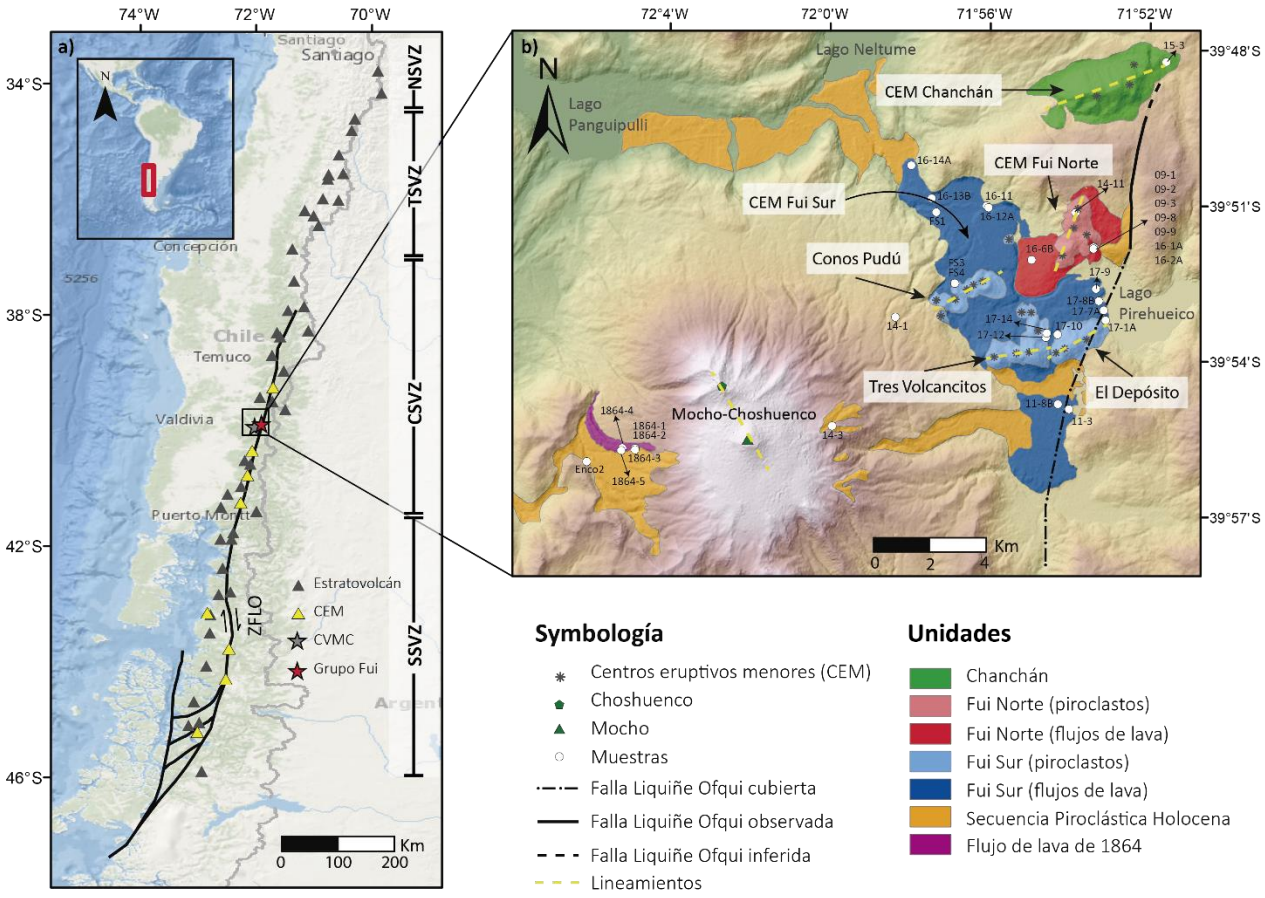

Fig. 1.1: *(a) Mapa de volcanes en la ZVS. Se incluyen los segmentos de la subdivisión de la ZVS (basado en López-Escobar et al., 1995). Mapa elaborado con "Oceans" basemap en el software ArcGIS v.10.3. (b) Mapa geológico simplificado del Complejo Volcánico Mocho-Choshuenco (incluyendo solo las unidades volcánicas de interés para este trabajo), Grupo Fui y volcanes Chanchán. Modificado de Moreno y Lara (2007). La Secuencia Piroclástica Holocena incluye la erupción sub-pliniana Enco. Se incluyen los lineamientos observados y los nombres locales de los subgrupos de CEM del Grupo Fui. Chanchán se incluye dentro del subgrupo Fui Norte en este trabajo, mientras que los conos Pudú, Tres Volcancitos y conos de El Depósito conforman el subgrupo Fui Sur.*

1.3 Objetivos

1.3.1 Objetivo general

Establecer las condiciones físico-químicas (presión, temperatura, contenido de H_2O, y fugacidad de oxígeno) de los reservorios de los CEM del Grupo Fui, y sus implicancias en sus historias pre-eruptivas.

1.3.2 Objetivos específicos

-Determinar la composición química de materiales volcánicos de los centros volcánicos.

-Determinar la mineralogía de los productos volcánicos, su composición, texturas y las asociaciones de fases minerales presentes en los sistemas.

-Determinar la geotermobarometría, condiciones de oxidación y contenido de agua para las erupciones holocenas de los CEM del Grupo Fui.

-Simular las condiciones de formación para la mineralogía presente en las muestras de lava.

-Describir los procesos pre-eruptivos para cada sistema volcánico estudiado.

1.3.3 Hipótesis

Los CEM de los subgrupos Fui Norte y Fui Sur tienen historias y orígenes diferentes e independientes en la corteza. Existe una relación entre los magmas del CVMC y los de Fui Sur, mientras que el subgrupo Fui Norte es un sistema independiente.

1.4 Marco geológico

1.4.1 Marco geológico regional

El CVMC, los CEM del Grupo Fui y los volcanes Chanchán se ubican en la Cordillera Principal en el sur de Los Andes chilenos, donde se encuentra el arco volcánico actual. Específicamente, se ubican en la ZVS, definida como el arco volcánico comprendido entre los 33°S y 46°S al oeste de la placa sudamericana, y con orientación general NNE-SSW (López-Escobar et al., 1995; Cembrano y Lara, 2009).

La ZVS a su vez tiene cuatro subdivisiones (Fig. 1.1a) basadas en la configuración tectónica, composiciones geoquímicas y características petrológicas de los productos volcánicos (López Escobar et al., 1995; Stern, 2004). Estas corresponden al segmento Norte (NSVZ de *"North Southern Volcanic Zone"* en inglés, 33.3 – 34.5°S), Transicional (TSVZ, 34.5 – 37°S), Central (CSVZ, 37 – 41.5°S) y Sur (SSVZ, 41.5 – 46°S). La zona de estudio que comprende al Grupo Fui y al CVMC se ubica en el segmento Central de la ZVS, en la cual también se encuentran los volcanes más activos y riesgosos de Chile, tales como el volcán Villarrica, Llaima, Calbuco, entre otros (de acuerdo con el ranking de riesgo específico; SERNAGEOMIN, 2020a).

Los centros volcánicos en estudio se emplazan sobre un basamento heterogéneo compuesto por rocas metamórficas, granitoides y rocas estratificadas (Fig. 1.2) que dan cuenta de la evolución geológica del territorio desde el Paleozoico hasta el Pleistoceno Inferior (Moreno y Lara, 2007). A continuación, se presenta una síntesis de las unidades del basamento y de las unidades que afloran en la zona de estudio (Fig. 1.2), basado en el trabajo de Moreno y Lara (2007).

1.4.1.1 Unidades metamórficas

Complejo Metamórfico Trafún (Devónico-Carbonífero): Aflora al SW de la zona de estudio cercano al Lago Riñihue (fuera del área mostrada en la Fig. 1.2; Lago Riñihue referenciado en la Fig. 1.3). Consta de meta-areniscas, cuarcitas, pizarras y filitas verdes. Estas rocas forman parte de

la Serie Oriental del basamento Metamórfico de la Costa de Chile central-sur (Aguirre et al., 1972). Fuera del área de estudio de este trabajo, la edad máxima datada en circones en meta-conglomerados es de ca. 383 Ma, mientras que la edad mínima queda restringida por el Batolito Futrono-Riñihue (ca. 300 Ma) que intruye a esta unidad.

1.4.1.2 Unidades estratificadas

Formación Panguipulli (Triásico Superior): Reconocida en la zona NW de la zona de estudio, principalmente en la ribera del Lago Panguipulli y en el extremo suroriental del Lago Riñihue, y fuera de la zona de estudio correspondiente a la ribera del Lago Calafquén. Corresponde a una sucesión estratificada fuertemente plegada de lutitas, areniscas, cuarcitas y conglomerados. La flora fósil recolectada en esta unidad correspondería al Carniense-Noriense (Herbst et al., 2005).

Estratos de Lago Ranco (Oligoceno-Mioceno): Aflora en el segmento sur de la zona de estudio, corresponde a una secuencia volcanosedimentaria plegada, compuesta por conglomerados, brechas volcánicas, tobas, tufitas y lavas andesíticas porfídicas, de color gris verde. Fuera del área de estudio se reportaron edades de ca. 13 Ma (K-Ar en roca total; García et al., 1988) para rocas volcánicas e hipabisales de la secuencia, y de ca. 20 Ma (K-Ar en plagioclasa; Campos et al., 1998), sin descartar que la base de la secuencia alcance edades oligocenas.

Secuencias Volcánicas Indiferenciadas (Pleistoceno Inferior a Medio): Corresponden a remanentes de antiguos estratovolcanes desgastados por erosión glacial, compuesta principalmente por lavas andesítico-basálticas de olivino y clinopiroxeno, junto a escasas andesitas y dacitas con algunas intercalaciones de brechas y conglomerados volcánicos. Se reconoce esta unidad principalmente en el segmento NE de la zona de estudio, cubierta parcialmente por depósitos volcánicos de los centros eruptivos Fui y Chanchán, y también aflora en zonas SW del CVMC. Las edades determinadas han sido: <1 Ma en K-Ar roca total en lava del sector SO (Campos et al., 1998); <1.5 Ma en K-Ar en áreas vecinas hacia el este del sector de estudio (Lara et al., 2001 y Lara y Moreno

2004); y ca. 0.6-0.7 Ma en $^{40}Ar/^{39}Ar$ masa fundamental, para secuencias volcánicas similares situadas en la zona fronteriza a similar latitud (Lara y Folguera, 2006).

1.4.1.3 Intrusivos

Batolito Futrono-Riñihue (Carbonífero Superior-Pérmico Inferior): Aflora en el sector occidental al oeste del Río Enco (fuera del área mostrada en la Fig. 1.2), corresponde a una unidad plutónica constituida por granitos, granodioritas y tonalitas de biotita y hornblenda, de carácter metaluminoso a peraluminoso. Fuera del área de estudio, edades K-Ar y $^{40}Ar/^{39}Ar$ de ca. 282-307 Ma fueron reportadas por Munizaga et al. (1988), Beck et al. (1991), Campos et al. (1998) y Rodríguez et al. (1999). También, edades U-Pb en circones definen un rango entre ca. 282-304 Ma (Campos et al., 1998).

Plutón Panguipulli (Jurásico): Unidad plutónica que forma una franja NW-SE entre los lagos Panguipulli, Riñihue y Pirehueico. Compuesto principalmente por tonalitas de hornblenda y biotita, también con presencia de granitos y granodioritas. Edades de enfriamiento de K-Ar y $^{40}Ar/^{39}Ar$ entre 142-184 Ma han sido reportadas para esta unidad por Munizaga et al. (1988), Rodríguez et al. (1999) y Lara y Moreno (2004). Además, Rodríguez et al. (1999) reporta una edad de ca. 176 Ma (U-Pb en circones).

Plutón Choshuenco (Cretácico Inferior): Localizado al sur y este de la localidad de Choshuenco (localidad referenciada en Fig. 1.3), constituido principalmente por dioritas y tonalitas de hornblenda. Edades de enfriamiento de ca.142 Ma con K-Ar en biotita y ca. 134 Ma $^{40}Ar/^{39}Ar$ plateau en biotita (Rodríguez et al., 1999), también se determinó una edad K-Ar en anfíbol de tonalita correspondiente 74±8 Ma, que debido a su ubicación (al Norte del Río Llanquihue) se interpreta como una edad mínima debido a su proximidad con un cuerpo porfídico del Mioceno Superior.

Granitoides Miocenos (Mioceno): Cuerpos intrusivos dispuestos en franjas longitudinales de orientación NNE y limitadas por la traza principal de la ZFLO o algunas estructuras subsidiarias a ella. Las litologías corresponden desde granitos y granodioritas a dioritas y tonalitas de biotita y hornblenda, además cuerpos hipabisales andesítico-dacíticos subordinados. La edad de estos granitoides está constreñida en el rango entre 5 y 18 Ma (Lara y Moreno, 2004; Munizaga et al., 1988; Campos et al., 1998).

Pórfidos Miocenos (Mioceno): Conjunto de intrusivos porfídicos que afloran en el extremo norte del área, al W del Lago Neltume. Son cuerpos tipo *stock* con diques asociados de composición andesítica a dacítica, algunos de los cuales han sido datados por Rodríguez et al. (1999) en 9 Ma (K-Ar en roca total).

1.4.1.4 Depósitos sedimentarios

Los depósitos sedimentarios cuaternarios en la zona se diferencian dependiendo de su origen. En general, están asociados a la erosión de los centros volcánicos y basamento durante los diferentes eventos glaciares en la zona. A continuación, se presentan de manera sintetizada las principales características de los depósitos sedimentarios cuaternarios, basado en Moreno y Lara (2007).

Los depósitos glaciales y glaciofluviales se encuentran formando morrenas y abanicos fluvioglaciales compuestos por diamictos de bolones, arena y limo, junto a bancos de gravas y arenas moderadamente consolidados asociados a los avances y retrocesos del hielo durante la Glaciación Llanquihue (110-14 ka; Clapperton, 1993; Clayton et al., 1997) y el último máximo glacial (ca. 32-14 ka; Lowell et al., 1995). Los depósitos glaciales asociados al glaciar del CVMC están conformados por diamictos de bolones volcánicos inmersos en una matriz gravo-arenosa, formando morrenas frontales, laterales y de fondo ubicadas en la parte alta del edificio volcánico.

Los depósitos fluviales antiguos (Pleistoceno Superior-Holoceno) corresponden a bancos de gravas y arenas con intercalaciones de limos y arcillas, como remanentes de terrazas antiguas más elevadas que el nivel actual del Lago Panguipulli; constituidos por depósitos fluviales con intercalaciones de depósitos lacustres. Actualmente, se identifican depósitos clásticos de gravas con intercalaciones de arenas, relativamente bien seleccionados dispuestos en capas de espesor variable (decenas de cm a m) en los cauces de los ríos Blanco-Pillanleufú, Fuy, Neltume, Llanquihue y Enco.

Los depósitos de remoción en masa y coluviales actuales son de mala selección, con fragmentos angulosos tamaños grava, con o sin matriz de arena y arcilla-limo; con morfologías de conos o lóbulos con pendientes superiores a 20°, formados por flujos de detritos, coluviales y de deslizamiento de roca, generados por colapso gravitacional de taludes en condiciones inestables. Los flujos de detritos habrían sido gatillados por lluvias torrenciales.

Finalmente, los depósitos deltaicos clásticos dispuestos en la desembocadura del río Llanquihue en el lago Panguipulli, y en el sector de la entrada del río Enco en el lago Riñihue, están formados por gravas medias e intercalaciones de arenas. Los depósitos de playas lacustres compuestos de sedimentos finos (arena media a fina) bien seleccionados, de origen mayoritariamente volcánico, se ubican principalmente en el sector NW del lago Pirehueico (Puerto Fuy; localidad referenciada en la Fig. 1.3) y en el litoral del lago Panguipulli, en la localidad de Choshuenco.

1.4.2 Marco tectónico

La configuración tectónica de la ZVS está caracterizada por la convergencia ligeramente dextral-oblicua entre las placas de Nazca y Sudamericana, cuya tasa de convergencia es de 7 – 9 cm/año que se ha mantenido por 20 Ma (Cembrano y Lara, 2009). El espesor de la corteza en la ZVS decrece desde 50 km en el extremo norte de esta zona (33°S) hasta alcanzar 35 km de espesor en

el extremo sur de la misma (46°S; López-Escobar et al., 1995; Stern, 2004; Cembrano y Lara, 2009), a su vez considerando los espesores de la corteza presentados en el estudio de Tašárová (2007), la zona de estudio que incluye al Grupo Fui y al CVMC posee un espesor cortical de 40 km.

La tectónica de la zona de estudio está principalmente controlada por la acción de la ZFLO. La ZFLO corresponde a un sistema de fallas de ~1200 km de longitud (Cembrano y Lara, 2009) ubicada en el intra-arco de un segmento de la ZVS (Fig. 1.1a), que controla la tectónica dextral-transpresiva entre los ~38° y ~46°S (Cembrano y Lara, 2009). La ZFLO acomoda la deformación a través de la falla principal de orientación NNE y a través de estructuras subsidiarias transtensivas dextrales ENE; además existen estructuras de orientación WNW, las cuales han sido interpretadas como zonas de debilidad cortical asociadas a fallas pre-existentes (pre-andinas) que se reactivan como fallas transpresivas sinestrales (Cembrano y Lara, 2009).

La ZFLO también juega un rol fundamental en el volcanismo de la ZVS, se ha observado que los CEM y estratovolcanes de composiciones primitivas se distribuyen a lo largo de estructuras de orientación NE, mientras que los estratovolcanes con un rango composicional más amplio (incluyendo así composiciones más diferenciadas) se ubican alineados a las estructuras de orientación WNW (López-Escobar et al. 1995; Cembrano y Lara, 2009).

1.4.3 Marco geológico volcánico

1.4.3.1 CVMC

El CVMC es un complejo volcánico con productos desde el Pleistoceno Medio hasta el presente (Moreno y Lara, 2007), compuesto por dos cimas principales: el volcán Mocho corresponde a un cono de escoria en la zona sureste del complejo volcánico, construido al interior de una caldera

mientras que el volcán Choshuenco corresponde a un cuello volcánico ubicado en la parte noroeste de la caldera y que fue parcialmente afectado por este evento explosivo (Moreno y Lara, 2007).

EL CVMC se ubica en la posición 7 del ranking de riesgo específico de Sernageomin de un total de 92 sistemas volcánicos considerados (SERNAGEOMIN, 2020a), su última erupción confirmada data del año 1864 por lo que lleva más de un siglo sin actividad efusiva o explosiva. Sin embargo, el Observatorio Volcanológico de Los Andes del Sur (OVDAS) ha reportado actividad sísmica asociada a movimiento de fluidos y fracturas de roca recientemente (e.g., SERNAGEOMIN, 2018; SERNAGEOMIN, 2020b; SERNAGEOMIN, 2021). Mediante un detallado estudio tefroestratigráfico se determinó una ciclicidad eruptiva de 150 años (Rawson et al., 2015) para este complejo volcánico.

De acuerdo con Moreno y Lara (2007), las unidades evolutivas del complejo volcánico se dividieron de acuerdo con su centro emisor, existiendo tres unidades para el edificio Mocho ancestral pre-caldera, y dos unidades del Mocho post-caldera incluyendo las emisiones volcánicas más recientes del volcán, además de una unidad aparte que reúne los productos de eventos explosivos holocenos denominada Secuencia Piroclástica; mientras que para el Choshuenco se definieron dos unidades de edades pleistocenas. A continuación, se presenta una síntesis de las unidades anteriormente mencionadas, basadas en la Carta Geológica de Moreno y Lara (2007).

Unidad Mocho 1 (Pleistoceno Medio): Lavas, conglomerados volcánicos y tobas ubicadas en la sección sur del complejo volcánico, constituye la secuencia más antigua del edificio. Sus composiciones son de andesitas-basálticas a andesitas (52-59 wt% SiO_2). Existen en algunos sectores diques andesítico-basálticos y dacíticos (55-65 wt% SiO_2) que cortan la secuencia principal o alimentan coladas menores; uno de estos diques indica la edad de 86±17 ka. Las

dataciones $^{40}Ar/^{39}Ar$ en lavas indicaron edades de 350±20 ka, 260±60 ka, 220±78 y 202±54; con lo cual se definió que la época de esta unidad corresponde al Pleistoceno Medio.

Unidad Mocho 2 (Pleistoceno Medio-Superior): Lavas, tobas, brechas y conglomerados volcánicos con inyecciones filoneanas y lacolíticas; expuestas preferentemente en los flancos oriental y nororientales del CVMC formando gran parte de la secuencia pre-caldera del edificio volcánico. Las composiciones de estos productos volcánicos son de andesitas-basálticas a dacitas (52-68 wt% SiO_2). Edades de 130±30 ka se obtuvieron mediante el método $^{40}Ar/^{39}Ar$ en lavas cercanas al techo de la secuencia. No se tiene una edad máxima para la unidad, sin embargo, puede acotarse con la edad mínima definida para la Unidad Mocho1 (200 ka).

Unidad Mocho 3 (Pleistoceno Superior): Conjunto de lavas expuestas en la periferia de la caldera, de composiciones andesíticas y dacíticas (56-66 wt% SiO_2). Se obtuvo una datación en una lava mediante el método 40Ar/39Ar de 60±20 ka, y de acuerdo con observaciones morfológicas, esta unidad se puede considerar como enteramente intraglacial. Posteriormente a esta unidad el estratovolcán ancestral sufrió un evento de colapso del edificio y se habría generado la caldera; durante la última glaciación (>ca. 14 ka).

Unidad Mocho 4 (Holoceno): Conjunto de lavas expuestas principalmente en el sector occidental y en algunos lugares altos del flanco oriental del CVMC. Forma parte de la secuencia de coladas post-caldera emitidas desde el interior de la caldera y desde los flancos a través de fisuras, y que representan la primera etapa de construcción del cono moderno. Sus composiciones son de andesítico-basálticas a dacíticas (52-67 wt% SiO_2). La edad general de esta unidad es de <ca. 11 ka, la cual fue determinada mediante relaciones estratigráficas y análisis de eventos simultáneos con la Secuencia Piroclástica Holocena.

Unidad Mocho 5 (Holoceno tardío e Histórico): Conjunto de lavas, aglomerados volcánicos y depósitos laháricos asociados, que representan las emisiones más recientes del CVMC y construyen el cono central Mocho. Sus composiciones son andesíticas a dacíticas (57-65 wt% SiO_2). Incluye la colada de lava de bloques de composición dacítica emitida durante la última erupción del CVMC en el año 1864. La edad de esta unidad se indica como <ca. 1.7 ka, ya que la edad máxima se infiere a partir de la ausencia de depósitos de la Ignimbrita Enco (perteneciente a la Secuencia Piroclástica Holocena) sobre las coladas holocenas.

Secuencia Piroclástica (Holoceno): Secuencia estratificada que comprende los depósitos piroclásticos de flujo, caída y oleadas, producto de erupciones explosivas holocenas que en su conjunto constituyen cerca de 11,000 años de actividad eruptiva postglacial. La secuencia se distribuye ampliamente sobre los flancos del CVMC y sobre rocas del basamento en zonas distales. Se destacan en esta unidad a las Ignimbritas Neltume (edad entre 10.7 y 9.7 ka; volumen de 2.5 – 2.9 km^3), Pirehueico (edad entre 8.2 y 6.7 ka; volumen ~1 km^3) y Enco (edad de 1.7 ka).

Unidad Choshuenco 1 (Pleistoceno Medio): Secuencia constituida principalmente por lavas andesítico-basálticas a dacíticas (52 – 68 wt% SiO_2) que constituyen el edificio principal del volcán Choshuenco, y forman parte de la secuencia pre-caldera del complejo. El cuello volcánico Choshuenco se encuentra profusamente intruído por diques verticales, y algunos de disposición radial. Una lava de la base fue datada en 200±60 ka mediante $^{40}Ar/^{39}Ar$, mientras que otra lava cercana al techo de esta unidad indicó una edad de 170±70 ka mediante el mismo método.

Unidad Choshuenco 2 (Pleistoceno Superior): Conjunto de lavas expuestas emitidas por dos centros eruptivos en el flanco NO del volcán Choshuenco, de composiciones andesíticas y dacíticas (59 – 66 wt% SiO_2). Dos edades obtenidas mediante el método $^{40}Ar/^{39}Ar$ en la sección distal de las coladas arrojaron 53±30 ka y 46±20 ka, por lo que esta unidad puede considerarse equivalente al

techo de la Unidad Mocho3, sin embargo, también existe la posibilidad de que se hayan reactivado los centros emisores de los flancos posteriormente a la formación de la caldera en el Tardiglacial.

1.4.3.2 Centros volcánicos adventicios

En los flancos este y suroeste del CVMC se ubican alrededor de veinte centros volcánicos adventicios organizados en dos grupos: Grupo Alto Caunahue y Grupo Ranquil. El Grupo Alto Caunahue consiste en un conjunto de trece conos de piroclastos holocenos (en su mayoría fuera del área mostrada en la Fig. 1.2) con productos de composición andesítica (55-58 wt% SiO_2; Moreno y Lara, 2007). Por otro lado, el Grupo Ranquil se compone de cuatro conos de piroclastos postglaciales holocenos en una cadena de dirección NW sin lavas asociadas; los productos volcánicos son de composición andesítica (55-58 wt% SiO_2; Moreno y Lara, 2007).

1.4.3.3 CEM del Grupo Fui

El Grupo Fui corresponde a un conjunto de 20 CEM ubicados ~8 km al noreste del CVMC y adyacentes al oeste de la ZFLO (39°54 S). De acuerdo con SERNAGEOMIN, el Grupo Fui es considerado como un campo volcánico de bajo riesgo específico (ubicado en la posición 51° de un total de 92 sistemas volcánicos; SERNAGEOMIN, 2020a). Debido a variaciones composicionales, autores previos han señalado diferencias que permiten dividir el Grupo Fui en dos subgrupos:

1) Fui Norte, compuesto por cuatro CEM al norte del Río Fuy (polígonos de tonalidades rojas, Fig. 1.1b) referidos geográficamente en otros estudios como “Cerro Fui Alto” (Lara y Moreno, 2004), “Fui Alto” (Gardeweg y Sellés, 2012) y composicionalmente como parte de los conos de signatura “Kangechi” en el trabajo de Rawson et al. (2016).

2) Fui Sur, conformado por 16 CEM al sur del Río Fuy (polígonos de tonalidades azules, Fig. 1.1b), llamados de la misma manera por Gardeweg y Sellés (2012) e incluidos composicionalmente como parte de los “conos Normal de la ZVS” en la investigación de Rawson et al. (2016).

Todos los CEM están alineados en direcciones NE o NNE. Las edades para Fui Norte promedian ~1700 AP, mientras que para Fui Sur el rango es desde 1100 a 5780 AP en base a dataciones con el método ^{14}C de Moreno y Lara (2007), Pérez (2005) y Echegaray (2004). Sus alturas son entre 150 y 350 m, con diámetros de hasta 1250 m, mientras que los cráteres presentan diámetros entre 200 y 750 m (Moreno y Lara, 2007). Los volúmenes calculados del material emitido por el subgrupo Fui Norte suman un total de 0.171 km^3 mientras que en Fui Sur el volumen es de 0.535 km^3 (ambos volúmenes calculados en este estudio, ver Sección A.2). Los productos volcánicos del Grupo Fui tienen composiciones desde basálticas hasta dacíticas (50 – 64 wt% SiO_2; DiBiase, 1975; Echegaray, 2004; Moreno y Lara, 2007; Rawson et al., 2016).

1.4.3.4 Volcanes Chanchán

Conjunto de tres centros eruptivos principalmente postglaciales ubicados a 16 km al noreste del CVMC y al oeste de la ZFLO (39°48 S; Fig. 1.1); formando un lineamiento de dirección NE. Sus alturas alcanzan hasta 600 m y sus bases tienen hasta 3000 m de diámetro (Moreno y Lara, 2007). A pesar de no contar con dataciones directas, en base a observaciones morfológicas y estratigráficas se estima que su actividad fue durante el Pleistoceno Superior tardío – Holoceno temprano (Moreno y Lara, 2007). El volumen calculado de material emitido por estos volcanes es de 0.171 km^3 (este estudio, ver Sección A.2). Las composiciones geoquímicas de los productos volcánicos corresponden a los más primitivos de la zona (48 – 50 wt% SiO2; Moreno y Lara, 2007; Rawson et al., 2016). En este estudio se considerará a los volcanes Chanchán como parte del subgrupo Fui Norte debido a su ubicación geográfica y similitudes composicionales.

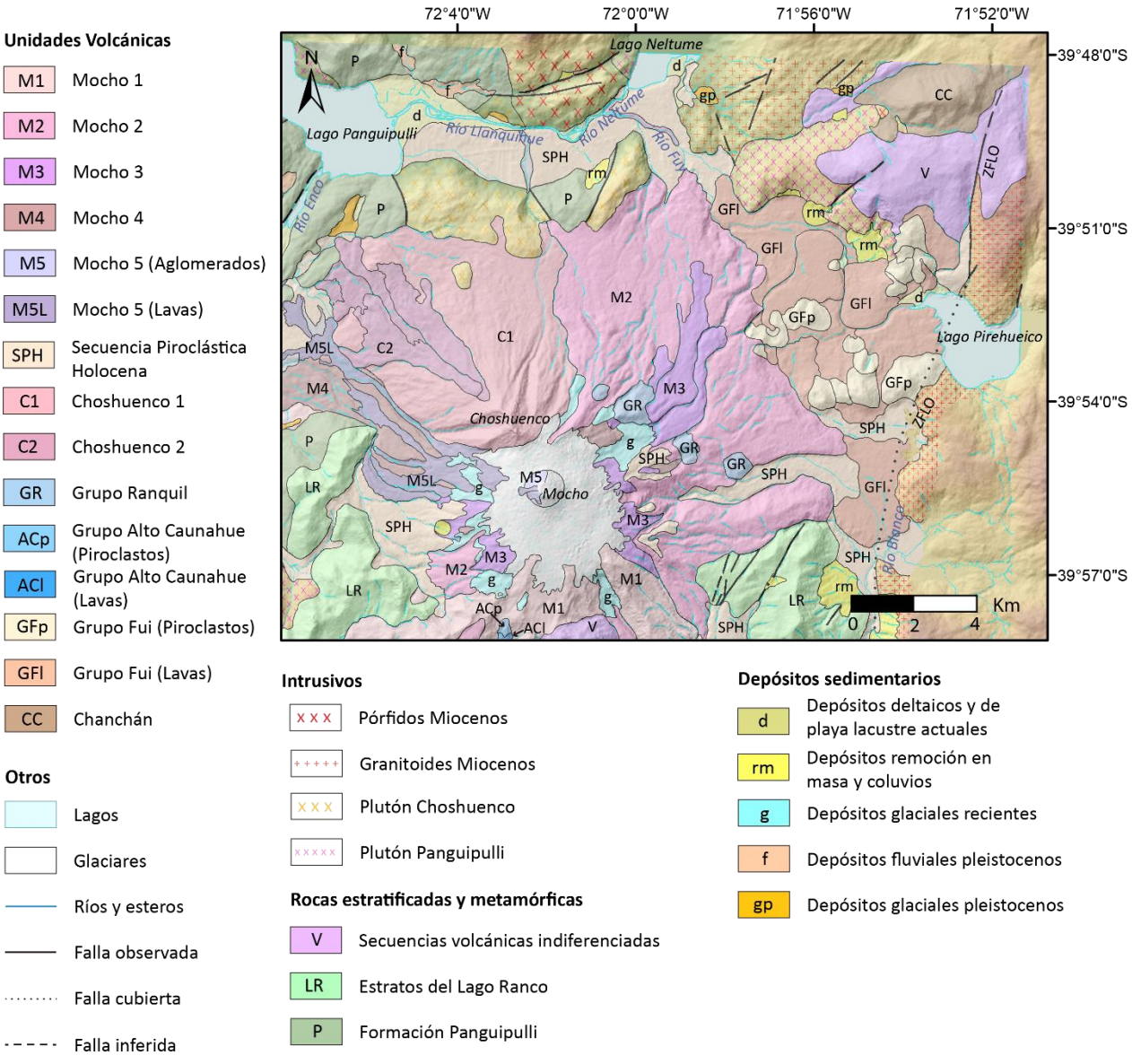

Fig. 1.2: *Mapa geológico simplificado, extraído y modificado de Moreno y Lara, (2007).*

1.5 Campaña de terreno y muestreo

Con el objetivo de muestrear materiales piroclásticos y lavas de los CEM del Grupo Fui y del Volcán Mocho-Choshuenco, se llevó a cabo una campaña de terreno por los alrededores de las localidades de Puerto Fuy, Neltume y Choshuenco (Fig. 1.3). La campaña se realizó durante enero de 2019, con una duración de 11 días en total y 9 días efectivos de muestreo; esta fecha fue

estratégicamente escogida durante el verano ya que en el resto del año las lluvias y nieve imposibilitan un adecuado trabajo de campo. Las muestras recolectadas se muestran en el mapa de la Fig. 1.1b, y sus ubicaciones se pueden encontrar en la Tabla A.1.

1.5.1 Ubicación y vías de acceso

El CVMC y los CEM del Grupo Fui se ubican entre los 39°56 S y 72°01 O en el sur de Chile. Comprende la Región de Los Ríos, entre las provincias de Valdivia y Ranco y las comunas de Panguipulli, Los Lagos y Futrono. Las localidades más cercanas a este complejo son Puerto Fuy, Neltume, Choshuenco y Panguipulli (esta última, fuera del área mostrada en la Fig. 1.3). En el Volcán Mocho-Choshuenco se ubica la Reserva Nacional Mocho-Choshuenco (administrada por CONAF; Fig. 1.3). La zona oriental del CVMC junto con los CEM del Grupo Fui pertenecen a la Reserva Biológica Huilo-Huilo.

Para acceder al Volcán Mocho-Choshuenco es posible ingresar desde el poblado de Choshuenco hacia la Reserva Nacional Mocho-Choshuenco o por las cercanías de Neltume y Puerto Fuy ingresando a la Reserva Huilo-Huilo (rutas de acceso marcadas en la Fig. 1.3), en ambos casos es necesario solicitar autorización a las respectivas instituciones tanto para el ingreso como para el retiro de muestras. En el caso de los CEM del Grupo Fui y volcanes Chanchán, el ingreso se realiza por caminos privados de la Reserva Huilo-Huilo (Fig. 1.3). Los caminos entre los poblados son pavimentados aptos para cualquier tipo de vehículo, no así los caminos internos pertenecientes a las reservas, en las cuales es necesario ingresar con vehículo de doble tracción (4x4).

1.5.1.1 Productos volcánicos de Fui Norte

Las muestras recolectadas de los CEM de Fui Norte fueron nueve (códigos, ubicación y breve descripción de las muestras en la Tabla A.1), obtenidas principalmente en tres puntos. El primero de ellos corresponde a la “Cantera Roja” (Fig. 1.4a), la cual es una excavación de origen antrópico

donde se puede observar la secuencia piroclástica de los productos volcánicos emitidos por uno de los conos de Fui Norte y una lava en un nivel intermedio de la secuencia. Para acceder a la Cantera Roja es necesario seguir por un camino local en el extremo oeste de Puerto Fuy, e ingresar a un camino que pertenece a la Reserva Huilo-Huilo. Desde esta cantera se tomaron muestras de tefras en 3 niveles (base, medio y alto) y muestras de la lava. El segundo punto corresponde a las cercanías del Mirador del Teleférico Cóndor Andino (ver Fig. 1.3) perteneciente a la Reserva Huilo-Huilo, al cual se puede acceder mediante vehículo con doble tracción siguiendo el camino desde la Cantera Roja. En este punto se tomaron muestras de una lava que aflora en un corte del camino. Finalmente, el tercer punto de muestreo corresponde a un corte del camino principal de la ruta 203 que une la localidad de Neltume con Puerto Fuy, de donde se obtuvieron muestras de lava provenientes de los conos Fui Norte.

1.5.1.2 Productos volcánicos de Fui Sur

En Fui Sur se reconocieron tres lineamientos de CEM: conos de El Depósito, conos Pudú y Tres Volcancitos (Fig. 1.1b). Se obtuvieron un total de 15 muestras recolectadas para los CEM de Fui Sur, incluyendo tefras, bombas y lavas (códigos, ubicación y breve descripción de las muestras en la Tabla A.1). Los puntos de muestreo fueron seis: 1) Cercanías del Salto Huilo-Huilo, 2) cercanías de Pampa Pilmaiquén, 3) cantera en la ladera de un cono de los Tres Volcancitos (Fig. 1.4c y d), 4) Condominio El Depósito, 5) corte de camino de la Ruta 203 (Fig. 1.4b) y 6) orillas del Rio Fuy (ver localización en el mapa de la Fig. 1.3). Los tres primeros sitios de muestreo pertenecen a la Reserva Huilo-Huilo, y para acceder a ellos es necesario seguir caminos privados de la reserva con la guía de un guardaparques. Dentro del Condominio El Depósito se ubica una colada de lava proveniente de uno de los conos de los Tres Volcancitos, para ingresar se solicitó autorización a los administradores del recinto. Finalmente, los puntos 5) y 6) se encuentran en zonas de libre acceso.

1.5.1.3 Productos volcánicos de Chanchán

Para acceder a las cercanías de los volcanes Chanchán es necesario ingresar por caminos privados de la Reserva Huilo-Huilo en las proximidades de la localidad de Neltume. Debido al denso bosque que se encuentra en esta zona, sumado a la ausencia de caminos o senderos y fuertes pendientes, los Volcanes Chanchán son de muy difícil acceso, por lo que solo se obtuvo una muestra de lava (muestra 15-3) de estos centros eruptivos, la cual aflora en un corte de camino en la zona este de los CEM.

1.5.1.4 Productos holocenos del CVMC

Se obtuvieron nueve muestras (códigos, ubicación y breve descripción de las muestras en la Tabla A.1) de los productos holocenos del CVMC en cuatro puntos: 1) lava de bloques de la última erupción del CVMC en 1864 (Fig. 1.4e), 2) corte de camino cercano al Refugio del Club Andino en la Reserva Nacional Mocho-Choshuenco (localización en Fig. 1.3), 3) ladera este del CVMC y 4) cercanías de la Pampa Pilmaiquén (Fig. 1.4f). Los productos incluyen lavas, bombas y tefras de la Ignimbrita Enco y erupción de 1864. Los tres primeros puntos se encuentran dentro de la Reserva Nacional Mocho-Choshuenco, donde es posible ingresar en un vehículo 4x4 y luego recorrer a pie, mientras que los dos últimos puntos pertenecen a la Reserva Huilo-Huilo, los cuales pueden ser recorridos en vehículo.

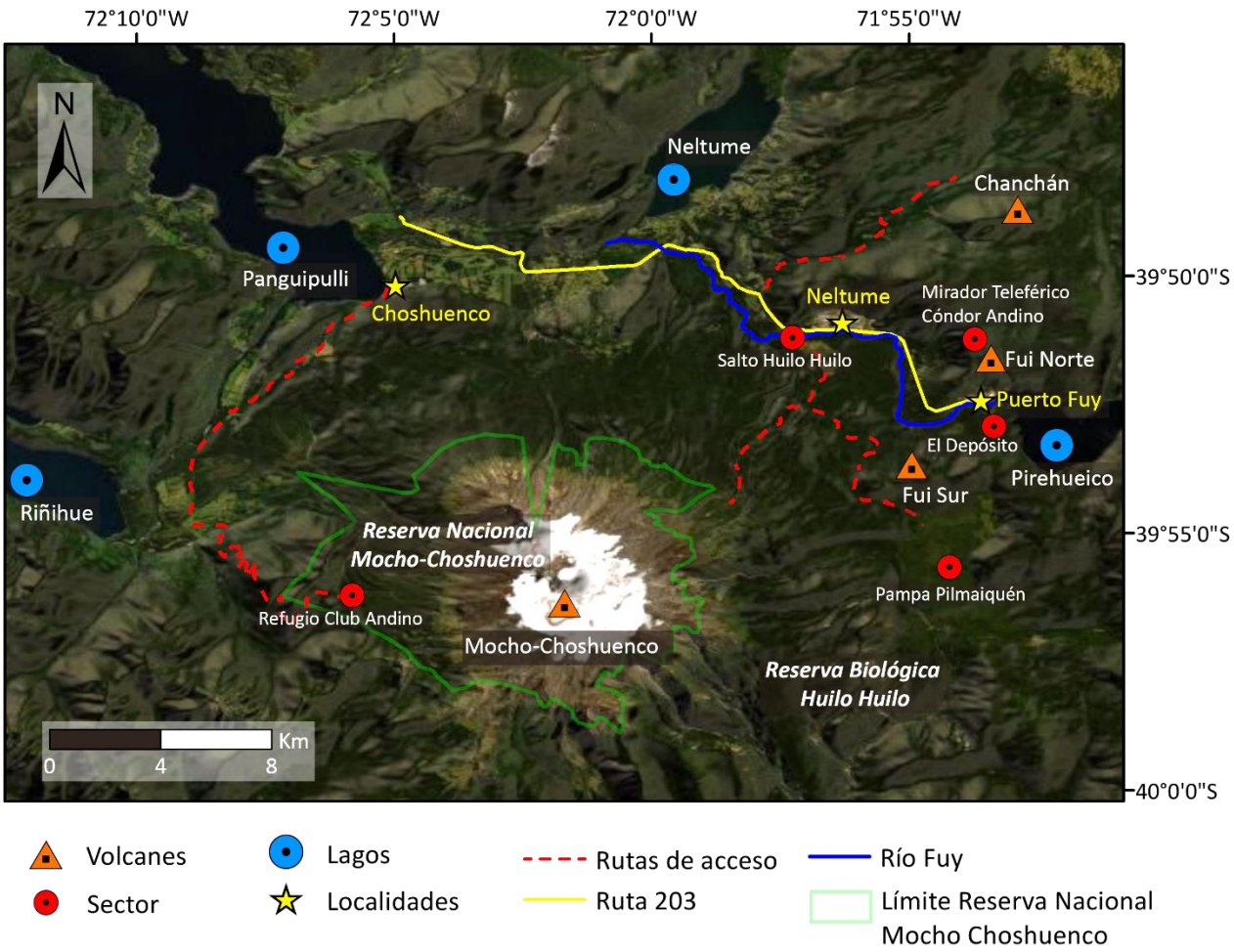

Fig. 1.3: *Mapa referencial de ubicación de volcanes, lagos, ríos, localidades, sectores de muestreo y rutas de acceso mencionadas en el texto. Contiene la delimitación de la Reserva Nacional Mocho-Choshuenco basada en Google maps y mapa de Andes Handbook. Al este de dicha reserva, se ubica la Reserva Biológica Huilo Huilo.*

Fig. 1.4: *Puntos de muestreo en terreno. (a) Tefras y lava en Cantera Roja en conos Fui Norte. Desde este sitio se obtuvieron las muestras 09-1, 09-2, 09-3 y 09-8 correspondientes a lavas, y 09-9, 16-1A y 16-2A correspondientes a tefras. (b) Muestra de lava 16-13B proveniente de los CEM Fui Sur, en corte de camino de la ruta 203. (c) Tefras en cantera en la ladera de un cono de los Tres Volcancitos (Fui Sur). Desde esta secuencia se obtuvo la muestra de bomba 17-12. (d) Lava 17-14 en nivel inferior de la misma cantera indicada en (c). (e) Lava de bloques de la erupción de 1864 del Volcán Mocho-Choshuenco, desde esta colada se obtuvieron las muestras 1864-1, 1864-2, 1864-3, 1864-4 y 1864-5. (f) Bomba 11-8B de la Ignimbrita Enco en la Pampa Pilmaiquén.*

1.6 Metodología

En enero de 2019 se llevó a cabo la campaña de terreno en las cercanías de las localidades de Puerto Fuy, Neltume y Choshuenco, en la Región de Los Ríos, para recolectar muestras holocenas de los diferentes centros volcánicos con la finalidad de analizar y caracterizar las composiciones geoquímicas y petrográficas de los productos volcánicos (códigos, coordenadas y tipo de muestra en la Tabla A.1). En el terreno se describieron las muestras macroscópicamente.

Los volúmenes de los materiales emitidos por los CEM fueron calculados tal como se indica en Larrea et al. (2019); utilizando modelos de elevación digital (DEM) en el software ArcGis, generando paleosuperficies utilizando las curvas de nivel, y *Triangulated Irregular Networks* "TIN" para posteriormente calcular el volumen sobre dicha paleosuperficie con la herramienta *Surface Difference*.

Se realizó un estudio petrográfico microscópico y geoquímico a un total de 34 muestras. La composición geoquímica de roca total fue analizada mediante ICP-ES e ICP-MS, para elementos mayores y trazas, respectivamente, en Bureau Veritas Mineral Laboratories en Vancouer, Canadá, utilizando el estándar SO-19 (resultados completos en la Sección A.3). La exactitud para elementos mayores es mejor que un 3% (relativo) excepto para el Cr_2O_3 (18% relativo), y para elementos traza es mejor que un 9% (relativo), excepto para el Sn con <11% (relativo) y Be con <40% (relativo). Se analizaron muestras duplicadas (muestra 1864-1 para elementos mayores y 1864-4 para elementos trazas) donde en general los resultados del duplicado tienen errores menores al 3% relativo a la muestra original en elementos mayores, y menor al 6% (relativo) en elementos trazas, excepto para el Be (50%), Ta (33%), U (23%) y V (17%). En el mismo laboratorio, se analizó la abundancia de FeO en las muestras a través de la técnica *Titration*, se utilizaron los estándares OREAS-700 y SY-4 presentando una exactitud mejor que 4% (relativo). Se midieron tres

duplicados de los cuales dos presentaron errores <1% relativo a la muestra original (muestras 17-2 y 16-1) y el tercero presenta un error de 15% relativo (muestra 09-3).

Las 34 láminas delgadas se realizaron en Vancouver Petrographics Ltd. (VanPetro), para un posterior estudio en microscopio óptico (Olympus, BX51) y microscopio electrónico de barrido (SEM) en el Departamento de Geología de la Universidad de Chile (FEI Quanta250) y en la Pontificia Universidad Católica de Chile (FE-SEM, FEI Quanta 250 FEG). Las láminas fueron escaneadas para procesar las imágenes en el *freeware* JMicroVision, donde se cuantificaron los cristales, vesículas y masa fundamental de las muestras con conteo modal en una base de 500 puntos aleatorios para cada lámina (resultados de la cuantificación en Table 3).

Luego de la caracterización petrográfica, se escogieron muestras representativas para medir puntualmente fenocristales de olivino, plagioclasa y clinopiroxeno con una Microsonda Electrónica (EPMA, JEOL JXA-8230) en LAMARX – Universidad Nacional de Córdoba, Argentina. Las composiciones minerales se obtuvieron con un potencial de aceleración de 15 keV y una corriente del haz de electrones de 20 nA, con un haz enfocado de 1 a 4 μm para todas las fases minerales, excepto para la plagioclasa, en la cual se utilizó un haz desenfocado de 10 μm para minimizar la pérdida de alkalis. Los tiempos de conteo fueron 10/5 s (peak/cada background) para elementos mayores y menores, con excepción del Ca en cristales de olivino donde el tiempo de conteo fue 20/10 s.

Adicionalmente, las composiciones de microlitos y microfenocristales de olivino, plagioclasa y clinopiroxeno fueron medidas con una Microsonda Electrónica JEOL JXA-8530F en la Univesity of Bristol (Inglaterra); donde los microlitos y microfenocristales de olivinos y clinopiroxenos fueron medidos con un potencial de aceleración de 20 keV y una corriente del haz de electrones de 20 nA, con un haz enfocado de 1 μm; los tiempos de conteo fueron 30/15 s (peak/ cada background)

para Si, Mg, Fe, y Mn; 40/20 s para Na; y 60/30 s para K, Al, Ti, Ca, Cr y Ni. Los microfenocristales y microlitos de plagioclasas fueron medidos con un potencial de aceleración de 10 keV y una corriente del haz de electrones de 5nA, con un haz desenfocado de 0.5 μm, con un tiempo de conteo de 10/5 s en Si, Ca, Na y Al; 30/15 s para K; 40/20 s para Ti y Mg; y 60/30 s para Fe.

Finalmente, se realizaron perfiles composicionales en olivino y plagioclasa en la University of Bristol (Inglaterra), mediante el uso de Microsonda Electrónica CAMECA SX-100; con un potencial de aceleración de 20 keV y una corriente del haz de electrones de 20 nA, con un haz enfocado de 1 μm para olivinos y un haz desenfocado de 5 μm para plagioclasas. El espaciado de medida en los perfiles fue entre 10 y 3 μm dependiendo del tamaño del cristal. Los tiempos de conteo para olivinos fueron de 10/5 s para Mg y Si; 20/10 s para Mn y Fe; 30/15 s para Ca y Ti; y 60/30 s para Al, Cr y Ni; mientras que para las plagioclasas los tiempos de conteo fueron de 10/5 s para Si, Ca y Na; 20/10 s para Al y K; 30/15 s para Ti; y 60/30 para Mg, Fe y Sr.

Los cálculos del contenido de Fe^{2+} y Fe^{3+} en piroxenos fueron calculados siguiendo el procedimiento de Droop (1987).

Capítulo 2: Shallow reservoir conditions in the Fui Group small eruptive centres in the Southern Volcanic Zone (Chilean Andes)

Francisca Mallea-Lillo[1,2,*], Miguel A. Parada[1,2], Eduardo Morgado[2,3], Claudio Contreras[4], Darío Hübner[1,2]

[1] *Departamento de Geología, Facultad de Ciencias Físicas y Matemáticas, Universidad de Chile, 803 Plaza Ercilla, 8370450 Santiago, Chile.*

[2] *Centro de Excelencia en Geotermia de los Andes (CEGA), Universidad de Chile, 803 Plaza Ercilla, 8370450 Santiago, Chile.*

[3] *Escuela de Geología, Universidad Mayor, Manuel Montt 367, Providencia, Chile.*

[4] *School of Earth Sciences, University of Bristol, Wills Memorial Building, Bristol BS8 1RJ, UK.*

*Corresponding author at: francisca.mallea@ug.uchile.cl; Centro de Excelencia en Geotermia de los Andes (CEGA), Universidad de Chile, 803 Plaza Ercilla, 8370450 Santiago, Chile.

Abstract

The Fui Group are clusters of Holocene Small Eruptive Centres (SECs) located at the east and north-east from the Mocho-Choshuenco Volcanic Complex (MCVC), in the Central Southern Volcanic Zone of the Andes, segment in which the most hazardous volcanoes of Chile are located. We recognised two subgroups of volcanic products based on geochemical signatures, petrographic features, and geographical position: Fui Norte (north) and Fui Sur (south). The distance between those subgroups is ~2 km. The Fui Norte volcanic products are olivine-rich basalts (49 – 52 wt% SiO_2), enriched in incompatible elements, whilst the Fui Sur material are more evolved (basaltic andesites to andesites; 55 – 58 wt% SiO_2) with less phenocrysts and microphenocrysts of olivine and more plagioclase and clinopyroxene, and depleted in incompatible elements. We classified

olivine and plagioclase phenocrysts and microphenocrysts from both subgroups based on two compositional zones: High-Fo, High-An (Zone 1, Fo_{78-89} and An_{76-93}) and Low-Fo, Low-An (Zone 2, Fo_{60-78} and An_{57-73}). Olivine and plagioclase phenocrysts and microphenocrysts, together with clinopyroxene, form crystal clots that are abundant in all the studied samples. We determined shallow reservoir conditions for Zone 2 crystallisation in equilibrium with the groundmass melt compositions (up to 7.6 km in the Fui Norte SECs and up to 18.9 km in the Fui Sur SECs) by geobarometry and modelling via rhyolite-MELTS v.1.0.2 freeware. Maximum water content between 0.4 – 2 wt% and 0.9 – 3 wt% were determined for Zone 2 compositions of the Fui Norte and Fui Sur SECs respectively, under QFM, QFM-1 and NNO oxidation conditions. Contrarily, Zone 1 crystallisation are in disequilibrium with the groundmass melts. We infer that Zone 1 of both subgroups of SECs formed during an earlier stage of crystallization in a mushy zone of the reservoir according to their relative more primitive compositions and their common occurrence as part of crystal clots. Despite the short distance between the Fui Norte and Fui Sur SECs, we propose that their origins are independent from each other, due to relevant differences in their geochemical signatures, and the Fui Sur SECs have a likely genetic relation with the MCVC.

2.1 Introduction

Monogenetic volcanoes or small eruptive centres (SECs; see Németh and Kereszturi, 2015; Cañón Tapia, 2016; McGee and Smith, 2016; for recent discussion about this term) are the most common form of volcanism on Earth (Németh and Kereszturi, 2015) and are present in different tectonic settings (Németh, 2010; Cañón-Tapia, 2016). This type of volcanism is characterized by small amount of erupted material (<1 km^3; Németh & Kereszturi, 2015) during a limited time from days to some years (≤10 years; Németh & Kereszturi, 2015). The compositions of these volcanic

products are not restricted to a specific range, nevertheless, they are commonly basaltic (Valentine and Gregg, 2008; Németh, 2010).

Volcanism of SECs was commonly considered as a simple batch of magmas that ascends directly from the mantle with minimal interaction with the crust (e.g., Walker, 1993; Valentine and Perry, 2007; Rasoazanamparany et al., 2015; McGee and Smith, 2016). These are the cases of Carrán - Los Venados and Caburgua - Huelemolle monogenetic volcanic fields in the SVZ (Bucchi et al., 2015, Morgado et al., 2017) where no reservoir (or transient reservoirs) and differentiation in the upper crust are identified. In the mentioned volcanic fields, low magma flux and extensional regime were invoked to explain why eruptions took place in different centres instead a single stratovolcano. However, recent studies evidence that some SECs formed by polybaric crustal crystallisation, suggesting complex plumbing systems and upper-middle crust magma reservoirs in a variety of tectonic settings (e.g., Johnson et al., 2008; Erlund et al., 2010; Gao et al., 2017; Morgado et al., 2017; Coote et al., 2018; Coote and Shane, 2018; Shane and Coote, 2018; Larrea et al., 2021). It is therefore important to characterize their pre-eruptive conditions and magmatic histories, to decipher the complexity and depth of their magma reservoirs.

SECs from Southern Volcanic Zone (SVZ; 33-46°S) are located close to large active stratovolcanoes and controlled tectonically by the NS structure Liquiñe Ofqui Fault Zone (LOFZ; Cembrano and Lara, 2009; Bucchi et al., 2015; Morgado et al., 2015; among others). Similarities (Brahm et al., 2018) and differences (Morgado et al., 2015; McGee et al., 2017) between SECs and stratovolcanoes recorded in the SVZ give insights on the magma sources and the role of the LOFZ. Products from some SVZ SECs are derived from the mantle-crust boundary (Morgado et al., 2015) or have a lower slab-derived fluid input than products from stratovolcanoes (McGee et al., 2017). Unlike stratovolcanoes, the magma ascent of most SECs would have been facilitated for the LOFZ (Morgado et al., 2017). The study of the Fui Group SECs provided the chance to characterize the

magmatic processes and pre-eruptive reservoir conditions, identify two subgroups of SECs with contrasting evolution, despite they are located in the LOFZ, and evaluate the genetic relation between the studied SECs and the neighbouring stratovolcanoes (Mocho-Choshuenco Volcanic Complex, MCVC) of the SVZ (Fig. 2.1). For those purposes, we used detailed petrographic descriptions, whole-rock compositions, thermobarometric approaches and rhyolite-MELTS modelling.

2.2 Geological setting

The SVZ (33 – 46°S) of the Chilean Andes is a volcanic chain produced by the subduction of the oceanic Nazca Plate beneath the western margin of the continental South American Plate. Based on geochemical, petrographic, and tectonic features of volcanoes, SVZ is subdivided into four sections: North (NSVZ, 33.3 – 34.5°S), Transitional (TSVZ, 34.5 – 37°S), Central (CSVZ, 37 – 41.5°S) and South (SSVZ, 41.5 – 46°S) (Fig. 2.1a; López-Escobar et al., 1995; Stern, 2004). The tectonic setting of the studied zone is mainly controlled by the LOFZ, a ~1200 km-long intra-arc major structure developed between ~38º and ~46ºS (López-Escobar et al., 1995; Stern, 2004; Cembrano and Lara, 2009).

The Fui Group SECs and the MCVC are located in the CSVZ (37 – 41.5°S) section, that comprise the most active and hazardous volcanoes of Chile such as Villarrica, Llaima, Calbuco among others (SERNAGEOMIN, 2020a). The Fui Group and the MCVC were built over a basement composed by metamorphic, granitic, and stratified rocks with ages from Paleozoic to Lower Pleistocene (Moreno and Lara, 2007). The crustal thickness in the SVZ decreases to the south from 50 km-thick (33°S) to 35 km-thick (46°S; López-Escobar et al., 1995; Stern, 2004; Cembrano and Lara, 2009). Taking the data of Tašárová (2007), a thickness of 40 km is assumed for the crust beneath the Fui Group and MCVC.

The Fui Group (39°48 S – 39°54 S) are clusters of Late Pleistocene - Holocene SECs (Moreno and Lara, 2007) located between 8 – 16 km east and north-east from the central vent of the MCVC. The Fui Group SECs are aligned in NE or NNE direction (Moreno and Lara, 2007) and lie over and adjacent to the west of the LOFZ (Fig. 2.1b). According to SERNAGEOMIN, the Fui Group is considered a volcanic field with low specific risk (51st position of 92 volcanic systems, SERNAGEOMIN, 2020a).

The Fui Group is subdivided into Fui Norte and Fui Sur subgroups. Fui Norte includes four SECs (also referred as Cerro Fui Alto and Kangechi cones by Lara and Moreno, 2004; Rawson et al., 2016, respectively) and three partially eroded cones named Chanchán SECs (Moreno and Lara, 2007). Fui Sur is formed by sixteen SECs, previously referred as Normal SVZ cones (Rawson et al., 2016). The main features and ages of the Fui Norte, Fui Sur and Chanchán SECs are shown in Table 1. Based on whole-rock compositions, Rawson et al. (2016) distinguished chemical differences in rocks of Fui Norte and Fui Sur attributed to a direct magma evacuation through the LOFZ in the case of the Fui Norte SECs, and an origin related to the MCVC (parasitic cones) in the case of the Fui Sur SECs.

The MCVC is a Late Quaternary volcanic complex with two major summits forming a volcanic NW-SE alignment (Fig. 2.1b). Mocho is a scoria cone built within the south-eastern zone of the MCVC caldera (Moreno and Lara, 2007) and Choshuenco corresponds to remnant of the volcanic edifice after the explosive event that formed the caldera. According to Rawson et al. (2015), the MCVC is one of the most productive (ca. 1 km^3/kyr) and active volcanic centres of the SVZ since deglaciation, recording at least 75 post-glacial explosive eruptions, including large Plinian and subplinian eruptions (Rawson et al., 2015). SERNAGEOMIN's specific risk ranking (SERNAGEOMIN, 2020a), considers the MCVC as one of the most dangerous volcanoes of Chile (7th position between a total of 92 active volcanic systems). For comparison purposes we include

geochemical data from bombs of the MCVC Enco ignimbrite (sub-Plinian eruption; Rawson et al., 2015; dated 1700 BP, Moreno and Lara, 2007; Pérez, 2005; Echegaray, 2004) and from bombs and lavas of the 1864 eruption (the last eruption of MCVC, Moreno and Lara, 2007).

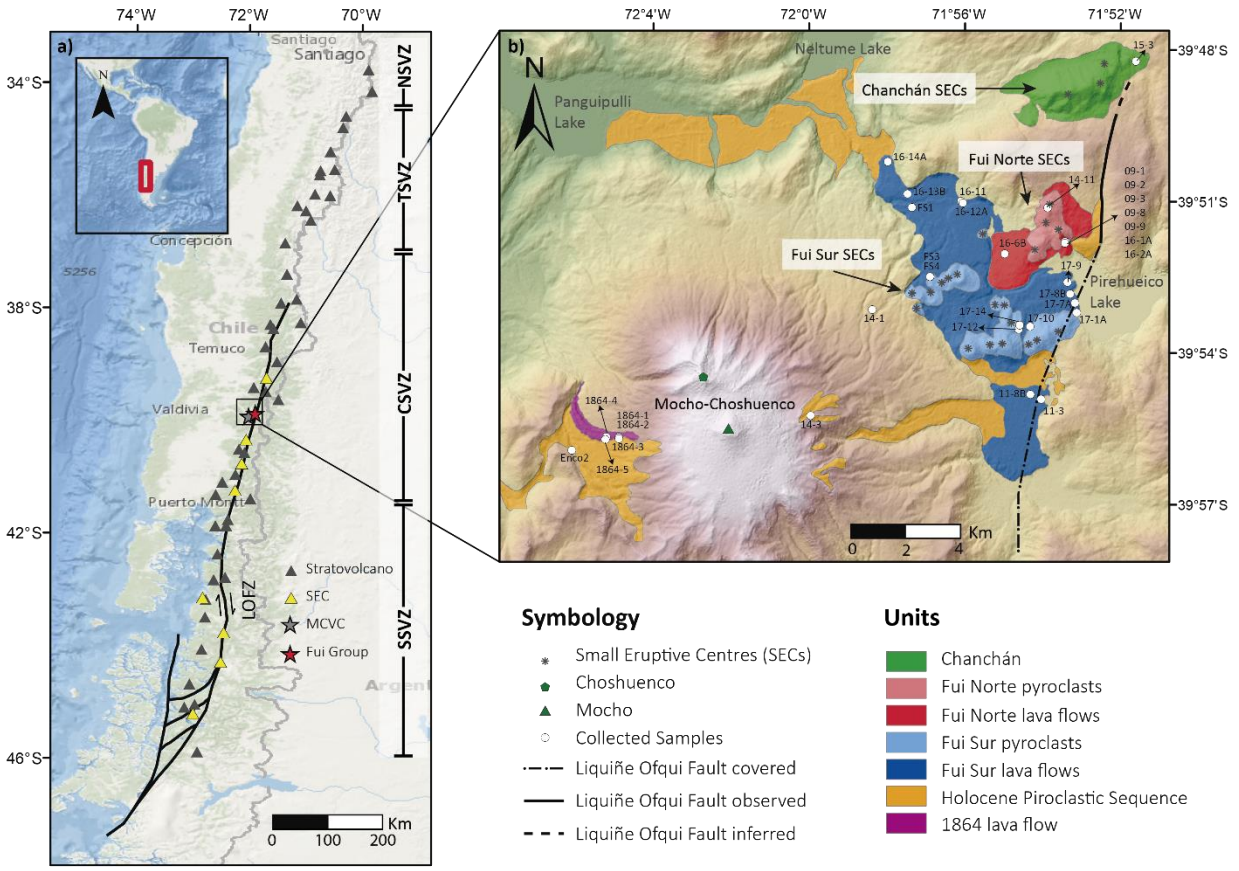

Fig. 2.1: *(a) Stratovolcanoes and SECs in the SVZ. Subdivision of the SVZ is included (after López-Escobar et al., 1995). Map elaborated with "Oceans" basemap in ArcGIS v.10.3 software. (b) Simplified geologic map modified from Moreno and Lara (2007) of the MCVC (including only the volcanic units of interest in this study), Fui Group and Chanchán SECs. Sampling locations are marked with white circles. Holocene Pyroclastic Sequence includes Enco sub-Plinian eruption.*

Table 1: *Main features and ages of the Fui Norte and Fui Sur SECs, including Chanchán SECs.*

Eruptive centres	Number of centres	Age	Height (m)	Total volume DRE (km^3)
Chanchán	3	Later Upper-Pleistocene - Early Holocene	600	0.171
Fui Norte	4	~1700 BP	150-280	0.171
Fui Sur	16	1100-5780 BP	150-350	0.535

Ages were estimated based on ^{14}C dating from Moreno and Lara (2007); and unpublished data from Echegaray (2004) and Pérez (2005). Volumes were calculated in this study and are presented as Dense Rock Equivalent (DRE; more details of the methodology in Sections 2.3 and A.2).

2.3 Methodology

We calculated the volume of the volcanic products emitted from the SECs following Larrea et al. (2019) approach and using Digital Elevation Models (DEM) via the software ArcGis v.10.3. In detail, we generated paleosurfaces with contour lines, used *Triangulated Irregular Networks* "TIN", and applied the *"Surface Difference"* tool over the paleosurface. We calculated separated bulk volumes for lavas and tephras and applied correction by vesicularity to present the results in terms of Dense Rock Equivalent (DRE; see Section A.2 for more details).

We collected 34 samples including lavas, tephras and bombs from Fui Group and MCVC holocene events. Ten samples are from Fui Norte, including one from Chanchán SECs, fifteen samples from Fui Sur and nine samples from MCVC (sample codes, location coordinates and type of sample are in Table A.1).

Whole-rock compositions of the 34 extrusive samples were analysed by Arcos Spectro ICP-OES and Perkin Elmer ELAN 9000 ICP-MS, for major and trace elements, respectively, at Bureau Veritas Mineral Laboratories (Vancouver, Canada) using SO-19 standard. Accuracy for major elements is better than 3% (relative) except for Cr_2O_3 (18% relative), and better than 9% (relative) for trace elements, except for Sn which were <11% (relative) and Be <40% (relative). Two samples were duplicated (sample 1864-1 for major elements and 1864-4 for trace elements) which in general were in good agreement with original samples with differences better than 3% (relative) in major elements and better than 6% (relative) in trace elements, except for Be (50%), Ta (33%), U (23%) and V (17%). Quantification of FeO in samples were determined by Titration technique, using OREAS-700 and SY-4 standards, with accuracy better than 4% (relative). Three samples were duplicated, reporting differences of <1% relative in two samples (samples 17-2 and 16-1), and 15% relative in the third (sample 09-3). Complete data are included in Section A.3.

We quantified crystal, vesicle and groundmass contents by point counting via the freeware JMicroVision. On each section we performed 500 random points (results of the quantification in Table 3). Then, we described and recognised mineral phases using a Scanning Electron Microprobe (SEM) at Universidad de Chile (FEI Quanta 250) and at Pontificia Universidad Católica de Chile (FEI Quanta 250 FEG). Single point compositional measurements in phenocrysts, microphenocrysts and microlites of olivine, plagioclase and clinopyroxene were performed with Electron Probe Micro-Analizer (EPMA; JEOL JXA-8230) at LAMARX National University of Córdoba. We use an accelerating potential of 15 keV, an electron beam current of 20 nA, and a focused beam of 1 to 4 μm for all phases except for plagioclase, in which a defocused beam of 10 μm was applied to minimise alkali loss. Counting times were 10/5 s (peak/each background) for major and minor elements, except for Ca in olivines, where counting times were 20/10 s. Microlites and microphenocrysts compositions were measured with an EPMA (JEOL JXA-8530F) at the University of Bristol. Olivine and clinopyroxene microphenocrysts and microlites were measured using an accelerating potential of 20 keV, an electron beam current of 20 nA and a focused beam of 1 μm. Counting times were 30/15 s (peak/each background) for Si, Mg, Fe and Mn, 40/20 s for Na, and 60/30 s for K, Al, Ti, Ca, Cr and Ni. Plagioclase microphenocrysts and microlites were measured with an accelerating potential of 10 keV, an electron beam current of 5 nA and a defocused beam of 0.5 μm. Counting times were 10/5 s on Si, Ca, Na and Al, 30/15 s for K, 40/20 s for Ti and Mg and 60/30 s for Fe. Compositional profiles in olivines and plagioclases phenocrysts were obtained with a CAMECA SX-100 EPMA at the University of Bristol. The EPMA settings used were an accelerating potential of 20 keV and an electron beam current of 20 nA. A focused beam of 1 μm for olivines and defocused beam of 5 μm for plagioclase were applied. The profile spacing were between 10 and 3 μm depending on the size of the crystal. Counting times for olivines were 10/5 s for Mg and Si, 20/10 s for Mn and Fe, 30/15 s for Ca and Ti, and 60/30 s for Al, Cr

and Ni. For plagioclases, the counting times were 10/5 s for Si, Ca and Na, 20/10 s for Al and K, 30/15 s for Ti and 60/30 s for Mg, Fe and Sr.

We calculated the Fe^{2+} and Fe^{3+} contents in pyroxenes following the procedure of Droop (1987).

2.4 Results

2.4.1 Whole rock compositions

According to Le Bas et al. (1986) TAS diagram, the compositions of the 34 analysed samples vary from basalts to dacites, (48.56 – 63.03 wt% SiO_2, Fig. 2.2a; Table 2). The lava sample from the Chanchán SECs is a basalt (48.56 wt% SiO_2), the samples from the Fui Norte SECs are basalts (48.65 – 51.6 wt% SiO_2), the samples from the Fui Sur SECs are basaltic andesites and andesites (54.80 – 57.84 wt% SiO_2) and the volcanic products from the MCVC vary from basaltic andesites to dacites (53.52 – 63.03 wt% SiO_2).

Among the major elements, Na_2O and K_2O positively correlate with SiO_2 (Fig. 2.2b, c), but in the K_2O diagram, samples from the Fui Norte and Chanchán SECs form a cluster separated from the rest of the data (Fig. 2.2c). In contrast, negative trends are identified for Al_2O_3, MgO, CaO, Fe_2O_3* (Fe_2O_3* corresponding to the total Fe measured as Fe_2O_3 in the samples) and Cr_2O_3 respect to SiO_2 (Fig. 2.2d, e, f, g, h). The samples from the Chanchán and Fui Norte SECs presents the highest contents in MgO, CaO and Cr_2O_3 forming clusters separated from the rest of the samples, and the sample from the Chanchán SECs contains the highest values of Cr_2O_3 (0.083 wt%). Rocks from the Fui Norte SECs form a separated trend in the Fe_2O_3* - SiO_2 diagram (Fig. 2.2g) from rocks of the Fui Sur SECs and the MCVC, and rocks from the Fui Sur SECs plot slightly separated from the MCVC samples. The volcanic products from the Fui Norte and Fui Sur SECs contains variable amounts of TiO_2 respect to similar SiO_2 contents (Fig 2.2i), however, the Fui Sur SECs samples

contain higher amounts of TiO_2. Finally, the MCVC rocks shows a negative correlation between TiO_2 and SiO_2.

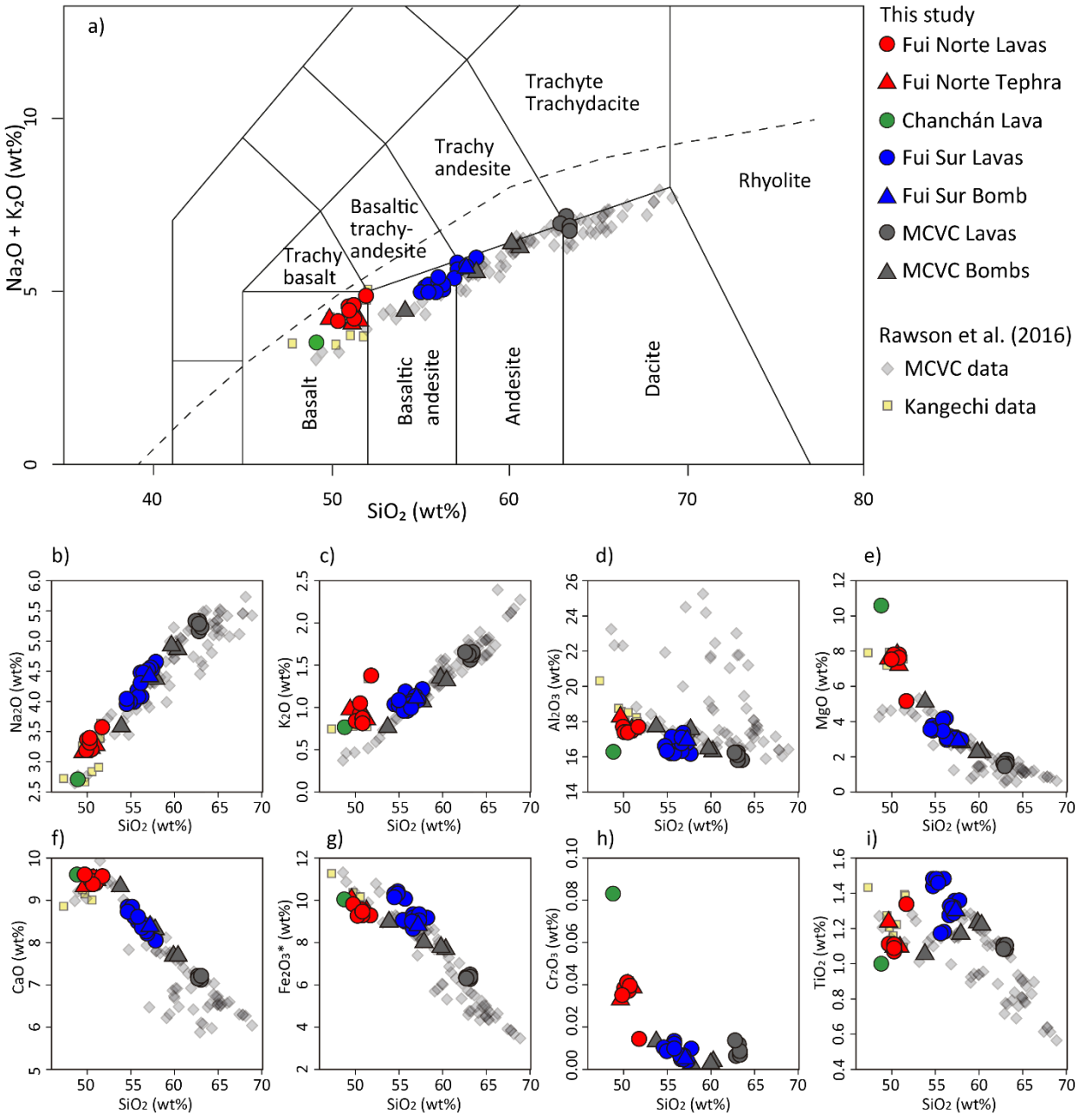

Fig. 2.2**:** *a) Total Alkali vs Silica (TAS) after Le Bas et al. (1986) for analysed samples and data obtained from literature (Rawson et al., 2016). b) to i) are representative Harker diagrams for analysed samples and available published data (Rawson et al., 2016).*

All the samples present negative anomalies of Nb-Ta, Ti and Zr in the spider diagram (Fig. 2.3a), typical of calc-alkaline magmas in a subduction setting. In the REE diagram, all the samples have small negative Eu anomaly of 0.99 – 0.79 (Eu/Eu*, where Eu* derived from the interpolation between Sm and Gd abundances, Fig. 2.3b). Samples from the Fui Norte SECs have higher La_N/Yb_N values (6.65 – 10.3) than the volcanic material from the Fui Sur SECs and MCVC (3.00 – 3.89; Fig 2.3b). Ni content decreases with an increase in SiO_2 for all the studied samples (Fig. 2.3c), while Ba, Zr and La shows an increase with SiO_2 content for the samples from the Fui Sur SECs and MCVC (Fig. 2.3d, e, f respectively). The rocks from the Fui Norte and Chanchán SECs present variable contents of the trace elements despite the narrow range of silica content. The Chanchán sample contains the highest content of Ni and the lowest contents of Ba, Zr and La (Fig. 2.3c, d, e, f) with the exception of one sample from the Fui Norte SECs, which has lower Ba than the Chanchán SECs sample (Fig. 2.3d).

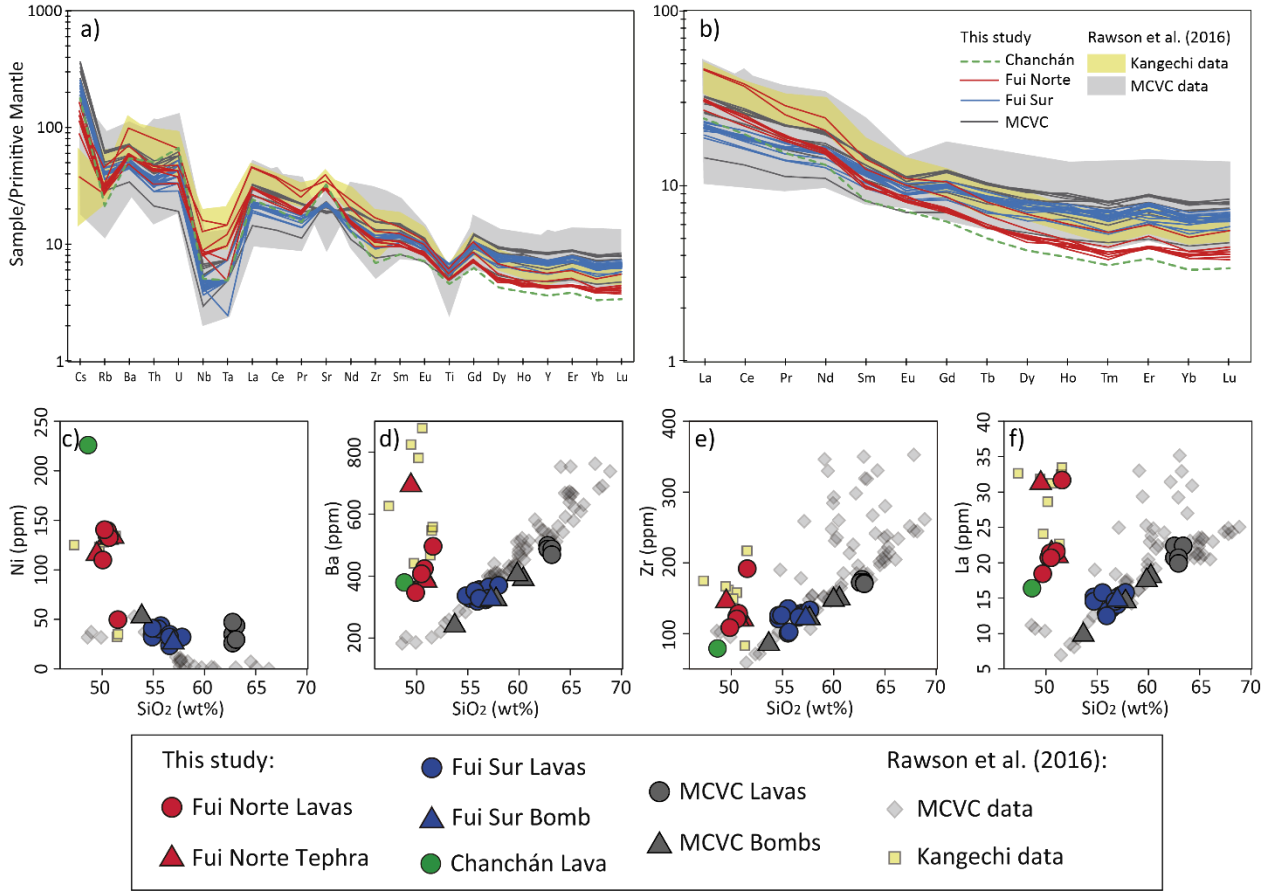

Fig. 2.3: *Trace elements diagrams. a) Spider and b) REE pattern data were normalized to the primitive mantle composition from Sun & McDonough (1989). c) to f) are bivariant diagrams of trace elements vs. SiO_2.*

Table 2: *Whole rock geochemistry of representative volcanic products from the Chanchán, Fui Norte, Fui Sur SECs and the MCVC. FeO obtained by Titration. Complete database can be found in supplementary material (Section A.3).*

		Chanchán	Fui Norte			Fui Sur			MCVC	
	DL	15-3	14-11	16-6B	09-3	16-11	FS1	FS4	Enco2	1864-2
SiO_2	0.01 (%)	48.56	49.77	51.60	50.22	54.80	55.62	55.74	57.38	62.95
Al_2O_3	0.01 (%)	16.13	17.60	17.64	17.28	16.37	16.23	16.90	17.42	15.93
FeO	0.2 (%)	7.15	6.96	6.61	0.41	6.65	6.46	5.80	5.07	3.81
Fe_2O_3*	0.04 (%)	10.02	9.71	9.30	9.42	10.39	10.08	9.05	8.02	6.37
MgO	0.01 (%)	10.62	7.60	5.11	7.57	3.66	3.41	4.16	2.84	1.71
CaO	0.01 (%)	9.16	9.23	9.08	8.85	7.51	7.11	7.27	6.67	4.33
Na_2O	0.01 (%)	2.71	3.16	3.56	3.20	3.99	4.15	4.07	4.35	5.22
K_2O	0.01 (%)	0.75	0.91	1.37	0.89	1.08	1.17	0.96	1.08	1.59
TiO_2	0.01 (%)	0.99	1.10	1.34	1.09	1.47	1.47	1.18	1.17	1.09
P_2O_5	0.01 (%)	0.21	0.29	0.50	0.32	0.27	0.28	0.22	0.27	0.35
MnO	0.01 (%)	0.16	0.16	0.16	0.16	0.18	0.18	0.17	0.16	0.16
Cr_2O_3	0.002 (%)	0.083	0.036	0.014	0.040	0.009	0.011	0.012	0.002	0.007
LOI		0.2	0.1	0.0	0.6	0.0	0.0	0.0	0.4	0.1
Cs	0.1 (ppm)	1.4	0.3	1.0	0.9	1.8	2.0	1.8	1.9	2.9
Rb	0.1 (ppm)	13.5	17.3	29.0	19.0	25.4	28.5	23.1	25.5	39.9
Ba	1 (ppm)	380	343	492	422	340	352	310	325	502
Th	0.2 (ppm)	4.3	2.8	4.0	3.8	2.9	3.2	2.4	2.8	3.6
U	0.1 (ppm)	1.4	0.7	1.0	0.9	0.7	1.1	0.6	0.7	1.2
Nb	0.1 (ppm)	3.6	5.9	11.5	6.3	3.0	3.5	2.8	3.2	4.6
Ta	0.1 (ppm)	0.2	0.4	0.6	0.5	0.2	0.2	0.2	0.2	0.3
La	0.1 (ppm)	16.6	18.5	31.8	21.1	14.8	15.6	12.8	14.7	22.0
Ce	0.1 (ppm)	34.9	38.8	67.4	43.1	33.5	36.4	28.6	32.8	47.4
Pr	0.02 (ppm)	4.25	4.96	7.91	5.38	4.50	4.79	3.82	4.43	6.15
Sr	0.5 (ppm)	686.3	646.7	739.6	663.9	457.5	445.8	470.2	486.7	405.6
Nd	0.3 (ppm)	17.8	20.5	33.0	20.8	20.7	20.8	17.1	19.4	26.4
Zr	0.1 (ppm)	77.0	107.3	190.7	123.7	126.4	132.8	104.0	121.2	174.9
Sm	0.05 (ppm)	3.64	4.27	6.28	4.70	5.17	5.26	4.28	4.79	6.67
Eu	0.02 (ppm)	1.20	1.47	1.84	1.39	1.48	1.64	1.37	1.53	1.77
Gd	0.05 (ppm)	3.72	4.21	6.27	4.37	5.82	5.96	4.92	5.45	7.08
Tb	0.01 (ppm)	0.54	0.63	0.87	0.63	0.89	0.92	0.75	0.85	1.09
Dy	0.05 (ppm)	3.14	3.64	5.06	3.84	5.42	6.03	4.87	5.50	6.99
Ho	0.02 (ppm)	0.64	0.73	0.99	0.77	1.14	1.26	0.97	1.09	1.44
Tm	0.01 (ppm)	0.26	0.30	0.40	0.31	0.47	0.48	0.39	0.44	0.57
Y	0.1 (ppm)	16.5	19.1	25.8	19.8	29.8	31.9	25.1	27.6	37.6
Er	0.03 (ppm)	1.84	2.11	2.87	2.15	3.50	3.69	2.90	3.30	4.20
Yb	0.05 (ppm)	1.63	1.89	2.50	1.98	3.02	3.23	2.73	3.03	3.95
Lu	0.01 (ppm)	0.25	0.29	0.41	0.32	0.46	0.48	0.41	0.47	0.62

FeO measured by Titration. Fe_2O_3* corresponds to the total Fe measured as Fe_2O_3 in the samples.

2.4.2 Petrography

All the samples are porphyritic and contain 3-20 vol.% of phenocrysts and microphenocryst (herein all the crystallinity values are on a vesicle free basis) in a crystal-rich groundmass. They contain phenocrysts and microphenocryst of olivine, plagioclase and clinopyroxene, except the sample from the Chanchán SECs, that contain exclusively olivine phenocrysts. The highest olivine modal contents are observed in the Chanchán SECs sample followed by the samples from the Fui Norte SECs. Plagioclase and clinopyroxene phenocrysts and microphenocrysts are more abundant in the volcanic material from the Fui Sur SECs (Fig. 2.4, Table 3) where the plagioclase phenocrysts are the largest. Groundmass of the studied samples comprise microlites of plagioclase (<100 μm), olivine (<60 μm), clinopyroxene (<50 μm), Ti-magnetite (<20 μm), Cr-spinel (<40 μm, only in more primitive samples), and glass. In the samples from the Fui Norte SECs, the vesicle contents vary from 2 to 22 vol.% in lava and from 28 to 48 vol.% in tephra. The lava from the Chanchán SECs have a vesicle content of 2.4 vol. %. Finally, the vesicle contents in samples from the Fui Sur SECs vary from 2 to 12 vol.% in lava and reach up to 28 vol.% in the bombs.

2.4.2.1 Fui Norte

Phenocrysts and microphenocrysts in the lavas and tephras from the Fui Norte SECs correspond to olivine (3.6 – 6.8 vol.%), plagioclase (0 – 13.3 vol.%) and clinopyroxene (0 – 2.7 vol.%). Crystal clots of 0.5 – 2.5 mm-size are abundant and consist of olivine + plagioclase ± clinopyroxene (in order of decreasing abundance; Fig. 2.5a, b, 2.8d). Some clots show a brecciated and fragmented aspect (Fig. 2.5a, b, c). The ratio ol/(cpx+pl) varies from 0.2 to 0.8.

Olivine phenocryst and microphenocryst are normally zoned with sizes in the range 0.4 – 1.2 mm and 95 – 400 μm, respectively. The phenocrysts have cores that commonly contain Cr-spinel inclusions (Fig. 2.5c) and rims are subtly reabsorbed. Poikilitic textures are recognised, where

granular crystals of olivine are chadacryst in crystals of clinopyroxene and plagioclase. Olivine-clinopyroxene intergrowth are also identified.

Plagioclase phenocrysts are commonly in the range of 200 – 600 μm (hereafter the indicated plagioclase crystal size corresponds to the longest dimension) but few of them reach up to 1.5 mm long, while microphenocrysts are between 100 and 200 μm. Plagioclase phenocrysts are normally zoned, but cores exhibit reverse zoning (Fig. 2.9a, b), whereas plagioclase microphenocrysts are normally or oscillatory zoned (Fig. 2.9c). Most of plagioclase correspond to well-preserved euhedral-subhedral phenocrysts but with fragmentated aspect. Clinopyroxene phenocrysts sizes vary between 70 and 700 μm.

The lava sample from the Chanchán SECs shows only olivine phenocrysts (17 vol.%) as both isolated and forming glomerocrysts (Fig. 2.8a). Phenocrysts have sizes that vary from 150 μm to 2.6 mm and commonly exhibit normal zoning although few of them show reverse zoning (Fig. 2.5d, 2.8b). Cr-spinel inclusions in the cores are commonly observed. Resorption textures are common for all olivine phenocrysts rims, but also in some cores. Some skeletal textures in olivine have also been recognised. Despite this sample does not contain clinopyroxene or plagioclases as phenocrysts, scarce plagioclase crystals occur filling resorption features of olivine phenocrysts (Fig. 2.5d).

2.4.2.2 Fui Sur

Samples from the Fui Sur SECs (lavas and bomb) comprise phenocrysts and microphenocrysts of plagioclase (2.4 – 15.6 vol. %), clinopyroxene (0.6 – 6.6 vol. %) and olivine (0 – 3.5 vol. %). The ratio ol/(cpx+pl) is <0.3. The mentioned phases occur as isolated phenocrysts, microphenocrysts and forming crystal clots of up to 2 mm size where plagioclase followed by clinopyroxenes are the most abundant phases (Fig. 2.5e, 2.8f).

Olivine phenocryst sizes vary from 0.12 to 2.2 mm and microphenocryst from 35 to 120 μm. Phenocrysts of olivine shows normal zoning, with oscillatory zoning in cores (Fig. 2.5f, 2.8e) while microphenocryst are slightly normally zoned (Fig. 2.8f). Resorption textures are recognised in rims of olivine phenocrysts. Clinopyroxene phenocryst sizes are in the range of 100 – 390 μm while microphenocrysts in the range of 60 – 100 μm. They are commonly forming part of crystal clots and rarely isolated.

Plagioclase phenocryst and microphenocryst sizes are in the range of 0.3 – 2 mm, and 120-300 μm, respectively. Phenocrysts of plagioclase are normally zoned with well-preserved cores (Fig. 2.9d), or with sieve texture and patchy zoning (Fig. 2.9e). Microphenocrysts of plagioclase are commonly oscillatory zoned (Fig. 2.8f), but a few exhibits similar texture features recognized in phenocrysts.

Table 3: *Modal point counting in percentage for the main minerals and vesicles of studied samples. Crystallinity percentage does not consider vesicles and is obtained from contents of phenocrysts and microphenocrysts of plagioclase, olivine and clinopyroxene.*
*Crystallinity= [(Pl+Ol+Cpx)/(Groundmass+Pl+Ol+Cpx)]*100.*

	Chanchán	Fui Norte					Fui Sur						
Sample	15-3	09-8	09-9	14-11	16-6B	16-1	16-11	FS4	17-12	17-14A	17-7AXEN	17-1A	17-10
Vesicles (vol. %)	2.4	12.8	47.8	2.0	21.8	27.6	4.2	9.9	27.8	11.6	4.0	1.8	19.7
Groundmass (vol. %)	84.3	81.7	50.2	86.7	67.0	68.4	79.9	75.4	58.5	82.4	77.5	79.4	77.9
Plagioclase (vol. %)	0.0	0.0	0.0	6.9	11.1	0.0	11.5	7.8	11.2	3.5	12.2	13.0	1.9
Olivine (vol. %)	17.1	5.5	2.0	6.9	3.0	3.9	2.2	3.2	0.5	1.2	0.5	1.0	0.0
Clinopyroxene (vol. %)	0.0	0.0	0.0	1.7	2.2	0.0	2.2	3.6	2.1	1.2	6.4	4.8	0.5
Crystallinity (%) *	16.9	6.3	3.9	15.2	19.6	5.5	16.7	16.2	19.0	6.7	19.8	19.2	3.0

*Percentage not considering vesicles.

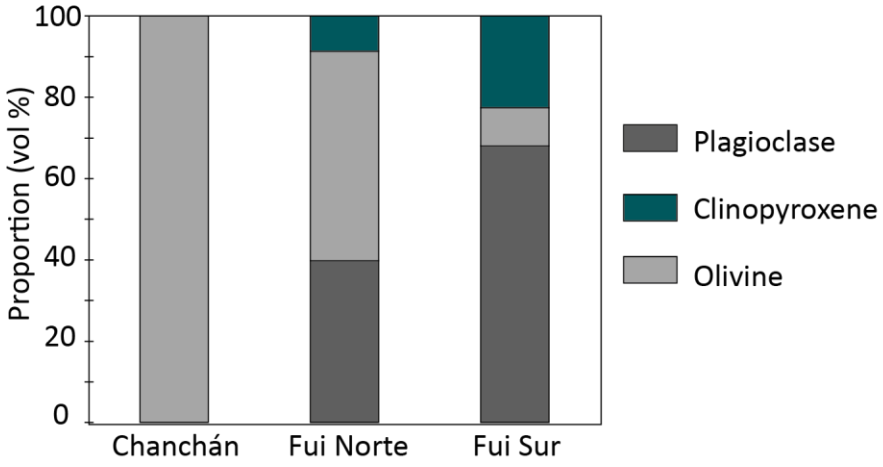

Fig. 2.4: *Normalized average of phenocryst and microphenocryst content of the studied samples estimated by point counting of thin sections on a vesicle-free basis, using JMicroVision freeware. Data from Table 3.*

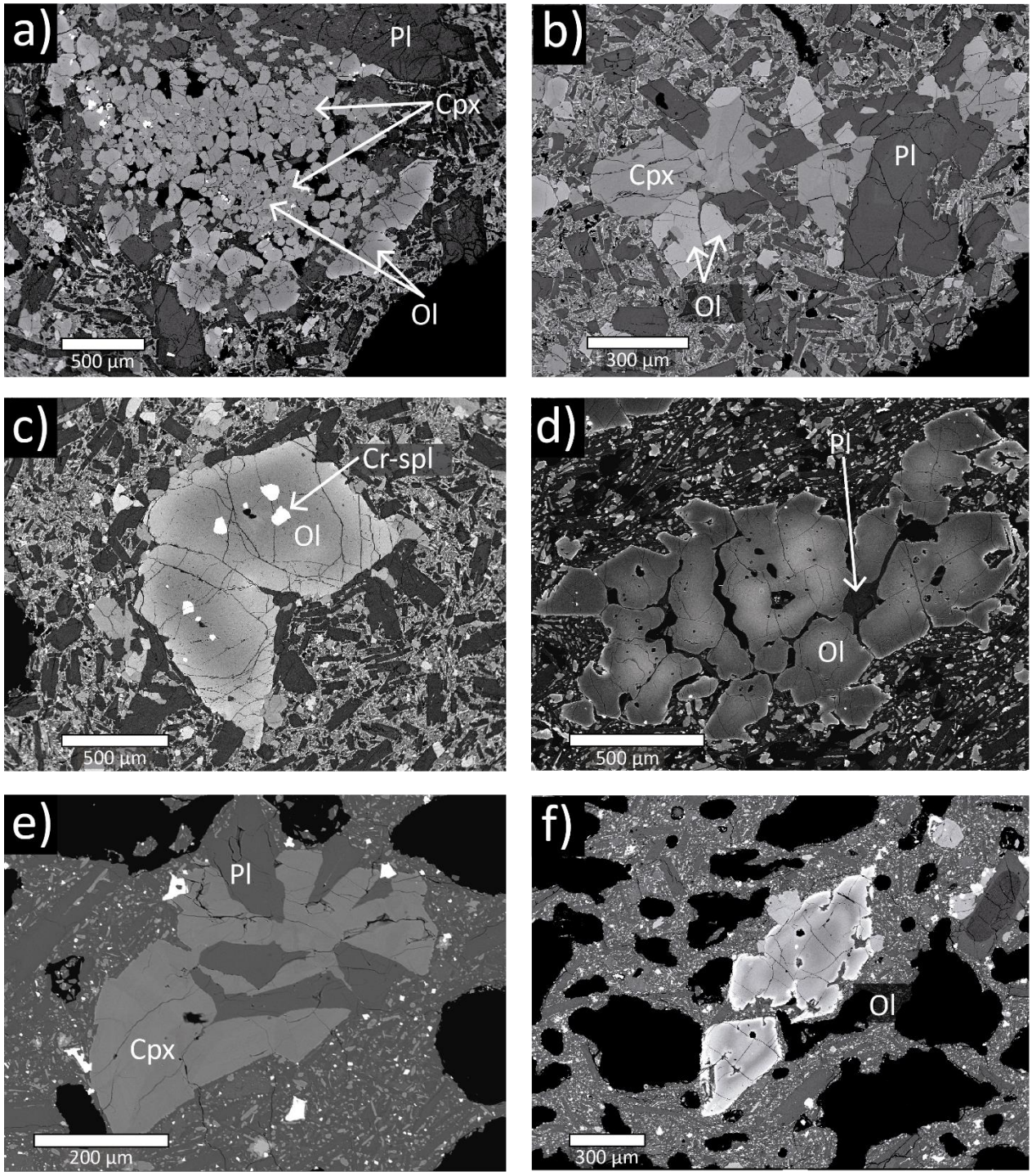

Fig. 2.5: *BSE images of crystal clots from selected samples. (a), (b) and (c) images are from 16-6B lava sample from the Fui Norte SECs, (d) 15-3 lava sample from the Chanchán SECs, and (e) and (f) are from FS4 lava sample from the Fui Sur SECs. (a) Crystal clot with granular/anhedral olivine and clinopyroxene crystals. (b) Crystal clot composed by olivine, clinopyroxene and plagioclase with brecciated and fragmented aspects. (c) Olivine phenocryst with Cr-spinel inclusions. (d) Olivine with reverse zoning, plagioclase filling reabsorbed areas are shown. (e) Crystal clot of clinopyroxene and plagioclase. (f) Olivine with oscillatory zoning and resorption.*

2.4.3 Mineral chemistry

2.4.3.1 Olivines

We report compositional zonation in olivine crystals of all the studied samples. Two compositional zones have been identified for olivine phenocrysts and microphenocrysts: Zone 1 and Zone 2 correspond to High-Fo compositions (Fo_{78-89}) and Low-Fo compositions (Fo_{60-78}), respectively. Details of olivine phenocryst compositions are shown in Fig. 2.6 and 2.7. Compositional profiles of representative olivine crystals are shown in Fig. 2.8 and complete compositional EPMA data are presented in Table A.4.1.

In the samples from the Fui Norte SECs, the compositional ranges of Zones 1 and 2 are Fo_{79-82} and Fo_{68-77}, respectively. The olivine phenocryst cores and rims have a Zone 1 and Zone 2 compositions, respectively. Olivine rims show gradual normal zoning and subtle resorption. Olivine microphenocrysts present Zone 2 cores with slight normal zoning in the same compositional range. Olivine microlites have a composition of $Fo_{68–70}$ like the lower values of Zone 2 compositions. Olivine phenocryst cores of the samples from the Fui Sur SECs correspond to Zone 1 (Fo_{78-85}). Some cores show oscillatory zoning within the compositional range of Zone 1 (Fig. 2.5f, 2.8e). Partially resorbed rims of Zone 2 compositions (Fo_{61-74}) surround the olivine phenocryst cores. Olivine microphenocrysts present cores of Zone 2 compositions with slight normal zoning (Fig. 2.8f). Olivine microlites are in the compositional range of $Fo_{47–53}$, which is lower than the zone compositions of phenocrysts and microphenocryts.

Zone 1 compositions in olivine crystals of the lava sample from the Chanchán SECs, corresponds to normally-zoned cores (Fo_{81-89}) of olivine phenocrysts (Fig. 2.8a), and cores of skeletal olivine phenocrysts. Zone 2 (Fo_{71-79}) corresponds to all phenocryst rims, and to a few olivine cores with reverse zoning surrounded by Zone 1 composition (Fig. 2.5d, 2.8b). Microlites of olivine are in the range Fo_{63-75}, which is slightly lower than Zone 2 olivine compositions.

2.4.3.2 Plagioclase

Two compositional zones are also recorded in plagioclase phenocrysts and microphenocrysts in the studied samples of Fui Norte and Fui Sur SECs: Zone 1 and Zone 2 correspond to High-An (An_{76-93}) and Low-An (An_{57-73}) compositions. Details of plagioclase compositions are shown in Fig. 2.6 and 2.7. Compositional profiles in selected plagioclase phenocrysts are shown in Fig. 2.9 and complete EPMA data are listed in Table A.4.2.

Plagioclase phenocryst cores of samples from the Fui Norte SECs have compositional range of An_{79-87} (Zone 1) and exhibit reverse zoning in the Zone 1 compositional range. It is interesting to note that the highest An contents correspond to a Transitional Zone which is abruptly surrounded by compositions of Zone 2 (An_{62-73}) (Fig. 2.9a, b). Plagioclase microphenocrysts exhibit oscillatory zoning in Zone 2 compositional range (Fig. 2.9c) whereas microlites have a compositional range of An_{51-63}.

The samples from the Fui Sur SECs include isolated plagioclase phenocrysts with An_{76-93} (Zone 1) cores, exhibiting reverse or patchy zoning with a Transitional Zone (highest An content, Fig. 2.9d, e). All the studied plagioclase phenocrysts present Zone 2 (An_{57-71}) rim compositions. Microphenocrysts shows oscillatory zoning in Zone 2 compositional range (Fig. 2.9f) and few of them have similar compositions to the phenocrysts. Microlites show a wide compositional range of An_{37-62}.

2.4.3.3 Clinopyroxene

Most of the pyroxene phenocrysts of the studied samples from the Fui Norte SECs are augite ($Wo_{41-45}\ En_{40-48}\ Fs_{10-17}$), although diopsides were found in the compositional range of $Wo_{45-47}\ En_{40-44}\ Fs_{10-15}$ (Table 4). The analysed clinopyroxene phenocrysts of the samples from the Fui Sur SECs are augite ($Wo_{32-44}\ En_{40-49}\ Fs_{15-21}$). Microlites of Fui Norte and Fui Sur have compositions of $Wo_{38-45}\ En_{41-46}\ Fs_{13-16}$ and $Wo_{17-40}\ En_{41-54}\ Fs_{18-37}$, respectively, which are similar to phenocryst

compositions, except for a few Fs-rich and Wo-poor microlites (Fig. 2.6 g, h, i). Clinopyroxene microlites of Chanchán sample have compositions of $Wo_{38-45}\,En_{40-48}\,Fs_{12-16}$. Complete EPMA data are listed in Table A.4.3.

Table 4: *Compositional ranges for olivine, plagioclase and clinopyroxene phenocrysts, microphenocrysts and microlites in the studied samples. Zone 1 and Zone 2 can describe the compositions of phenocrysts and microphenocrysts.*

		Chanchán	Fui Norte	Fui Sur
Olivine	Zone 1	Fo81 - Fo89	Fo79 - Fo82	Fo78 - Fo85
	Zone 2	Fo71 - Fo79	Fo69 - Fo77	Fo61 - Fo74
	Microlites	Fo63 - Fo75	Fo68 - Fo70	Fo47 - Fo53
Plagioclases	Zone 1	-	An79 - An87	An76 - An93
	Zone 2	-	An62 - An73	An57 - An71
	Microlites	An60 - An81	An51 - An63	An37 - An62
Clinopyroxene	Phenocrysts	-	Wo41-47 En40-48 Fs10-17	Wo32-44 En40-49 Fs15-21
	Microlites	Wo38-45 En40-48 Fs12-16	Wo38-45 En41-46 Fs13-16	Wo17-40 En41-54 Fs18-37

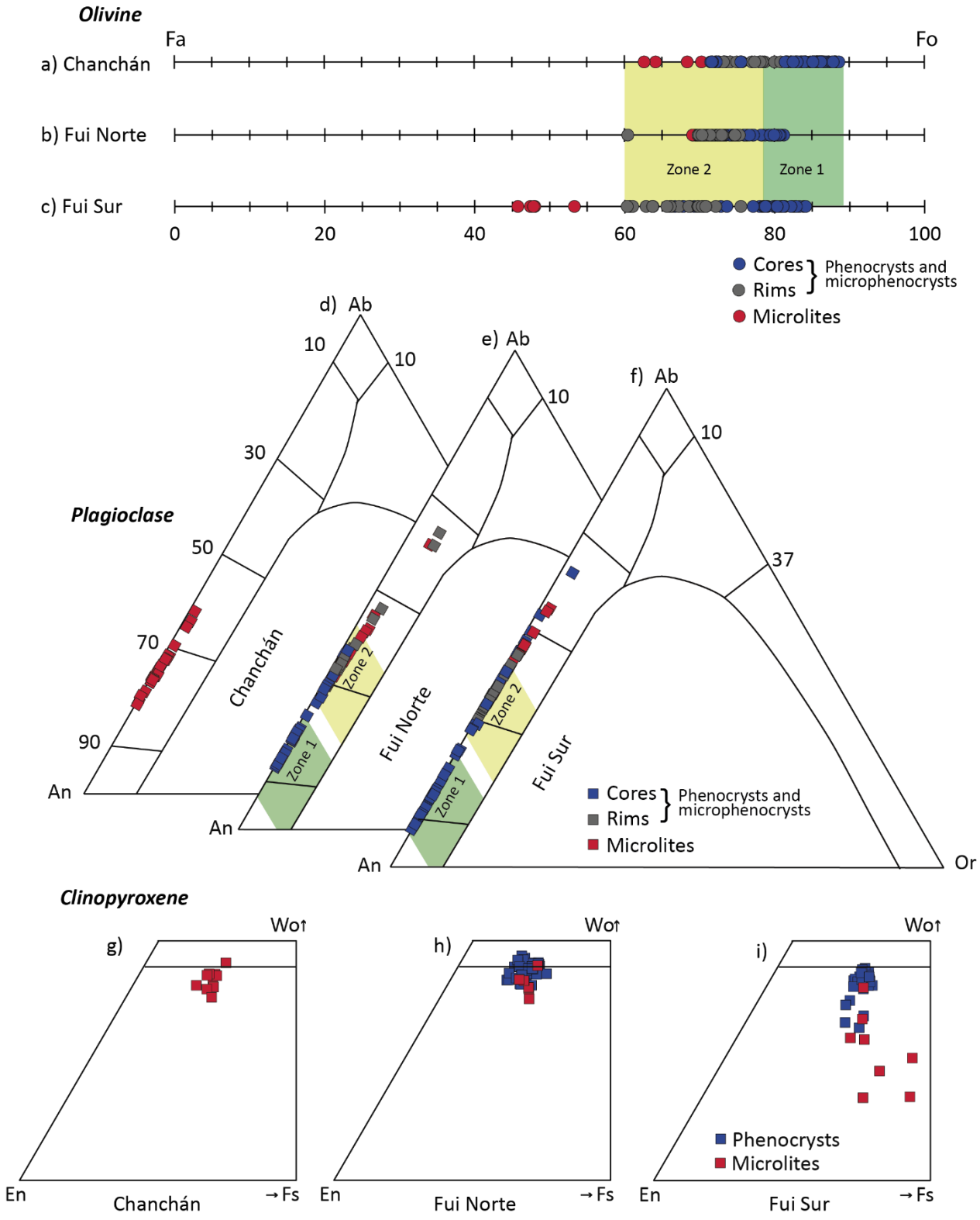

Fig. 2.6: *Olivine (a, b, c), plagioclase (d, e, f) and pyroxene (g, h, i) compositions for the studied samples. In plagioclase and olivine diagrams, Zones 1 and 2 are indicated with coloured areas.*

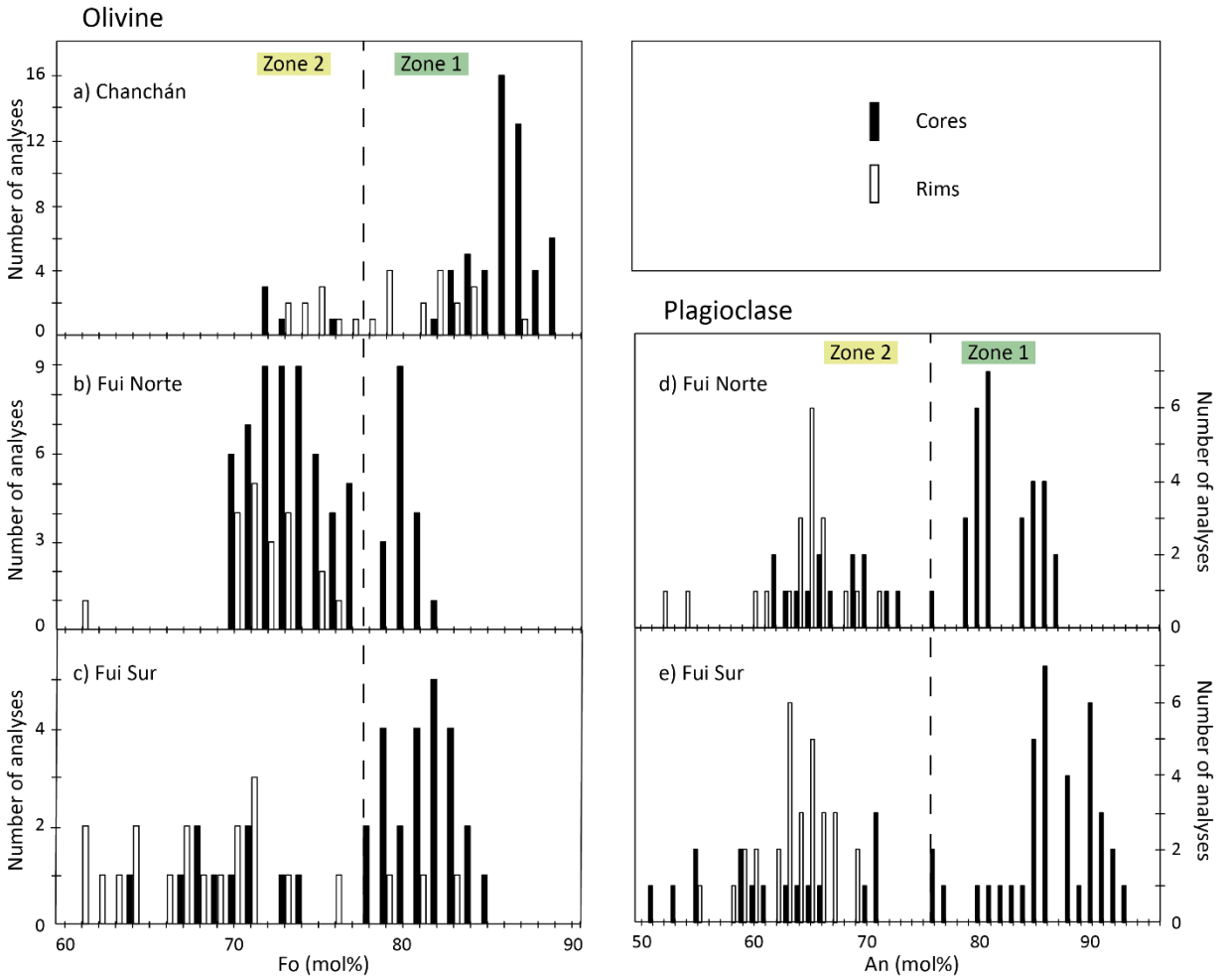

Fig. 2.7**:** *Histograms of the Fo and An (mol%) contents of cores and rims of olivine (left) and plagioclase (right) phenocrysts and microphenocrysts, from the different SECs. Dashed lines separate Zone 1 and Zone 2. Data are based on the total number of punctual analyses carried out per mineral and crystal type in each SEC using EPMA. Microlites compositions are not shown.*

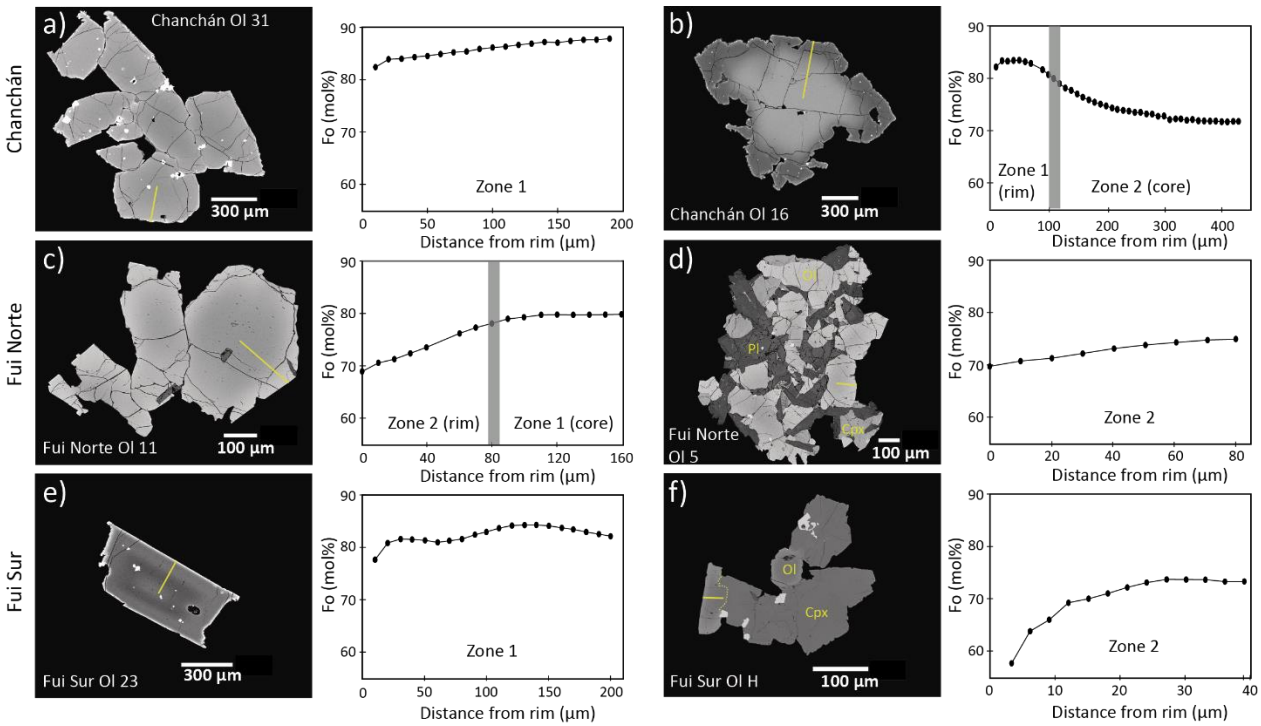

Fig. 2.8**:** *BSE images and forsterite compositional profiles of selected olivines. (a) and (b) are olivine phenocrysts from sample 15-3 of the Chanchán SECs, (a) is a glomerocryst with slight normal zoning within High-Fo composition (Fo_{82-88}), and (b) is an isolated olivine with reverse zoning. (c) and (d) are representative olivine crystals from the Fui Norte SECs (sample 16-6B) forming glomerocryst and crystal clot, respectively. (e) and (f) are representative olivine phenocryst and micrphenocryst respectively, from the Fui Sur SECs (sample FS4). (e) shows slight High-Fo variations and (f) shows a microphenocryst in a crystal clot with Low-Fo composition. Grey lines separate Zone 1 and 2.*

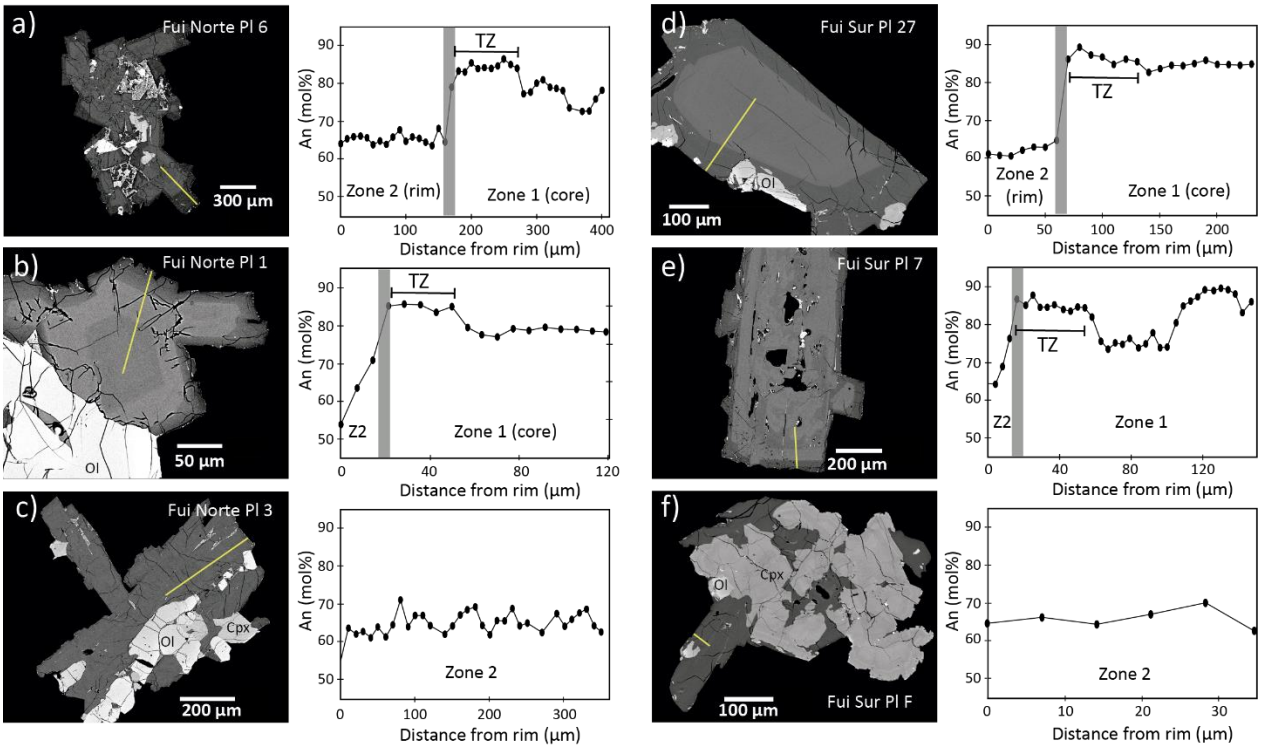

Fig. 2.9: *BSE images and anorthite compositional profiles of selected plagioclase crystals as part of clots or individual phenocrysts. (a), (b) and (c) are plagioclase phenocrysts from the Fui Norte SECs (sample 16-6B) and (d), (e) and (f) are plagioclase phenocryst and microphenocrysts from the Fui Sur SECs (FS4 sample). Grey lines separate Zone 1 and 2. Zone 2 is referred as "Z2" in (b) and (e) diagrams. Transitional Zone is referred as "TZ" in (a), (b), (d) and (e) diagrams.*

2.5 Magmatic intensive conditions

We applied three different methods to determine intensive conditions in the Fui Group. Geothermobarometry approaches developed using punctual clinopyroxene and olivine compositions, based on the equilibrium between these two phases. Secondly, a numerical solution for P and H_2O content were performed using punctual plagioclase composition along with the groundmass composition. Finally, to gather multivariable conditions while mineral phases crystallise, rhyolite-MELTS simulations were run to evaluate the intensive conditions in which known compositions of the crystals are in equilibrium with a melt of a groundmass composition. All these approaches allow us to determine a crystallization history based on a rigorous analysis of the intensive magmatic conditions.

2.5.1 Thermobarometry

Because Chanchán SECs have only olivine as phenocryst, no thermobarometric values could obtain. To determine intensive physical conditions, we used the olivine-augite Fe-Mg exchange geothermometer (Loucks, 1996), the Ca in olivine geothermometer (Shejwalkar and Coogan, 2013) and the olivine-clinopyroxene Ca-exchange geobarometer (Köhler & Brey, 1990). We determined the equilibrium conditions between olivine and clinopyroxene following Morgado et al. (2015) and using the Grove's et al. (1997) equations (details in Fig. A.5.1.1). Only Zone 2 compositions of olivine are in equilibrium with clinopyroxene according to the test. Consequently, all the olivine compositions used in geothermobarometers corresponds to Zone 2 (Low-Fo). We applied the Ca-in-olivine thermometer in the Zone 2 of the same olivine phenocrysts and microphenocryst used for the Fe-Mg exchange geothermometer, but in this case, only olivine crystals of clots with plagioclase and clinopyroxenes were selected, as this thermometer requires coetaneous growth of olivine and plagioclase. For the olivine-clinopyroxene Ca-exchange geobarometer, we consider only the positive pressure values, obtained from temperatures of the olivine-augite Fe-Mg exchange thermometer (negative values are consequence of the error ranges of the thermobarometric methods). Both geothermometers show consistent values between 1079 and 1175°C in Fui Norte, and from 1060 to 1192°C in Fui Sur. Details of pairs of crystals used in calculations and thermodynamic variables are given in Section A.5.2.

2.5.1.1 Fui Norte

The olivine-augite Fe-Mg exchange geothermometer yielded temperatures from 1079 to 1174°C with an average of 1130°C (± 6 ºC) and a standard deviation of 26°C in 44 olivine-augite pairs. The Ca in olivine geothermometer gave temperatures from 1082 to 1175°C with an average of 1129°C (± 20 ºC) with a standard deviation of 22°C in 32 olivine phenocrysts and microphenocrysts. The olivine-clinopyroxene Ca-exchange barometer, considering the

temperature values obtained by Loucks (1996) method, yielded pressure values between 1.2 and 5.1 kbar, with an average of 3.3 kbar (± 1.7 kbar), obtained in 5 pairs of olivine-augite phenocrysts and microphenocrysts.

2.5.1.2 Fui Sur

The olivine-augite Fe-Mg exchange geothermometer yielded temperatures from 1087 to 1192°C with an average of 1158°C (± 6 ºC) and a standard deviation of 31°C in 14 olivine-augite pairs. The Ca in olivine geothermometer yielded temperatures from 1060 to 1134°C with an average of 1094°C (± 20 ºC) and a standard deviation of 29°C in five olivine phenocrysts and microphenocrysts. The geothermobarometer of Köhler & Brey (1990), yielded pressure values between 0.2 and 7.5 kbar, with an average of 2.8 (± 1.7 kbar), obtained in seven pairs of olivine-augite phenocrysts and microphenocrysts.

2.5.2 Numerical solution for H_2O content and pressure conditions

We calculated the magma H_2O solubility and pressure conditions by applying an iterative combination of expressions from Lange et al. (2009) and Moore et al. (1998) (see Lohmar et al., 2012 and Morgado et al., 2015 for details of the numerical solution) based on An contents of plagioclase and groundmass compositions. These groundmasses compositions were calculated taking the whole-rock compositions of representative samples (16-6B sample from the Fui Norte SECs and FS4 sample from the Fui Sur SECs) after the extraction of phenocryst compositions according to their mineral chemistry and modal counting results (details in Table 5 and Section A.5.3). These groundmasses compositions would represent the final stage of the pre-eruptive melt evolution of each system before microlites crystallisation. We used the Zone 2 compositions of plagioclase as representative of the pre-eruptive final stage plagioclase composition, and temperature of olivine + clinopyroxene + plagioclase clots obtained from the thermometer of Loucks (1996).

For the samples from Fui Norte SECs, we select seven ol + cpx + pl clots where temperature data were obtained from Zone 2 of olivine. The values used were between 1118 – 1163°C and plagioclase composition of An_{62-64} (Zone 2). The results yielded a maximum dissolved H_2O content in magma of 0.4 – 1.6 wt% and pressure values up to 1.2 kbar. For the samples from the Fui Sur SECs, we select five clots (ol + cpx + pl) where also, temperature data were obtained from Zone 2 olivine. The temperature values and plagioclase compositions used for calculations were in the range 1138 – 1160°C and An_{62-70} (Zone 2), respectively and the resulting maximum H_2O contents were between 0.9 and 2.3%, while pressures values reached up to 2.1 kbar. Representative P-H_2O solubility diagrams are shown in Fig. 2.10 and summary of the clots temperatures, and anorthite content used in the iterative calculations as well as their respective results of pressure and H_2O content are given in Section A.5.4.

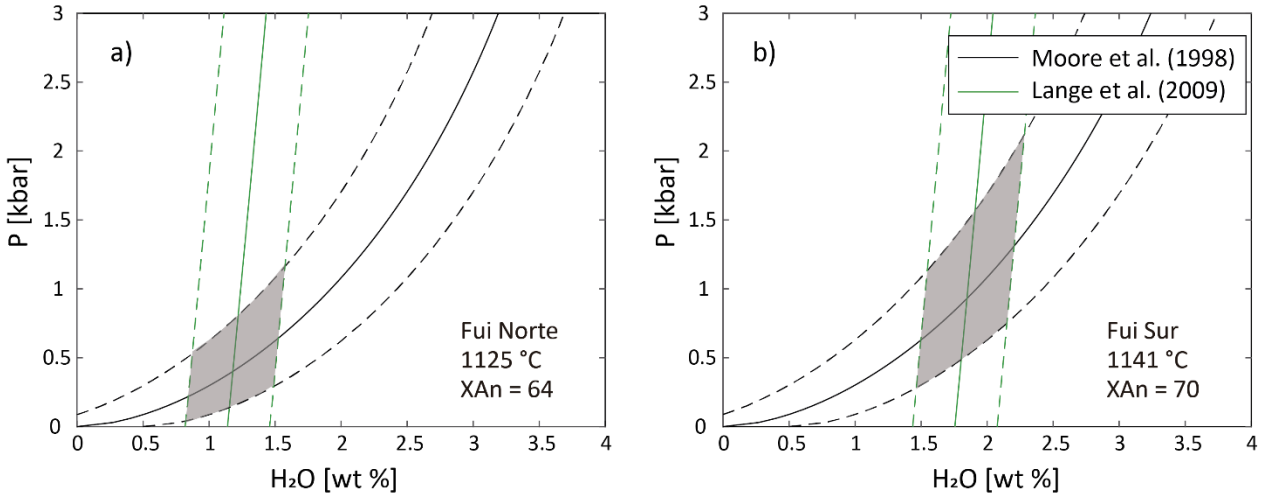

Fig. 2.10: *Representative P – H_2O solubility diagrams obtained from numerical solution using Moore et al. (1998) and Lange et al. (2009) equations. a) and b): Results of H_2O content (wt%) and pressure (kbar) from numerical solution for a representative clot from the Fui Norte SECs (clot "CP4") and Fui Sur SECs (clot "F"), respectively (more details in Section A.5.4). Grey fields indicate the intersection of the solution of both equations considering the errors of each method.*

Table 5: *Representative (Rep.) compositions of crystals used to calculate the groundmass (GM) compositions for the Fui Norte (including the Chanchán SECs), and Fui Sur SECs. Modal contents (vol. %) of the mineralogy on vesicle free basis. Whole rock (WR) composition corresponds to the sample 16-6B from the Fui Norte SECs, sample 15-3 is from the Chanchán SECs and sample FS4 is from the Fui Sur SECs. FeO* corresponds to the total Fe content expressed as FeO.*

	SiO_2	Al_2O_3	FeO*	MgO	CaO	Na_2O	K_2O	TiO_2	P_2O_5	MnO	Cr_2O_3	vol. %
Fui Norte WR	51.60	17.64	8.36	5.11	9.08	3.56	1.37	1.34	0.50	0.16	0.014	100.00
Fui Norte GM	53.41	16.78	9.02	4.27	8.12	3.99	1.71	1.64	0.63	0.17	0.002	80.45
Rep. Olivine	37.99	0.04	24.39	36.80	0.27	0.03	0.00	0.00	-	0.46	0.000	3.58
Rep. Pl (cores)	47.73	32.55	0.51	0.10	16.36	2.29	0.07	0.00	0.02	0.00	0.000	8.50
Rep. Pl (rims)	51.05	29.80	0.87	0.17	13.62	3.87	0.17	0.05	0.04	0.00	0.000	4.80
Rep. Cpx	49.34	4.33	8.80	14.28	21.43	0.36	0.00	1.32	-	0.19	0.470	2.69
Fui Sur WR	55.74	16.90	8.13	4.16	7.27	4.07	0.96	1.18	0.22	0.17	0.012	100.00
Fui Sur GM	58.22	16.80	8.36	2.58	6.15	4.62	1.15	1.35	0.27	0.18	0.008	83.81
Rep. Olivine	39.31	0.01	20.19	41.45	0.20	0.00	0.00	0.00	-	0.24	0.010	3.51
Rep. Pl (cores)	46.97	33.43	0.71	0.10	17.45	1.77	0.03	0.08	0.00	0.02	0.000	5.76
Rep. Pl (rims)	52.70	29.88	0.85	0.10	13.25	4.33	0.09	0.05	0.01	0.09	0.000	2.90
Rep. Cpx	48.83	5.22	10.87	13.97	19.63	0.44	0.01	1.43	-	0.26	0.120	4.02
Chanchán WR	48.56	16.13	9.00	10.62	9.16	2.71	0.75	0.99	0.21	0.16	0.083	100.00
Chanchán GM	51.19	19.79	8.29	3.30	11.21	3.32	0.92	1.21	0.26	0.16	0.096	83.10
Rep. olivine	40.48	0.01	13.29	46.93	0.14	0.00	0.00	0.00	0.00	0.17	0.027	16.90

2.5.3 Rhyolite-MELTS modelling for Fui Norte and Fui Sur

The initial melt compositions we used in rhyolite-MELTS modelling (v.1.0.2, Gualda et al., 2012) correspond to the anhydrous groundmass composition (as representative of the final pre-eruptive melt) of samples 16-6B and FS4 (same used in numerical solution, see Table 5 and Section A.5.3 for more details about this procedure) for the Fui Norte and Fui Sur SECs, respectively. This modelling could not reproduce olivine phenocrysts compositions for the Chanchán sample (15-3 sample) nor the Fui Sur sample.

We performed simulations of isobaric equilibrium crystallisation at pressures from 1 bar to 6 kbar (with increments of 1 kbar). The simulations were run for crystallisation temperatures from 1300 to 900°C (with decrements of 0.5°C), at different oxygen fugacity conditions (QFM±2 including NNO), and at H_2O content of 0 – 6 wt% (with increments of 1 wt%). The runs were performed

tolerating a maximum of 20% of solids phases and checking the compositions of the simulated crystallizing phases.

The P, T equilibrium conditions of the final stage of evolution of the system that we could obtained, correspond to the intersection of stability fields in which clinopyroxene compositions, Zone 2 compositions of olivine and plagioclase crystallises from a melt equivalent to the groundmass compositions. This is also consistent with results of equilibrium test applied in thermobarometry section, and textural features consisting in crystal clots with the phases and compositions mentioned. Summary of the modelling are in Section A.5.5.

In the case of Fui Norte, the Zone 2 compositions of olivine (Fo_{69-77}) and plagioclase (An_{62-73}) together with the compositions of clinopyroxene ($Wo_{41-47}\,En_{40-48}\,Fs_{10-17}$) of crystal clots reproduced at a temperature range of 1036 – 1119°C, pressure range of 0.5 – 2 kbar, and dissolve H_2O content in the melt of 1 – 2 wt% under QFM-1, QFM and NNO oxygen fugacity buffers (Fig. 2.11). Simulations for Fui Sur could reproduce p plagioclase (Zone 2: An_{57-71}) and clinopyroxene ($Wo_{32-44}\,En_{40-49}\,Fs_{15-21}$) of crystal clots at a temperature range of 980 – 1082°C, pressure of 1.5 – 5 kbar, and H_2O dissolved in melt of 2 – 3 wt% and under QFM-1, QFM and NNO oxygen fugacity buffers (Fig. 2.11).

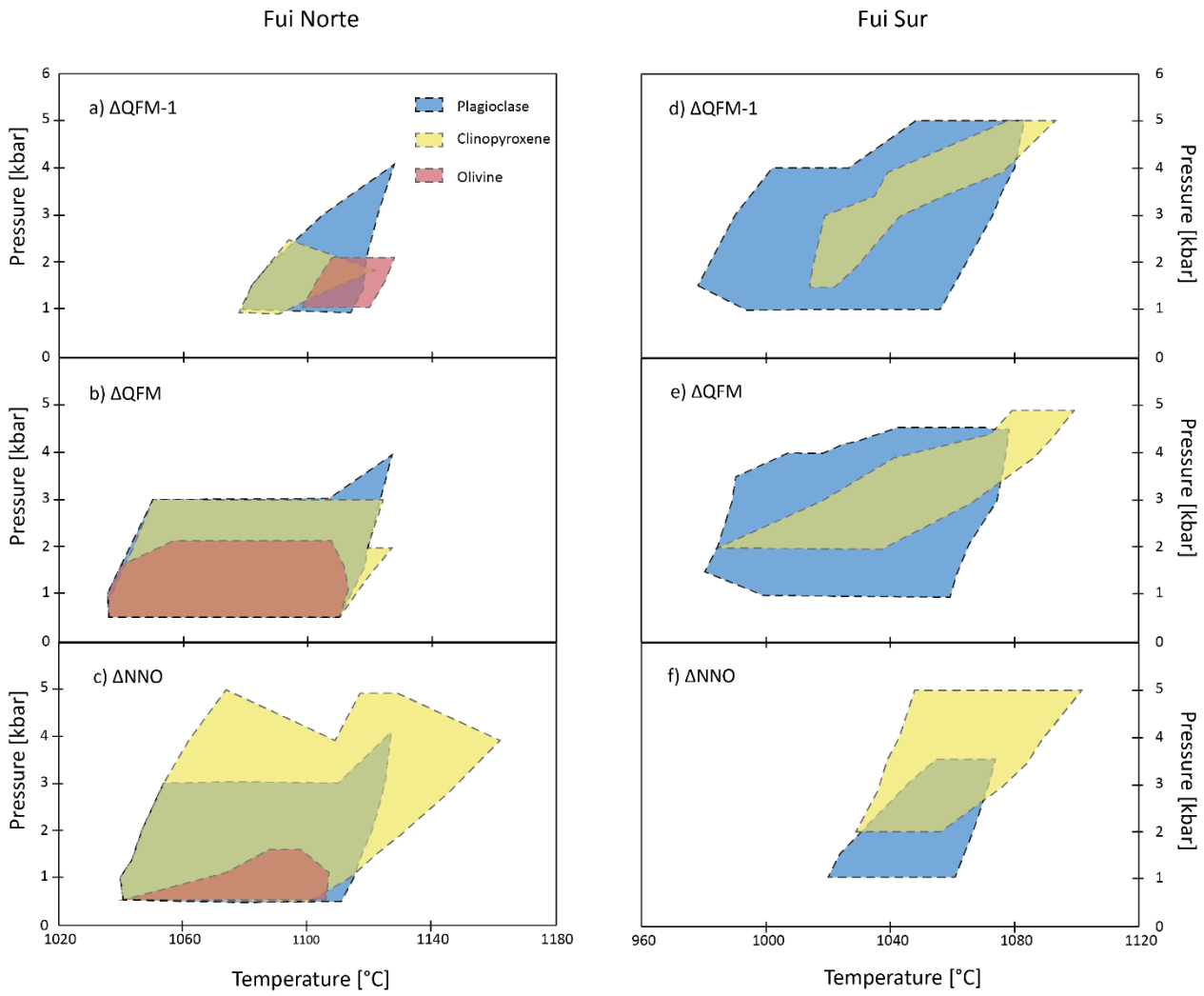

Fig. 2.11**:** *P-T stability fields for Zone 2 of olivine (when it is present), plagioclase and clinopyroxene compositions obtained by rhyolite-MELTS at different oxygen fugacity conditions for Fui Norte and Fui Sur samples. Water content used for the simulations are 1 – 2 wt% and 2 – 3 wt% in the Fui Norte and Fui Sur SECs samples, respectively.*

The overlapped fields in the P-T diagram for Low-Fo olivine, Low-An plagioclase and clinopyroxene crystallisation for the sample from Fui Norte SECs (Fig. 2.11 a-c), indicates pressure conditions (0.5 – 2 kbar) that are consistent with those obtained from geobarometers. This could indicate the presence of a crustal reservoir where isolated crystals and crystal clots of compositional range of Zone 2 (Low-Fo for olivine and Low-An for plagioclase) were formed. In the case of the Fui Sur SECs, rhyolite-MELTS modelling yielded pressure conditions of 1.5 – 5 kbar where the

Zone 2 of plagioclase and clinopyroxene crystallise. These results are also consistent with geobarometry, indicating the presence of a crustal reservoir.

2.6 Discussion

2.6.1 Pre-eruptive conditions and evidence of SECs shallow reservoirs from different approaches

Summarizing the intensive conditions calculated via different approaches, these are consistent with each other. The lower temperatures obtained through geothermometers (Loucks, 1996; Shejwalkar & Coogan, 2013) agree with ranges yielded by rhyolite-MELTS simulations (Fig. 2.12). In the case of H_2O content, the results of the numerical solution are slightly lower compared with those obtained by the thermodynamic modelling. We reproduced the compositions of mineral phases (only Zone 2 in the case of plagioclase and olivine) using rhyolite-MELTS, in simulations considering an H_2O content between 1 and 2 wt% for the Fui Norte SECs and between 2 and 3 wt% for the Fui Sur SECs. These values do not substantially differ from those obtained by numerical solution based on H_2O solubility equations (see Fig. 2.10). Despite the absence of Fe-Ti oxide pairs, the estimated oxidizing conditions (QFM-1, QFM and NNO) were those necessary to reproduce by rhyolite-MELTS the compositions of the mineral phases of Fui Norte and Fui Sur SECs.

In comparison with other magmatic systems of the SVZ, water contents and oxygen fugacity results obtained here are in the same magnitude order. For example, in Villarrica volcano values between 0.3 – 3 wt% for H_2O and QFM and NNO buffers are reported (Lohmar et al., 2012; Morgado et al., 2015), and in Quetrupillán Volcano, values of 2.9 – 3.3 wt% of H_2O and QFM and NNO buffers are reported (Brahm et al., 2018).

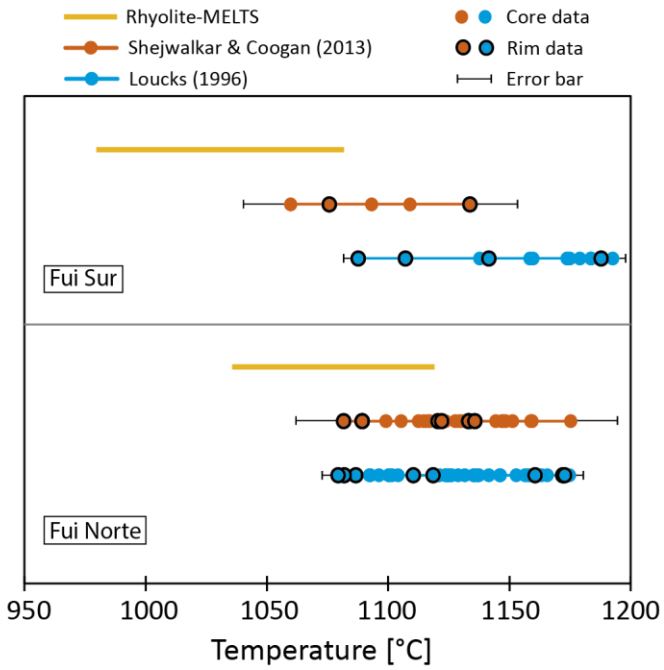

Fig. 2.12: *Comparison of temperature ranges obtained by rhyolite-MELTS simulations and geothermometers of Loucks (1996) and Shejwalkar & Coogan (2013), for the samples from the Fui Norte and Fui Sur SECs (16-6B and FS4 respectively). Temperatures obtained from cores and rims of olivine are shown. Black bars correspond to the error of the methods (±6°C for Loucks (1996) and ±20°C for Shejwalkar & Coogan (2013)).*

Considering the pressure ranges obtained from rhyolite-MELTS simulations, Ol-Cpx Ca-exchange barometer (Köhler & Brey, 1990) and numerical solution for P-H_2O content of the crystallizing melts, together with a density equivalent to 2700 kg/m^3 (typical value used for the upper crust in the SVZ; e.g., Tassara et al., 2006; Tašárová, 2007) for a transformation to depth (km), we could infer the presence of crustal reservoirs. The pressures obtained using Köhler & Brey (1990) method, yielded depths values up to 25.7 and 34.8 km for the Fui Norte and Fui Sur SECs, respectively. This information is only useful to constrain a crystallisation event within the crust with no major details about the depth range of the reservoir formation in the crust. Nevertheless, considering the numerical solution and rhyolite-MELTS modelling methods, in the Fui Norte SECs the conditions correspond to a shallow reservoir in upper crust up to 7.6 km, whereas in the Fui Sur SECs, the conditions are between upper and middle crust corresponding to depths up to 18.9 km (Fig. 2.13). In consequence, despite the deeper values for the

magmatic reservoir, we found melt-mineral equilibrium at shallow crustal reservoir conditions for both subgroups, Fui Norte and Fui Sur.

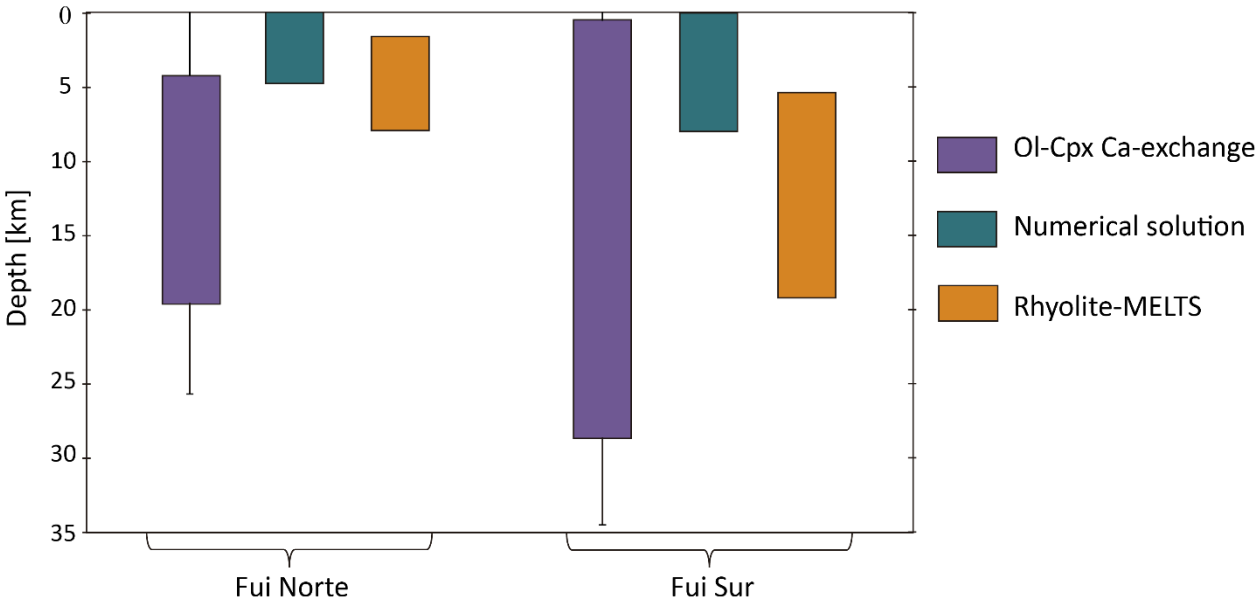

Fig. 2.13: *Estimation of the reservoir depth for the Fui Norte (left) and Fui Sur (right) SECs with Köhler & Brey (1990) Ca-exchange between Cpx and Ol (purple bar), numerical solution using Lange et al. (2009) and Moore et al. (1989) expressions (green bar), and rhyolite-MELTS modelling (orange bar). Depths obtained through geobarometer from Köhler & Brey (1990) Ol-Cpx Ca-exchange (purple bar) includes the error of the method (black lines in purple bars).*

As it was inferred from our rhyolite-MELTS simulations, the crystallisations of Zone 1 for olivine and plagioclase phenocrysts (many of them forming crystal clots) took place from a melt of composition different from the groundmass in the SECs. These results are consistent with equilibrium test for olivine using the chemical filter of Roeder and Emslie (1970) in the cases of the Chanchán and Fui Sur SECs (see section A.5.1). Nevertheless, in the case of the Fui Norte SECs, Zone 1 olivine compositions show equilibrium with the groundmass, but these compositions could not be reproduced by rhyolite-MELTS. Similar situations occur with Chanchán and Fui Sur Zone 2 olivine compositions that cannot be reproduced by rhyolite-MELTS despite equilibrium conditions are indicated by the Fe-Mg olivine-groundmass chemical filter. These differences are

expected because rhyolite-MELTS simulations consider multiple variables such as water content, oxygen fugacity, pressure, and temperature for a given melt composition. Thus, we infer that Zone 1 compositions of olivine and plagioclase phenocrysts would correspond to antecryst compositions formed in deeper crustal levels, or in a crystal mush, where the interstitial melt composition differs from that of the groundmass.

Table 6: *Summary of the pre-eruptive conditions for the Zone 2 compositions of Fui Norte and Fui Sur SECs. Conditions using Köhler & Brey (1990) Ca-exchange between Cpx and Ol (pressure), numerical solution using Lange et al. (2009) and Moore et al. (1989) expressions (pressure and H_2O content), Loucks (1996) Fe-Mg exchange between Ol and Aug (temperature), Shejwalkar & Coogan (2013) Ca in olivine (temperature) and rhyolite-MELTS modelling (Pressure, temperature, H_2O content and oxygen fugacity) are listed. Uncertainties are not considered.*

	Fui Norte		Fui Sur	
	Pressure [kbar]	Depth [km]	Pressure [kbar]	Depth [km]
Ol-Cpx barometer	1.2 - 5.1 (±1.7)	4.5 - 19.3 (±6.4)	0.2 - 7.5 (±1.7)	0.8 - 28.3 (±6.4)
Numerical solution	up to 1.2	up to 4.5	up to 2.1	up to 7.9
Rhyolite-MELTS	0.5 - 2	1.9 - 7.6	1.5 - 5	5.7 - 18.9
T Ol-Aug [±6°C]	1079 - 1174		1087 - 1192	
T Ca-in-Ol [±20°C]	1082 - 1175		1060 - 1134	
T rhyolite-MELTS [°C]	1036 - 1119		980 - 1082	
H_2O Numerical sol. [wt%]	0.4 - 1.6		0.9 - 2.4	
H_2O Rhyolite-MELTS [wt%]	1 - 2		2 - 3	
Buffer fO_2 rhyolite-MELTS	QFM-1, QFM, NNO		QFM-1, QFM, NNO	

2.6.2 Crystal mush reservoirs and interpretation of olivine and plagioclase textures and compositions

Several studies proposed complex crustal processes for other SECs in different tectonic settings, some of them including a crustal reservoir (e.g., Johnson et al., 2008; Erlund et al.; 2010; Gao et al., 2017) and crystal mush-bearing within magmatic reservoirs (Coote et al., 2018; Coote & Shane, 2018; Shane & Coote, 2018). In the central SVZ, other studies proposed crustal magmatic reservoirs beneath SECs and near to stratovolcanoes such as Caburgua-Huelemolle (Morgado et al., 2017) and Carrán Los Venados (Bucchi et al., 2015). Additionally, several works proposed

crystal mushes in reservoirs beneath stratovolcanoes of the CSVZ (e.g., Llaima volcano, Bouvet de Maisonneuve et al., 2012; Quetrupillán, volcano, Brahm et al., 2018; Calbuco volcano, Morgado et al., 2019.). We discuss the presence of crystal mush in the reservoirs of the studied SECs based on textural and mineralogical data.

2.6.2.1 Interpretations from textural data

The presence of abundant crystal clots and disequilibrium textures in the studied samples are consistent with a mush type reservoir in the upper crust (Bachmann and Bergantz, 2004; Hildreth, 2004). The phenocrysts of olivine, plagioclase and glomerocryst with cores of Zone 1 would be testimony of an early mush residing in a reservoir with a fractionated residual melt (groundmass) that allowed the crystallisation of Zone 2 as part of clots, rims and isolated microphenocrysts with Low-Fo and Low-An composition for olivine and plagioclase respectively. Disequilibrium conditions for plagioclase crystallisation generated resorption and patchy textures of the inner core followed by a Transitional Zone crystallisation (Fig. 2.9).

The relatively low crystallinity of the studied volcanic products (3 – 20 %; low compared to other volcanic products from proposed crystal mush reservoirs around ~40 %) is not contradictory with the presence of a crystal mush within the magmatic reservoir. According to the model of Dufek and Bachmann (2010), residual melts are efficiently extracted from a mushy solidification front (cf. Marsh, 1996), where the crystallinity is in the window of 50 – 70 vol. % crystals in the mush. Field evidence and numerical modelling reported in plutonic bodies also suggests efficient melt extraction (as dikes) at high crystal contents (e,g. Molina et al., 2015; Aravena et al., 2017). Crystal clots and isolated antecrysts of the studied samples could be extracted from the crystal mush and transported to the eruptible melt accumulation zone of the reservoir (Huber et al., 2011). A melt remobilisation process from a crystal mush was also inferred in the nearby Quetrupillán volcano to explain disequilibrium textures in their holocene materials (Brahm et al., 2018).

2.6.2.2 Interpretations from mineralogical data

Plagioclases are good tracer of magmatic histories and have been used to elucidate magmatic processes (e.g., Humphreys et al., 2006; Bouvet de Maisonneuve et al., 2013; Cashman and Blundy, 2013; Pizarro et al., 2019). For example, anorthite contents can vary according to four variables: melt composition, dissolve water content, temperature, and pressure (Nelson and Montana, 1992; Streck, 2008; Lange et al., 2009; Waters and Lange, 2015). Nevertheless, it has been mentioned that temperature produce significant changes in Anorthite content (e.g., Lange et al., 2009), being one of the most relevant variables that influences the composition of the crystallizing plagioclase. As it was mentioned, plagioclases with Zone 1 compositions of Fui Norte and Fui Sur SECs, commonly form clots and exhibit partially resorbed High-An cores followed by the Transitional Zone growth with the highest An content (Fig. 2.9a, b, d, e). We cannot determine if the mentioned disequilibrium features in plagioclases could be associated with changes in melt composition, increase of dissolved water in melt, increase pressure, increase temperature or a combination of them. Disaggregation of the crystal mush that gave rise to crystal clots recording crystallisation of Zone 2 plagioclase composition from residual melt, could also be consequence of the mentioned physicochemical changes in the reservoir. Taking into account the Transitional Zone in plagioclase plus the determined temperature ranges, a heating event is a more likely process that favoured the crystal mush disaggregation and disequilibrium textures.

The presence in Chanchán SECs of olivine as glomerocrysts, resorbed phenocrysts (in cores and rims) or with reverse zoning (Fig. 2.8b) among other disequilibrium textures, together with the olivine-groundmass compositiona disequilibrium, suggest that the olivine phenocrysts are antecrysts. The presence of reverse zoned olivine along with being the only phenocryst-size phase, would indicate that they come from an accumulation zone dragged during the eruptions. Recently Pankhurst et al. (2018) proposed that reverse-zoned olivine phenocrysts could be consequence of

a process denominated “Crystal Rain”, that consist of a fractional crystallization in which olivine phenocrysts fall from the top of a reservoir (with lower temperatures), settling and forming a crystal mush zone in the floor. Whichever are the reservoir processes to explain Chanchán rocks, they differ from those of the neighbouring Fui Norte and Fui Sur SECs, although similarities in magma genesis between Chanchán and adjacent Fui Norte SECs are observed, as it is discussed below.

2.6.3 Genetic relation between magmas from the MCVC, the Fui Norte SECs and the Fui Sur SECs

According to Harker diagrams (Fig. 2.2b – i and Fig. 2.3c – f), there is a trend that correlates the evolution of the Fui Sur SECs and the MCVC, while the Fui Norte and Chanchán SECs do not always fit this evolution trend, particularly in incompatible elements (Fig. 2.3d-f). Major elements compositions show that the Fui Sur SECs and the MCVC volcanic products are more differentiated than the volcanic material from the Fui Norte and Chanchán SECs, which is consistent with the higher abundance of olivine in the Chanchán and Fui Norte SECs samples.

Volcanic products from the MCVC and the Fui Sur SECs show higher SiO_2 content and fluid mobile/immobile ratios (Fig. 2.14c, d) and lower La/Yb ratios (Fig. 2.14b) than the products from the Fui Norte and Chanchán SECs. This could indicate that the former two centres would have had higher influence of the slab-derived fluid component and higher partial melting degree (Fig. 2.14). Conversely, samples from the Fui Norte and Chanchán SECs show higher Zr/Hf ratios than the Fui Sur SECs and the MCVC (Fig. 2.14a). As Hf is more compatible than Zr (clinopyroxene DZr/DHf ≈ 0.5; Hart & Dunn, 1993; Blundy et al.,1998; Lundstrom et al., 1998; Green et al., 2000) a higher Zr/Hf ratio could be related to the presence of clinopyroxene in the source resulting in a more fertile mantle source for the Fui Norte and Chanchán SECs. The influence of the slab-derived fluid component in SECs relative to stratovolcanoes and their location away from the trench has been subject of study in the SVZ. They indicate that SECs located to the east of stratovolcanoes presents

lower fluid component than the large composite volcanic centre relatively nearest to the trench (e.g., Villarrica Volcano and adjacent SECs; Hickey-Vargas et al., 2002). However, recent studies proposed that there is no correlation between compositions and distance from the arc front in the SVZ, instead, the local tectonics have influence on the compositions of SECs along the LOFZ (McGee et al., 2017).

Based on our geochemical and mineralogical results, the magmatic systems of the two subgroups of Fui Group (Fui Norte and Fui Sur) are independent from each other, registering different geochemical signatures, while only the Fui Sur SECs are likely genetic related to the MCVC (Fig. 2.15). These interpretations are consistent with Rawson's et al. (2016) proposition of Fui Sur SECs would be parasitic cones of the MCVC, while the Fui Norte SECs would have derived from magmas directly evacuated across the LOFZ (see also Cembrano and Lara, 2009; Bucchi et al., 2015). In this scenario, however, despite we observe geochemical similarities between the MCVC and the Fui Sur SECs (Fig. 2.2, 2.3 and 2.14), there are differences in some clue elements (Fe_2O_3* and TiO_2; Fig. 2.2g, i), thus we cannot determine if they belong to the same plumbing system or are independent from each other. If one assumes the scenario of Fui Sur SECs - MCVC dependence (Fig. 2.15), the spatial distribution of Fui Sur SECs adjacent to the MCVC and following NE-SW trends towards the main branch of the LOFZ, could be indicative of feeder dykes from MCVC reservoir following the well-known NE-SW extensional strike-slip duplexes resulting of the dextral LOFZ movements (López-Escobar et al., 1995; Cembrano et al., 1996; Arancibia et al., 1999; Cembrano & Lara, 2009). It is interesting to note that along the LOFZ a glacial valley of about 1,200 m depth and 10 km wide formed. Thus, the large amount of rocks removed by glacier activities together with glacial unloading would produce the necessary decompression and degasification for dyke propagation. A rough estimation of decompression at depth of the top of

the MCVC reservoir after remotion of glacial valley rocks is about 0.5 kb and the associated decrease of about 0.6 wt % in melt dissolve H_2O content.

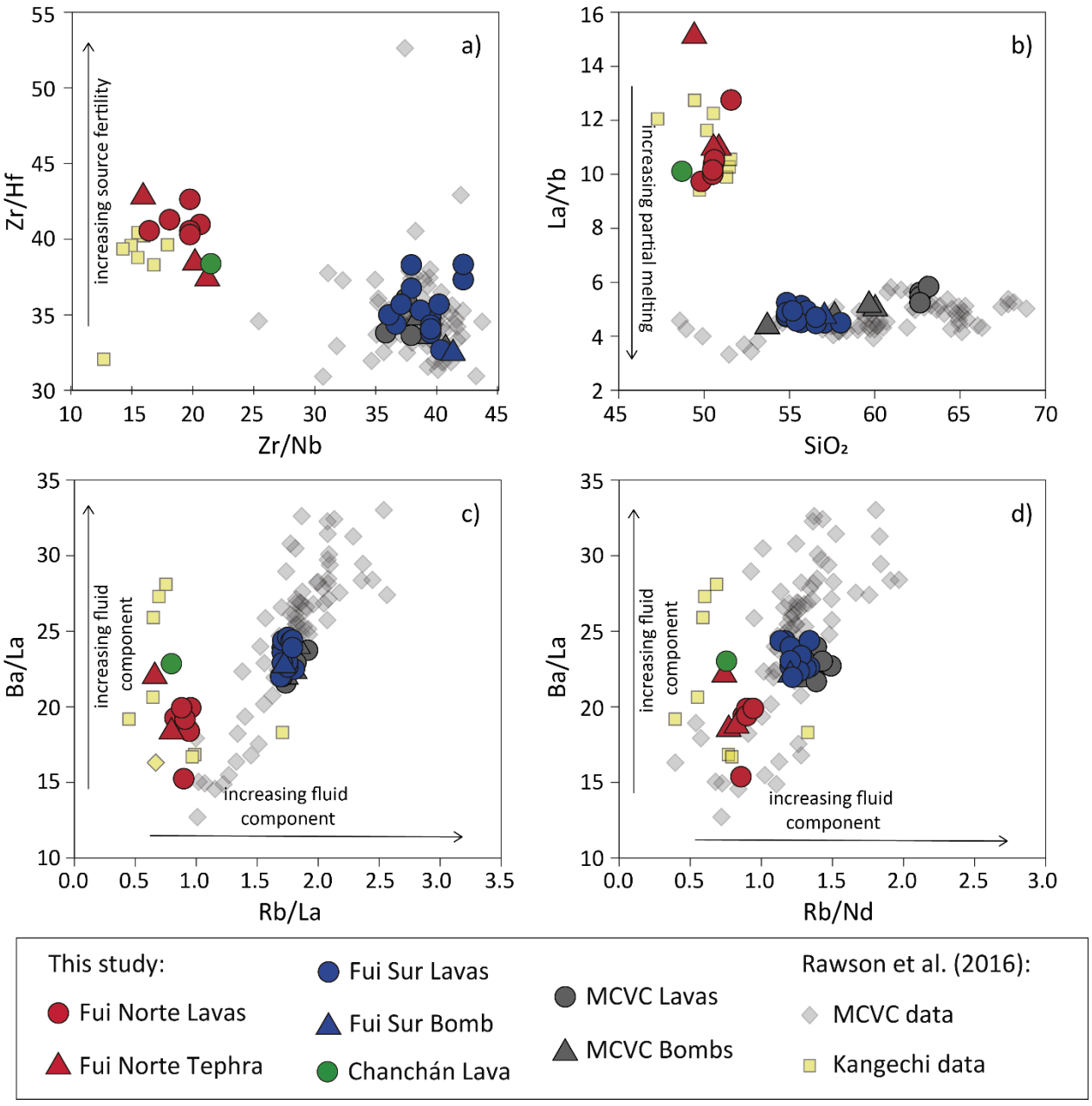

Fig. 2.14: *a) Plot of Zr/Nb vs. Zr/Hf. b) Plot of La/Yb vs. SiO_2, arrow indicates the direction in which partial melting increases. c) Plot of Ba/La vs. Rb/La. d) Plot of Ba/La vs. Rb/Nd. Arrows in c) and d) indicates the direction in which fluid component of the source increases. Note that Kangechi rocks of Rawson et al., (2016) correspond to our Chanchán and Fui Norte SECs.*

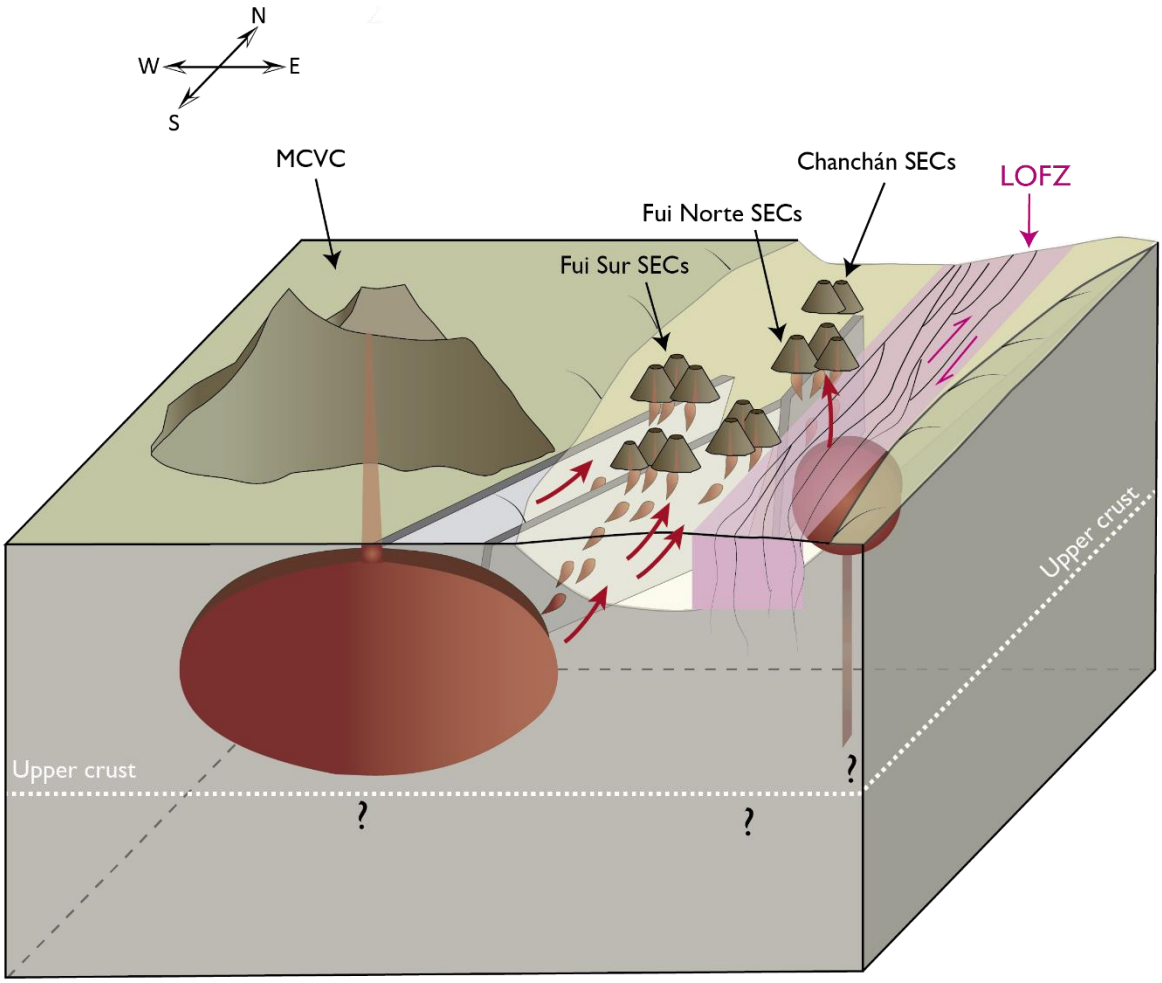

Fig. 2.15: *Schematic representation of the main characteristics of the Fui Group SECs and MCVC reservoirs in the upper crust. The Fui Group SECs are located in the glacial valley (filled by glacial and fluvial sediments along with volcanic products) and adjacent to the west of the LOFZ. The magmas that feed the Fui Sur SECs ascend from the MCVC reservoir, through NE structures associated to the dextral movements of the LOFZ. The reservoir from the Fui Norte SECs is independent of the Fui Sur SECs and MCVC, and magmas tap the surface through NNE structures. Not to scale.*

2.7 Conclusions

The Fui Group SECs is formed by Fui Norte, Fui Sur and Chanchán SECs forming clusters of volcanic cones close to each other and spatially related to the LOFZ, however, they exhibit compositional differences related to the proximity to the MCVC. In fact, the Fui Sur SECs have andesites and basaltic andesites depleted in incompatible trace elements similar to the MCVC rocks and differ from the Fui Norte and Chanchán SECs, which are basalts that are more primitive and enriched in incompatible trace elements. From mineralogical point of view, differences and similarities are observed among the clusters. Volcanic material from the Fui Norte and Fui Sur SECs include olivine, clinopyroxene and plagioclase as phenocrysts, microphenocrysts or forming part of crystal clots, however Chanchán SECs have antecryst olivines as the only large-size phase what prevents, to some extent, estimate their intensive conditions. Olivine and plagioclase phenocrysts and microphenocrysts of the studied SECs are compositionally zoned in High-Fo/High-An (Zone 1, Fo_{78-89} and An_{76-93}) and Low-Fo/Low-An (Zone 2, Fo_{60-78} and An_{57-73}) compositional ranges, respectively. Zone 2 compositions yielded shallow crustal pressures of up to 2 kbar for Fui Norte and up to 5 kbar Fui Sur SECs equivalent to ≤ 7.6 and ≤ 18.9 km, respectively. Additionally, temperatures obtained from different thermometer and rhyolite-MELTS simulations are in the range 1036 – 1175°C and 980 – 1192°C for Fui Norte and Fui Sur SECs, respectively. We infer that crystal clots could be testimonies of crystal mush zones due to long magma residence in reservoirs that underwent perturbations, evidenced by disequilibrium textures.

Taking together the whole-rock compositions and mineralogical results, the Fui Norte and Fui Sur SECs are considered as independent systems despite the closeness between them. A genetic relation between magmas from Fui Sur and MCVC is discussed based on whole-rock compositions (including slab-derived fluid components), and tectonic relationships.

Acknowledgments

This work was mainly funded by CONICYT-FONDAP project 15090013 “Centro de Excelencia en Geotermia de los Andes” (CEGA) and the Department of Geology of the Universidad de Chile. F.M. acknowledges to Reserva Biológica Huilo-Huilo and Reserva Nacional Mocho-Choshuenco for their collaboration and assistance in fieldwork, as well as N. Mendoza and A. Bordeu for valuable assistance and discussion in the field. Many thanks to the personnel of LAMARX – Universidad Nacional de Córdoba for the assistance in EPMA, to S. Kearns and B. Buse who provided great assistance with EPMA in the University of Bristol, and to Fondequip EQM150101 project for sessions in FE-SEM at Universidad Católica de Chile.

Capítulo 3: Conclusiones

El Grupo Fui está compuesto por los CEM de Fui Norte, Fui Sur y Chanchán, formando subgrupos volcánicos cercanos entre sí, y espacialmente relacionados a la ZFLO, sin embargo, exhiben diferencias composicionales relacionadas a su proximidad con el CVMC. Los productos volcánicos de Fui Norte son más primitivos, enriquecidos en elementos incompatibles, mientras que el material volcánico emitido desde Fui Sur presenta productos más diferenciados, empobrecido en elementos traza incompatibles, siendo similares a las rocas del CVMC. Mineralógicamente, similitudes y diferencias son observadas entre los subgrupos. Los productos volcánicos de Fui Norte y Fui Sur incluyen olivino, clinopiroxeno y plagioclasa como fenocristales, microfenocristales y formando parte de cúmulos cristalinos, sin embargo, en los CEM de Chanchán la única fase presente como fenocristales es olivino, los cuales son antecristales y por lo tanto, no permiten determinar condiciones intensivas para este subgrupo. Los fenocristales y microfenocristales de olivino y plagioclasa del Grupo Fui están zonados composicionalmente en los rangos de Alta-Fo y Alta-An (Zona 1, Fo_{78-89} and An_{76-93}) y de Baja-Fo y Baja-An (Zona 2, Fo_{60-78} and An_{57-73}) respectivamente. La Zona 2 registra presiones de hasta 2 kbar (Fui Norte) y hasta 5 kbar (Fui Sur), las cuales son interpretadas como cristalización en niveles de corteza superior de hasta 7.6 km para los CEM de Fui Norte; y hasta 18.9 km para los CEM de Fui Sur. Adicionalmente, las temperaturas obtenidas por los diferentes termómetros y el modelamiento en rhyolite-MELTS están en el rango de 1036 – 1175°C y 980 – 1192°C para Fui Norte y Fui Sur, respectivamente. Se infiere que los cúmulos cristalinos presente en las muestras son testimonios de una zona de acumulación de cristales *(mush zone)*, evidenciado a través de las texturas de desequilibrio, las cuales demuestran las perturbaciones magmáticas ocurridas en el reservorio.

Tomando en consideración las composiciones geoquímicas de roca total y los resultados mineralógicos, los sistemas magmáticos de Fui Norte y Fui Sur son independientes, a pesar de la cercanía entre ambos subgrupos. Una relación genética entre los magmas de Fui Sur y los del CVMC es discutida basada en las composiciones geoquímicas de roca total (incluyendo la componente de fluidos derivados desde el *slab*) y relaciones tectónicas.

Como se ha demostrado, el volcanismo monogenético o los CEM pueden presentar historias magmáticas corticales complejas, incluyendo reservorios corticales con procesos registrados a escala de pequeños cristales.

Bibliografía

Aguirre, L., Hervé, F., & Godoy, E. (1972). Distribution of metamorphic facies in Chile: an outline. *Krystallinikum*, *9*(1), 7-19.

Arancibia, G., Cembrano, J., & Lavenu, A. (1999). Transpresión dextral y partición de la deformación en la Zona de Falla Liquiñe-Ofqui, Aisén, Chile (44-45ºS). *Revista geológica de Chile*, *26*(1), 03-22.

Aravena, Á., Gutiérrez, F. J., Parada, M. A., Payacán, Í., Bachmann, O., & Poblete, F. (2017). Compositional zonation of the shallow La Gloria pluton (Central Chile) by late-stage extraction/redistribution of residual melts by channelization: Numerical modeling. *Lithos*, *284*, 578-587.

Bachmann, O., & Bergantz, G. W. (2004). On the origin of crystal-poor rhyolites: extracted from batholithic crystal mushes. *Journal of Petrology*, *45*(8), 1565-1582.

BAS, M. L., Maitre, R. L., Streckeisen, A., Zanettin, B., & IUGS Subcommission on the Systematics of Igneous Rocks. (1986). A chemical classification of volcanic rocks based on the total alkali-silica diagram. *Journal of petrology*, *27*(3), 745-750.

Blundy, J. D., Robinson, J. A. C., & Wood, B. J. (1998). Heavy REE are compatible in clinopyroxene on the spinel lherzolite solidus. *Earth and Planetary Science Letters*, *160*(3-4), 493-504.

Brahm, R., Parada, M. A., Morgado, E., Contreras, C., & McGee, L. E. (2018). Origin of Holocene trachyte lavas of the Quetrupillán volcanic complex, Chile: Examples of residual melts in a rejuvenated crystalline mush reservoir. *Journal of Volcanology and Geothermal Research*, *357*, 163-176.

Bouvet De Maisonneuve, C., Dungan, M. A., Bachmann, O., & Burgisser, A. (2012). Insights into shallow magma storage and crystallization at Volcán Llaima (Andean southern volcanic zone, Chile). *Journal of Volcanology and Geothermal Research*, *211*, 76-91.

Bouvet De Maisonneuve, C., Dungan, M. A., Bachmann, O., & Burgisser, A. (2013). Petrological insights into shifts in eruptive styles at Volcán Llaima (Chile). *Journal of Petrology*, *54*(2), 393-420.

Bucchi, F., Lara, L. E., & Gutiérrez, F. (2015). The Carrán–Los Venados volcanic field and its relationship with coeval and nearby polygenetic volcanism in an intra-arc setting. *Journal of Volcanology and Geothermal Research*, *308*, 70-81.

Campos, A., Moreno, H., Muñoz, J., Antinao, J., Clayton, J., & Martin, M. (1998). Area de Futrono-Lago Ranco, Región de los Lagos. *Servicio Nacional de Geología y Minería, Mapas Geológicos, 8*(1).

Cañón-Tapia, E. (2016). Reappraisal of the significance of volcanic fields. *Journal of volcanology and Geothermal Research*, *310*, 26-38.

Cashman, K., & Blundy, J. (2013). Petrological cannibalism: the chemical and textural consequences of incremental magma body growth. *Contributions to Mineralogy and Petrology*, *166*(3), 703-729.

Cembrano, J., Hervé, F., & Lavenu, A. (1996). The Liquiñe Ofqui fault zone: a long-lived intra-arc fault system in southern Chile. *Tectonophysics*, *259*(1-3), 55-66.

Cembrano, J., & Lara, L. (2009). The link between volcanism and tectonics in the southern volcanic zone of the Chilean Andes: a review. *Tectonophysics*, *471*(1-2), 96-113.

Clapperton, C. (1993). Quaternary geology and geomorphology of South America. *Elsevier Science Publishers* 779.

Clayton, J. D., Clapperton, C. M., & Antinao, J. L. (1997). Las glaciaciones pleistocenas en la cuenca del lago Villarrica, Andes del Sur. *Congreso Geológico Chileno*, *8*, 307-311.

Coote, A., & Shane, P. (2018). Open-system magmatic behaviour beneath monogenetic volcanoes revealed by the geochemistry, texture and thermobarometry of clinopyroxene, Kaikohe-Bay of Islands volcanic field (New Zealand). *Journal of Volcanology and Geothermal Research*, *368*, 51-62.

Coote, A., Shane, P., Stirling, C., & Reid, M. (2018). The origin of plagioclase phenocrysts in basalts from continental monogenetic volcanoes of the Kaikohe-Bay of Islands field, New Zealand: implications for magmatic assembly and ascent. *Contributions to Mineralogy and Petrology*, *173*(2), 14.

Di Biase, F. (1975). Geología del Grupo Volcánico Mocho-Choshuenco, Provincia de Valdivia, Chile. *Memoria de Título (Inédito), Universidad de Chile, Departamento de Geología*.

Droop, G. T. R. (1987). A general equation for estimating Fe 3+ concentrations in ferromagnesian silicates and oxides from microprobe analyses, using stoichiometric criteria. *Mineralogical magazine*, *51*(361), 431-435.

Dufek, J., & Bachmann, O. (2010). Quantum magmatism: Magmatic compositional gaps generated by melt-crystal dynamics. *Geology*, *38*(8), 687-690.

Echegaray, J. (2004). *Evolución geológica y geoquímica del Centro Volcánico Mocho-Choshuenco, Andes del Sur* (Doctoral dissertation, Master Thesis, Universidad de Chile, Chile).

Erlund, E. J., Cashman, K. V., Wallace, P. J., Pioli, L., Rosi, M., Johnson, E., & Granados, H. D. (2010). Compositional evolution of magma from Parícutin Volcano, Mexico: the tephra record. *Journal of Volcanology and Geothermal Research*, *197*(1-4), 167-187.

Gao, R., Lassiter, J. C., & Ramirez, G. (2017). Origin of temporal compositional trends in monogenetic vent eruptions: Insights from the crystal cargo in the Papoose Canyon sequence, Big Pine Volcanic Field, CA. *Earth and Planetary Science Letters*, *457*, 227-237.

García, A., Beck, M., Burmester, R., Munizaga, F., Hervé, F. (1988). Paleomagnetic Reconnaissance of the Región de Los Lagos, Sourthern Chile and its tectonic implications. *Revista Geológica de Chile 15*(1), 13-30.

Gardeweg, M., & Sellés, D. (2012) Los volcanes Chanchán y el Grupo Volcánico Fui: volcanes monogenéticos al norte del CV Mocho-Choshuenco, Región de los Ríos, sur de Chile.

Green, T. H., Blundy, J. D., Adam, J., & Yaxley, G. M. (2000). SIMS determination of trace element partition coefficients between garnet, clinopyroxene and hydrous basaltic liquids at 2–7.5 GPa and 1080–1200 C. *Lithos*, *53*(3-4), 165-187.

Grove, T. L., Donnelly-Nolan, J. M., & Housh, T. (1997). Magmatic processes that generated the rhyolite of Glass Mountain, Medicine Lake volcano, N. California. *Contributions to Mineralogy and Petrology*, *127*(3), 205-223.

Gualda G.A.R., Ghiorso M.S., Lemons R.V., Carley T.L. (2012) Rhyolite-MELTS: A modified calibration of MELTS optimized for silica-rich, fluid-bearing magmatic systems. *Journal of Petrology, 53, 875-890.*

Hart, S. R., & Dunn, T. (1993). Experimental cpx/melt partitioning of 24 trace elements. *Contributions to Mineralogy and Petrology*, *113*(1), 1-8.

Herbst, R., Troncoso, A., & Munoz, J. (2005). The Triassic taphofloras from the Lake District, Xth Region, Chile. *Ameghiniana, 42*(2), 377-394.

Hickey-Vargas, R., Sun, M., López-Escobar, L., Moreno-Roa, H., Reagan, M. K., Morris, J. D., & Ryan, J. G. (2002). Multiple subduction components in the mantle wedge: evidence from eruptive centers in the Central Southern volcanic zone, Chile. *Geology*, *30*(3), 199-202.

Hildreth, W. (2004). Volcanological perspectives on Long Valley, Mammoth Mountain, and Mono Craters: several contiguous but discrete systems. *Journal of Volcanology and Geothermal Research*, *136*(3-4), 169-198.

Huber, C., Bachmann, O., & Dufek, J. (2011). Thermo-mechanical reactivation of locked crystal mushes: Melting-induced internal fracturing and assimilation processes in magmas. *Earth and Planetary Science Letters*, *304*(3-4), 443-454.

Humphreys, M. C., Blundy, J. D., & Sparks, R. S. J. (2006). Magma evolution and open-system processes at Shiveluch Volcano: Insights from phenocryst zoning. *Journal of Petrology*, *47*(12), 2303-2334.

Johnson, E. R., Wallace, P. J., Cashman, K. V., Granados, H. D., & Kent, A. J. (2008). Magmatic volatile contents and degassing-induced crystallization at Volcán Jorullo, Mexico: Implications for melt evolution and the plumbing systems of monogenetic volcanoes. *Earth and Planetary Science Letters*, *269*(3-4), 478-487.

Köhler, T. P., & Brey, G. (1990). Calcium exchange between olivine and clinopyroxene calibrated as a geothermobarometer for natural peridotites from 2 to 60 kb with applications. *Geochimica et Cosmochimica Acta*, *54*(9), 2375-2388.

Lange, R. A., Frey, H. M., & Hector, J. (2009). A thermodynamic model for the plagioclase-liquid hygrometer/thermometer. *American Mineralogist, 94*(4), 494-506.

Lara, L., Rodríguez, C., Moreno, H., & Pérez de Arce, C. (2001). Geocronología K-Ar y geoquímica del volcanismo plioceno superior-pleistoceno de los Andes del sur (39-42 S). *Revista geológica de Chile, 28*(1), 67-90.

Lara, L., & Moreno, H. (2004). Geología del Área Liquiñe-Neltume, Regiones de Los Lagos y de la Araucanía. Servicio Nacional de Geología y Minería. Carta Geológica de Chile, Serie Geología Básica, 83, 1. *Scale 1: 100.000.*

Lara, L. E., & Folguera, A. (2006). The Pliocene to Quaternary narrowing of the Southern Andean volcanic arc between 37° and 41°S latitude. *Special Papers-Geological Society of America*, 407, 299-315.

Larrea, P., Siebe, C., Juárez-Arriaga, E., Salinas, S., Ibarra, H., & Böhnel, H. (2019). The~ AD 500–700 (Late Classic) El Astillero and El Pedregal volcanoes (Michoacán, Mexico): a new monogenetic cluster in the making?. *Bulletin of Volcanology*, *81*(10), 1-19.

Larrea, P., Albert, H., Ubide, T., Costa, F., Colás, V., Widom, E., & Siebe, C. (2021). From explosive vent opening to effusive outpouring: mineral constraints on magma dynamics and timescales at paricutin monogenetic volcano. Journal of Petrology.

Lohmar, S., Parada, M., Gutiérrez, F., Robin, C., & Gerbe, M. C. (2012). Mineralogical and numerical approaches to establish the pre-eruptive conditions of the mafic Lican Ignimbrite, Villarrica Volcano (Chilean Southern Andes). *Journal of Volcanology and Geothermal Research*, *235*, 55-69.

López-Escobar, L., Cembrano, J., & Moreno, H. (1995). Geochemistry and tectonics of the Chilean Southern Andes basaltic Quaternary volcanism (37-46 S). *Andean geology*, *22*(2), 219-234.

Loucks, R. R. (1996). A precise olivine-augite Mg-Fe-exchange geothermometer. *Contributions to Mineralogy and Petrology*, *125*(2-3), 140-150.

Lowell, T. V., Heusser, C. J., Andersen, B. G., Moreno, P. I., Hauser, A., Heusser, L. E., Schluchter, C., Marchant, D. R., & Denton, G. H. (1995). Interhemispheric correlation of late Pleistocene glacial events. *Science*, *269*(5230), 1541-1549.

Lundstrom, C. C., Shaw, H. F., Ryerson, F. J., Williams, Q., & Gill, J. (1998). Crystal chemical control of clinopyroxene-melt partitioning in the Di-Ab-An system: implications for elemental fractionations in the depleted mantle. *Geochimica et Cosmochimica Acta*, *62*(16), 2849-2862.

McGee, L. E., & Smith, I. E. (2016). Interpreting chemical compositions of small scale basaltic systems: a review. *Journal of Volcanology and Geothermal Research*, *325*, 45-60.

McGee, L. E., Brahm, R., Rowe, M. C., Handley, H. K., Morgado, E., Lara, L. E., Turner, M. B., Vinet, N., Parada, M. A., & Valdivia, P. (2017). A geochemical approach to distinguishing competing tectono-magmatic processes preserved in small eruptive centres. *Contributions to Mineralogy and Petrology*, *172*(6), 44.

Molina, P. G., Parada, M. A., Gutiérrez, F. J., Ma, C., Li, J., Yuanyuan, L., Reich, M., & Aravena, Á. (2015). Protracted late magmatic stage of the Caleu pluton (central Chile) as a consequence of heat redistribution by diking: Insights from zircon data and thermal modeling. *Lithos*, *227*, 255-268.

Moore, G., Vennemann, T., & Carmichael, I. S. E. (1998). An empirical model for the solubility of H2O in magmas to 3 kilobars. *american Mineralogist*, *83*(1), 36-42.

Moreno, H., & Lara, L. (2007). Geologia del Complejo Volcánico Mocho-Choshuenco: Carta Geológica de Chile. *Serie Geología Básica*, *107*, 1-27.

Morgado, E., Parada, M. A., Contreras, C., Castruccio, A., Gutiérrez, F., & McGee, L. E. (2015). Contrasting records from mantle to surface of Holocene lavas of two nearby arc volcanic complexes: Caburgua-Huelemolle Small Eruptive Centers and Villarrica Volcano, Southern Chile. *Journal of Volcanology and Geothermal Research*, *306*, 1-16.

Morgado, E., Parada, M. A., Morgan, D. J., Gutiérrez, F., Castruccio, A., & Contreras, C. (2017). Transient shallow reservoirs beneath small eruptive centres: Constraints from Mg-Fe interdiffusion in olivine. *Journal of Volcanology and Geothermal Research*, *347*, 327-336.

Morgado, E., Morgan, D. J., Harvey, J., Parada, M. Á., Castruccio, A., Brahm, R., Gutiérrez, F., Georgiev, B., & Hammond, S. J. (2019). Localised heating and intensive magmatic conditions prior

to the 22–23 April 2015 Calbuco volcano eruption (Southern Chile). *Bulletin of Volcanology*, *81*(4), 24.

Munizaga, F., Hervé, F., Drake, R., Pankhurst, R. J., Brook, M., & Snelling, N. (1988). Geochronology of the Lake Region of south-central Chile (39–42 S): Preliminary results. *Journal of South American Earth Sciences*, *1*(3), 309-316.

Nelson, S. T., & Montana, A. (1992). Sieve-textured plagioclase in volcanic rocks produced by rapid decompression. *American Mineralogist*, *77*(11-12), 1242-1249.

Németh, K. (2010). Monogenetic volcanic fields: Origin, sedimentary record, and relationship with polygenetic volcanism. *What is a Volcano?*, *470*, 43.

Németh, K., & Kereszturi, G. (2015). Monogenetic volcanism: personal views and discussion. *International Journal of Earth Sciences*, *104*(8), 2131-2146.

Pizarro, C., Parada, M. A., Contreras, C., & Morgado, E. (2019). Cryptic magma recharge associated with the most voluminous 20th century eruptions (1921, 1948 and 1971) at Villarrica Volcano. *Journal of Volcanology and Geothermal Research*, *384*, 48-63.

Pérez, S. (2005). Volcanismo explosivo postglacial del complejo volcánico Mocho-Choshuenco, Andes del Sur (408 S). *Undergraduate thesis, Universidad de Concepción, Chile*.

Rasoazanamparany, C., Widom, E., Valentine, G. A., Smith, E. I., Cortés, J. A., Kuentz, D., & Johnsen, R. (2015). Origin of chemical and isotopic heterogeneity in a mafic, monogenetic volcanic field: A case study of the Lunar Crater Volcanic Field, Nevada. *Chemical Geology*, *397*, 76-93.

Rawson, H., Naranjo, J. A., Smith, V. C., Fontijn, K., Pyle, D. M., Mather, T. A., & Moreno, H. (2015). The frequency and magnitude of post-glacial explosive eruptions at Volcán Mocho-Choshuenco, southern Chile. *Journal of Volcanology and Geothermal Research*, *299*, 103-129.

Rawson, H., Keller, T., Fontijn, K., Pyle, D. M., Mather, T. A., Smith, V. C., & Naranjo, J. A. (2016). Compositional variability in mafic arc magmas over short spatial and temporal scales: Evidence for the signature of mantle reactive melt channels. *Earth and Planetary Science Letters*, *456*, 66-77.

Roeder, P. L., & Emslie, R. (1970). Olivine-liquid equilibrium. *Contributions to mineralogy and petrology*, *29*(4), 275-289.

Rodríguez, C., Pérez, Y., Moreno, H., Clayton, J., Antinao, J. L., Duhart, P., & Martin, M. (1999). Área de Panguipulli-Riñihue, Región de Los Lagos. *Servicio Nacional de Geología y Minería, Mapas Geológicos*, *10*(1).

Pankhurst, M. J., Morgan, D. J., Thordarson, T., & Loughlin, S. C. (2018). Magmatic crystal records in time, space, and process, causatively linked with volcanic unrest. *Earth and Planetary Science Letters*, *493*, 231-241.

SERNAGEOMIN (2020a). Ranking de riesgo específico de volcanes activos de Chile 2019.

SERNAGEOMIN (2020b). Reporte de Actividad Volcánica (RAV) N°8, Abril 2020, Región de Los Ríos.

SERNAGEOMIN (2018). Reporte Especial de Actividad Volcánica (REAV), Región de Los Ríos, C.V. Mocho-Choshuenco. 28 de marzo de 2018, 09:00 hora local.

SERNAGEOMIN (2021). Reporte Especial de Actividad Volcánica (REAV), Región de Los Ríos, C.V. Mocho-Choshuenco. 11 de mayo de 2021, 22:05 hora local.

Shejwalkar, A., & Coogan, L. A. (2013). Experimental calibration of the roles of temperature and composition in the Ca-in-olivine geothermometer at 0.1 MPa. *Lithos*, *177*, 54-60.

Stern, C. R. (2004). Active Andean volcanism: its geologic and tectonic setting. *Revista geológica de Chile*, *31*(2), 161-206.

Shane, P., & Coote, A. (2018). Thermobarometry of Whangarei volcanic field lavas, New Zealand: Constraints on plumbing systems of small monogenetic basalt volcanoes. *Journal of Volcanology and Geothermal Research*, *354*, 130-139.

Streck, M. J. (2008). Mineral textures and zoning as evidence for open system processes. *Reviews in Mineralogy and Geochemistry*, *69*(1), 595-622.

Sun, S. S., & McDonough, W. F. (1989). Chemical and isotopic systematics of oceanic basalts: implications for mantle composition and processes. *Geological Society, London, Special Publications*, *42*(1), 313-345.

Tašárová, Z. A. (2007). Towards understanding the lithospheric structure of the southern Chilean subduction zone (36 S–42 S) and its role in the gravity field. *Geophysical Journal International*, *170*(3), 995-1014.

Tassara, A., Götze, H. J., Schmidt, S., & Hackney, R. (2006). Three-dimensional density model of the Nazca plate and the Andean continental margin. *Journal of Geophysical Research: Solid Earth*, *111*(B9).

Valentine, G. A., & Perry, F. V. (2007). Tectonically controlled, time-predictable basaltic volcanism from a lithospheric mantle source (central Basin and Range Province, USA). *Earth and Planetary Science Letters*, *261*(1-2), 201-216.

Valentine, G. A., & Gregg, T. K. P. (2008). Continental basaltic volcanoes—processes and problems. *Journal of Volcanology and Geothermal Research*, *177*(4), 857-873.

Walker, G. P. (1993). Basaltic-volcano systems. *Geological Society, London, Special Publications*, *76*(1), 3-38.

Waters, L. E., & Lange, R. A. (2015). An updated calibration of the plagioclase-liquid hygrometer-thermometer applicable to basalts through rhyolites. *American Mineralogist*, *100*(10), 2172-2184.

Anexos

A.1 Ubicación muestras

Tabla A.1: Ubicación de las 34 muestras del Grupo Fui (Chanchán, Fui Norte y Fui Sur) y el CVMC.

Código	Unidad	Material	Huso	Este WGS84 (m)	Norte WGS84 (m)	Ubicación relativa
09-1	Fui Norte	Lava	19H	253047	5583303	Cantera Roja, nivel inferior
09-2	Fui Norte	Lava	19H	253047	5583303	Cantera Roja, nivel inferior
09-3	Fui Norte	Lava	19H	253047	5583303	Cantera Roja, nivel inferior
09-8	Fui Norte	Lava	19H	253047	5583303	Cantera Roja, nivel inferior
09-9	Fui Norte	Tefra	19H	253047	5583303	Cantera Roja, nivel inferior
16-1A	Fui Norte	Tefra	19H	253015	5583302	Cantera Roja, nivel medio
16-2A	Fui Norte	Tefra	19H	253021	5583254	Cantera Roja, nivel superior
16-6B	Fui Norte	Lava	19H	250836	5582712	Corte de camino ruta 203
14-11	Fui Norte	Lava	19H	252302	5584511	Mirador Teleférico
15-3	Chanchán	Lava	19H	255173	5590079	Sector Chanchán
11-3	Fui Sur	Lava	19H	252528	5577484	Pampa Pilmaiquén
FS1	Fui Sur	Lava	19H	247322	5584178	Cerca de Salto Huilo Huilo
FS3	Fui Sur	Lava	19H	248157	5581693	Corte de camino hacia Pampa Pilmaiquén
FS4	Fui Sur	Lava	19H	248157	5581693	Corte de camino hacia Pampa Pilmaiquén
16-11	Fui Sur	Lava	19H	249105	5584538	Rio Fuy, cerca de Neltume
16-12A	Fui Sur	Lava	19H	249177	5584479	Rio Fuy, cerca de Neltume
16-13B	Fui Sur	Lava	19H	247122	5584663	Corte de camino ruta 203
16-14A	Fui Sur	Lava	19H	246322	5585792	Corte de camino ruta 203
17-1A	Fui Sur	Lava	19H	253621	5580739	Sector El Depósito, Lago Pirehueico
17-7A	Fui Sur	Lava	19H	253533	5581086	Sector El Depósito, Lago Pirehueico
17-8B	Fui Sur	Lava	19H	253330	5581406	Sector El Depósito, Lago Pirehueico
17-9	Fui Sur	Lava	19H	253202	5581828	Sector El Depósito, Lago Pirehueico
17-10	Fui Sur	Lava	19H	251944	5580113	Sector El Depósito, camino interior
17-12	Fui Sur	Bomba	19H	251533	5579983	Cantera en cono de Tres Volcancitos
17-14	Fui Sur	Lava	19H	251554	5580135	Cantera en cono de Tres Volcancitos
1864-1	Erupción 1864	Lava	18H	749848	5575477	Lava de bloques erupción 1864
1864-2	Erupción 1864	Lava	18H	749848	5575477	Lava de bloques erupción 1864
1864-3	Erupción 1864	Lava	18H	749842	5575428	Lava de bloques erupción 1864
1864-4	Erupción 1864	Lava	18H	749396	5575498	Lava de bloques erupción 1864
1864-5	Erupción 1864	Lava	18H	749353	5575401	Lava de bloques erupción 1864
14-3	Erupción 1864	Bomba	19H	244118	5576320	Ladera este Volcán Mocho-Choshuenco
Enco2	Ignimbrita Enco	Bomba	18H	748116	5575009	Corte de camino cerca de Refugio Andino
11-8B	Ignimbrita Enco	Bomba	19H	252124	5577631	Pampa Pilmaiquén
14-1	CVMC	Bomba	19H	246121	5580350	Camino hacia ladera este del Volcán

A.2 Volúmenes del material volcánico emitido por los CEM

Los volúmenes del material emitido por los CEM fueron calculados a través del procesamiento de un modelo de elevación digital (DEM, sigla en inglés de *Digital Elevation Model*) en el *software* ArcGIS v.10.3, siguiendo el procedimiento detallado en Larrea et al. (2019). La resolución del DEM utilizado es de 12.5 m.

En primer lugar, se construyeron polígonos delimitando el área de los flujos de lava y de los conos de piroclastos, con la finalidad de realizar un cálculo por separado de los volúmenes correspondientes a lavas y piroclastos. Luego, se reconstruyó el relieve topográfico antes del emplazamiento del material volcánico del Grupo Fui, a través de la interpolación de las curvas de nivel de 10 m, y considerando la topografía del área circundante.

La reconstrucción de la topografía se realizó utilizando modelos de redes triangulares irregulares (TIN, sigla en inglés de *Triangulated Irregular Networks*). Primero se construyó una TIN utilizando las curvas de nivel del DEM sin modificar. Luego, se modificaron los datos de elevación de la zona de interés (flujos de lava o conos de piroclastos) restando los espesores de los flujos de lavas y alturas de los conos de piroclastos a través de la observación de la imagen satelital y perfiles de elevación. Posteriormente, se utilizaron los datos de curvas de nivel modificadas para construir una nueva TIN (sin lava y sin cono de piroclasto, según corresponde). De esta manera, fue posible utilizar la herramienta *"Surface Difference"* para calcular la diferencia de volumen entre la TIN original y la modificada.

Este volumen total fue corregido utilizando la vesicularidad de lavas y piroclastos por separado, con datos de las muestras estudiadas en este trabajo (Table 3).

Tabla A.2: Resumen de los resultados de volumen calculados para los distintos CEM, separados por lavas y piroclastos. Bulk corresponde al volumen total sin modificaciones, y DRE es el volumen corregido por las vesículas. Los volúmenes corregidos fueron sumados para estimar un total por subgrupo.

CEM	Vesicularidad [%]	Vol. Bulk [km^3]	Vol. DRE [km^3]	Vol. DRE total [km^3]
Chanchán	2.4	0.175	0.171	0.171
Fui Norte Lava	37.7	0.126	0.079	
Fui Norte Piroclastos	12.2	0.105	0.092	0.171
Fui Sur Lava	27.8	0.374	0.270	
Fui Sur Piroclastos	8.5	0.290	0.265	0.535

A.3 Geoquímica de roca total

Tabla A.3: Análisis de geoquímica de roca total de las 34 muestras seleccionadas del Grupo Fui (Chanchán, Fui Norte y Fui Sur) y el CVMC. FeO determinado por Titration. Fe_2O_3* corresponde al Fe total expresado como Fe_2O_3 (resultado entregado por laboratorio). QC data (*Quality Control*) corresponde a los análisis de estándares y réplicas (REP).

		Chanchán	Fui Norte						
	Detection Limit	15-3	09-1	09-2	09-3	09-8	14-11	16-6B	09-9
SiO_2	0.01 (%)	48.56	50.09	50.10	50.22	50.25	49.77	51.60	50.57
Al_2O_3	0.01 (%)	16.13	17.21	17.27	17.28	17.28	17.60	17.64	17.53
FeO	0.2 (%)	7.15	0.42	0.41	0.41	2.32	6.96	6.61	<0.20
Fe_2O_3*	0.04 (%)	10.02	9.29	9.33	9.42	9.38	9.71	9.30	9.42
MgO	0.01 (%)	10.62	7.61	7.78	7.57	7.72	7.60	5.11	7.15
CaO	0.01 (%)	9.16	8.80	8.81	8.85	8.96	9.23	9.08	8.93
Na_2O	0.01 (%)	2.71	3.33	3.30	3.20	3.18	3.16	3.56	3.24
K_2O	0.01 (%)	0.75	1.01	0.95	0.89	0.92	0.91	1.37	0.85
TiO_2	0.01 (%)	0.99	1.09	1.08	1.09	1.07	1.10	1.34	1.08
P_2O_5	0.01 (%)	0.21	0.32	0.32	0.32	0.31	0.29	0.50	0.31
MnO	0.01 (%)	0.16	0.15	0.16	0.16	0.15	0.16	0.16	0.15
Cr_2O_3	0.002 (%)	0.083	0.040	0.042	0.040	0.041	0.036	0.014	0.039
LOI		0.2	0.7	0.5	0.6	0.4	0.1	0.0	0.4
Cs	0.1 (ppm)	1.4	1.1	1.0	0.9	0.7	0.3	1.0	0.9
Rb	0.1 (ppm)	13.5	20.3	19.8	19.0	18.2	17.3	29.0	16.8
Ba	1 (ppm)	380	411	410	422	404	343	492	391
Th	0.2 (ppm)	4.3	4.0	4.0	3.8	3.7	2.8	4.0	3.7
U	0.1 (ppm)	1.4	0.9	0.9	0.9	0.9	0.7	1.0	0.8
Nb	0.1 (ppm)	3.6	6.0	6.3	6.3	5.9	5.9	11.5	5.9
Ta	0.1 (ppm)	0.2	0.4	0.3	0.5	0.4	0.4	0.6	0.2
La	0.1 (ppm)	16.6	20.7	21.0	21.1	20.9	18.5	31.8	21.1
Ce	0.1 (ppm)	34.9	43.6	44.8	43.1	41.4	38.8	67.4	43.6
Pr	0.02 (ppm)	4.25	5.33	5.28	5.38	5.06	4.96	7.91	5.19
Sr	0.5 (ppm)	686.3	624.9	657.5	663.9	659.9	646.7	739.6	655.1
Nd	0.3 (ppm)	17.8	22.0	21.4	20.8	21.0	20.5	33.0	21.9
Zr	0.1 (ppm)	77.0	123.1	125.3	123.7	116.8	107.3	190.7	119.0
Sm	0.05 (ppm)	3.64	4.76	4.67	4.70	4.43	4.27	6.28	4.38
Eu	0.02 (ppm)	1.20	1.43	1.38	1.39	1.35	1.47	1.84	1.35
Gd	0.05 (ppm)	3.72	4.45	4.32	4.37	4.18	4.21	6.27	4.30
Tb	0.01 (ppm)	0.54	0.65	0.65	0.63	0.63	0.63	0.87	0.62
Dy	0.05 (ppm)	3.14	3.70	3.74	3.84	3.78	3.64	5.06	3.75
Ho	0.02 (ppm)	0.64	0.74	0.80	0.77	0.71	0.73	0.99	0.77
Tm	0.01 (ppm)	0.26	0.31	0.30	0.31	0.28	0.30	0.40	0.30
Y	0.1 (ppm)	16.5	19.5	19.8	19.8	20.0	19.1	25.8	19.4
Er	0.03 (ppm)	1.84	2.10	2.17	2.15	2.17	2.11	2.87	2.15
Yb	0.05 (ppm)	1.63	2.01	2.08	1.98	1.96	1.89	2.50	1.90
Lu	0.01 (ppm)	0.25	0.30	0.33	0.32	0.30	0.29	0.41	0.28

		Fui Norte		Fui Sur					
	Detection Limit	16-1	16-2	16-11	16-12A	FS1	FS3	FS4	17-12
SiO_2	0.01 (%)	50.10	48.65	54.80	55.02	55.62	55.63	55.74	56.88
Al_2O_3	0.01 (%)	17.42	17.93	16.37	16.26	16.23	17.07	16.90	17.05
FeO	0.2 (%)	4.88	5.30	6.65	6.01	6.46	5.66	5.80	6.02
Fe_2O_3*	0.04 (%)	9.40	9.87	10.39	10.33	10.08	9.08	9.05	8.97
MgO	0.01 (%)	7.75	7.39	3.66	3.69	3.41	4.11	4.16	2.84
CaO	0.01 (%)	8.88	8.50	7.51	7.55	7.11	7.27	7.27	6.81
Na_2O	0.01 (%)	3.19	3.12	3.99	3.98	4.15	4.06	4.07	4.44
K_2O	0.01 (%)	0.84	0.96	1.08	1.07	1.17	0.96	0.96	1.09
TiO_2	0.01 (%)	1.08	1.22	1.47	1.46	1.47	1.17	1.18	1.31
P_2O_5	0.01 (%)	0.30	0.37	0.27	0.27	0.28	0.22	0.22	0.27
MnO	0.01 (%)	0.15	0.19	0.18	0.18	0.18	0.17	0.17	0.18
Cr_2O_3	0.002 (%)	0.040	0.032	0.009	0.010	0.011	0.013	0.012	0.006
LOI		0.5	1.4	0.0	-0.1	0.0	0.0	0.0	-0.1
Cs	0.1 (ppm)	1.0	1.3	1.8	1.9	2.0	1.6	1.8	1.8
Rb	0.1 (ppm)	17.8	20.5	25.4	26.3	28.5	22.7	23.1	25.5
Ba	1 (ppm)	400	696	340	328	352	317	310	333
Th	0.2 (ppm)	3.6	6.9	2.9	3.2	3.2	2.4	2.4	2.8
U	0.1 (ppm)	0.9	1.4	0.7	0.9	1.1	0.7	0.6	0.8
Nb	0.1 (ppm)	5.7	9.2	3.0	2.9	3.5	2.6	2.8	3.0
Ta	0.1 (ppm)	0.4	0.6	0.2	0.2	0.2	0.2	0.2	0.2
La	0.1 (ppm)	21.5	31.4	14.8	14.6	15.6	13.3	12.8	15.1
Ce	0.1 (ppm)	43.2	65.5	33.5	33.0	36.4	29.0	28.6	32.2
Pr	0.02 (ppm)	5.29	7.02	4.50	4.51	4.79	3.85	3.82	4.46
Sr	0.5 (ppm)	671.8	835.1	457.5	467.7	445.8	470.6	470.2	466.6
Nd	0.3 (ppm)	22.0	28.0	20.7	21.0	20.8	17.7	17.1	21.4
Zr	0.1 (ppm)	119.6	145.6	126.4	122.5	132.8	101.6	104.0	123.6
Sm	0.05 (ppm)	4.39	5.52	5.17	5.01	5.26	4.58	4.28	5.49
Eu	0.02 (ppm)	1.37	1.69	1.48	1.51	1.64	1.39	1.37	1.62
Gd	0.05 (ppm)	4.38	5.14	5.82	5.90	5.96	5.06	4.92	6.01
Tb	0.01 (ppm)	0.63	0.73	0.89	0.89	0.92	0.77	0.75	0.92
Dy	0.05 (ppm)	3.49	4.15	5.42	5.32	6.03	4.62	4.87	5.68
Ho	0.02 (ppm)	0.76	0.80	1.14	1.18	1.26	1.05	0.97	1.15
Tm	0.01 (ppm)	0.29	0.33	0.47	0.46	0.48	0.40	0.39	0.48
Y	0.1 (ppm)	20.2	22.1	29.8	29.6	31.9	25.2	25.1	33.1
Er	0.03 (ppm)	2.10	2.47	3.50	3.41	3.69	2.97	2.90	3.68
Yb	0.05 (ppm)	1.95	2.07	3.02	3.08	3.23	2.60	2.73	3.15
Lu	0.01 (ppm)	0.31	0.31	0.46	0.47	0.48	0.43	0.41	0.49

		Fui Sur						MCVC	
	Detection Limit	17-14A	17-1A	17-7A	17-8B	17-9	17-10	11-3	14-1
SiO_2	0.01 (%)	56.95	56.37	56.51	56.72	56.53	57.84	56.30	59.96
Al_2O_3	0.01 (%)	16.47	16.73	16.85	16.65	16.93	16.16	17.22	16.33
FeO	0.2 (%)	5.45	5.29	6.13	4.94	6.02	6.26	3.56	4.47
Fe_2O_3*	0.04 (%)	9.30	9.24	9.29	9.13	9.20	9.13	8.92	7.76
MgO	0.01 (%)	2.97	2.90	2.93	2.87	2.92	2.92	2.95	2.38
CaO	0.01 (%)	6.57	6.74	6.78	6.58	6.74	6.09	6.88	5.36
Na_2O	0.01 (%)	4.48	4.43	4.41	4.40	4.44	4.66	4.27	4.86
K_2O	0.01 (%)	1.10	1.09	1.08	1.12	1.11	1.21	1.03	1.32
TiO_2	0.01 (%)	1.36	1.34	1.34	1.33	1.33	1.36	1.27	1.22
P_2O_5	0.01 (%)	0.27	0.26	0.26	0.27	0.27	0.30	0.26	0.31
MnO	0.01 (%)	0.18	0.18	0.18	0.18	0.18	0.19	0.17	0.17
Cr_2O_3	0.002 (%)	0.003	0.005	0.007	0.005	0.006	0.009	0.007	0.004
LOI		0.1	0.5	0.1	0.5	0.1	-0.1	0.5	0.1
Cs	0.1 (ppm)	1.7	1.8	1.8	1.9	1.8	2.0	1.5	2.0
Rb	0.1 (ppm)	25.9	25.9	25.6	25.8	26.2	28.7	24.9	30.6
Ba	1 (ppm)	360	334	340	335	333	376	319	393
Th	0.2 (ppm)	2.9	2.8	2.6	2.7	2.8	3.0	2.7	3.4
U	0.1 (ppm)	0.8	0.8	1.0	0.8	0.9	0.9	0.7	1.0
Nb	0.1 (ppm)	3.3	3.4	3.1	3.1	3.1	3.7	3.1	3.9
Ta	0.1 (ppm)	0.2	0.2	0.2	0.2	0.2	0.3	0.2	0.3
La	0.1 (ppm)	14.7	14.8	14.6	14.0	15.3	15.9	14.6	18.1
Ce	0.1 (ppm)	33.3	34.2	33.0	34.4	33.4	36.3	31.6	39.8
Pr	0.02 (ppm)	4.60	4.50	4.46	4.46	4.49	4.86	4.17	5.17
Sr	0.5 (ppm)	455.0	455.1	481.2	444.2	444.9	443.0	462.4	433.1
Nd	0.3 (ppm)	22.5	21.6	20.3	21.3	20.9	22.3	19.2	22.9
Zr	0.1 (ppm)	127.2	123.6	122.0	122.1	124.5	133.2	118.1	149.6
Sm	0.05 (ppm)	5.26	5.46	5.61	5.13	5.37	5.58	5.03	5.81
Eu	0.02 (ppm)	1.64	1.57	1.56	1.64	1.49	1.72	1.48	1.68
Gd	0.05 (ppm)	6.08	5.94	5.95	5.81	5.99	6.31	5.55	6.33
Tb	0.01 (ppm)	0.92	0.94	0.91	0.92	0.91	0.99	0.89	1.02
Dy	0.05 (ppm)	6.03	5.88	5.46	5.49	5.81	5.92	5.16	5.96
Ho	0.02 (ppm)	1.22	1.21	1.22	1.19	1.23	1.28	1.18	1.34
Tm	0.01 (ppm)	0.50	0.48	0.49	0.49	0.50	0.53	0.48	0.52
Y	0.1 (ppm)	31.4	31.9	31.9	30.9	30.9	33.2	29.6	32.9
Er	0.03 (ppm)	3.76	3.42	3.71	3.49	3.64	3.81	3.47	3.88
Yb	0.05 (ppm)	3.31	3.35	3.15	3.12	3.28	3.45	3.18	3.57
Lu	0.01 (ppm)	0.50	0.52	0.50	0.50	0.51	0.54	0.48	0.55

		MCVC							
	Detection Limit	16-13B	16-14A	11-8B	14-3	Enco2	1864-1	1864-2	1864-3
SiO_2	0.01 (%)	54.68	54.85	59.57	53.52	57.38	62.99	62.95	63.03
Al_2O_3	0.01 (%)	16.48	16.39	16.47	17.66	17.42	15.91	15.93	16.02
FeO	0.2 (%)	6.31	6.50	5.05	4.32	5.07	4.46	3.81	4.41
Fe_2O_3*	0.04 (%)	10.28	10.41	7.78	8.96	8.02	6.37	6.37	6.44
MgO	0.01 (%)	3.67	3.63	2.38	5.11	2.84	1.70	1.71	1.74
CaO	0.01 (%)	7.62	7.54	5.38	8.60	6.67	4.28	4.33	4.36
Na_2O	0.01 (%)	3.93	4.00	4.92	3.58	4.35	5.24	5.22	5.27
K_2O	0.01 (%)	1.06	1.07	1.33	0.78	1.08	1.60	1.59	1.61
TiO_2	0.01 (%)	1.44	1.47	1.23	1.06	1.17	1.09	1.09	1.09
P_2O_5	0.01 (%)	0.27	0.26	0.32	0.18	0.27	0.35	0.35	0.36
MnO	0.01 (%)	0.18	0.18	0.17	0.16	0.16	0.16	0.16	0.16
Cr_2O_3	0.002 (%)	0.010	0.010	0.003	0.013	0.002	0.011	0.007	0.008
LOI		0.1	-0.1	0.2	0.1	0.4	0.1	0.1	-0.3
Cs	0.1 (ppm)	1.7	1.8	2.1	1.4	1.9	2.4	2.9	2.8
Rb	0.1 (ppm)	25.9	26.5	32.0	18.2	25.5	38.1	39.9	38.9
Ba	1 (ppm)	329	339	403	238	325	492	502	479
Th	0.2 (ppm)	2.9	3.1	3.5	1.8	2.8	4.4	3.6	4.0
U	0.1 (ppm)	1.0	0.9	1.1	0.4	0.7	1.2	1.2	1.2
Nb	0.1 (ppm)	3.0	3.2	3.8	2.1	3.2	4.4	4.6	4.6
Ta	0.1 (ppm)	0.1	0.2	0.3	0.2	0.2	0.3	0.3	0.3
La	0.1 (ppm)	14.4	15.2	17.8	9.9	14.7	22.3	22.0	20.1
Ce	0.1 (ppm)	34.1	33.8	39.8	23.3	32.8	48.7	47.4	47.6
Pr	0.02 (ppm)	4.49	4.57	5.16	3.11	4.43	6.12	6.15	6.02
Sr	0.5 (ppm)	462.8	475.1	447.3	482.7	486.7	391.3	405.6	392.8
Nd	0.3 (ppm)	21.0	20.8	23.6	14.9	19.4	27.6	26.4	28.0
Zr	0.1 (ppm)	120.9	126.6	147.8	85.2	121.2	174.4	174.9	173.1
Sm	0.05 (ppm)	5.23	5.13	5.82	3.62	4.79	6.46	6.67	6.41
Eu	0.02 (ppm)	1.50	1.48	1.70	1.18	1.53	1.84	1.77	1.86
Gd	0.05 (ppm)	5.75	5.75	6.28	4.19	5.45	7.30	7.08	7.23
Tb	0.01 (ppm)	0.90	0.88	1.02	0.63	0.85	1.12	1.09	1.09
Dy	0.05 (ppm)	5.39	5.68	6.18	3.96	5.50	6.81	6.99	6.72
Ho	0.02 (ppm)	1.19	1.18	1.29	0.81	1.09	1.38	1.44	1.48
Tm	0.01 (ppm)	0.46	0.50	0.55	0.35	0.44	0.60	0.57	0.60
Y	0.1 (ppm)	30.3	31.7	32.4	21.6	27.6	37.8	37.6	37.3
Er	0.03 (ppm)	3.35	3.40	3.85	2.38	3.30	4.23	4.20	4.17
Yb	0.05 (ppm)	2.94	3.01	3.49	2.23	3.03	3.89	3.95	3.81
Lu	0.01 (ppm)	0.47	0.49	0.55	0.35	0.47	0.58	0.62	0.60

		MCVC		QC Data				
	Detection Limit	1864-4	1864-5	SO-19	SO-19	SO-19 cert	1864-1 REP	1864-4 REP
SiO_2	0.01 (%)	62.88	62.81	60.57	60.45	61.13	63.06	-
Al2O3	0.01 (%)	16.09	16.05	13.91	13.94	13.95	15.95	-
FeO	0.2 (%)	4.50	4.45	-	-	-	-	-
Fe_2O_3*	0.04 (%)	6.40	6.41	7.49	7.52	7.47	6.29	-
MgO	0.01 (%)	1.71	1.72	2.92	2.93	2.88	1.69	-
CaO	0.01 (%)	4.32	4.35	5.92	5.93	6	4.27	-
Na_2O	0.01 (%)	5.30	5.29	4.01	4.02	4.11	5.23	-
K_2O	0.01 (%)	1.62	1.61	1.26	1.29	1.29	1.59	-
TiO_2	0.01 (%)	1.10	1.10	0.70	0.70	0.69	1.09	-
P_2O_5	0.01 (%)	0.36	0.35	0.33	0.32	0.32	0.36	-
MnO	0.01 (%)	0.16	0.16	0.13	0.13	0.13	0.16	-
Cr_2O_3	0.002 (%)	0.006	0.013	0.497	0.504	0.5	0.009	-
LOI		-0.2	-0.1	1.9	1.9	-	0.1	-
Cs	0.1 (ppm)	2.8	2.6	4.9	4.6	4.5	-	2.6
Rb	0.1 (ppm)	38.9	38.2	20.1	20.1	19.5	-	38.2
Ba	1 (ppm)	487	483	469	471	486	-	484
Th	0.2 (ppm)	4.1	4.0	13.1	13.2	13	-	3.9
U	0.1 (ppm)	1.3	1.2	19.7	20.6	19.4	-	1.0
Nb	0.1 (ppm)	4.8	4.8	65.5	72.7	68.5	-	5.1
Ta	0.1 (ppm)	0.3	0.3	4.6	5.0	4.9	-	0.4
La	0.1 (ppm)	21.2	22.2	73.4	74.8	71.3	-	21.3
Ce	0.1 (ppm)	45.2	46.1	162.2	163.0	161	-	46.1
Pr	0.02 (ppm)	6.08	6.08	19.18	19.56	19.4	-	6.03
Sr	0.5 (ppm)	387.9	388.7	327.0	324.8	317.1	-	388.1
Nd	0.3 (ppm)	26.9	27.2	74.8	77.2	75.7	-	26.7
Zr	0.1 (ppm)	172.7	174.2	110.9	115.5	112	-	174.1
Sm	0.05 (ppm)	6.59	6.51	12.72	13.38	13.7	-	6.62
Eu	0.02 (ppm)	1.89	1.77	3.58	3.67	3.81	-	1.80
Gd	0.05 (ppm)	7.27	7.17	10.25	10.62	10.53	-	6.97
Tb	0.01 (ppm)	1.10	1.09	1.38	1.42	1.41	-	1.14
Dy	0.05 (ppm)	6.87	6.98	7.51	7.08	7.5	-	6.71
Ho	0.02 (ppm)	1.44	1.42	1.36	1.41	1.39	-	1.44
Tm	0.01 (ppm)	0.59	0.60	0.54	0.51	0.55	-	0.58
Y	0.1 (ppm)	38.5	37.0	33.2	36.0	35.5	-	36.5
Er	0.03 (ppm)	4.28	4.24	3.80	3.82	3.78	-	4.32
Yb	0.05 (ppm)	3.87	3.99	3.32	3.51	3.55	-	3.94
Lu	0.01 (ppm)	0.58	0.59	0.51	0.51	0.53	-	0.60

Titration	
QC Data	FeO
OREAS 700	11.88
OREAS 700	11.74
OREAS 700 cert	12.07
SY-4	2.74
SY-4	2.76
SY-4 cert	2.86
09-3 REP	0.47
17-2 REP	6.01
16-1 REP	4.87

A.4 Química mineral (EPMA) de lavas del Grupo Fui

Tabla A.4.1: Análisis de química mineral mediante microsonda electrónica (EPMA) de fenocristales (ph), microfenocristales (mph) y microlitos (m) de olivino. (c=core, núcleo y r=rim, borde).

	Análisis Puntuales - LAMARX - Universidad Nacional de Córdoba														
	Point	Type	Na_2O (Wt%)	MgO (Wt%)	Al_2O_3 (Wt%)	SiO_2 (Wt%)	TiO_2 (Wt%)	Cr_2O_3 (Wt%)	MnO (Wt%)	FeO (Wt%)	K_2O (Wt%)	CaO (Wt%)	NiO (Wt%)	ZnO (Wt%)	Total (Wt%)
Chanchán	15-3-Ol-30-1	ph-c	0.006	46.63	0.007	40.33	0.034	0.044	0.185	12.92	0	0.136	0.319	0.024	100.6
	15-3-Ol-30-2	ph-c	0.034	46.96	0.019	40.21	0	0.028	0.208	12.21	0	0.129	0.343	0	100.1
	15-3-Ol-30-3	ph-c	0	46.58	0.017	39.16	0	0	0.173	12.36	0	0.138	0.347	0	98.78
	15-3-Ol-22-4	ph-c	0.005	36.78	0.034	37.81	0	0	0.48	25.12	0.005	0.076	0.11	0.07	100.5
	15-3-Ol-22-5	ph-r	0.002	44.23	0.031	39.34	0	0.065	0.241	16.09	0	0.183	0.127	0.064	100.4
	15-3-Ol-B-6	ph-c	0	45.02	0.023	39.5	0.046	0.03	0.184	14.38	0	0.147	0.165	0.03	99.52
	15-3-Ol-S2-7	ph-c	0	44.25	0.011	39.29	0.046	0	0.253	15.81	0	0.166	0.135	0.047	100
	15-3-Ol-S2-8	ph-r	0	37.27	0.028	37.83	0.045	0.037	0.477	23.15	0	0.266	0	0.124	99.23
	15-3-Ol-2-9	ph-c	0.008	46.16	0.024	39.64	0.069	0	0.161	13.38	0	0.138	0.242	0.05	99.87
	15-3-Ol-2-10	ph-c	0	45.13	0.016	39.41	0	0.073	0.196	15.06	0.001	0.158	0.193	0	100.2
	15-3-Ol-9-11	ph-c	0.014	45.62	0.031	39.5	0.16	0.005	0.173	13.51	0	0.147	0.288	0	99.45
	15-3-Ol-9-12	ph-r	0.015	40.33	0.027	38.27	0.09	0.011	0.419	19.44	0	0.234	0.135	0.053	99.02
	15-3-Ol-29-13	ph-c	0	48.13	0.04	40.78	0.08	0.039	0.166	11.65	0	0.124	0.404	0.01	101.4
	15-3-Ol-31-14	ph-c	0.012	47.26	0.031	40.45	0.092	0.052	0.204	12.29	0	0.119	0.41	0	100.9
	15-3-Ol-31-15	ph-c	0	47.55	0.02	40.38	0.115	0.044	0.189	11.23	0	0.14	0.529	0	100.2
	15-3-Ol-31-16	ph-c	0	46.08	0	39.63	0	0.022	0.123	13.05	0	0.123	0.342	0.045	99.41
	15-3-Ol-27-17	ph-r	0	46.2	0.033	39.12	0	0.033	0.258	13.3	0	0.16	0.236	0	99.34
	15-3-Ol-28-18	ph-c	0	44.8	0.005	39.7	0.034	0.03	0.284	15.42	0	0.191	0.189	0	100.7
	15-3-Ol-28-19	ph-r	0.027	37.24	0.031	38.09	0	0.013	0.466	24.13	0.007	0.323	0.028	0.017	100.4
	15-3-Ol-21-20	ph-c	0	45.66	0.032	39.37	0	0.03	0.192	13.62	0	0.159	0.276	0	99.34
	15-3-Ol-21-21	ph-c	0.012	46.15	0.038	40.21	0	0.011	0.208	13.74	0	0.134	0.17	0.04	100.7
	15-3-Ol-21-22	ph-c	0	45.85	0.007	39.55	0.046	0.057	0.234	13.6	0	0.15	0.24	0.058	99.79
	15-3-Ol-16-23	ph-c	0.009	36.21	0	37.84	0.1	0.003	0.411	25.68	0	0.018	0.131	0.046	100.4
	15-3-Ol-16-24	ph-r	0	44.85	0.033	39.6	0	0.027	0.169	15.27	0	0.158	0.172	0.08	100.4
	15-3-Ol-11-25	ph-c	0.002	46.23	0	39.67	0	0.033	0.142	13.59	0	0.153	0.255	0.01	100.1
	15-3-Ol-11-26	ph-c	0.01	46.41	0.011	39.27	0.023	0.036	0.192	13.33	0.003	0.141	0.324	0	99.75
	15-3-Ol-8-27	ph-c	0	44.33	0.026	39.09	0.046	0.022	0.226	15.46	0.002	0.142	0.204	0.061	99.61
	15-3-Ol-3-28	ph-c	0.201	46.11	0.02	39.35	0.103	0.014	0.215	12.96	0.028	0.245	0.294	0.017	99.56
	15-3-Ol-3-29	ph-c	0	45.9	0.027	39.88	0	0.055	0.246	13.63	0.012	0.151	0.281	0	100.2
	15-3-Ol-4-30	ph-c	0	46.93	0.013	40.48	0	0.027	0.169	13.29	0	0.138	0.3	0.074	101.4
	15-3-Ol-4-31	ph-r	0	42.04	0	38.72	0	0.016	0.263	18.62	0	0.219	0.186	0.091	100.2
	15-3-Ol-4-32	ph-c	0	47.45	0.035	40.4	0.081	0.05	0.177	11.36	0	0.124	0.432	0.028	100.1
	15-3-Ol-4-33	ph-c	0.018	45.66	0.015	39.93	0.023	0.03	0.162	13.65	0	0.139	0.22	0.022	99.87
	15-3-Ol-20-34	ph-c	0.002	46.16	0.037	39.91	0.069	0.06	0.188	13.68	0.01	0.143	0.316	0.047	100.6
	15-3-Ol-19-35	ph-c	0	44.79	0	39.65	0	0.022	0.219	14.95	0	0.169	0.208	0	100

	Análisis Puntuales - LAMARX - Universidad Nacional de Córdoba														
	Point	Type	Na_2O (Wt%)	MgO (Wt%)	Al_2O_3 (Wt%)	SiO_2 (Wt%)	TiO_2 (Wt%)	Cr_2O_3 (Wt%)	MnO (Wt%)	FeO (Wt%)	K_2O (Wt%)	CaO (Wt%)	NiO (Wt%)	ZnO (Wt%)	Total (Wt%)
Chanchán	15-3-Ol-18-36	ph-c	0.021	44.94	0.005	39.21	0	0	0.196	15.03	0.012	0.167	0.223	0.07	99.87
	15-3-Ol-18-37	ph-r	0	43.74	0.015	39.33	0	0.057	0.321	17.43	0	0.228	0.094	0.065	101.3
	15-3-Ol-18-38	ph-r	0.016	37.88	0.026	37.65	0.011	0	0.36	23.51	0.008	0.281	0.035	0.074	99.85
	15-3-Ol-15-39	ph-c	0.006	47.1	0.038	40.42	0	0.094	0.077	11.41	0.008	0.123	0.501	0	99.78
	15-3-Ol-14-40	ph-c	0.006	46.29	0.021	39.94	0.023	0.008	0.15	13.28	0	0.145	0.306	0	100.2
	15-3-Ol-14-41	ph-c	0	46.42	0.014	40.43	0.034	0.107	0.169	13.1	0	0.145	0.217	0	100.6
	15-3-Ol-14-42	ph-c	0.03	46.56	0.04	39.65	0.046	0	0.177	13.02	0	0.153	0.219	0.005	99.9
	15-3-Ol-5-43	ph-c	0.012	47.75	0.009	40.15	0	0.019	0.066	11.51	0	0.136	0.406	0.031	100.1
	15-3-Ol-5-44	ph-c	0.016	47.03	0.032	40.28	0	0.044	0.181	12.79	0	0.125	0.302	0	100.8
	15-3-Ol-5-45	ph-c	0	46.84	0.029	40.35	0.023	0.033	0.2	13.03	0.006	0.141	0.317	0.025	101
	15-3-Ol-6-46	ph-c	0.006	45.44	0.011	40.06	0.011	0.014	0.238	14.15	0.003	0.158	0.284	0.073	100.4
	15-3-Ol-6-47	ph-r	0.013	38.61	0.061	38.3	0.045	0	0.455	22.91	0	0.319	0	0.023	100.7
	15-3-Ol-6-48	ph-c	0.006	47.02	0.015	39.91	0.138	0.055	0.196	11.79	0	0.135	0.422	0.049	99.74
	15-3-Ol-6-49	ph-r	0.019	42.8	0.007	39.52	0	0	0.363	17.2	0	0.207	0.11	0	100.2
	15-3-Ol-6-50	ph-c	0.031	45.53	0.019	39.46	0.069	0.016	0.223	14.17	0.006	0.166	0.285	0.031	100
	15-3-Ol-7-51	ph-c	0.015	44.21	0.026	39.37	0	0.003	0.287	16.34	0	0.172	0.095	0.062	100.6
	15-3-Ol-25-52	ph-c	0.008	46.01	0.04	39.66	0.034	0.041	0.265	13.27	0.007	0.145	0.308	0.084	99.87
	15-3-Ol-25-53	ph-3	0.015	43.63	0.032	38.75	0.079	0	0.264	16.77	0.006	0.2	0.119	0.006	99.87
	15-3-Ol-D-54	ph-c	0.013	44.06	0.025	39.24	0.023	0.03	0.249	16.83	0.01	0.193	0.125	0.15	100.9
	15-3-Ol-D-55	ph-c	0.011	43.59	0.02	39.35	0	0.005	0.226	16.84	0	0.195	0.139	0	100.4
	15-3-Ol-mf-56	m	0.048	31.09	0.058	35.82	0.055	0.005	0.493	30.84	0.01	0.451	0.013	0.037	98.92
	15-3-Ol-mf-58	m	0	38.52	0.039	37.54	0.112	0	0.29	22.3	0	0.272	0.018	0.062	99.15
	15-3-Ol-mf-59	m	0.036	36.28	0.027	37.21	0.19	0	0.361	24.72	0.003	0.351	0.062	0	99.24
	15-3-Ol-mf-60	m	0	37.06	0.047	37.42	0.09	0	0.483	23.79	0.008	0.35	0.035	0.068	99.35
	15-3-Ol-mf-62	m	0	30.23	0.028	35.93	0.219	0	0.379	32.09	0	0.391	0	0.053	99.32
Fui Norte	166B-Ol-A-1	mph-c	0.046	35.19	0.021	37.91	0.056	0.066	0.501	26.61	0.008	0.346	0.027	0	100.8
	166B-Ol-A-7	mph-c	0.028	34.15	0.038	37.62	0.034	0.008	0.642	26.89	5E-04	0.394	0.07	0.148	100
	166B-Ol-B-8	mph-c	0	35.4	0.021	37.42	0.101	0	0.506	25.43	0.006	0.339	0.008	0.045	99.28
	166B-Ol-CP1-14	mph-c	0	36.84	0.029	38.14	0.091	0.059	0.35	23.88	0	0.369	0.067	0.013	99.84
	166B-Ol-8-18	mph-c	0.04	34.27	0.004	37.61	0.034	0	0.452	26.72	0	0.376	0.001	0.015	99.52
	166B-Ol-8-23	mph-c	0.032	35.54	0.03	37.95	0	0.005	0.464	25.57	0.006	0.371	0.026	0.062	100.1
	166B-Ol-8-24	mph-c	0.007	38.96	0.006	38.87	0	0.016	0.343	22.27	0	0.211	0.124	0.148	101
	166B-Ol-H-25	mph-c	0.035	35.06	0.035	38.1	0.068	0.05	0.505	26.34	0.018	0.386	0.068	0.056	100.7
	166B-Ol-H-26	mph-c	0.009	34.27	0.041	37.5	0	0	0.505	26.98	0	0.347	0.011	0	99.66
	166B-Ol-H-31	mph-c	0.014	35.57	0.086	37.74	0.011	0	0.429	24.82	0.004	0.493	0.039	0.059	99.26
	166B-Ol-G-34	mph-c	0	35.2	0.041	37.5	0	0.008	0.524	25.95	0.006	0.292	0.027	0.035	99.58
	166B-Ol-CP4-35	mph-c	0	36.25	0.022	37.8	0	0	0.368	25.8	0	0.273	0.013	0.109	100.6
	166B-Ol-CP4-36	mph-c	0	36.49	0.024	38.44	0.011	0.037	0.445	25.13	0.009	0.342	0.002	0.011	100.9

	Análisis Puntuales - LAMARX - Universidad Nacional de Córdoba														
	Point	Type	Na_2O (Wt%)	MgO (Wt%)	Al_2O_3 (Wt%)	SiO_2 (Wt%)	TiO_2 (Wt%)	Cr_2O_3 (Wt%)	MnO (Wt%)	FeO (Wt%)	K_2O (Wt%)	CaO (Wt%)	NiO (Wt%)	ZnO (Wt%)	Total (Wt%)
Fui Norte	166B-Ol-CP4-37	mph-c	0.03	36.8	0.036	37.99	0	0	0.46	24.39	0	0.271	0.004	0.139	100.1
	166B-Ol-CP4-38	mph-c	0	35.85	0.031	37.83	0	0.034	0.456	25.52	0.012	0.355	0.013	0.026	100.1
	166B-Ol-17-45	ph-c	0	41.13	0	39	0.046	0.084	0.283	18.93	0.005	0.173	0.054	0.068	99.77
	166B-Ol-17-46	ph-r	0	34.82	0.07	37.66	0.022	0	0.512	26.45	0	0.321	0.022	0.059	99.94
	166B-Ol-9-47	ph-c	0	42	0.017	39.19	0.138	0.027	0.325	18.48	0.007	0.17	0.071	0.026	100.4
	166B-Ol-9-48	ph-r	0	37.73	0.026	38.38	0.045	0	0.373	23.11	0	0.206	0.109	0.131	100.1
	166B-Ol-9-53	ph-r	0.605	26.64	1.687	37.62	0.4	0	0.452	31.32	0.321	0.496	0.025	0.033	99.6
	166B-Ol-5-59	mph-c	0	34.49	0	37.61	0.09	0	0.508	27.24	0	0.328	0	0.04	100.3
	166B-Ol-5-60	mph-c	0.005	35.06	0.029	37.65	0.112	0.003	0.524	26.75	0	0.31	0.048	0.052	100.5
	166B-Ol-5-61	mph-c	0.023	34.27	0.02	37.46	0.124	0	0.478	26.67	0	0.334	0	0.025	99.4
	166B-Ol-5-62	mph-c	0	34.57	0.021	37.25	0	0	0.474	27.25	0	0.364	0.048	0.051	100
	166B-Ol-5-65	mph-c	0	34.49	0.045	37.16	0.067	0	0.584	26.95	0.003	0.337	0.018	0.05	99.7
	166B-Ol-c-66	mph-c	0	35.76	0.014	37.83	0.146	0.021	0.62	25.28	0.001	0.3	0.048	0	100
	166B-Ol-1-69	ph-c	0.017	41.48	0.032	39.07	0.034	0.016	0.321	19.3	0.002	0.18	0.165	0.128	100.7
	166B-Ol-1-70	ph-r	0	37.91	0	38.4	0.102	0.035	0.381	22.38	0	0.224	0.042	0.011	99.48
	166B-Ol-1-78	mph-c	0	37.44	0.009	38.08	0.102	0.005	0.472	23.5	0.013	0.297	0.066	0.008	99.99
	166B-Ol-1-79	mph-c	0.037	34.87	0.03	37.35	0	0.026	0.497	26.2	0	0.368	0.016	0.043	99.44
	166B-Ol-1-80	mph-r	0	34.82	0.029	38.24	0	0	0.463	26.33	0	0.33	0.047	0.091	100.3
	166B-Ol-1-81	ph-c	0.002	42.87	0.025	39.21	0.069	0.003	0.215	17.89	0	0.171	0.222	0	100.7
	166B-Ol-1-82	ph-r	0.007	36.29	0.026	37.67	0.034	0	0.428	25.49	8E-04	0.238	0.031	0	100.2
	166B-Ol-10-85	ph-c	0.02	42.05	0.003	39.13	0	0	0.295	19.1	0	0.19	0.108	0	100.9
	166B-Ol-10-89	mph-c	0	39.06	0.002	38.06	0.046	0	0.448	21.81	0.003	0.247	0.071	0.001	99.75
	166B-Ol-10-90	mph-c	0	38.7	0.003	38.55	0	0.016	0.467	22.11	0	0.304	0.126	0.07	100.3
	166B-Ol-D1-92	mph-c	0.011	36.67	0.016	38.1	0	0.005	0.461	25.01	0	0.281	0.036	0.166	100.8
	166B-Ol-2-98	mph-c	0	41.22	0.01	39.18	0.092	0.043	0.329	19.46	0	0.189	0.104	0.077	100.7
	166B-Ol-11-102	ph-c	0	41.51	0.01	38.86	0	0.014	0.259	19.16	0	0.183	0.131	7E-04	100.1
	166B-Ol-11-103	ph-r	0.009	36.74	0.038	38.07	0.056	0.053	0.491	25.05	0	0.223	0.073	0.03	100.8
	166B-Ol-11-104	ph-r	0	36.64	0.012	37.64	0.158	0.027	0.334	24.9	0	0.232	0.067	0.111	100.1
	166B-Ol-16-107	ph-c	0	40.69	0.015	39.02	0.183	0.024	0.363	20.32	0	0.199	0.087	0.114	101
	166B-Ol-16-111	mph-c	0	35.38	0.039	37.35	0.067	0.039	0.486	26.42	0	0.33	0	0.004	100.1
	166B-Ol-E-116	mph-c	0.016	35.95	0.006	37.53	0.011	0.037	0.502	25.29	0	0.262	0.077	0.014	99.7
	166B-Ol-F-117	mph-c	0	36.71	0.056	37.74	0	0.042	0.457	24.7	0.008	0.276	0.041	0.045	100.1
	166B-Ol-F-118	mph-c	0	36.63	0.049	37.69	0	0.013	0.449	24.91	0.003	0.302	0.058	0.069	100.2
	166B-Ol-MF1-123	m	0.007	34.5	0.024	37.76	0.09	0	0.493	27	0.018	0.343	0.002	0.055	100.3
	166B-Ol-MF1-122	m	0.014	34.56	0.017	37.66	0	0	0.558	27.09	0	0.339	0.034	0.115	100.4
	166B-Ol-MF2-127	m	0	35.17	0.034	37.94	0	0.005	0.463	26.92	0.001	0.301	0.002	0	100.8
	166B-Ol-MF2-128	m	0	34.52	0.021	37.03	0	0	0.436	26.96	0	0.303	0	0.059	99.33

	Análisis Puntuales - LAMARX - Universidad Nacional de Córdoba														
	Point	Type	Na_2O (Wt%)	MgO (Wt%)	Al_2O_3 (Wt%)	SiO_2 (Wt%)	TiO_2 (Wt%)	Cr_2O_3 (Wt%)	MnO (Wt%)	FeO (Wt%)	K_2O (Wt%)	CaO (Wt%)	NiO (Wt%)	ZnO (Wt%)	Total (Wt%)
Fui Sur	FS4-Ol-6-2	ph-r	0.026	32.6	0.011	37.29	0.111	0	0.624	29.71	0.006	0.229	0.051	0.06	100.7
	FS4-Ol-6-3	mph-c	0.051	31.34	0	36.92	0	0.028	0.565	31.74	2E-04	0.201	0.019	0	100.9
	FS4-Ol-6-4	ph-c	0.043	42.62	0.021	39.35	0	0.027	0.287	17.43	0	0.189	0.164	0	100.1
	FS4-Ol-11-13	ph-c	0.022	41.51	0	38.43	0.069	0.027	0.351	19.56	1E-04	0.192	0.144	0.07	100.4
	FS4-Ol-11-14	ph-r	0.004	43.96	0.046	39.84	0.023	0.036	0.241	16.51	0	0.161	0.167	0	101
	FS4-Ol-X2-16	ph-c	0	42.98	0.008	39.6	0	0.014	0.379	17.96	0.017	0.166	0.125	0	101.2
	FS4-Ol-L-25	mph-c	0	35.28	0.01	37.57	0	0.026	0.504	27.24	0.005	0.171	0.052	0	100.9
	FS4-Ol-29-28	ph-c	0	43.66	0.213	39.81	0.069	0.003	0.268	16.75	0	0.193	0.161	0.024	101.1
	FS4-Ol-23-30	ph-c	0	43.21	0.023	39.09	0.057	0.011	0.318	17.84	0.016	0.179	0.249	0	101
	FS4-Ol-23-31	ph-c	0.002	44.93	0.027	39.76	0.058	0.036	0.256	15.39	0.002	0.166	0.225	0.006	100.9
	FS4-Ol-23-32	ph-r	0	42.49	0.016	39.13	0.08	0	0.368	18.21	0.008	0.171	0.151	0	100.6
	FS4-Ol-22-34	ph-c	0	34.99	0.002	38.15	0	0.003	0.454	27.7	0	0.163	0	0	101.5
	FS4-Ol-13-39	ph-c	0.022	41.1	0.013	39.1	0.011	0.057	0.278	19.63	0	0.193	0.053	0	100.5
	FS4-Ol-14-42	ph-c	0.031	40.7	0.037	39.33	0.057	0.008	0.293	20.47	0.002	0.181	0.121	0.028	101.3
	FS4-Ol-10-43	ph-c	0.023	43.98	0	40.01	0	0.017	0.221	16.3	0	0.195	0.127	0	100.9
	FS4-Ol-H-49	mph-c	0	35.91	0.027	37.81	0.135	0	0.592	26.34	0.005	0.187	0.068	0.119	101.2
	FS4-Ol-H-50	mph-c	0.068	37.23	0.022	38.33	0	0.021	0.433	24.78	0.003	0.183	0	0	101.1
	FS4-Ol-2-53	ph-c	0	43.16	0.026	39.68	0.057	0	0.236	17.79	0	0.199	0.167	0	101.3
	FS4-Ol-2-54	ph-r	0.02	41.09	0.021	38.96	0.023	0.089	0.386	20.18	0	0.148	0.237	0	101.2
	FS4-Ol-2-55	ph-r	0.02	39.38	0.038	38.42	0	0.029	0.419	22.75	0.006	0.168	0.063	0.019	101.3
	FS4-Ol-A-61	mph-c	0	34.22	0.013	37.29	0.078	0	0.491	28.97	0.004	0.192	0.055	0.033	101.3
	FS4-Ol-F-64r	mph-c	0	33.58	0.013	37.37	0.077	0	0.657	29.22	0.005	0.231	0	0	101.2
	FS4-Ol-8-67	ph-c	0	44.73	0.016	40.03	0.012	0.006	0.167	15.99	0	0.19	0.142	0	101.3
	FS4-Ol-9-68	ph-c	0	42.78	0.005	39.04	0.011	0.033	0.282	17.77	0	0.162	0.164	0.057	100.3
	FS4-Ol-30-79	ph-c	0	41.45	0.007	39.31	0	0.008	0.243	20.19	0	0.201	0.033	0.013	101.5
	FS4-Ol-MF1-105	m	0	21.41	0.571	33.59	0.075	0	1.039	42.26	0.016	0.313	0	0	99.27
	FS4-Ol-MF1-106	m	0	22.06	0.036	34.61	0.14	0	0.764	42.63	0.02	0.318	0	0.076	100.7
	FS4-Ol-4S-107	ph-r	0	29.24	0.007	35.86	0.165	0.028	0.582	33.78	0.011	0.196	0.012	0.096	99.98
	FS4-Ol-4S-108	ph-r	0.017	32.98	0.02	36.68	0	0.01	0.62	28.64	0	0.254	0.011	0.093	99.32
	FS4-Ol-4S-109	ph-r	0.009	34.06	0.03	36.73	0	0	0.488	27.78	0	0.194	0	0	99.29

	Análisis Puntuales - University of Bristol (Jeol)													
	Point	Type	Na_2O (Wt%)	MgO (Wt%)	Al_2O_3 (Wt%)	SiO_2 (Wt%)	TiO_2 (Wt%)	Cr_2O_3 (Wt%)	MnO (Wt%)	FeO (Wt%)	K_2O (Wt%)	CaO (Wt%)	NiO (Wt%)	Total (Wt%)
Fui Norte	16-6B-ol3-1	mph-c	0.013	37	0.05	37.94	0.025	0.002	0.437	23.37	0	0.294	0.056	99.19
	16-6B-ol3-2	mph-c	6E-04	37.42	0.046	37.86	0.021	0.008	0.434	23.59	0.003	0.243	0.05	99.68
	16-6B-ol3-3	mph-c	0.012	37.33	0.028	37.93	0.02	0.018	0.419	23.33	0	0.246	0.056	99.39
	16-6B-ol5-1	mph-c	0.001	35.97	0.024	37.7	0.013	0.019	0.471	25	0	0.224	0.057	99.48
	16-6B-ol5-2	mph-c	0	37.81	0.028	38.2	0.014	0.025	0.412	22.83	0.006	0.193	0.067	99.57
	16-6B-ol5-3	mph-c	0	38.58	0.02	38.19	0.01	0	0.396	21.93	0	0.191	0.08	99.37
	16-6B-olD-1	mph-c	0	36.17	0.038	37.61	0.026	0.027	0.461	24.41	0.006	0.261	0.034	99.04
	16-6B-ol8-1	mph-c	0	40.4	0.035	38.81	0.015	0.005	0.352	19.71	0.008	0.212	0.105	99.65
	16-6B-ol8-2	ph-r	0.013	34.56	0.056	37.23	0.038	0.007	0.509	26.6	0	0.305	0.028	99.35
	16-6B-ol8-3	ph-c	0.012	40.24	0.048	38.87	0.017	0.009	0.336	20.23	0	0.248	0.101	100.1
	16-6B-ol10-1	mph-c	0.015	39.17	0.027	38.46	0.009	0.019	0.367	20.98	0.008	0.217	0.099	99.38
	16-6B-ol10-2	mph-c	0	39.11	0.025	38.43	0.02	0.028	0.38	20.84	0	0.267	0.099	99.2
	16-6B-ol10-3	mph-c	0	39.08	0.026	38.51	0.01	0.024	0.401	21.46	0	0.241	0.095	99.84
	16-6B-ol13-1	ph-c	0	41.83	0.009	39.01	0.007	0	0.294	18	0.005	0.178	0.134	99.46
	16-6B-ol13-2	ph-r	0	35.31	0.043	37.87	0.026	0.013	0.495	26.2	0.005	0.277	0.04	100.3
	16-6B-ol16-1	mph-c	0.001	41.73	0.029	39.26	0.011	0.002	0.3	18.13	0	0.18	0.139	99.77
	16-6B-ol16-2	mph-c	0.005	40.96	0.031	38.96	0.013	0.029	0.313	18.99	0.005	0.225	0.111	99.64
	16-6B-ol16-4	mph-c	0.004	41	0.03	39.05	0.016	0	0.331	19.18	0.007	0.208	0.121	99.94
	16-6B-ol16-5	mph-r	0.006	36.51	0.034	37.73	0.022	0.016	0.444	24.15	0	0.335	0.067	99.32
	16-6B-ol17-1	ph-c	0.012	41.29	0.028	39.06	0.007	0	0.303	18.4	0	0.176	0.112	99.37
	16-6B-olC-1	mph-c	0.003	36.23	0.033	37.81	0.015	0	0.46	24.64	0.001	0.248	0.032	99.46
	16-6B-ol-CP1-1	mph-c	0.007	37.67	0.021	38.02	0.02	0.012	0.417	22.96	0.003	0.318	0.053	99.49
	16-6B-ol-CP1-2	mph-c	0.007	37.91	0.031	38.4	0.022	0.009	0.425	22.65	0	0.282	0.055	99.78
	16-6B-ol-CP1-3	mph-c	7E-04	37.21	0.035	37.83	0.029	0.008	0.425	23.12	3E-04	0.34	0.034	99.02
	16-6B-ol-CP1-4	mph-c	0.007	37.25	0.041	37.82	0.023	0.02	0.418	23.14	6E-04	0.295	0.052	99.07
	16-6B-ol-CP1-5	mph-r	0	36.49	0.032	37.89	0.028	0.012	0.471	24.36	0.01	0.305	0.037	99.64
	16-6B-ol-CP4-1	mph-c	0.006	36.97	0.043	38.05	0.025	0	0.446	23.95	0.004	0.29	0.036	99.81
	16-6B-ol-CP4-2	mph-c	0.009	36.57	0.036	37.98	0.025	0	0.454	23.98	0	0.278	0.032	99.36
	16-6B-ol-CP4-3	mph-r	3E-04	35.27	0.029	37.58	0.023	0	0.472	25.65	0.001	0.295	0.051	99.37
	16-6B-ol-E-1	mph-r	0	34.41	0.038	37.2	0.029	0	0.528	26.56	0.002	0.335	0.042	99.13
	16-6B-ol-E-2	mph-c	0.005	36.65	0.05	37.87	0.022	0.015	0.445	24.06	0	0.329	0.048	99.49
	16-6B-ol-E-3	mph-c	0.007	37.09	0.038	37.94	0.029	0.025	0.444	23.41	0	0.38	0.036	99.4
	16-6B-ol-E-4	mph-c	0	36.43	0.033	37.99	0.033	0	0.45	23.84	5E-04	0.43	0.038	99.21
	16-6B-ol-F-1	mph-c	0	36.08	0.05	37.7	0.032	0.015	0.456	24.26	0.005	0.484	0.048	99.12
	16-6B-ol-F-2	mph-r	0.008	35.36	0.045	37.37	0.021	0.029	0.472	25.47	0	0.295	0.05	99.11
	16-6B-ol-F-3	mph-c	0.006	35.17	0.027	37.27	0.031	0.007	0.505	25.58	0.008	0.373	0.045	99.02
	16-6B-ol-MF-1	m	0.035	33.7	0.068	36.79	0.062	0.005	0.524	27.06	0.002	0.438	0.038	98.72

	Análisis Puntuales - University of Bristol (Jeol)													
	Point	Type	Na_2O (Wt%)	MgO (Wt%)	Al_2O_3 (Wt%)	SiO_2 (Wt%)	TiO_2 (Wt%)	Cr_2O_3 (Wt%)	MnO (Wt%)	FeO (Wt%)	K_2O (Wt%)	CaO (Wt%)	NiO (Wt%)	Total (Wt%)
Fui N.	16-6B-ol-MF-3	m	0.012	33.64	0.047	37.03	0.056	0.013	0.521	27.1	0.017	0.402	0.029	98.87
	16-6B-ol-MC-2	mph-c	0	34.88	0.039	37.45	0.027	0.006	0.482	26.54	0.004	0.301	0.034	99.76
Chanchán	15-3-ol-MC1-core1	ph-c	0	35.85	0.019	37.39	0	0	0.552	25.27	0.002	0.032	0.084	99.17
	15-3-ol-MC1-rim1	ph-r	0	43.29	0.035	39.11	0.012	0.009	0.272	15.96	0.007	0.217	0.133	99.05
	15-3-ol-MC2-1	ph-c	5E-04	44.47	0.04	39.56	0.013	0.034	0.237	15.11	0.003	0.18	0.144	99.79
	15-3-ol-MC3-1	ph-c	0.003	43.46	0.05	39.44	0.018	0.021	0.271	15.81	0.003	0.2	0.128	99.4
	15-3-ol-MC4-1	ph-c	0	45.27	0.044	40.16	0.006	0.027	0.21	14.07	0.007	0.167	0.199	100.1
	15-3-ol-MC5-1	ph-c	0	43.18	0.034	39.32	0.008	0.023	0.275	16.32	0	0.184	0.115	99.44
	15-3-ol-MF-1	m	0.015	36.68	0.063	37.89	0.045	0.035	0.423	23.82	0.008	0.35	0.02	99.36
	15-3-ol-MF-2	m	0.012	33.45	0.081	37.2	0.078	0	0.474	27.56	0.014	0.681	0.022	99.56
	15-3-ol-MF-3	m	0.025	35.98	0.081	37.62	0.03	0	0.424	24.27	0.008	0.386	0.039	98.85
	15-3-ol-MF-4	m	0.004	34.44	0.069	37.26	0.027	0.017	0.451	25.94	4E-04	0.404	0.029	98.64
	15-3-ol-2-rim	ph-r	0.007	39.21	0.037	38.25	0.013	0.019	0.348	20.88	0	0.207	0.105	99.06
	15-3-ol-8-rim	ph-r	0	36.87	0.058	37.96	0.026	0.032	0.458	24.77	0.008	0.305	0.074	100.6
	15-3-ol-15-rim	ph-r	0	40.22	0.055	38.89	0.026	0.034	0.354	20.13	0.008	0.284	0.068	100.1
	15-3-ol-19-rim	ph-r	0.003	36.45	0.056	37.9	0.031	0.002	0.396	23.74	0.009	0.305	0.048	98.94
	15-3-ol-27-rim	ph-r	0.004	40.3	0.06	39.04	0.011	0.009	0.347	20.12	0.009	0.232	0.107	100.2
	15-3-ol-30-rim	ph-r	0.01	39.83	0.046	38.67	0.023	0.022	0.326	20.75	0.005	0.261	0.082	100
Fui Sur	FS4-ol-4s-core	ph-c	0.006	40.42	0.03	38.85	0.007	0.028	0.335	19.62	0	0.182	0.093	99.56
	FS4-ol-4s-2	ph-r	0.016	35.08	0.031	37.72	0.024	0	0.479	25.94	0.001	0.199	0.033	99.52
	FS4-ol-4s-3	ph-r	0.012	34.13	0.04	37.22	0.023	0.02	0.538	26.42	0	0.226	0.036	98.67
	FS4-ol-8-rim	ph-r	0	35.92	0.018	37.7	0.018	0	0.454	24.75	0.003	0.148	0.044	99.05
	FS4-ol-9-rim	ph-r	0	34.36	0.022	37.21	0.023	0	0.482	26.48	0.007	0.169	0.043	98.76
	FS4-ol-13-1	ph-c	0.002	42.09	0.031	39.23	0.014	0.005	0.288	17.47	0	0.179	0.114	99.42
	FS4-ol-13-2	ph-r	0.006	32.08	0.031	37.11	0.022	0	0.553	29.35	0	0.172	0.027	99.35
	FS4-ol-14-rim	ph-r	0	30.65	0.039	36.46	0.012	0	0.578	31.12	0	0.174	0.029	99.06
	FS4-ol-20-rim	ph-r	0	34.77	0.019	37.37	0.024	0.006	0.483	26.17	0	0.162	0.034	99.03
	FS4-ol-20-a	ph-c	0.008	41.8	0.017	39.05	0.013	0	0.278	18.26	0	0.178	0.117	99.71
	FS4-ol-20-core	ph-c	0	40.94	0.022	38.95	0.009	0	0.321	19.69	0	0.18	0.112	100.2
	FS4-ol-28-core	ph-c	0	39.44	0.028	38.43	0.012	0.019	0.367	20.87	0.001	0.165	0.058	99.37
	FS4-ol-28-rim	ph-r	0	34.91	0.03	37.85	0.012	0.019	0.474	25.69	0.01	0.186	0.098	99.27
	FS4-ol-J-1	mph-c	0	34.02	0.035	36.97	0.032	0	0.543	27.64	0.005	0.196	0.017	99.45
	FS4-ol-L-1	mph-r	0.008	31.75	0.035	36.46	0.059	0.004	0.586	29.68	7E-04	0.336	0.024	98.93
	FS4-ol-L-2	mph-c	0.016	32.58	0.336	37.3	0.109	0.019	0.537	27.56	0.05	0.444	0.03	98.98
	FS4-ol-H-1	mph-c	0	36.77	0.036	37.77	0.029	0.01	0.437	23.68	0.011	0.254	0.047	99.04
	FS4-ol-H-2	mph-r	0.006	34.45	0.028	36.99	0.045	0	0.51	26.78	0.005	0.332	0.025	99.17
	FS4-ol-H-3	mph-c	0.002	37.05	0.036	37.8	0.027	0	0.437	23.8	0	0.204	0.059	99.39
	FS4-ol-F-1	mph-c	0.01	34.89	0.027	37.33	0.024	0.01	0.465	26.25	0.001	0.251	0.046	99.31

Análisis Puntuales - University of Bristol (Jeol)

	Point	Type	Na_2O (Wt%)	MgO (Wt%)	Al_2O_3 (Wt%)	SiO_2 (Wt%)	TiO_2 (Wt%)	Cr_2O_3 (Wt%)	MnO (Wt%)	FeO (Wt%)	K_2O (Wt%)	CaO (Wt%)	NiO (Wt%)	Total (Wt%)
Fui Sur	FS4-ol-MC1	mph-c	0	34.04	0.037	37.07	0.029	0.043	0.54	27.39	0.007	0.173	0.029	99.35
	FS4-ol-MC2	mph-c	0.014	35.88	0.03	37.52	0.022	0.006	0.47	25.17	0	0.167	0.041	99.31
	FS4-ol-MC3	mph-c	0.006	36.15	0.044	37.57	0.032	0.019	0.458	24.65	0	0.189	0.035	99.16
	FS4-ol-MC4	mph-c	0.008	35.17	0.032	37.33	0.02	0	0.513	26.05	0.009	0.163	0.018	99.31
	FS4-ol-MC5	mph-c	0.002	35.51	0.045	37.25	0.022	0.004	0.478	25.23	0.005	0.168	0.032	98.75
	FS4-ol-MF-1	m	0.022	21.37	0.042	34.33	0.117	0	0.94	41.56	0.013	0.309	0.005	98.69

Perfiles - University of Bristol (Jeol)

	Point	Na_2O (Wt%)	MgO (Wt%)	Al_2O_3 (Wt%)	SiO_2 (Wt%)	TiO_2 (Wt%)	Cr_2O_3 (Wt%)	MnO (Wt%)	FeO (Wt%)	K_2O (Wt%)	CaO (Wt%)	NiO (Wt%)	Total (Wt%)	Distance from rim (µm)
Fui Norte	16-6Bpr1-9	0	37.59	0.033	38.1	0.027	0.004	0.417	22.92	0.005	0.221	0.066	99.39	0.00
	16-6Bpr1-8	0	40.36	0.039	38.7	0.018	0	0.349	19.61	0	0.2	0.098	99.37	10.06
	16-6Bpr1-7	0	40.83	0.034	38.8	0.011	5E-04	0.329	19.19	0.003	0.194	0.086	99.46	20.00
	16-6Bpr1-6	0	40.84	0.028	38.85	0.012	0.009	0.332	19.14	0	0.19	0.083	99.49	30.01
	16-6Bpr1-5	0	41.08	0.019	38.76	0.014	0.011	0.326	19.1	0	0.187	0.106	99.6	40.08
	16-6Bpr1-4	0	41.35	0.03	38.87	0.007	0	0.318	19.04	0.003	0.184	0.105	99.9	50.01
	16-6Bpr1-3	0	41.17	0.029	38.92	0.009	0.022	0.328	18.85	0.002	0.183	0.111	99.61	60.03
	16-6Bpr1-2	0.01	41.26	0.022	39.08	0.01	0	0.32	18.78	0	0.179	0.118	99.76	70.01
	16-6Bpr1-1	0	41.35	0.022	38.97	0.011	0.032	0.32	18.77	0.002	0.177	0.101	99.74	80.02
	16-6BprH-7	0	34.88	0.049	37.45	0.032	0.003	0.516	26.48	0.003	0.298	0.024	99.73	0.00
	16-6BprH-6	0.01	35.08	0.052	37.27	0.024	0	0.483	25.78	0	0.276	0.042	99.02	10.04
	16-6BprH-5	0.01	35.58	0.066	37.04	0.03	0	0.476	25.32	3E-04	0.276	0.05	98.85	20.00
	16-6BprH-4	0	36.21	0.041	37.5	0.027	0.021	0.455	24.85	3E-04	0.257	0.033	99.39	29.98
	16-6BprH-3	0	36.28	0.044	37.52	0.018	0	0.452	24.52	0	0.254	0.055	99.13	40.03
	16-6BprH-2	0	36.36	0.042	37.43	0.023	0	0.439	24.27	0	0.257	0.034	98.83	49.98
	16-6BprH-1	0.02	36.54	0.034	37.61	0.017	0.024	0.438	24.22	0	0.256	0.034	99.19	60.02

	Perfiles - University of Bristol (CAMECA)											
	Point	MgO (Wt%)	Al_2O3 (Wt%)	SiO_2 (Wt%)	TiO_2 (Wt%)	Cr_2O_3 (Wt%)	MnO (Wt%)	FeO (Wt%)	CaO (Wt%)	NiO (Wt%)	Total (Wt%)	Distance from rim (μm)
Chanchán	15-3-Ol9-p1	43.3	0.031	39.88	0.011	0.022	0.272	17.13	0.208	0.116	101	0
	15-3-Ol9-p2	44.5	0.022	40.2	7E-04	0.017	0.228	15.33	0.18	0.132	100.6	9.27
	15-3-Ol9-p3	45.1	0.016	39.99	0	0.019	0.241	14.88	0.174	0.167	100.6	19.13
	15-3-Ol9-p4	45.5	0.028	40.18	0.01	0.024	0.222	14.5	0.171	0.168	100.8	29.75
	15-3-Ol9-p5	45.9	0.02	40.4	0.003	0.023	0.216	14.23	0.166	0.202	101.1	39.64
	15-3-Ol9-p6	45.8	0.018	40.2	0.003	0.022	0.212	14.02	0.166	0.19	100.6	49.56
	15-3-Ol9-p7	45.7	0.031	40.57	0.002	0.025	0.222	13.93	0.165	0.212	100.8	59.5
	15-3-Ol9-p8	45.9	0.027	40.4	0.003	0.035	0.201	13.67	0.153	0.229	100.6	69.38
	15-3-Ol9-p9	45.7	0.025	40.22	0.003	0.035	0.202	13.71	0.15	0.228	100.3	80.01
	15-3-Ol9-p10	46.2	0.009	40.49	0.009	0.029	0.196	13.7	0.151	0.25	101	89.92
	15-3-Ol9-p11	46.2	0.025	40.18	0.008	0.034	0.202	13.39	0.152	0.253	100.4	99.81
	15-3-Ol9-p12	46.2	0.025	40.2	0	0.04	0.205	13.56	0.16	0.269	100.7	109.8
	15-3-Ol9-p13	46.1	0.025	40.15	0.002	0.03	0.2	13.5	0.155	0.255	100.4	119.6
	15-3-Ol9-p14	45.9	0.022	40.29	0.003	0.025	0.197	13.59	0.158	0.258	100.5	129.6
	15-3-Ol9-p15	45.6	0.029	40.5	0.006	0.036	0.213	13.98	0.158	0.244	100.8	140.2
	15-3-Ol9-p16	45.1	0.032	40.63	0.007	0.033	0.221	14.39	0.158	0.236	100.8	150.1
	15-3-Ol9-p17	42.7	0.082	39.89	0.017	0.028	0.279	17.14	0.211	0.171	100.5	160.7
	15-3-Ol16-p1	36.8	0.048	37.84	0.01	0.011	0.434	25.37	0.317	0.052	100.9	0
	15-3-Ol16-p2	43.4	0.014	39.39	8E-04	0.023	0.272	16.67	0.221	0.136	100.2	10.34
	15-3-Ol16-p3	44.5	0.014	40.08	0.014	0.026	0.25	15.7	0.194	0.126	100.9	20.62
	15-3-Ol16-p4	44.2	0.015	40.25	0	0.02	0.251	15.7	0.176	0.132	100.8	30.43
	15-3-Ol16-p5	44.2	0.017	40.06	0.008	0.013	0.249	15.54	0.174	0.165	100.4	40.72
	15-3-Ol16-p6	44.6	0.025	39.93	0.011	0.014	0.236	15.61	0.168	0.138	100.7	50.55
	15-3-Ol16-p7	44.1	0.024	39.61	0.002	0.013	0.247	15.74	0.163	0.156	100.1	60.84
	15-3-Ol16-p8	43.8	0.048	39.39	0.004	0.025	0.255	16.03	0.156	0.166	99.89	70.67
	15-3-Ol16-p10	43.1	0.033	39.37	0	0.015	0.27	17.13	0.138	0.149	100.2	90.79
	15-3-Ol16-p11	42.5	0.005	39.44	3E-04	0.012	0.296	17.98	0.122	0.14	100.5	101.1
	15-3-Ol16-p12	42	0.009	39.14	0.001	0.015	0.304	18.61	0.099	0.136	100.3	110
	15-3-Ol16-p13	41.6	0.006	39.11	0	0.001	0.314	19.59	0.082	0.109	100.8	120.3
	15-3-Ol16-p14	40.8	7E-04	38.94	8E-05	0.011	0.334	20.18	0.07	0.092	100.4	130.2
	15-3-Ol16-p15	40.7	0.015	38.88	0	0.004	0.358	20.71	0.055	0.081	100.8	140.5
	15-3-Ol16-p16	40.1	0.012	38.99	0	0.008	0.367	21.19	0.048	0.08	100.8	150.7
	15-3-Ol16-p17	39.6	0	38.65	0	0.002	0.375	21.7	0.035	0.087	100.5	160.6
	15-3-Ol16-p18	39.2	0.002	38.27	0	0.001	0.389	22.06	0.032	0.083	100	170.9
	15-3-Ol16-p19	39	0.008	38.55	0	0.002	0.396	22.53	0.026	0.101	100.6	180.7
	15-3-Ol16-p20	38.8	0.008	38.42	0	0.004	0.378	22.8	0.037	0.086	100.5	191
	15-3-Ol16-p21	38.5	0	38.4	0	0	0.404	23.08	0.027	0.093	100.5	200.8
	15-3-Ol16-p22	38.5	0.015	38.29	0.002	0.006	0.4	23.57	0.026	0.08	100.9	211.1

	Perfiles - University of Bristol (CAMECA)											
	Point	MgO (Wt%)	Al_2O3 (Wt%)	SiO_2 (Wt%)	TiO_2 (Wt%)	Cr_2O_3 (Wt%)	MnO (Wt%)	FeO (Wt%)	CaO (Wt%)	NiO (Wt%)	Total (Wt%)	Distance from rim (µm)
Chanchán	15-3-Ol16-p23	38.2	0.002	38.03	0	0.008	0.401	23.7	0.028	0.078	100.4	220.1
	15-3-Ol16-p24	38	0.006	37.99	0	0.005	0.412	23.82	0.022	0.085	100.4	230.4
	15-3-Ol16-p25	38	0.006	37.96	5E-04	0.001	0.414	23.99	0.026	0.078	100.5	240.2
	15-3-Ol16-p26	37.8	0.011	38.06	0	0.006	0.397	24.15	0.03	0.082	100.5	250.5
	15-3-Ol16-p27	37.8	0.006	38.04	0	0.005	0.409	24.17	0.019	0.078	100.5	260.3
	15-3-Ol16-p28	37.7	0	37.93	0	0.002	0.414	24.5	0.022	0.086	100.7	270.6
	15-3-Ol16-p29	37.2	0.033	37.25	0	0	0.401	24.18	0.022	0.084	99.17	280.4
	15-3-Ol16-p30	37.7	0	37.88	0.004	0.002	0.411	25.02	0.021	0.069	101.1	290.7
	15-3-Ol16-p31	37.6	0.003	37.81	0.003	0.003	0.41	24.92	0.017	0.08	100.9	301
	15-3-Ol16-p32	36.1	0.609	38.07	0.018	0.002	0.411	24.76	0.046	0.07	100.1	310.8
	15-3-Ol16-p33	36.9	0.002	38.07	0	0	0.419	25.15	0.026	0.064	100.7	321.1
	15-3-Ol16-p34	37	0.02	37.97	0.002	0	0.421	25.19	0.021	0.07	100.7	330.1
	15-3-Ol16-p35	36.8	0.012	37.91	0.003	0	0.425	25.41	0.025	0.062	100.6	340.4
	15-3-Ol16-p36	37	0.005	37.57	0	0	0.413	25.36	0.023	0.077	100.5	350.2
	15-3-Ol16-p37	36.8	0.006	37.98	0	5E-04	0.413	25.53	0.017	0.081	100.8	360.5
	15-3-Ol16-p38	36.8	8E-04	37.88	5E-04	1E-03	0.423	25.51	0.027	0.079	100.7	370.3
	15-3-Ol16-p39	36.7	0.012	37.67	0.006	0	0.419	25.5	0.02	0.068	100.4	380.6
	15-3-Ol16-p40	36.7	0.006	37.63	0	0.006	0.406	25.53	0.016	0.058	100.4	390.5
	15-3-Ol16-p41	36.5	0.016	37.59	0	0.002	0.429	25.53	0.022	0.072	100.2	400.7
	15-3-Ol16-p42	36.5	0.004	37.87	0	0.003	0.414	25.59	0.022	0.055	100.5	410.6
	15-3-Ol16-p43	36.7	0.02	37.87	0	0	0.418	25.58	0.021	0.059	100.6	420.9
	15-3-Ol16-p44	36.6	0	37.91	0.006	0.001	0.426	25.53	0.022	0.069	100.6	429.8
	15-3-Ol29-p2	43.3	0.036	39.41	0.018	0.024	0.291	17.44	0.209	0.099	100.8	10.05
	15-3-Ol29-p4	45.4	0.012	39.45	0	0.02	0.254	15.07	0.185	0.158	100.6	30.02
	15-3-Ol29-p5	45.6	0.027	39.61	0.004	0.024	0.227	14.93	0.171	0.145	100.7	40.01
	15-3-Ol29-p6	45.6	0.034	39.7	0.005	0.022	0.219	14.52	0.161	0.192	100.5	50.01
	15-3-Ol29-p7	45.7	0.027	39.98	0.01	0.025	0.21	14.23	0.156	0.2	100.5	60.01
	15-3-Ol29-p8	45.9	0.028	40.15	0	0.031	0.217	14.11	0.155	0.234	100.8	70.01
	15-3-Ol29-p9	46	0.021	40.03	0.005	0.04	0.223	13.77	0.158	0.219	100.5	80.01
	15-3-Ol29-p10	46.4	0.024	40.19	0.002	0.04	0.199	13.58	0.16	0.234	100.9	90.01
	15-3-Ol29-p11	46.3	0.028	39.99	0	0.028	0.201	13.35	0.155	0.247	100.3	100
	15-3-Ol29-p12	46.4	0.037	40.2	0.003	0.03	0.199	13.27	0.159	0.256	100.6	110
	15-3-Ol29-p13	46.9	0.022	40.3	0.003	0.034	0.198	13.16	0.148	0.252	101	120
	15-3-Ol29-p14	46.7	0.028	40.4	0.01	0.026	0.186	13.07	0.148	0.274	100.8	130
	15-3-Ol29-p15	46.7	0.043	40.26	8E-04	0.028	0.188	13	0.143	0.256	100.6	140
	15-3-Ol29-p16	46.8	0.026	40.07	0.006	0.026	0.186	12.72	0.155	0.288	100.3	150
	15-3-Ol29-p17	46.7	0.029	40.33	0.005	0.027	0.179	12.55	0.147	0.275	100.2	160
	15-3-Ol29-p18	46.9	0.024	40.27	6E-04	0.032	0.179	12.57	0.136	0.308	100.4	170

	Perfiles - University of Bristol (CAMECA)											
	Point	MgO (Wt%)	Al_2O3 (Wt%)	SiO_2 (Wt%)	TiO_2 (Wt%)	Cr_2O_3 (Wt%)	MnO (Wt%)	FeO (Wt%)	CaO (Wt%)	NiO (Wt%)	Total (Wt%)	Distance from rim (µm)
Chanchán	15-3-Ol29-p19	46.9	0.036	40.56	0.003	0.042	0.183	12.47	0.146	0.324	100.6	180
	15-3-Ol29-p20	46.6	0.023	40.33	0.005	0.043	0.177	12.28	0.148	0.326	99.98	190
	15-3-Ol29-p21	47.2	0.025	40.72	0.002	0.038	0.166	12.15	0.135	0.354	100.8	200
	15-3-Ol29-p23	47.3	0.041	40.31	0.01	0.04	0.17	11.84	0.135	0.377	100.2	220
	15-3-Ol29-p24	47.5	0.034	40.26	0	0.039	0.169	11.65	0.137	0.404	100.2	230
	15-3-Ol29-p25	47.5	0.044	40.43	0.006	0.05	0.174	11.53	0.133	0.389	100.2	240
	15-3-Ol29-p26	47.5	0.033	40.24	0	0.048	0.15	11.54	0.139	0.414	100.1	250
	15-3-Ol29-p27	47.4	0.03	40.48	0.011	0.049	0.156	11.46	0.132	0.421	100.1	260
	15-3-Ol29-p28	47.2	0.048	40.88	0.007	0.057	0.159	11.44	0.12	0.431	100.4	270
	15-3-Ol29-p29	48.4	0.026	40.9	0.003	0.055	0.162	11.21	0.126	0.43	101.3	280
	15-3-Ol29-p30	48.1	0.049	40.3	0	0.063	0.155	11.34	0.136	0.426	100.6	290
	15-3-Ol29-p31	48.3	0.046	39.58	7E-04	0.05	0.154	11.24	0.136	0.409	99.92	300
	15-3-Ol29-p32	48.1	0.038	40.46	0.006	0.055	0.158	11.12	0.129	0.43	100.5	310
	15-3-Ol29-p33	48.2	0.036	40.57	0.001	0.056	0.154	11.06	0.129	0.444	100.6	320
	15-3-Ol29-p34	47.9	0.043	40.59	0.004	0.056	0.16	11.14	0.134	0.443	100.5	330
	15-3-Ol29-p35	48.2	0.025	40.39	0.005	0.051	0.155	11.11	0.13	0.445	100.5	340
	15-3-Ol29-p36	48	0.032	40.35	0	0.051	0.154	11.04	0.132	0.449	100.2	350
	15-3-Ol29-p37	48	0.029	40.4	0.005	0.057	0.144	11.01	0.135	0.42	100.3	360
	15-3-Ol29-p38	47.8	0.039	40.3	0.001	0.049	0.162	11	0.131	0.437	99.88	370
	15-3-Ol29-p39	47.9	0.029	40.6	0.006	0.047	0.152	11.1	0.124	0.451	100.5	380
	15-3-Ol29-p40	47.8	0.029	40.32	0	0.049	0.155	11.08	0.129	0.436	99.98	390
	15-3-Ol29-p41	48	0.037	40.66	0.008	0.049	0.157	11.02	0.13	0.424	100.5	400
	15-3-Ol29-p42	48	0.033	40.61	0	0.051	0.143	11	0.135	0.445	100.4	410
	15-3-Ol29-p43	47.6	0.034	40.53	0.001	0.048	0.153	10.92	0.118	0.45	99.88	420
	15-3-Ol31-p1	39.2	0.031	37.97	0.024	0.016	0.382	22.44	0.278	0.052	100.4	0
	15-3-Ol31-p2	43.9	0.018	39.2	0.007	0.019	0.262	16.69	0.201	0.126	100.4	10
	15-3-Ol31-p3	44.9	0.037	39.6	0.006	0.012	0.235	15.35	0.185	0.151	100.5	20
	15-3-Ol31-p4	44.9	0.012	39.75	0.016	0.016	0.223	15.23	0.182	0.159	100.5	30
	15-3-Ol31-p5	45.1	0.029	39.73	0.017	0.019	0.242	14.91	0.172	0.146	100.3	40
	15-3-Ol31-p6	45.4	0.033	40.12	0.004	0.02	0.221	14.8	0.164	0.164	100.9	50
	15-3-Ol31-p7	45.3	0.031	39.69	0.003	0.023	0.212	14.34	0.168	0.208	99.93	60
	15-3-Ol31-p8	45.6	0.027	40	0.007	0.03	0.21	14.09	0.155	0.205	100.3	70
	15-3-Ol31-p9	46.1	0.021	39.97	0	0.027	0.212	14.03	0.156	0.226	100.7	80
	15-3-Ol31-p10	46.1	0.018	39.98	0	0.027	0.2	13.51	0.159	0.241	100.2	90
	15-3-Ol31-p11	46.5	0.025	40.22	0	0.027	0.199	13.32	0.144	0.267	100.7	100
	15-3-Ol31-p12	46.3	0.037	40.15	0.004	0.031	0.185	13.05	0.142	0.283	100.2	110
	15-3-Ol31-p13	46.4	0.016	40.05	0	0.032	0.18	12.75	0.135	0.28	99.88	120
	15-3-Ol31-p14	46.9	0.029	40.29	0.005	0.043	0.183	12.61	0.152	0.316	100.6	130

	Perfiles - University of Bristol (CAMECA)											
	Point	MgO (Wt%)	Al_2O3 (Wt%)	SiO_2 (Wt%)	TiO_2 (Wt%)	Cr_2O_3 (Wt%)	MnO (Wt%)	FeO (Wt%)	CaO (Wt%)	NiO (Wt%)	Total (Wt%)	Distance from rim (µm)
Chanchán	15-3-Ol31-p15	47.2	0.038	40.27	0.005	0.044	0.184	12.32	0.144	0.322	100.5	140
	15-3-Ol31-p16	47	0.038	40.32	0	0.038	0.169	12.42	0.143	0.348	100.5	150
	15-3-Ol31-p17	47.3	0.035	40.42	0.002	0.051	0.181	12.14	0.146	0.346	100.6	160
	15-3-Ol31-p18	47.1	0.027	40.32	0.007	0.064	0.169	11.85	0.136	0.352	100	170
	15-3-Ol31-p19	47.4	0.031	40.46	0.003	0.055	0.173	11.91	0.133	0.383	100.5	180
	15-3-Ol31-p20	47.6	0.033	40.43	0.004	0.054	0.169	11.73	0.136	0.411	100.6	190
	15-3-Ol25-p2	40.8	0.018	38.99	0.011	0.017	0.35	20.03	0.263	0.076	100.6	10
	15-3-Ol25-p3	44	0.023	39.63	0.003	0.017	0.269	16.67	0.209	0.127	100.9	20
	15-3-Ol25-p4	44	0.029	39.53	0.004	0.019	0.261	16.45	0.196	0.132	100.6	30
	15-3-Ol25-p6	43	0.02	39.59	0.013	0.007	0.267	17.48	0.168	0.102	100.7	50
	15-3-Ol25-p7	43.8	0.019	39.81	0.004	0.011	0.254	16.75	0.17	0.129	100.9	60
	15-3-Ol25-p8	44.4	0.03	39.54	0.01	0.018	0.248	15.97	0.169	0.15	100.5	70.6
	15-3-Ol25-p9	45.2	0.006	39.79	0.011	0.022	0.23	15.09	0.176	0.176	100.7	80.6
	15-3-Ol25-p10	45.7	0.023	40.1	0.009	0.022	0.221	14.44	0.158	0.202	100.9	90.6
	15-3-Ol25-p11	45.6	0.017	39.85	8E-04	0.027	0.217	13.96	0.166	0.205	100.1	99.81
	15-3-Ol25-p12	46.1	0.021	39.88	0.002	0.027	0.209	14.09	0.171	0.233	100.7	109.8
	15-3-Ol25-p13	45.8	0.017	40.2	0.003	0.032	0.202	13.81	0.153	0.216	100.5	119.8
	15-3-Ol25-p14	46.2	0.028	40.25	0.007	0.024	0.216	13.64	0.155	0.246	100.7	130.4
	15-3-Ol25-p15	45.9	0.026	40.11	0	0.038	0.199	13.57	0.158	0.254	100.3	140.4
	15-3-Ol25-p16	46.1	0.023	40.33	0	0.041	0.199	13.41	0.161	0.253	100.5	150.4
	15-3-Ol25-p17	46.5	0.019	40.27	0.011	0.042	0.184	13.54	0.159	0.275	101	160.4
	15-3-Ol25-p18	46.3	0.03	40.06	0.005	0.049	0.199	13.41	0.149	0.266	100.5	170.4
	15-3-Ol25-p19	46.1	0.022	40.36	0.007	0.061	0.203	13.31	0.162	0.278	100.5	180.4
	15-3-Ol25-p20	46.1	0.026	40.42	0.01	0.076	0.198	13.17	0.186	0.269	100.5	190.2
Fui Norte	16-6B-Ol5-p1	34.9	0.018	37.7	0.032	0.008	0.497	26.94	0.326	0.026	100.5	0
	16-6B-Ol5-p2	35.7	0.013	37.63	0.013	0.02	0.49	26.2	0.278	0.039	100.4	10.05
	16-6B-Ol5-p3	36.2	0.005	37.67	0.01	0.033	0.467	25.89	0.24	0.044	100.6	20.22
	16-6B-Ol5-p4	36.9	0.021	37.96	0.018	0.029	0.456	25.2	0.22	0.039	100.8	30.27
	16-6B-Ol5-p5	37.3	0.019	38.33	0.01	0.027	0.432	24.32	0.215	0.075	100.8	40.45
	16-6B-Ol5-p6	38.1	0.014	38.11	0.012	0.02	0.408	23.96	0.195	0.076	100.9	50.64
	16-6B-Ol5-p7	38.2	0.022	38.3	0.011	0.018	0.405	23.42	0.195	0.069	100.6	60.67
	16-6B-Ol5-p8	38.5	0.022	38.3	0.007	0.006	0.414	23.08	0.191	0.077	100.6	70.86
	16-6B-Ol5-p9	38.7	0.019	38.02	0.007	0.013	0.394	22.95	0.189	0.074	100.4	80.06
	16-6B-Ol11-p1	34.2	0.08	37.3	0.074	0.01	0.503	27.54	0.331	0.025	100	0
	16-6B-Ol11-p2	35.4	0.014	37.33	0.023	0.003	0.489	26.42	0.309	0.05	100	10
	16-6B-Ol11-p3	36	0.006	37.58	0.013	0	0.467	26	0.267	0.057	100.4	19.85
	16-6B-Ol11-p4	36.7	0.033	37.57	0.019	0.005	0.453	25.03	0.254	0.059	100.1	29.73
	16-6B-Ol11-p5	37.5	0.009	37.67	0.02	0.008	0.429	24.2	0.225	0.044	100.1	39.64

	Perfiles - University of Bristol (CAMECA)											
	Point	MgO (Wt%)	Al_2O3 (Wt%)	SiO_2 (Wt%)	TiO_2 (Wt%)	Cr_2O_3 (Wt%)	MnO (Wt%)	FeO (Wt%)	CaO (Wt%)	NiO (Wt%)	Total (Wt%)	Distance from rim (µm)
Fui Norte	16-6B-Ol11-p7	39.1	0.023	38.85	1E-03	0.011	0.383	21.88	0.185	0.076	100.5	60.15
	16-6B-Ol11-p8	40.1	0.019	38.47	0.008	0.01	0.346	21.09	0.177	0.103	100.3	70.06
	16-6B-Ol11-p9	40.7	0.011	38.84	0.007	0.009	0.331	20.48	0.18	0.091	100.7	79.96
	16-6B-Ol11-p10	41.1	0.029	38.91	0.015	0.009	0.325	19.59	0.182	0.113	100.2	89.85
	16-6B-Ol11-p11	41.5	0.01	38.88	0.01	0.01	0.332	19.41	0.167	0.101	100.4	99.77
	16-6B-Ol11-p12	41.8	0.022	39.02	0.01	0.009	0.31	19.06	0.172	0.119	100.5	110.4
	16-6B-Ol11-p13	42.2	0.019	38.7	0.014	0.009	0.309	19.18	0.171	0.099	100.7	120.3
	16-6B-Ol11-p14	41.7	0.028	39.14	0.014	0.012	0.306	19.02	0.18	0.108	100.5	130.2
	16-6B-Ol11-p15	42	0.019	38.96	0.003	0.009	0.298	19.13	0.173	0.125	100.7	140.1
	16-6B-Ol11-p16	42.1	0.031	38.81	0.003	0.012	0.299	19.12	0.177	0.115	100.7	150
	16-6B-Ol11-p17	41.9	0.012	39.04	0.012	0.012	0.305	18.95	0.17	0.109	100.5	159.9
Fui Sur	FS4-Ol23-p1	29.4	0.021	36.41	0.034	1E-03	0.662	33.5	0.226	0.022	100.3	0
	FS4-Ol23-p2	40.2	0.029	38.9	0.017	0.011	0.354	20.69	0.167	0.096	100.5	10.2
	FS4-Ol23-p3	42.4	0.01	39.25	0.011	0.013	0.279	17.96	0.19	0.146	100.2	20.4
	FS4-Ol23-p4	42.9	0.014	39.26	0.001	0.014	0.265	17.32	0.174	0.165	100.2	30.81
	FS4-Ol23-p5	42.8	0.02	39.36	0.011	0.013	0.278	17.34	0.17	0.159	100.1	40.02
	FS4-Ol23-p6	42.6	0.021	39.49	0.013	0.012	0.271	17.46	0.166	0.124	100.1	50.45
	FS4-Ol23-p7	42.3	0.018	39.48	0	0.007	0.254	17.76	0.183	0.117	100.1	60.64
	FS4-Ol23-p8	42.6	0.015	39.22	0	0.01	0.256	17.58	0.171	0.104	99.98	70.09
	FS4-Ol23-p9	42.8	0.014	39.41	0.005	0.007	0.267	17.29	0.162	0.143	100.1	80.28
	FS4-Ol23-p10	43.6	0.013	39.31	0.002	0.012	0.231	16.63	0.162	0.16	100.1	90.71
	FS4-Ol23-p11	43.8	0.023	39.84	0.003	0.02	0.244	16.08	0.161	0.219	100.4	99.92
	FS4-Ol23-p12	44.2	0.025	40.09	0.001	0.027	0.229	15.45	0.158	0.281	100.5	110.1
	FS4-Ol23-p13	44.3	0.031	39.7	0	0.026	0.225	14.9	0.16	0.284	99.6	120.5
	FS4-Ol23-p14	44.8	0.029	39.86	0	0.018	0.216	14.95	0.161	0.262	100.3	130.7
	FS4-Ol23-p15	44.8	0.027	39.88	0.006	0.017	0.218	14.94	0.168	0.232	100.3	140.2
	FS4-Ol23-p16	44.7	0.027	39.96	0	0.013	0.224	15.1	0.158	0.223	100.4	150.4
	FS4-Ol23-p17	44.4	0.031	39.72	0.003	0.015	0.235	15.44	0.172	0.223	100.2	160.8
	FS4-Ol23-p18	44.2	0.029	39.61	0	0.02	0.23	15.69	0.169	0.237	100.1	170
	FS4-Ol23-p19	44	0.021	39.44	0.011	0.017	0.247	16.18	0.173	0.213	100.3	180.5
	FS4-Ol23-p20	43.4	0.018	39.48	0.005	0.021	0.251	16.42	0.175	0.219	99.97	190.6
	FS4-Ol23-p21	43.1	0.031	39.4	0	0.013	0.263	16.77	0.168	0.21	99.95	200.1
	FS4-OlH-p2	27.2	0.007	35.79	0.05	0.002	0.732	35.86	0.261	0	99.93	3.32
	FS4-OlH-p3	31	0.008	36.91	0.031	0.003	0.63	31.54	0.213	0.018	100.3	6.16
	FS4-OlH-p4	32.5	0.012	37.16	0.037	0.003	0.601	30.01	0.196	0.016	100.5	9.11
	FS4-OlH-p5	34.3	0.016	37.61	0.038	0.005	0.558	27.34	0.189	0.023	100.1	12.08
	FS4-OlH-p6	35.1	0.013	37.55	0.025	8E-04	0.529	26.94	0.18	0.01	100.4	15.17
	FS4-OlH-p7	35.7	0.021	37.8	0.031	0.005	0.51	26.08	0.196	0.026	100.4	18.14

	Perfiles - University of Bristol (CAMECA)											
	Point	MgO (Wt%)	Al_2O3 (Wt%)	SiO_2 (Wt%)	TiO_2 (Wt%)	Cr_2O_3 (Wt%)	MnO (Wt%)	FeO (Wt%)	CaO (Wt%)	NiO (Wt%)	Total (Wt%)	Distance from rim (µm)
Fui Sur	FS4-OlH-p8	36.5	0.021	38.02	0.022	0.009	0.469	25.21	0.207	0.037	100.5	21.12
	FS4-OlH-p9	37.1	0.015	38.33	0.034	0.009	0.456	24.45	0.209	0.047	100.6	24.1
	FS4-OlH-p10	37.1	0.017	38.36	0.028	0.004	0.426	23.74	0.218	0.051	99.99	27.18
	FS4-OlH-p11	37.2	0.025	38.13	0.021	0.009	0.433	23.84	0.243	0.044	100	30.17
	FS4-OlH-p12	37.2	0.028	37.93	0.029	0.013	0.443	23.87	0.259	0.065	99.87	33.15
	FS4-OlH-p13	37	0.019	38.06	0.021	0.009	0.44	24.14	0.29	0.056	100	36.14
	FS4-OlH-p14	37.1	0.022	38.01	0.029	0.011	0.442	24.2	0.294	0.051	100.2	39.13
	FS4-Ol29-1-p2	29	0.023	35.91	0.051	0.006	0.673	34.08	0.297	0.016	100.1	2.45
	FS4-Ol29-1-p3	33.8	0.021	37.22	0.034	1E-04	0.527	28.59	0.174	0.026	100.4	5.48
	FS4-Ol29-1-p4	35.5	0.023	37.57	0.022	0.007	0.481	26.36	0.175	0.055	100.2	8.6
	FS4-Ol29-1-p5	36.9	0.003	38.05	0.015	0.006	0.448	24.91	0.157	0.044	100.5	11.75
	FS4-Ol29-1-p6	37.3	0.011	38.21	0.028	0.009	0.417	23.86	0.172	0.058	100.1	13.96
	FS4-Ol29-1-p7	38.5	0.012	38.68	0.013	0.009	0.415	22.64	0.161	0.061	100.5	17.12
	FS4-Ol29-1-p8	39.3	0.02	38.87	0.025	0.016	0.37	21.48	0.175	0.091	100.3	20.27
	FS4-Ol29-1-p9	40.7	0.013	39.26	0.004	0.009	0.325	19.9	0.178	0.11	100.5	23.43
	FS4-Ol29-1-p10	41.7	0.033	39.36	0.007	0.01	0.306	18.98	0.178	0.119	100.7	26.94
	FS4-Ol29-2-p1	41.6	0.025	39.52	0.006	0.009	0.296	18.72	0.187	0.113	100.5	0
	FS4-Ol29-2-p2	42.7	0.022	39.59	0.004	0.009	0.274	17.46	0.162	0.143	100.3	9.49
	FS4-Ol29-2-p3	42.8	0.029	39.95	0.016	0.017	0.261	16.87	0.181	0.15	100.3	19.92
	FS4-Ol29-2-p5	44	0.02	39.38	0.004	0.015	0.272	16.45	0.194	0.146	100.5	39.85
	FS4-Ol29-2-p6	43.8	0.029	39.61	0.006	0.016	0.264	16.31	0.185	0.146	100.4	49.34
	FS4-Ol29-2-p8	43.9	0.019	39.46	0.001	0.014	0.26	16.38	0.193	0.14	100.4	69.26
	FS4-Ol29-2-p9	44	0.029	39.54	0.013	0.015	0.24	16.45	0.199	0.134	100.6	79.7
	FS4-Ol29-2-p10	44	0.035	39.75	0.014	0.013	0.26	16.29	0.191	0.136	100.7	89.19
	FS4-Ol29-2-p11	44	0.017	39.98	0.002	0.01	0.274	16.31	0.194	0.137	101	99.62
	FS4-Ol29-2-p12	43.6	0.026	39.61	0.012	0.013	0.254	16.18	0.188	0.154	100	109.1
	FS4-Ol29-2-p13	43.6	0.024	39.5	0.006	0.016	0.263	16.31	0.188	0.142	100	119.6
	FS4-Ol29-2-p14	43.8	0.016	39.9	0.01	0.012	0.256	16.31	0.201	0.142	100.7	129
	FS4-Ol29-2-p15	43.8	0.041	39.7	0.007	0.013	0.253	16.2	0.192	0.137	100.4	139.5
	FS4-Ol29-2-p16	43.8	0.01	39.81	0.012	0.021	0.253	16.39	0.196	0.132	100.7	149
	FS4-Ol29-2-p17	43.8	0.018	39.72	0.012	0.016	0.254	16.13	0.183	0.144	100.3	159.4
	FS4-Ol29-2-p18	43.8	0.008	39.74	0.004	0.014	0.255	16.16	0.19	0.151	100.4	168.9
	FS4-Ol29-2-p19	43.5	0.012	39.98	0	0.019	0.266	16.42	0.192	0.16	100.5	179.3
	FS4-Ol29-2-p20	43.7	0.016	39.65	0.004	0.014	0.26	16.39	0.19	0.151	100.4	188.8
	FS4-Ol29-2-p21	43.9	0.028	40.07	0.009	0.015	0.261	16.26	0.197	0.138	100.9	199.3
	FS4-Ol29-2-p22	43.9	0.027	39.96	3E-04	0.011	0.259	16.39	0.193	0.13	100.8	209.7
	FS4-Ol11-1-p1	30.2	0.024	36.92	0.053	0.004	0.627	31.89	0.231	0.017	99.99	0
	FS4-Ol11-1-p2	32.8	0.02	37.66	0.026	0.005	0.525	29.21	0.177	0.037	100.5	5.1

	Perfiles - University of Bristol (CAMECA)											
	Point	MgO (Wt%)	Al_2O3 (Wt%)	SiO_2 (Wt%)	TiO_2 (Wt%)	Cr_2O_3 (Wt%)	MnO (Wt%)	FeO (Wt%)	CaO (Wt%)	NiO (Wt%)	Total (Wt%)	Distance from rim (µm)
Fui Sur	FS4-Ol11-1-p3	35.8	0.014	38.05	0.018	0.008	0.421	25.51	0.15	0.075	100	10.05
	FS4-Ol11-1-p4	39.4	0.017	38.84	0.015	0.011	0.329	21.01	0.182	0.084	99.9	15.13
	FS4-Ol11-1-p5	42.1	0.026	39.66	0.004	0.005	0.272	18.23	0.174	0.134	100.7	20.1
	FS4-Ol11-1-p6	42.2	0.027	39.57	0.006	0.011	0.263	17.3	0.176	0.147	99.7	25.08
	FS4-Ol11-1-p7	42.6	0.016	39.68	0.008	0.01	0.259	16.95	0.175	0.169	99.82	30.15
	FS4-Ol11-1-p8	43.3	0.016	39.83	0.003	0.011	0.262	16.84	0.166	0.173	100.6	35.13
	FS4-Ol11-1-p9	43.1	0.023	40.13	0.009	0.015	0.244	16.72	0.18	0.164	100.6	40.12
	FS4-Ol11-1-p10	43.2	0.032	39.8	0.003	0.01	0.255	16.46	0.173	0.182	100.1	45.19
	FS4-Ol11-1-p11	43.3	0.027	39.89	0.009	0.013	0.253	16.51	0.173	0.167	100.4	50.17
	FS4-Ol11-1-p12	43.3	0.013	39.8	0.005	0.013	0.258	16.59	0.168	0.167	100.3	55.15
	FS4-Ol11-1-p13	43.1	0.034	39.64	0.011	0.015	0.252	16.73	0.175	0.148	100.1	60.22
	FS4-Ol11-1-p14	43	0.015	39.77	0.003	0.012	0.27	16.72	0.17	0.175	100.1	65.2
	FS4-Ol11-1-p15	42.9	0.022	39.67	0.003	0.01	0.257	16.85	0.184	0.156	100.1	70.26
	FS4-Ol11-1-p16	42.7	0.015	39.61	0.01	0.013	0.269	16.99	0.169	0.144	99.97	75.27
	FS4-Ol11-1-p17	42.8	0.022	39.65	0.001	0.007	0.27	17.07	0.188	0.149	100.1	80.25
	FS4-Ol11-1-p18	43	0.013	39.65	0.009	0.009	0.264	17.31	0.188	0.143	100.6	85.31
	FS4-Ol11-1-p19	42.9	0.028	39.62	4E-04	0.009	0.277	17.51	0.175	0.14	100.7	90.29
	FS4-Ol11-1-p20	42.6	0.018	39.48	0.01	0.013	0.293	17.48	0.178	0.137	100.2	95.28
	FS4-Ol11-1-p21	42.7	0.016	39.55	0.006	0.01	0.286	17.74	0.182	0.139	100.6	100.3
	FS4-Ol11-1-p22	42.5	0.016	39.28	0.002	0.015	0.297	17.73	0.186	0.124	100.2	105.3
	FS4-Ol11-1-p23	42.5	0.012	39.48	0.009	0.009	0.285	17.96	0.182	0.115	100.6	110.3
	FS4-Ol11-2-p1	42.2	0.012	39.55	0.006	0.008	0.281	17.7	0.181	0.128	100.1	0
	FS4-Ol11-2-p2	42.1	0.024	39.66	0.005	0.012	0.289	17.92	0.174	0.124	100.3	10.05
	FS4-Ol11-2-p3	42.1	0.012	39.5	0.005	0.01	0.291	18.22	0.178	0.124	100.5	20.1
	FS4-Ol11-2-p4	42.1	0.015	39.46	0.002	0.013	0.297	18.33	0.175	0.109	100.5	30.15
	FS4-Ol11-2-p5	41.7	0.012	39.15	0.014	0.012	0.295	18.48	0.176	0.119	99.98	40.2
	FS4-Ol11-2-p6	41.7	0.013	39.25	0.015	0.007	0.311	18.41	0.182	0.106	99.97	50.25
	FS4-Ol11-2-p7	41.9	0.02	39.32	0	0.012	0.3	18.54	0.183	0.1	100.3	60.3
	FS4-Ol11-2-p8	41.7	0.015	39.19	0.002	0.017	0.309	18.79	0.179	0.104	100.3	70.35
	FS4-Ol11-2-p10	41.3	0.028	39.58	0.008	0.011	0.307	18.88	0.18	0.105	100.4	90.45
	FS4-Ol11-2-p11	41.6	0.019	39.32	0.002	0.008	0.309	19.03	0.173	0.121	100.6	100.5
	FS4-Ol11-2-p12	41.4	0.022	39.29	0.008	0.016	0.309	19.1	0.181	0.121	100.4	110.6
	FS4-Ol11-2-p13	41.5	0.032	39	0	0.01	0.32	19.07	0.176	0.11	100.2	120.6
	FS4-Ol11-2-p16	41	0.028	39.39	0.008	0.008	0.311	19.15	0.186	0.107	100.2	150.8
	FS4-Ol11-2-p17	41.2	0.019	39.25	0.002	0.012	0.311	19.29	0.176	0.108	100.4	159.8
	FS4-Ol11-2-p18	41.4	0.018	39.38	0	0.012	0.314	19.31	0.173	0.108	100.7	169.9
	FS4-Ol11-2-p19	41.2	0.011	39.54	0.011	0.01	0.296	19.19	0.19	0.111	100.5	179.9
	FS4-Ol11-2-p20	41	0.025	39.27	0.003	0.01	0.318	19.32	0.181	0.11	100.2	190

	Perfiles - University of Bristol (CAMECA)											
	Point	MgO (Wt%)	Al_2O3 (Wt%)	SiO_2 (Wt%)	TiO_2 (Wt%)	Cr_2O_3 (Wt%)	MnO (Wt%)	FeO (Wt%)	CaO (Wt%)	NiO (Wt%)	Total (Wt%)	Distance from rim (µm)
Fui Sur	FS4-Ol11-2-p21	41	0.013	39.22	0.006	0.01	0.317	19.25	0.198	0.1	100.1	200
	FS4-Ol11-2-p22	41	0.02	39.14	0	0.012	0.318	19.31	0.171	0.094	100	210.1
	FS4-Ol11-2-p23	41.1	0.007	39.2	0.008	0.012	0.317	19.27	0.175	0.106	100.2	220.1
	FS4-Ol11-2-p24	40.4	0.033	39.81	0.015	0.012	0.32	19.29	0.185	0.127	100.2	230.2
	FS4-Ol11-2-p25	41.2	0.018	39.5	0.01	0.006	0.313	19.24	0.179	0.107	100.6	240.2
	FS4-Ol11-2-p26	41	0.013	39.09	0.013	0.01	0.321	19.4	0.174	0.108	100.2	250.3
	FS4-Ol11-2-p27	40.8	0.013	39.39	0.006	0.008	0.322	19.04	0.169	0.11	99.87	260.3
	FS4-Ol11-2-p29	41.2	0.024	39.28	0.006	0.01	0.306	19.26	0.189	0.113	100.4	280.4
	FS4-Ol11-2-p30	41.1	0.026	39.16	0	0.004	0.313	19.25	0.176	0.116	100.1	290.5
	FS4-Ol11-2-p31	41.3	0.015	39.36	0	0.01	0.31	19.24	0.175	0.112	100.5	300.5
	FS4-Ol11-2-p32	41.5	0.023	39.48	0.007	0.012	0.321	19.13	0.18	0.109	100.7	310.6
	FS4-Ol11-2-p33	41.5	0.019	39.19	0	0.008	0.317	19.5	0.188	0.1	100.8	319.5

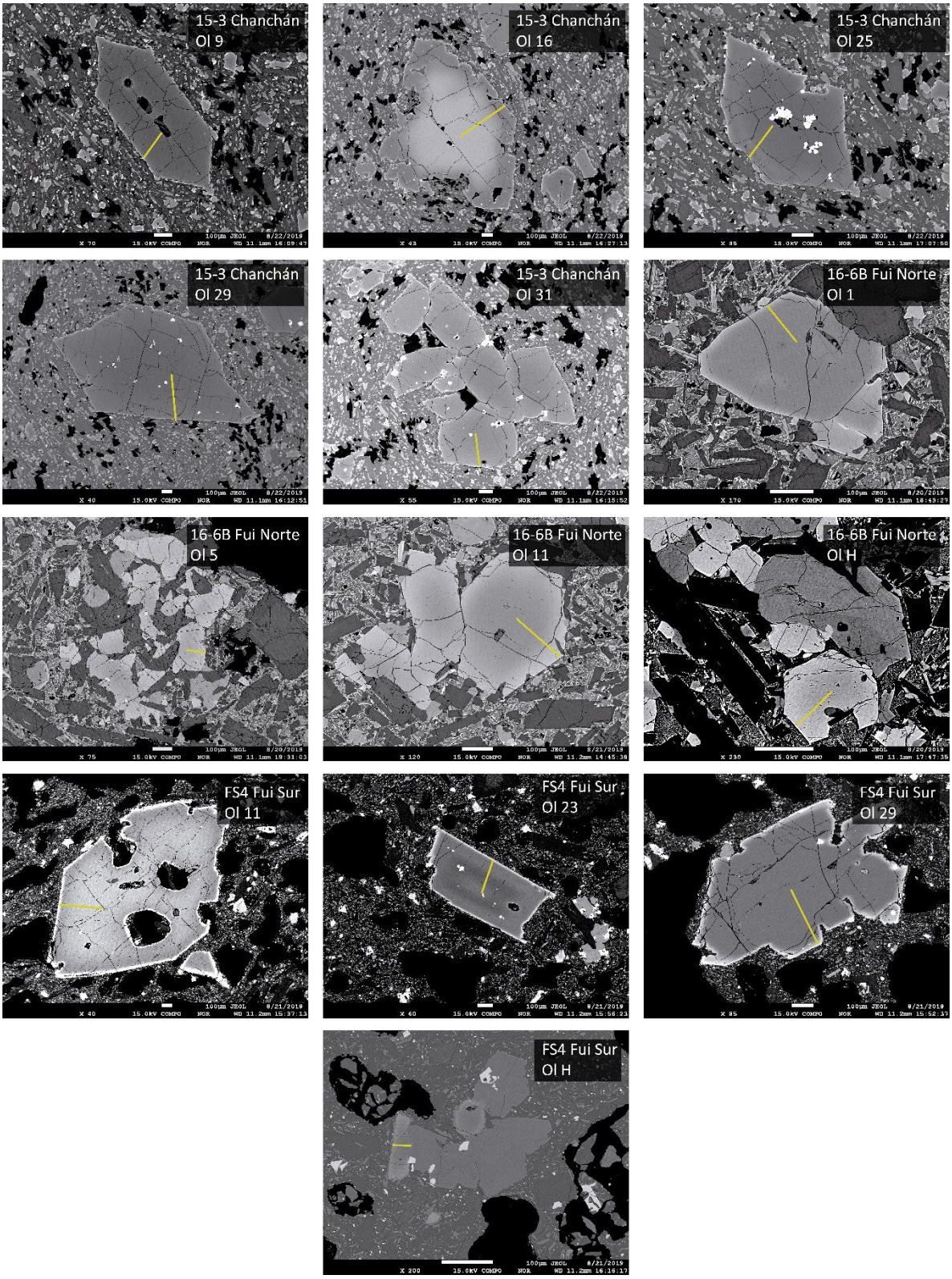

Fig. A.4.1: Ubicación de los perfiles composicionales en cristales de olivino.

Tabla A.4.2: Análisis de química mineral mediante microsonda electrónica (EPMA) de fenocristales (ph), microfenocristales (mph) y microlitos (m) de plagioclasa. (c=core, núcleo y r=rim, borde).

	Análisis Puntuales - LAMARX - Universidad Nacional de Córdoba														
	Point	Type	Na_2O (Wt%)	MgO (Wt%)	Al_2O_3 (Wt%)	SiO_2 (Wt%)	FeO (Wt%)	MnO (Wt%)	TiO_2 (Wt%)	BaO (Wt%)	K_2O (Wt%)	CaO (Wt%)	P_2O_5 (Wt%)	SrO (Wt%)	Total (Wt%)
Chanchán	15-3-Pl-mf-01	m	3.55	0.175	31.61	49.42	1.107	0.028	0.084	0.281	0.166	14.14	0	0.115	100.7
	15-3-Pl-mf-02	m	3.13	0.156	32.29	48.74	0.866	0	0	0.281	0.119	14.85	0.031	0.136	100.6
	15-3-Pl-mf-03	m	3.27	0.135	32.29	49.1	0.839	0.043	0.012	0.102	0.128	14.63	0.017	0.125	100.7
	15-3-Pl-mf-04	m	3.01	0.172	32.87	48.56	0.72	0	0.156	0.179	0.086	15.34	0.008	0.07	101.2
	15-3-Pl-mf-05	m	2.9	0.193	32.93	47.81	0.85	0.032	0.024	0.026	0.085	15.35	0.015	0.063	100.3
Fui Norte	166B-B-Pl-10	ph-c	2.21	0.108	32.53	48.89	0.653	0	0.073	0.154	0.077	16.49	0.021	0	101.2
	166B-B-Pl-11	ph-c	2.26	0.09	32.84	47.97	0.586	0.024	0	0.051	0.083	16.89	0.051	0.032	100.9
	166B-Pl-4-94	ph-c	2.3	0.107	32.73	47.68	0.588	0.036	0.048	0	0.094	16.42	0.015	0.063	100.1
	166B-Pl-4-95	ph-r	3.93	0.119	29.44	51.33	1.04	0	0	0	0.241	13.2	0.052	0.11	99.46
	166B-Pl-2-97	ph-r	4.35	0.131	28.86	52.51	0.741	0.016	0.048	0.077	0.283	12.69	0.007	0.167	99.88
	166B-Pl-6-99	ph-c	2.29	0.098	32.55	47.73	0.508	0	0	0	0.074	16.36	0.019	0.124	99.75
	166B-Pl-6-100	ph-c	1.75	0.082	33.06	46.9	0.598	0	0	0.154	0.055	17.31	0.021	0.087	100
	166B-Pl-6-101	ph-r	3.87	0.166	29.8	51.05	0.87	0	0.048	0	0.172	13.62	0.043	0.104	99.74
	166B-Pl-14-114	ph-c	2.2	0.08	32.38	46.73	0.604	0.055	0.024	0.077	0.059	16.4	0.007	0.105	98.72
	166B-Pl-MF1-120	m	4.01	0.146	29.51	52.19	0.841	0	0.024	0.051	0.236	13.12	0	0.025	100.2
	166B-Pl-MF1-121	m	3.96	0.12	29.59	51.29	0.891	0.036	0.12	0.026	0.245	13.37	0.039	0.096	99.78
	166B-Pl-MF2-129	m	4.04	0.109	29.44	51.54	0.824	0.055	0	0.128	0.292	13.12	0.038	0.1	99.69
	166B-Pl-MF2-130	m	3.68	0.124	30.45	51.1	0.953	0.008	0	0.026	0.253	13.8	0	0.111	100.5
	166B-B-Pl-12	ph-r	3.88	0.155	29.42	53.16	0.787	0	0	0.103	0.236	13.26	0.023	0.064	101.1
	166B-8-Pl-15	ph-c	4.12	0.052	29.28	52.68	0.534	0.032	0	0	0.152	12.83	0.016	0.088	99.78
	166B-8-Pl-16	ph-c	2.35	0.087	32.19	48.51	0.527	0	0.024	0	0.066	16.26	0	0.039	100.1
	166B-8-Pl-17	ph-r	5.03	0.148	27.3	54.92	0.847	0.04	0	0.154	0.426	11.1	0.009	0.038	100
	166B-5-Pl-54	mph-c	2.09	0.12	32.27	48.2	0.607	0.056	0.048	0	0.112	16.52	0.022	0.016	100.1
	166B-5-Pl-55	mph-r	3.43	0.113	30.37	51.44	0.993	0.071	0.386	0	0.215	14.17	0.016	0.092	101.3
	166B-1-Pl-71	ph-c	2.43	0.122	31.99	48.76	0.527	0.016	0	0.052	0.101	16.29	0.012	0.151	100.4
	166B-1-Pl-72	ph-c	1.62	0.125	33.44	47.27	0.533	0	0	0	0.066	17.59	0.025	0.132	100.8
	166B-1-Pl-73	ph-r	3.33	0.146	30.63	50.92	0.72	0.032	0.217	0.154	0.165	14.63	0.071	0.056	101.1
	166B-3-Pl-74	ph-c	4.23	0.138	29.16	53.31	0.76	0.103	0	0	0.237	12.83	0.043	0.127	100.9
	166B-Pl-10-86	ph-c	1.86	0.083	32.98	46.95	0.716	0.04	0.121	0	0.059	17.51	0.029	0.077	100.4
	166B-Pl-10-88	mph-c	2.27	0.124	32.29	47.28	0.756	0	0.157	0.077	0.083	16.52	0.021	0.04	99.62
Fui Sur	FS4-Pl-7-6	ph-c	1.7	0.086	33.46	46.37	0.628	0	0	0	0.02	17.77	0.02	0.024	100.1
	FS4-Pl-7-7	ph-c	1.84	0.086	33.37	47.01	0.671	0.012	0	0.026	0.023	17.63	0.022	0.031	100.7
	FS4-Pl-7-8	ph-r	4.02	0.089	29.91	52.45	0.532	0	0.108	0	0.095	13.47	0	0.161	100.8
	FS4-Pl-7-9	ph-c	2.05	0.09	33.32	47.18	0.628	0	0	0	0.045	17.17	0.006	0.076	100.6
	FS4-Pl-7-10	ph-c	2.7	0.104	31.97	48.81	0.582	0	0	0	0.048	15.93	0	0	100.1

	Análisis Puntuales - LAMARX - Universidad Nacional de Córdoba														
	Point	Type	Na_2O (Wt%)	MgO (Wt%)	Al_2O_3 (Wt%)	SiO_2 (Wt%)	FeO (Wt%)	MnO (Wt%)	TiO_2 (Wt%)	BaO (Wt%)	K_2O (Wt%)	CaO (Wt%)	P_2O_5 (Wt%)	SrO (Wt%)	Total (Wt%)
Fui Sur	FS4-Pl-7-11	ph-c	1.64	0.09	33.43	46.7	0.624	0.004	0.133	0	0.035	17.58	0	0.044	100.3
	FS4-Pl-7-12	ph-r	4.15	0.084	29.99	51.69	0.482	0	0.096	0.154	0.059	13.41	0.028	0.052	100.2
	FS4-Pl-12-15	ph-c	5.22	0.078	28.08	53.89	0.638	0.012	0.168	0.179	0.133	11.44	0.018	0.025	99.88
	FS4-Pl-12-16	ph-r	3.82	0.11	30.17	50.99	0.665	0	0.048	0	0.069	14.05	0.017	0.023	99.96
	FS4-Pl-28-19	ph-c	1.74	0.083	33.45	45.95	0.571	0.044	0	0	0.026	17.73	0	0.009	99.6
	FS4-Pl-28-20	ph-r	3.63	0.14	30.59	49.99	0.651	0	0	0.128	0.069	14.56	0	0.034	99.79
	FS4-Pl-22-37	ph-c	7.19	0.012	25.39	58.49	0.2	0.028	0	0.051	0.413	7.71	0.03	0.027	99.54
	FS4-Pl-13-38	ph-c	1.239	0.063	34.19	44.74	0.644	0	0	0	0.006	18.37	0.016	0.032	99.3
	FS4-Pl-14-41	ph-r	3.54	0.13	30.54	50.28	0.734	0	0	0	0.067	14.4	0.009	0.032	99.73
	FS4-Pl-26-44	ph-c	2.37	0.089	32.75	47.53	0.594	0	0.012	0.205	0.042	16.59	0.029	0.047	100.3
	FS4-Pl-26-45	ph-c	1.19	0.084	34.3	45.28	0.575	0	0.133	0	0.023	18.58	0.018	0.021	100.2
	FS4-Pl-26-46	ph-r	4.57	0.132	28.99	53.58	0.682	0	0.06	0.051	0.107	12.46	0.012	0.071	100.7
	FS4-Pl-27-47	ph-c	1.77	0.098	33.43	46.97	0.708	0.02	0.085	0	0.028	17.45	0	0.047	100.6
	FS4-Pl-27-48	ph-r	4.33	0.096	29.88	52.7	0.851	0.087	0.048	0	0.094	13.25	0.007	0.086	101.4
	FS4-Pl-A-59	ph-c	6.11	0.032	27.04	55.89	0.519	0	0.072	0	0.155	9.81	0.024	0.074	99.73
	FS4-Pl-A-60	ph-r	4.29	0.115	29.7	52.48	0.685	0.052	0	0	0.092	13.28	0.022	0.019	100.7
	FS4-Pl-F-63	mph-c	4.14	0.171	29.34	52.08	0.954	0.016	0.084	0	0.122	13.05	0.023	0.018	100
	FS4-Pl-8.2-65	mph-c	4.01	0.146	29.94	51.11	0.844	0.044	0	0	0.103	13.66	0	0.028	99.88
	FS4-Pl-9-69	ph-c	1.43	0.098	33.95	45.66	0.429	0	0	0.103	0.034	18.36	0.01	0.033	100.1
	FS4-Pl-9-70	ph-r	3.97	0.144	29.84	51.34	0.811	0	0	0.154	0.104	13.63	0	0	99.99
	FS4-Pl-16-73	ph-c	1.64	0.11	33.49	46.3	0.644	0.008	0	0.154	0.023	17.9	0.025	0.025	100.3
	FS4-Pl-16-74	ph-r	4.45	0.096	29.77	52.76	0.715	0	0.072	0	0.093	12.99	0.029	0	101
	FS4-Pl-17-75	ph-c	5.44	0.063	27.87	55.18	0.592	0.004	0.072	0	0.147	10.89	0	0.084	100.3
	FS4-Pl-17-76	ph-r	4.3	0.117	29.85	52.08	0.652	0.052	0.048	0	0.101	13.04	0.012	0.063	100.3
	FS4-Pl-31-80	ph-c	1.039	0.033	34.88	45.39	0.501	0	0.121	0.077	0.024	18.91	0.006	0.031	101
	FS4-Pl-31-81	ph-r	4.22	0.124	29.71	52.38	0.734	0	0.12	0	0.086	13.32	0.005	0.1	100.8
	FS4-Pl-25-82	ph-c	1.12	0.096	34.64	45.89	0.551	0	0	0	0.009	18.7	0.024	0.006	101
	FS4-Pl-25-83	ph-r	3.99	0.114	30.27	51.64	0.625	0.012	0.012	0	0.08	14.01	0.034	0.028	100.8
	FS4-Pl-18-88	ph-c	4.61	0.106	28.77	53.29	0.718	0.012	0.096	0	0.11	12.33	0.004	0.125	100.2
	FS4-Pl-3S-94	ph-c	0.949	0.058	34.74	45.03	0.554	0	0.145	0.051	0.011	19.08	0.02	0.068	100.7
	FS4-Pl-3S-95	ph-r	4.23	0.121	29.63	52.13	0.675	0.028	0.096	0	0.101	13.19	0.011	0.038	100.2
	FS4-Pl-32-102	ph-c	2.1	0.096	33.22	47.13	0.588	0.016	0.012	0.051	0.045	17.26	0.01	0.009	100.5
	FS4-Pl-32-103	ph-r	4.19	0.141	29.89	52.33	0.751	0.032	0.096	0	0.092	13.32	0.017	0	100.9
	FS4-Pl-mf-104	m	5.29	0.121	27.85	54.2	1.206	0.016	0.156	0	0.207	11.18	0.005	0.043	100.3
	FS4-Pl-mf-105	m	4.75	0.116	28.64	53.04	1.052	0.055	0.036	0	0.138	11.9	0.051	0.006	99.78
	FS4-Pl-mf-106	m	5.31	0.12	27.43	53.59	0.996	0.075	0.204	0.026	0.197	10.87	0.029	0.094	98.94
	FS4-Pl-mf-107	m	4.95	0.123	28.57	53.33	0.913	0.016	0.024	0	0.13	11.85	0.033	0.076	100
	FS4-Pl-mf-108	m	4.17	0.106	29.78	52.07	0.813	0.043	0.144	0	0.096	13.09	0.002	0	100.3

	Análisis Puntuales - University of Bristol (Jeol)										
	Point	Type	Na_2O (Wt%)	MgO (Wt%)	Al_2O_3 (Wt%)	SiO_2 (Wt%)	FeO (Wt%)	TiO_2 (Wt%)	K_2O (Wt%)	CaO (Wt%)	Total (Wt%)
Fui Norte	16-6B-pl-MF-core2	m	4.827	0.162	27.07	54.53	0.999	0.173	0.468	11.61	99.85
	16-6B-pl-MF-core3	m	6.923	0.106	24.63	58.66	1.394	0.15	0.888	7.515	100.3
	16-6B-pl-MF-c4	m	5.198	0.089	27.3	55.6	1.319	0.054	0.399	11.23	101.2
	16-6B-pl-MF-c5	m	4.802	0.12	28.26	54.1	1.155	0.061	0.412	11.83	100.7
	16-6B-pl2-core	ph-c	2.75	0.119	31.8	48.38	0.528	0.03	0.094	15.86	99.56
	16-6B-pl14-core	ph-c	2.346	0.105	32.49	48.2	0.597	0	0.059	16.7	100.5
	16-6B-pl14-rim	ph-r	5.172	0.127	28.04	55.19	0.876	0.08	0.495	10.38	100.4
	16-6B-plCP1-incl	mph-c	3.854	0.115	29.62	52.09	0.947	0.015	0.218	12.99	99.85
	16-6B-pl-c6	mph-c	3.134	0.125	30.78	51.3	1.097	0.114	0.205	14.57	101.3
	16-6B-pl-r6	mph-r	6.811	0.08	23.86	59.38	1.197	0.274	1.016	7.278	99.89
	16-6B-pl-CP4-core	mph-c	4.026	0.169	29.33	52.08	0.606	0.115	0.208	13.2	99.73
	16-6B-pl-CP4-rim	mph-r	7.144	0.084	23.34	60.34	1.171	0.152	0.963	6.823	100
	16-6B-pl10-core	ph-c	1.793	0.082	32.61	47.04	0.874	0	0.078	17.04	99.51
	16-6B-pl-MF-c7	m	4.146	0.088	28.95	52.61	0.914	0.187	0.302	12.5	99.7
	16-6B-pl-MF-c8	m	4.767	0.113	27.96	53.72	1.407	0.128	0.393	12.4	100.9
	16-6B-pl-pr1-1	mph-c	3.528	0.084	31.06	51.16	0.79	0.059	0.181	14.46	101.3
	16-6B-pl-pr1-8	mph-c	3.928	0.1	29.45	51.49	0.768	0.102	0.194	14.04	100.1
	16-6B-pl-pr1-12	mph-r	3.874	0.143	29.34	52.07	1.099	0.002	0.271	13.55	100.4
	16-6B-pl-pr2-1	mph-c	1.609	0.08	33.25	47.36	0.653	0.139	0.061	17.84	101
	16-6B-pl-pr2-13	mph-r	4.127	0.127	29.75	52.83	0.985	0.015	0.212	13.06	101.1
	16-6B-pl-pr3-1	mph-c	2.158	0.108	33.05	47.89	0.6	0.048	0.07	16.59	100.5
	16-6B-pl-pr3-7	mph-c	1.553	0.08	32.92	47.5	0.551	0.018	0.062	17.6	100.3
	16-6B-pl-pr3-12	mph-r	3.845	0.124	29.13	51.4	0.854	0.077	0.215	13.21	98.85
	16-6B-pl-pr4-8	mph-c	3.486	0.144	30.21	50.94	0.797	0.059	0.156	14.6	100.4
	16-6B-pl-pr4-13	mph-r	3.864	0.172	29.43	52.28	0.745	0.049	0.223	12.95	99.72
	16-6B-pl-pr5-3	mph-c	1.766	0.07	33.8	46.49	0.75	0.093	0.06	18.19	101.2
	16-6B-pl-pr5-6	mph-c	3.538	0.159	30.04	52.04	0.915	0.105	0.19	13.3	100.3
	16-6B-pl-pr5-9	mph-r	4.376	0.178	28.53	53.1	0.938	0.004	0.335	12.17	99.63
	16-6B-pl-pr6-1	mph-c	4.19	0.168	29.53	53.11	0.654	0.009	0.198	12.49	100.3
	16-6B-pl-pr6-4	mph-c	3.461	0.148	30.97	50.68	0.706	0.01	0.163	14.91	101
	16-6B-pl-pr6-5	mph-r	3.923	0.145	29.07	52.12	0.885	0.024	0.164	13.86	100.2
Chanchán	15-3-pl-D-int	m	2.818	0.207	31.28	48.55	1.126	0.06	0.151	15.32	99.51
	15-3-pl-22-int	m	2.909	0.163	31.12	49.37	0.92	0.056	0.087	15.84	100.5
	15-3-pl-8-int	m	2.95	0.199	30.59	50.12	1.022	0	0.117	15.07	100.1
	15-3-pl-MF-c1	m	2.7	0.119	31.4	49.08	0.844	0.064	0.103	15.94	100.2
	15-3-pl-MF-c2	m	3.215	0.164	30.61	50.75	0.878	0.084	0.178	14.17	100
	15-3-pl-MF-c3	m	2.975	0.131	31.68	49.41	0.861	0.066	0.164	16.03	101.3
	15-3-pl-MF-c4	m	2.808	0.132	31.57	48.78	0.78	0.099	0.078	16	100.3

	Análisis Puntuales - University of Bristol (Jeol)										
	Point	Type	Na_2O (Wt%)	MgO (Wt%)	Al_2O_3 (Wt%)	SiO_2 (Wt%)	FeO (Wt%)	TiO_2 (Wt%)	K_2O (Wt%)	CaO (Wt%)	Total (Wt%)
Chanchán	15-3-pl-MF-c5	m	3.119	0.152	31.41	49.8	0.801	0.011	0.101	15.34	100.7
	15-3-pl-MF-c6	m	2.75	0.182	31.46	48.75	0.627	0.035	0.057	15.51	99.37
	15-3-pl-pr1-1	m	2.664	0.169	31.61	49.25	0.777	0.03	0.108	15.72	100.3
	15-3-pl-pr1-9	m	4.23	0.099	28.93	52.78	1.136	0.057	0.235	13.3	100.8
	15-3-pl-pr1-12	m	6.391	0.09	25.46	58.01	1.093	0.123	0.571	8.115	99.85
	15-3-pl-pr2-1	m	2.45	0.144	31.81	48.62	0.781	0.084	0.07	16.23	100.2
	15-3-pl-pr2-12	m	3.222	0.174	29.73	50.39	0.785	0.043	0.121	14.21	98.68
	15-3-pl-pr3-1	m	2.747	0.183	31.57	48.86	0.446	0.119	0.073	15.65	99.66
	15-3-pl-pr3-9	m	2.191	0.099	32.76	48.04	0.705	0	0.052	16.54	100.4
	15-3-pl-pr3-18	m	3.202	0.134	30.23	50.36	0.956	0.103	0.174	14.58	99.74
	15-3-pl-pr4-1	m	2.206	0.148	31.65	49.07	0.655	0	0.014	15.53	99.23
	15-3-pl-pr4-15	m	3.182	0.21	30.51	50.42	0.857	0.006	0.129	14.55	99.86
	15-3-pl-pr4-16	m	4.106	0.166	28.95	52.49	1.056	0.001	0.22	13.64	100.6
	15-3-pl-pr5-1	m	2.124	0.137	32.58	47.95	0.887	0.056	0.066	16.64	100.4
	15-3-pl-pr5-13	m	2.796	0.179	31.38	48.52	0.673	0.08	0.11	16.1	99.84
Fui Sur	FS4-PL-13-rim	ph-r	4.735	0.112	28.84	53.46	0.72	0.054	0.096	12.36	100.4
	FS4-Pl-MF-c1	m	5.141	0.049	27.45	54.48	1.138	0.169	0.194	10.58	99.21
	FS4-Pl-14-anillo	ph-c	1.881	0.121	32.86	46.71	0.52	0.042	0.034	17.55	99.72
	FS4-Pl-14-core	ph-c	1.419	0.054	33.11	46.28	0.554	0	0.033	18.23	99.67
	FS4-Pl-28-core	ph-c	2.875	0.103	31.49	49.5	0.607	0.008	0.026	16.24	100.8
	FS4-Pl-28-anillo	ph-c	1.191	0.116	33.75	45.63	0.517	0.023	0.006	18.43	99.66
	FS4-Pl-MF-c2	m	4.144	0.127	30.03	53.14	0.928	0.156	0.118	12.77	101.4
	FS4-Pl-MF-c3	m	4.396	0.1	29.08	52.75	0.98	0.071	0.117	12.78	100.3
	FS4-Pl-MF-c4	m	5.322	0.111	27.41	54.86	1.042	0.194	0.246	9.775	98.96
	FS4-Pl-MF-c5	m	3.941	0.071	29.06	52.58	0.895	0	0.099	12.97	99.58
	FS4-Pl-MF-c6	m	4.93	0.089	28.25	54.24	1.011	0.096	0.178	10.99	99.78
	FS4-Pl-MF-c7	m	6.231	0.115	25.91	57.61	1.336	0.142	0.302	9.531	101.2
	FS4-pl-pr1-1	mph-c	0.892	0.072	34.49	43.98	0.464	0	0.002	18.83	98.7
	FS4-pl-pr1-6	mph-c	1.615	0.098	32.94	46.22	0.574	0.045	0.027	17.2	98.72
	FS4-pl-pr1-8	mph-c	0.963	0.081	34.22	44.93	0.668	0.115	0.012	17.87	98.86
	FS4-pl-pr1-13	mph-r	3.963	0.1	29.43	51.35	0.661	0	0.085	13.16	98.69
	FS4-pl-pr1-15	mph-r	4.691	0.139	29.03	53.58	0.802	0.002	0.114	11.98	100.3
	FS4-pl-pr2-2	mph-c	4.536	0.13	28.54	52.58	0.742	0.066	0.09	12.73	99.42
	FS4-pl-pr2-11	mph-r	4.848	0.144	27.64	54.44	0.76	0.096	0.122	11.94	100
	FS4-pl-pr3-1	mph-c	1.775	0.04	32.7	46.47	0.57	0.046	0.033	17.15	98.78
	FS4-pl-pr3-7	mph-c	1.361	0.043	33.42	46.1	0.65	0	0.009	17.9	99.42
	FS4-pl-pr3-11	mph-r	4.116	0.14	28.5	52.31	0.765	0	0.095	12.81	98.66
	FS4-pl-pr3-12	mph-r	4.618	0.102	28.38	52.22	0.978	0.056	0.136	12.33	98.82

	Análisis Puntuales - University of Bristol (Jeol)										
	Point	Ttype	Na_2O (Wt%)	MgO (Wt%)	Al_2O_3 (Wt%)	SiO_2 (Wt%)	FeO (Wt%)	TiO_2 (Wt%)	K_2O (Wt%)	CaO (Wt%)	Total (Wt%)
Fui Sur	FS4-pl-pr4-2	mph-c	3.915	0.133	29.28	52.11	0.792	0.082	0.079	13.69	100.1
	FS4-pl-pr4-7	mph-c	4.784	0.111	28.26	53.07	0.92	0.093	0.108	12.48	99.82
	FS4-pl-pr4-10	mph-r	5.067	0.126	28.14	54.56	1.052	0.223	0.168	11.38	100.7
	FS4-pl-pr5-1	mph-c	1.654	0.046	33.11	47.17	0.526	0.029	0.056	16.84	99.43
	FS4-pl-pr5-4	mph-c	1.27	0.073	33.44	45.72	0.826	0.081	0.011	18.88	100.3
	FS4-pl-pr5-10	mph-r	4.378	0.111	29.51	52.68	0.641	0.066	0.117	12.99	100.5

	Perfiles - University of Bristol (CAMECA)											
	Point	Na_2O (Wt%)	MgO (Wt%)	Al_2O_3 (Wt%)	SiO_2 (Wt%)	FeO (Wt%)	TiO_2 (Wt%)	K_2O (Wt%)	CaO (Wt%)	SrO (Wt%)	Total (Wt%)	Distance from rim (µm)
Fui Norte	16-6B-Pl1-p1	5.06	0.139	27.66	54.23	0.965	0.107	0.437	11.31	0.159	100.1	0
	16-6B-Pl1-p2	4.04	0.15	29.27	52.03	0.909	0.084	0.227	13.21	0.127	100	7.28
	16-6B-Pl1-p3	3.26	0.156	30.44	49.98	0.787	0.054	0.15	14.78	0.151	99.76	14.32
	16-6B-Pl1-p4	1.65	0.079	33.36	46.25	0.617	0.038	0.066	17.67	0.151	99.87	21.38
	16-6B-Pl1-p5	1.6	0.095	33.36	46.27	0.616	0.034	0.05	17.69	0.141	99.85	28.44
	16-6B-Pl1-p6	1.56	0.093	33.37	45.94	0.647	0.039	0.077	17.2	0.154	99.07	35.71
	16-6B-Pl1-p7	1.86	0.099	32.99	46.42	0.632	0.02	0.062	17.43	0.14	99.66	42.77
	16-6B-Pl1-p8	1.67	0.091	33.26	45.95	0.613	0.032	0.059	17.64	0.164	99.48	49.83
	16-6B-Pl1-p9	2.29	0.106	32.1	47.97	0.576	0.045	0.08	16.47	0.127	99.76	56.89
	16-6B-Pl1-p10	2.54	0.107	31.9	48.06	0.585	0.033	0.079	16.24	0.137	99.69	63.18
	16-6B-Pl1-p11	2.58	0.159	31.72	48.16	0.695	0.048	0.123	16.14	0.152	99.78	70.24
	16-6B-Pl1-p12	2.33	0.106	32.22	47.77	0.553	0.033	0.074	16.42	0.161	99.67	77.3
	16-6B-Pl1-p13	2.39	0.104	32.22	47.87	0.527	0.034	0.086	16.38	0.176	99.79	84.37
	16-6B-Pl1-p14	2.29	0.106	32.28	47.83	0.557	0.029	0.083	16.54	0.134	99.85	91.64
	16-6B-Pl1-p15	2.35	0.118	32.11	48.05	0.582	0.036	0.09	16.49	0.145	99.98	98.7
	16-6B-Pl1-p16	2.33	0.114	32.07	47.79	0.589	0.029	0.089	16.32	0.126	99.47	105.8
	16-6B-Pl1-p17	2.41	0.111	32.18	48.24	0.574	0.021	0.084	16.38	0.125	100.1	112.8
	16-6B-Pl1-p18	2.43	0.116	32.15	48.17	0.578	0.031	0.089	16.34	0.113	100	118.9
	16-6B-Pl3-p1	5.03	0.145	27.81	54.23	0.927	0.108	0.374	11.48	0.124	100.2	0
	16-6B-Pl3-p2	4.05	0.144	29.27	51.64	0.846	0.07	0.236	13.26	0.17	99.68	10.82
	16-6B-Pl3-p3	4.28	0.143	29.23	52.27	0.823	0.066	0.253	13.12	0.156	100.3	21.1
	16-6B-Pl3-p4	4.12	0.144	29.09	52.16	0.794	0.067	0.245	13.01	0.143	99.77	30.53
	16-6B-Pl3-p5	4.35	0.148	28.82	52.38	0.807	0.074	0.242	12.77	0.121	99.71	40.82
	16-6B-Pl3-p6	4.03	0.152	29.2	51.82	0.778	0.073	0.209	13.33	0.157	99.76	50.25
	16-6B-Pl3-p7	4.28	0.154	28.68	52.48	0.782	0.077	0.251	12.71	0.154	99.57	61.06
	16-6B-Pl3-p8	3.96	0.144	29.28	51.64	0.766	0.08	0.197	13.43	0.142	99.63	70.49
	16-6B-Pl3-p9	3.22	0.125	30.6	49.94	0.76	0.049	0.15	14.71	0.166	99.72	80.78
	16-6B-Pl3-p10	3.97	0.151	29.11	51.89	0.77	0.07	0.211	13.15	0.148	99.48	91.07
	16-6B-Pl3-p11	3.69	0.132	29.87	50.78	0.758	0.058	0.178	13.94	0.141	99.55	100.5
	16-6B-Pl3-p12	3.71	0.139	29.77	50.75	0.754	0.062	0.172	14.01	0.13	99.5	110.8
	16-6B-Pl3-p13	3.99	0.146	29.4	51.98	0.749	0.069	0.215	13.43	0.104	100.1	120.7
	16-6B-Pl3-p15	4.24	0.152	29	52.19	0.763	0.074	0.228	12.92	0.126	99.69	140.5
	16-6B-Pl3-p16	3.94	0.157	29.24	51.7	0.752	0.079	0.215	13.21	0.16	99.45	150.8
	16-6B-Pl3-p17	3.68	0.139	30.08	50.99	0.72	0.058	0.185	13.98	0.162	99.99	161
	16-6B-Pl3-p18	3.51	0.136	29.94	50.74	0.707	0.058	0.174	14.2	0.152	99.61	170.5
	16-6B-Pl3-p19	3.41	0.133	30.01	50.35	0.69	0.047	0.163	14.3	0.172	99.29	181.3
	16-6B-Pl3-p20	3.97	0.141	29.34	51.38	0.737	0.065	0.204	13.39	0.17	99.4	190.7
	16-6B-Pl3-p21	4.22	0.146	28.93	52.41	0.724	0.078	0.228	12.8	0.122	99.65	201

	Perfiles - University of Bristol (CAMECA)											
	Point	Na_2O (Wt%)	MgO (Wt%)	Al_2O_3 (Wt%)	SiO_2 (Wt%)	FeO (Wt%)	TiO_2 (Wt%)	K_2O (Wt%)	CaO (Wt%)	SrO (Wt%)	Total (Wt%)	Distance from rim (µm)
Fui Norte	16-6B-Pl3-p22	3.81	0.124	29.4	51.4	0.734	0.074	0.199	13.59	0.159	99.49	210.4
	16-6B-Pl3-p23	3.82	0.149	29.67	51.67	0.739	0.063	0.195	13.56	0.148	100	220.7
	16-6B-Pl3-p24	3.45	0.132	30	50.26	0.746	0.047	0.177	14.22	0.129	99.16	231
	16-6B-Pl3-p25	3.99	0.144	29.05	51.71	0.79	0.077	0.214	13.39	0.123	99.49	241
	16-6B-Pl3-p26	3.9	0.152	29.27	51.51	0.76	0.072	0.201	13.48	0.16	99.51	251.3
	16-6B-Pl3-p27	3.84	0.439	28.91	51.22	1.273	0.158	0.277	13.39	0.152	99.66	260.7
	16-6B-Pl3-p28	4.2	0.157	29.12	51.76	0.758	0.068	0.216	13.04	0.179	99.5	271
	16-6B-Pl3-p30	3.59	0.131	29.95	50.97	0.766	0.056	0.187	13.9	0.122	99.68	290.7
	16-6B-Pl3-p31	4	0.158	29.2	51.49	0.809	0.069	0.229	13.38	0.156	99.49	301.5
	16-6B-Pl3-p32	3.8	0.136	29.63	51.23	0.828	0.063	0.205	13.73	0.124	99.74	310.9
	16-6B-Pl3-p33	3.61	0.138	29.97	50.66	0.793	0.049	0.188	14.1	0.136	99.65	321.2
	16-6B-Pl3-p34	3.43	0.134	29.88	51.07	0.764	0.064	0.2	14.05	0.151	99.73	330.7
	16-6B-Pl3-p35	3.94	0.14	29.21	51.6	0.788	0.062	0.222	13.26	0.139	99.36	340.9
	16-6B-Pl3-p36	4.13	0.144	29.11	51.99	0.827	0.07	0.251	12.99	0.141	99.66	350.4
	16-6B-Pl4-p1	4.5	0.127	28.63	52.81	1.004	0.114	0.344	12.53	0.126	100.2	0
	16-6B-Pl4-p2	4.11	0.131	29.21	51.7	0.882	0.079	0.267	13.29	0.166	99.83	9.54
	16-6B-Pl4-p3	3.92	0.129	29.09	51.49	0.881	0.079	0.269	12.95	0.146	98.95	19.67
	16-6B-Pl4-p4	3.86	0.135	29.21	51.72	0.828	0.059	0.231	13.33	0.151	99.53	29.85
	16-6B-Pl4-p5	3.49	0.13	29.89	50.53	0.752	0.063	0.197	14.16	0.17	99.39	40.04
	16-6B-Pl4-p6	1.74	0.091	33	46.51	0.656	0.029	0.057	17.53	0.148	99.76	49.25
	16-6B-Pl4-p7	1.94	0.1	33	46.92	0.629	0.021	0.067	17.34	0.158	100.2	59.67
	16-6B-Pl4-p8	2.36	0.123	32.15	47.83	0.602	0.038	0.086	16.48	0.165	99.84	69.86
	16-6B-Pl4-p9	2.34	0.121	32.03	47.91	0.549	0.032	0.084	16.3	0.161	99.52	80.06
	16-6B-Pl4-p10	2.34	0.108	32.27	47.69	0.52	0.03	0.089	16.46	0.155	99.66	89.29
	16-6B-Pl4-p11	2.36	0.103	32.32	47.71	0.522	0.027	0.074	16.62	0.114	99.86	99.48
	16-6B-Pl4-p12	2.15	0.112	32.25	47.72	0.52	0.025	0.084	16.59	0.153	99.6	109.9
	16-6B-Pl4-p13	2.33	0.106	32.24	47.68	0.52	0.023	0.09	16.54	0.131	99.65	120.1
	16-6B-Pl4-p14	2.21	0.105	32.43	47.58	0.513	0.035	0.082	16.74	0.18	99.87	129.3
	16-6B-Pl4-p15	2.16	0.104	32.36	47.21	0.497	0.026	0.089	16.8	0.139	99.39	139.5
	16-6B-Pl4-p16	2.29	0.107	32.4	47.56	0.515	0.027	0.087	16.72	0.158	99.86	149.7
	16-6B-Pl4-p17	2.05	0.097	32.71	47.05	0.515	0.029	0.07	16.96	0.149	99.63	159.9
	16-6B-Pl4-p18	2.29	0.113	32.18	47.51	0.511	0.03	0.083	16.59	0.164	99.46	169.4
	16-6B-Pl4-p19	2.35	0.107	32.05	47.68	0.51	0.027	0.074	16.5	0.139	99.43	179.5
	16-6B-Pl4-p20	2.31	0.111	32.29	47.65	0.497	0.033	0.081	16.46	0.165	99.6	189.7
	16-6B-Pl4-p21	2.3	0.107	32.21	47.65	0.515	0.032	0.077	16.51	0.147	99.55	199.9
	16-6B-Pl4-p22	2.42	0.115	32.37	47.18	0.49	0.035	0.092	16.07	0.134	98.9	209.1
	16-6B-Pl4-p23	2.43	0.097	32.09	47.97	0.506	0.029	0.091	16.33	0.166	99.7	219.6
	16-6B-Pl4-p24	2.3	0.106	32.1	47.89	0.521	0.031	0.077	16.34	0.132	99.49	229.8

	Perfiles - University of Bristol (CAMECA)											
	Point	Na_2O (Wt%)	MgO (Wt%)	Al_2O_3 (Wt%)	SiO_2 (Wt%)	FeO (Wt%)	TiO_2 (Wt%)	K_2O (Wt%)	CaO (Wt%)	SrO (Wt%)	Total (Wt%)	Distance from rim (µm)
Fui Norte	16-6B-Pl4-p25	2.43	0.105	31.9	47.96	0.502	0.031	0.091	16.21	0.149	99.37	240
	16-6B-Pl4-p26	2.23	0.11	32.33	47.54	0.51	0.03	0.076	16.59	0.134	99.56	249.2
	16-6B-Pl4-p27	2.37	0.112	31.89	47.56	0.515	0.034	0.078	16.43	0.139	99.13	259.4
	16-6B-Pl4-p28	2.25	0.1	32.09	47.42	0.507	0.023	0.083	16.39	0.153	99.02	269.6
	16-6B-Pl4-p29	2.41	0.111	32.18	47.53	0.48	0.029	0.083	16.23	0.129	99.17	280
	16-6B-Pl4-p30	2.34	0.103	32.24	47.5	0.495	0.026	0.092	16.51	0.147	99.46	289.2
	16-6B-Pl4-p31	2.26	0.09	32.28	47.48	0.478	0.031	0.076	16.67	0.138	99.52	299.4
	16-6B-Pl4-p32	2.23	0.108	32.36	47.36	0.505	0.033	0.076	16.7	0.147	99.52	309.6
	16-6B-Pl4-p33	1.91	0.091	32.79	46.73	0.478	0.03	0.065	17.26	0.14	99.5	319.8
	16-6B-Pl4-p34	2.02	0.098	32.68	46.66	0.475	0.014	0.066	17.04	0.131	99.19	329.2
	16-6B-Pl4-p35	1.98	0.09	32.54	46.78	0.473	0.02	0.075	17.11	0.133	99.2	339.4
	16-6B-Pl4-p36	2.08	0.083	32.47	46.75	0.464	0.026	0.075	16.97	0.138	99.06	349.6
	16-6B-Pl4-p37	2.14	0.09	32.57	47.23	0.475	0.022	0.076	16.71	0.143	99.46	359.8
	16-6B-Pl4-p38	2.3	0.107	32.18	47.36	0.492	0.018	0.078	16.57	0.169	99.27	369
	16-6B-Pl4-p39	2.25	0.097	32.31	47.1	0.467	0.019	0.077	16.65	0.127	99.09	379.2
	16-6B-Pl4-p40	2.12	0.092	32.48	46.96	0.497	0.032	0.063	16.83	0.152	99.22	389.6
	16-6B-Pl4-p41	2.19	0.099	32.62	47.13	0.472	0.021	0.069	16.82	0.153	99.58	399.8
	16-6B-Pl4-p42	2.06	0.094	32.33	46.98	0.497	0.024	0.077	16.75	0.14	98.95	409.1
	16-6B-Pl4-p43	2.09	0.103	32.35	47.15	0.481	0.023	0.071	16.68	0.141	99.08	419.3
	16-6B-Pl4-p44	2.1	0.101	32.32	46.85	0.463	0.017	0.069	16.7	0.104	98.72	429.5
	16-6B-Pl4-p45	2.1	0.101	32.41	47.05	0.482	0.021	0.061	16.75	0.152	99.13	439.9
	16-6B-Pl4-p47	1.94	0.101	32.7	47.04	0.474	0.021	0.063	17.02	0.14	99.5	459.3
	16-6B-Pl4-p48	2	0.092	32.68	46.9	0.464	0.024	0.07	17.06	0.151	99.45	469.5
	16-6B-Pl4-p49	2	0.101	32.61	46.72	0.468	0.016	0.053	17.05	0.14	99.16	479.7
	16-6B-Pl4-p50	1.95	0.093	32.7	46.89	0.468	0.021	0.06	16.95	0.127	99.27	489.9
	16-6B-Pl5-1-p1	4.55	0.128	28.19	53.35	0.997	0.078	0.362	11.89	0.152	99.71	0
	16-6B-Pl5-1-p2	3.53	0.114	30.16	50.51	0.887	0.063	0.204	14.03	0.155	99.64	7.28
	16-6B-Pl5-1-p3	1.49	0.059	33.4	45.72	0.763	0.022	0.069	17.94	0.152	99.62	14.56
	16-6B-Pl5-1-p4	1.9	0.083	32.88	46.59	0.75	0.034	0.083	16.95	0.122	99.4	21.59
	16-6B-Pl5-1-p5	2.26	0.093	32.28	47.54	0.714	0.039	0.079	16.48	0.129	99.62	28.86
	16-6B-Pl5-1-p6	2.38	0.082	32.37	47.67	0.691	0.028	0.096	16.27	0.144	99.73	34.93
	16-6B-Pl5-2-p1	3.49	0.104	30.26	50.73	0.995	0.051	0.226	14.06	0.134	100.1	0
	16-6B-Pl5-2-p2	4.13	0.13	29.28	51.51	1.004	0.071	0.249	13.25	0.144	99.77	7.28
	16-6B-Pl5-2-p4	3.71	0.142	29.61	51.14	0.961	0.078	0.233	13.74	0.16	99.78	21.66
	16-6B-Pl5-2-p5	2.61	0.113	31.59	48.48	0.849	0.038	0.133	15.67	0.148	99.63	28.04
	16-6B-Pl5-2-p6	1.76	0.075	33.3	46.23	0.768	0.027	0.073	17.49	0.16	99.87	35.24
	16-6B-Pl5-2-p7	2.11	0.085	32.71	47.28	0.733	0.035	0.08	16.79	0.124	99.96	42.45
	16-6B-Pl5-2-p8	2.25	0.075	32.56	47.38	0.723	0.037	0.087	16.62	0.112	99.84	49.66

	Perfiles - University of Bristol (CAMECA)											
	Point	Na_2O (Wt%)	MgO (Wt%)	Al_2O_3 (Wt%)	SiO_2 (Wt%)	FeO (Wt%)	TiO_2 (Wt%)	K_2O (Wt%)	CaO (Wt%)	SrO (Wt%)	Total (Wt%)	Distance from rim (µm)
Fui Norte	16-6B-Pl5-2-p9	2.5	0.086	31.87	48.35	0.693	0.027	0.117	15.98	0.142	99.77	56.04
	16-6B-Pl6-p1	3.94	0.18	29.2	51.86	0.945	0.095	0.254	13.22	0.152	99.84	0
	16-6B-Pl6-p2	3.74	0.155	29.42	51.01	0.828	0.065	0.21	13.2	0.117	98.75	9.9
	16-6B-Pl6-p3	3.82	0.151	29.78	51.03	0.799	0.066	0.191	13.76	0.143	99.74	19.8
	16-6B-Pl6-p4	3.8	0.157	29.68	51.41	0.811	0.068	0.195	13.81	0.144	100.1	30.41
	16-6B-Pl6-p5	3.84	0.16	29.63	51.23	0.752	0.066	0.192	13.67	0.155	99.7	40.31
	16-6B-Pl6-p6	4.05	0.16	29.33	52.03	0.819	0.07	0.188	13.26	0.17	100.1	49.52
	16-6B-Pl6-p7	3.91	0.16	29.54	51.67	0.776	0.065	0.202	13.4	0.122	99.84	60.14
	16-6B-Pl6-p8	4.05	0.165	29.32	52.08	0.788	0.074	0.2	13.32	0.131	100.1	70.04
	16-6B-Pl6-p9	3.81	0.154	29.58	51.6	0.776	0.065	0.181	13.62	0.135	99.93	79.93
	16-6B-Pl6-p10	3.57	0.158	30.03	51.13	0.762	0.059	0.182	13.95	0.117	99.95	90.55
	16-6B-Pl6-p11	3.96	0.16	29.54	51.62	0.75	0.063	0.195	13.49	0.157	99.93	99.76
	16-6B-Pl6-p12	3.79	0.154	29.67	51.45	0.781	0.071	0.196	13.63	0.147	99.89	109.7
	16-6B-Pl6-p13	3.85	0.136	29.71	51.47	0.763	0.074	0.182	13.56	0.153	99.91	120.3
	16-6B-Pl6-p14	3.96	0.15	29.37	51.7	0.829	0.069	0.209	13.37	0.144	99.8	130.2
	16-6B-Pl6-p15	4.12	0.158	29.25	51.78	0.801	0.058	0.209	13.35	0.145	99.87	140.1
	16-6B-Pl6-p16	3.58	0.137	30.22	50.69	0.735	0.054	0.172	14.2	0.125	99.91	150
	16-6B-Pl6-p17	3.95	0.174	29.6	51.7	0.778	0.067	0.192	13.36	0.125	99.95	159.9
	16-6B-Pl6-p18	2.33	0.116	32.03	48.03	0.633	0.038	0.095	16.18	0.12	99.57	169.8
	16-6B-Pl6-p19	1.9	0.097	33.05	46.67	0.581	0.025	0.057	17.29	0.124	99.79	180.4
	16-6B-Pl6-p20	1.91	0.088	32.86	46.85	0.564	0.022	0.072	17.14	0.145	99.66	190.3
	16-6B-Pl6-p21	1.65	0.085	33.5	46.49	0.58	0.009	0.047	17.65	0.151	100.2	200.3
	16-6B-Pl6-p22	1.84	0.096	33.14	46.4	0.573	0.023	0.055	17.53	0.145	99.8	210.2
	16-6B-Pl6-p23	1.79	0.096	33.05	46.65	0.585	0.033	0.056	17.36	0.157	99.76	220.1
	16-6B-Pl6-p24	1.83	0.088	33.21	46.44	0.564	0.034	0.048	17.51	0.138	99.86	230.7
	16-6B-Pl6-p25	1.74	0.091	33.26	46.26	0.577	0.025	0.051	17.5	0.147	99.66	240.6
	16-6B-Pl6-p26	1.52	0.083	33.43	45.96	0.572	0.033	0.049	17.78	0.157	99.59	249.8
	16-6B-Pl6-p27	1.7	0.093	33.23	46.41	0.571	0.04	0.05	17.56	0.159	99.82	260.4
	16-6B-Pl6-p28	1.8	0.098	33.11	46.7	0.537	0.028	0.054	17.31	0.165	99.79	270.3
	16-6B-Pl6-p29	2.58	0.118	32.06	48.16	0.542	0.039	0.083	16.14	0.11	99.83	280.2
	16-6B-Pl6-p30	2.54	0.105	32.14	48.05	0.514	0.049	0.089	16.25	0.128	99.86	290.8
	16-6B-Pl6-p31	2.27	0.108	32.61	47.86	0.529	0.038	0.069	16.7	0.153	100.3	300
	16-6B-Pl6-p32	2.15	0.1	32.43	47.39	0.535	0.035	0.075	16.8	0.161	99.68	309.9
	16-6B-Pl6-p33	2.4	0.106	32.39	47.86	0.506	0.026	0.087	16.59	0.131	100.1	320.5
	16-6B-Pl6-p34	2.41	0.104	32.18	48.12	0.493	0.027	0.082	16.32	0.135	99.87	330.4
	16-6B-Pl6-p35	2.46	0.11	32.13	47.98	0.505	0.031	0.083	16.11	0.146	99.54	340.3
	16-6B-Pl6-p36	2.96	0.132	31.26	49.43	0.52	0.037	0.122	15.21	0.158	99.83	350.3
	16-6B-Pl6-p37	2.57	0.542	30.08	48.86	1.474	0.163	0.267	14.99	0.126	99.07	360.2

	Perfiles - University of Bristol (CAMECA)											
	Point	Na_2O (Wt%)	MgO (Wt%)	Al_2O_3 (Wt%)	SiO_2 (Wt%)	FeO (Wt%)	TiO_2 (Wt%)	K_2O (Wt%)	CaO (Wt%)	SrO (Wt%)	Total (Wt%)	Distance from rim (µm)
Fui Norte	16-6B-Pl6-p38	3.05	0.126	31.14	49.08	0.563	0.048	0.138	14.99	0.144	99.27	370.1
	16-6B-Pl6-p39	3.01	0.169	30.65	49.13	0.601	0.051	0.164	14.94	0.164	98.88	380.7
	16-6B-Pl6-p40	2.72	0.107	31.75	48.7	0.519	0.033	0.09	15.74	0.127	99.79	390.6
	16-6B-Pl6-p41	2.47	0.115	32.04	47.92	0.49	0.038	0.076	16.24	0.11	99.5	400.5
Fui Sur	FS4-PlF-p1	3.99	0.124	29.22	51.08	0.832	0.057	0.092	13.4	0.092	98.88	0
	FS4-PlF-p2	3.81	0.113	29.79	51.11	0.786	0.047	0.075	13.7	0.11	99.54	7.14
	FS4-PlF-p3	4.04	0.12	29.59	51.44	0.756	0.048	0.089	13.41	0.101	99.59	14.28
	FS4-PlF-p4	3.72	0.113	30.05	51.14	0.692	0.033	0.074	13.87	0.111	99.8	21.31
	FS4-PlF-p5	3.35	0.1	30.38	50.1	0.681	0.039	0.074	14.4	0.096	99.21	28.44
	FS4-PlF-p6	4.21	0.107	29.2	51.86	0.738	0.053	0.114	13.01	0.129	99.42	34.79
	FS4-PlS-p1	4.18	0.101	29.26	51.94	0.731	0.047	0.091	12.96	0.098	99.41	0
	FS4-PlS-p2	3.97	0.091	29.69	51.88	0.673	0.045	0.092	13.44	0.114	100	9.27
	FS4-PlS-p3	3.83	0.103	30.12	51.2	0.662	0.045	0.079	13.67	0.102	99.8	19.44
	FS4-PlS-p4	3.83	0.089	29.97	51.71	0.626	0.039	0.078	13.68	0.098	100.1	29.44
	FS4-PlS-p6	1.55	0.094	33.62	45.85	0.518	0.024	0.02	17.89	0.074	99.64	49.86
	FS4-PlS-p7	1.85	0.1	32.91	46.54	0.566	0.026	0.031	17.16	0.071	99.26	59.87
	FS4-PlS-p8	2.19	0.097	32.51	47.18	0.652	0.028	0.032	16.64	0.111	99.44	70.06
	FS4-PlS-p9	1.62	0.083	33.23	46.32	0.649	0.017	0.022	17.72	0.069	99.73	79.3
	FS4-PlS-p10	1.71	0.09	33.28	46.04	0.641	0.023	0.025	17.59	0.089	99.49	89.32
	FS4-PlS-p11	3.4	0.09	30.06	50.4	0.733	0.065	0.162	14.34	0.095	99.35	99.51
	FS4-PlS-p12	4.51	0.271	27.76	54.22	1.501	0.185	0.392	12.32	0.089	101.3	109.7
	FS4-PlS-p13	1.66	0.083	33.25	46.18	0.631	0.017	0.023	17.56	0.096	99.51	119.8
	FS4-PlS-p14	1.92	0.088	32.72	47	0.681	0.024	0.03	16.98	0.093	99.54	129.9
	FS4-PlS-p15	1.87	0.102	32.88	46.89	0.693	0.031	0.034	17.22	0.103	99.82	140.1
	FS4-PlS-p16	1.37	0.083	33.48	46.02	0.576	0.019	0.023	17.75	0.081	99.4	150.2
	FS4-Pl7-p1	4.04	0.079	29.95	51.82	0.519	0.037	0.087	13.43	0.095	100.1	0
	FS4-Pl7-p2	4.1	0.086	29.92	51.88	0.536	0.044	0.075	13.49	0.11	100.2	4.12
	FS4-Pl7-p3	3.53	0.101	30.49	50.51	0.604	0.036	0.063	14.32	0.057	99.71	8.06
	FS4-Pl7-p4	2.67	0.105	31.9	48.64	0.584	0.029	0.046	15.8	0.087	99.86	12.04
	FS4-Pl7-p5	1.5	0.095	33.34	45.96	0.543	0.015	0.017	17.94	0.092	99.51	16.03
	FS4-Pl7-p6	1.67	0.098	33.44	46.33	0.544	0.008	0.029	17.58	0.082	99.79	21.02
	FS4-Pl7-p7	1.37	0.077	33.8	45.87	0.49	0.021	0.021	18.02	0.059	99.73	25.02
	FS4-Pl7-p8	1.74	0.099	33.25	46.42	0.538	0.032	0.027	17.54	0.083	99.73	29.02
	FS4-Pl7-p9	1.74	0.088	33.15	46.7	0.585	0.013	0.026	17.52	0.062	99.89	33.02
	FS4-Pl7-p10	1.66	0.069	33.37	46.31	0.608	0.022	0.031	17.64	0.095	99.81	37.05
	FS4-Pl7-p11	1.8	0.078	33.24	46.69	0.655	0.027	0.025	17.29	0.073	99.89	42.05
	FS4-Pl7-p12	1.85	0.08	33.3	46.74	0.627	0.01	0.029	17.25	0.105	99.99	46.04
	FS4-Pl7-p13	1.72	0.075	33.19	46.57	0.631	0.011	0.028	17.39	0.083	99.7	50.04

	Perfiles - University of Bristol (CAMECA)											
	Point	Na_2O (Wt%)	MgO (Wt%)	Al_2O_3 (Wt%)	SiO_2 (Wt%)	FeO (Wt%)	TiO_2 (Wt%)	K_2O (Wt%)	CaO (Wt%)	SrO (Wt%)	Total (Wt%)	Distance from rim (µm)
Fui Sur	FS4-Pl7-p14	1.75	0.076	33.22	46.44	0.634	0.021	0.03	17.4	0.113	99.68	54.04
	FS4-Pl7-p15	2.04	0.093	32.71	47.21	0.633	0.017	0.032	17.01	0.116	99.86	58.03
	FS4-Pl7-p16	2.74	0.106	31.64	49.04	0.619	0.027	0.051	15.57	0.083	99.88	63.03
	FS4-Pl7-p17	3	0.111	31.39	49.17	0.647	0.027	0.063	15.26	0.109	99.78	67.03
	FS4-Pl7-p18	2.78	0.122	31.42	49.19	0.652	0.039	0.065	15.5	0.089	99.86	71.03
	FS4-Pl7-p19	2.85	0.113	31.5	48.91	0.684	0.023	0.055	15.51	0.081	99.73	75.07
	FS4-Pl7-p20	2.68	0.108	31.76	48.46	0.65	0.036	0.052	15.85	0.083	99.68	79.06
	FS4-Pl7-p21	2.96	0.114	31.26	49.18	0.652	0.028	0.055	15.3	0.075	99.63	84.06
	FS4-Pl7-p22	2.85	0.112	31.62	49.01	0.642	0.033	0.054	15.63	0.081	100	88.06
	FS4-Pl7-p23	2.48	0.11	31.94	48.49	0.641	0.033	0.051	16.03	0.095	99.86	92.05
	FS4-Pl7-p24	2.95	0.108	31.39	49.39	0.639	0.018	0.055	15.34	0.074	99.96	96.05
	FS4-Pl7-p25	2.94	0.112	31.37	49.21	0.6	0.028	0.057	15.4	0.087	99.81	100.1
	FS4-Pl7-p26	2.2	0.093	32.54	47.55	0.647	0.039	0.041	16.69	0.11	99.91	105.1
	FS4-Pl7-p27	1.69	0.089	33.04	46.24	0.629	0.018	0.031	17.5	0.086	99.33	109.1
	FS4-Pl7-p28	1.55	0.077	33.68	46.03	0.619	0.018	0.022	17.76	0.091	99.85	113.1
	FS4-Pl7-p29	1.42	0.08	33.57	45.46	0.606	0.016	0.017	17.99	0.089	99.25	117.1
	FS4-Pl7-p30	1.2	0.066	34.15	45.5	0.616	0.027	0.019	18.29	0.079	99.95	121.1
	FS4-Pl7-p31	1.24	0.068	34.12	45.34	0.612	0.012	0.019	18.39	0.086	99.89	126.1
	FS4-Pl7-p32	1.16	0.061	33.97	45.14	0.603	0.011	0.021	18.44	0.097	99.5	130.1
	FS4-Pl7-p33	1.22	0.067	33.96	45.3	0.623	0.019	0.015	18.42	0.091	99.72	134.1
	FS4-Pl7-p34	1.33	0.073	33.85	45.38	0.631	0.008	0.024	18.08	0.081	99.46	138.1
	FS4-Pl7-p35	1.88	0.078	32.93	46.91	0.635	0.02	0.039	17.04	0.088	99.62	142.1
	FS4-Pl7-p36	1.57	0.069	33.44	45.94	0.637	0.019	0.02	17.78	0.116	99.6	147.1
	FS4-Pl9-p1	4.23	0.101	29.24	53	0.74	0.061	0.102	12.72	0.132	100.3	0
	FS4-Pl9-p2	3.75	0.09	30.11	51.67	0.637	0.042	0.08	13.55	0.097	100	10.82
	FS4-Pl9-p3	1.59	0.094	33.32	46.83	0.546	0.013	0.028	17.44	0.082	99.96	20.81
	FS4-Pl9-p4	1.04	0.084	34.42	45.29	0.484	0.015	0.015	18.41	0.1	99.85	30.81
	FS4-Pl9-p5	1.41	0.088	34.07	45.7	0.481	0.02	0.027	18.26	0.086	100.1	40.8
	FS4-Pl9-p6	1.3	0.096	33.92	45.45	0.503	0.011	0.025	18.14	0.096	99.53	50.8
	FS4-Pl9-p7	1.31	0.098	33.92	45.63	0.476	0.011	0.026	18.16	0.047	99.67	60.8
	FS4-Pl9-p8	1.33	0.096	34	45.51	0.497	0.015	0.025	18.07	0.106	99.64	70.8
	FS4-Pl9-p9	1.32	0.097	33.79	45.78	0.502	0.012	0.026	18.09	0.088	99.71	80.8
	FS4-Pl9-p10	1.39	0.096	33.78	45.58	0.483	0.007	0.021	18.05	0.093	99.49	90.8
	FS4-Pl9-p11	1.33	0.102	33.87	45.5	0.487	0.018	0.024	18.07	0.065	99.48	100.8
	FS4-Pl9-p12	1.39	0.099	33.85	45.66	0.502	0.016	0.024	18.07	0.103	99.71	110.8
	FS4-Pl9-p13	1.42	0.106	33.7	45.79	0.486	0.015	0.027	18.06	0.087	99.7	120.8
	FS4-Pl9-p14	1.45	0.105	33.66	45.78	0.489	0.023	0.025	17.99	0.089	99.61	130.8
	FS4-Pl9-p15	1.41	0.098	33.8	45.9	0.499	0.012	0.028	18.07	0.079	99.89	140.8

	Perfiles - University of Bristol (CAMECA)											
	Point	Na_2O (Wt%)	MgO (Wt%)	Al_2O_3 (Wt%)	SiO_2 (Wt%)	FeO (Wt%)	TiO_2 (Wt%)	K_2O (Wt%)	CaO (Wt%)	SrO (Wt%)	Total (Wt%)	Distance from rim (µm)
Fui Sur	FS4-Pl9-p16	1.31	0.096	33.84	45.58	0.46	0.014	0.022	18.06	0.083	99.46	150.8
	FS4-Pl9-p17	1.34	0.098	33.9	45.28	0.476	0.015	0.033	18.01	0.098	99.25	160.8
	FS4-Pl9-p18	1.37	0.09	33.94	45.59	0.466	0.011	0.023	18.2	0.085	99.77	170.8
	FS4-Pl9-p19	1.32	0.098	33.86	45.46	0.464	0.018	0.023	18.15	0.077	99.47	180.8
	FS4-Pl9-p20	1.39	0.095	33.83	45.64	0.481	0.009	0.019	18.07	0.116	99.65	190.8
	FS4-Pl9-p21	1.35	0.091	33.79	45.37	0.465	0.021	0.024	18.08	0.076	99.26	200.8
	FS4-Pl9-p22	1.37	0.098	34.03	45.5	0.461	0.004	0.034	17.98	0.084	99.56	210.8
	FS4-Pl9-p23	1.42	0.09	33.77	45.47	0.455	0.006	0.03	18.02	0.09	99.35	220.8
	FS4-Pl9-p24	1.32	0.102	33.84	45.44	0.465	0.014	0.026	18.06	0.087	99.36	230.8
	FS4-Pl9-p25	1.38	0.09	33.77	45.27	0.466	0.004	0.03	18.1	0.085	99.2	240.8
	FS4-Pl9-p26	1.38	0.086	33.76	45.5	0.449	0.013	0.022	18.08	0.06	99.35	250.8
	FS4-Pl9-p27	1.42	0.091	33.79	45.5	0.467	0.014	0.024	18.09	0.087	99.48	260.8
	FS4-Pl9-p28	1.37	0.095	33.82	45.43	0.465	0.019	0.023	18.02	0.073	99.33	270.8
	FS4-Pl9-p29	1.34	0.096	33.71	45.59	0.46	0.01	0.026	18.01	0.088	99.33	280.8
	FS4-Pl9-p30	1.33	0.102	33.77	45.26	0.493	0.016	0.032	17.99	0.097	99.08	290.8
	FS4-Pl9-p31	1.36	0.089	33.71	45.47	0.5	0.014	0.027	18.02	0.094	99.29	300.8
	FS4-Pl9-p32	1.36	0.088	33.73	45.54	0.5	0.019	0.029	18.11	0.094	99.47	310.8
	FS4-Pl9-p33	1.26	0.091	33.69	45.4	0.498	0.015	0.021	18.07	0.073	99.12	320.8
	FS4-Pl9-p34	1.33	0.086	33.82	45.42	0.545	0.017	0.016	18.21	0.069	99.51	330.8
	FS4-Pl9-p35	1.3	0.089	34.14	45.45	0.566	0.009	0.024	18.25	0.048	99.88	340.8
	FS4-Pl9-p36	1.24	0.092	33.86	45.25	0.587	4E-04	0.022	18.27	0.083	99.41	350.2
	FS4-Pl12-1-p1	4.46	0.114	28.76	52.88	0.796	0.061	0.096	12.66	0.073	99.9	0
	FS4-Pl12-1-p2	3.79	0.118	29.7	51.19	0.743	0.039	0.067	13.55	0.098	99.3	7.21
	FS4-Pl12-1-p3	3.81	0.115	29.83	50.98	0.69	0.037	0.075	13.69	0.079	99.31	14.21
	FS4-Pl12-1-p4	4.05	0.136	29.39	52.07	0.706	0.052	0.081	13.22	0.104	99.81	21.26
	FS4-Pl12-1-p5	3.14	0.085	31.03	49.69	0.671	0.026	0.06	15.05	0.113	99.86	28.32
	FS4-Pl12-1-p6	3.31	0.078	30.92	49.84	0.672	0.034	0.059	14.73	0.101	99.75	35.38
	FS4-Pl12-1-p7	4.59	0.087	28.84	52.99	0.62	0.046	0.113	12.09	0.072	99.45	42.45
	FS4-Pl12-1-p8	4.77	0.088	28.55	53.63	0.634	0.044	0.115	12.09	0.111	100	49.52
	FS4-Pl12-2-p1	3.86	0.108	29.79	51.41	0.666	0.053	0.082	13.5	0.087	99.56	0
	FS4-Pl12-2-p2	3.25	0.087	30.58	49.17	0.692	0.031	0.066	14.58	0.088	98.55	7.21
	FS4-Pl12-2-p3	4.28	0.078	29.71	52.5	0.613	0.042	0.099	12.66	0.102	100.1	13.6
	FS4-Pl12-2-p4	4.83	0.086	28.71	53.59	0.599	0.054	0.114	11.97	0.137	100.1	21.4
	FS4-Pl12-2-p5	4.65	0.087	28.65	53.34	0.609	0.043	0.106	12.11	0.121	99.73	27.8
	FS4-Pl12-2-p6	4.76	0.088	28.32	53.82	0.589	0.046	0.119	11.81	0.068	99.62	35.61
	FS4-Pl12-2-p7	5.05	0.078	28.14	54.01	0.554	0.048	0.125	11.54	0.102	99.64	42.01
	FS4-Pl12-2-p8	5.11	0.085	27.99	54.44	0.537	0.044	0.132	11.37	0.115	99.82	49.04
	FS4-Pl12-2-p9	5.09	0.08	28.03	54.12	0.546	0.043	0.127	11.3	0.102	99.43	56.22

	Perfiles - University of Bristol (CAMECA)											
	Point	Na_2O (Wt%)	MgO (Wt%)	Al_2O_3 (Wt%)	SiO_2 (Wt%)	FeO (Wt%)	TiO_2 (Wt%)	K_2O (Wt%)	CaO (Wt%)	SrO (Wt%)	Total (Wt%)	Distance from rim (µm)
Fui Sur	FS4-Pl12-2-p10	5.37	0.076	27.68	54.92	0.527	0.051	0.138	10.84	0.111	99.72	62.63
	FS4-Pl12-2-p11	5.43	0.077	27.71	54.66	0.515	0.046	0.14	10.97	0.104	99.66	70.43
	FS4-Pl12-2-p12	5.08	0.072	28.13	54.17	0.579	0.049	0.122	11.5	0.116	99.82	76.84
	FS4-Pl12-2-p13	5.43	0.068	27.68	55.15	0.53	0.049	0.145	10.78	0.073	99.9	84.65
	FS4-Pl12-2-p14	5.18	0.074	28.23	54.19	0.539	0.041	0.133	11.3	0.113	99.81	91.05
	FS4-Pl12-2-p15	5.28	0.076	27.95	54.43	0.528	0.048	0.129	11.24	0.118	99.8	98.08
	FS4-Pl12-2-p16	5.17	0.264	27.66	54.71	0.735	0.052	0.133	10.97	0.119	99.81	105.3
	FS4-Pl12-2-p17	5.45	0.087	27.49	55.06	0.565	0.06	0.149	10.67	0.131	99.66	111.7
	FS4-Pl12-2-p18	5.63	0.076	27.13	55.5	0.514	0.053	0.156	10.47	0.096	99.63	119.5
	FS4-Pl12-2-p19	5.03	0.072	27.92	54.51	0.548	0.046	0.14	11.25	0.117	99.63	125.9
	FS4-Pl12-2-p20	5.1	0.08	28.09	54.38	0.532	0.042	0.138	11.28	0.1	99.74	133.7
	FS4-Pl12-2-p21	5.43	0.067	27.69	54.66	0.535	0.04	0.135	10.98	0.105	99.63	140.1
	FS4-Pl12-2-p22	5.26	0.065	27.95	54.52	0.53	0.056	0.133	11.25	0.116	99.88	147.1
	FS4-Pl12-2-p23	5.26	0.064	27.84	54.73	0.529	0.04	0.146	11.08	0.102	99.79	154.3
	FS4-Pl12-2-p24	5.15	0.077	27.88	54.67	0.516	0.05	0.136	11.08	0.127	99.68	160.7
	FS4-Pl12-2-p25	5.37	0.071	27.49	55.11	0.511	0.051	0.143	10.79	0.115	99.65	168.5
	FS4-Pl12-2-p26	5.2	0.065	27.85	54.67	0.513	0.05	0.136	11.12	0.117	99.73	174.9
	FS4-Pl12-2-p27	5.29	0.063	27.62	54.82	0.5	0.046	0.138	10.81	0.123	99.41	182.7
	FS4-Pl12-2-p28	5.17	0.068	27.87	54.88	0.517	0.048	0.142	11	0.079	99.76	189.1
	FS4-Pl12-2-p29	5.25	0.072	27.76	55.17	0.514	0.054	0.136	11.04	0.123	100.1	196.2
	FS4-Pl12-2-p30	5.39	0.062	27.63	55.3	0.514	0.051	0.149	10.71	0.104	99.91	203.3
	FS4-Pl12-2-p31	5.32	0.066	27.76	54.79	0.528	0.046	0.139	10.95	0.119	99.72	209.8
	FS4-Pl12-2-p32	5.28	0.071	27.91	54.53	0.518	0.045	0.131	11.06	0.101	99.65	217.6
	FS4-Pl12-2-p33	5.45	0.063	27.48	55.38	0.494	0.047	0.148	10.6	0.125	99.79	224
	FS4-Pl12-2-p34	5.23	0.068	27.74	54.88	0.516	0.046	0.145	10.97	0.121	99.71	231.8
	FS4-Pl12-2-p35	5.52	0.065	27.74	54.98	0.505	0.048	0.141	10.75	0.146	99.9	238.2
	FS4-Pl12-2-p36	5.48	0.062	27.48	55.31	0.512	0.045	0.151	10.76	0.128	99.93	245.2
	FS4-Pl12-2-p37	5.64	0.063	27.3	55.63	0.523	0.047	0.15	10.35	0.086	99.78	252.4
	FS4-Pl12-2-p38	5.41	0.063	27.56	55.07	0.507	0.052	0.137	10.77	0.116	99.68	258.8
	FS4-Pl12-2-p39	5.22	0.069	27.9	55.07	0.514	0.047	0.137	10.95	0.134	100	266.6
	FS4-Pl12-2-p40	5.3	0.069	27.79	55.18	0.548	0.047	0.155	10.84	0.108	100	273
	FS4-Pl12-2-p41	5.22	0.062	27.94	54.98	0.525	0.048	0.146	11.03	0.116	100.1	280.8
	FS4-Pl12-2-p42	5.3	0.067	27.54	55.13	0.488	0.05	0.152	10.74	0.121	99.59	287.2
	FS4-Pl12-2-p43	5.46	0.069	27.42	55.03	0.472	0.049	0.146	10.48	0.14	99.27	294.2
	FS4-Pl12-2-p44	5.46	0.073	27.29	55.49	0.505	0.048	0.147	10.54	0.112	99.66	301.4
	FS4-Pl12-2-p45	5.6	0.067	27.6	55.28	0.503	0.054	0.136	10.72	0.113	100.1	307.8
	FS4-Pl12-2-p46	5.68	0.071	27.39	55.77	0.527	0.041	0.16	10.5	0.117	100.2	315.6
	FS4-Pl12-2-p47	5.47	0.063	27.39	55.38	0.505	0.051	0.147	10.6	0.114	99.71	322

	Perfiles - University of Bristol (CAMECA)											
	Point	Na_2O (Wt%)	MgO (Wt%)	Al_2O_3 (Wt%)	SiO_2 (Wt%)	FeO (Wt%)	TiO_2 (Wt%)	K_2O (Wt%)	CaO (Wt%)	SrO (Wt%)	Total (Wt%)	Distance from rim (µm)
Fui Sur	FS4-Pl12-2-p48	5.41	0.064	27.61	55.31	0.533	0.038	0.146	10.68	0.104	99.89	329.9
	FS4-Pl12-2-p49	5.18	0.074	27.86	54.77	0.55	0.046	0.133	11.05	0.122	99.78	336.3
	FS4-Pl12-2-p50	5.28	0.068	27.91	54.77	0.535	0.052	0.132	11.01	0.14	99.91	343.3
	FS4-Pl27-p1	4.42	0.11	29.1	52.28	0.752	0.046	0.101	12.77	0.087	99.66	0
	FS4-Pl27-p2	4.42	0.116	28.7	51.7	0.796	0.053	0.092	12.52	0.118	98.51	9.9
	FS4-Pl27-p3	4.47	0.106	28.95	52.59	0.737	0.05	0.102	12.61	0.107	99.72	19.85
	FS4-Pl27-p4	4.27	0.112	29.11	52.07	0.737	0.051	0.098	12.85	0.107	99.4	29.83
	FS4-Pl27-p5	4.19	0.116	29.28	51.94	0.697	0.064	0.088	13.03	0.092	99.49	39.82
	FS4-Pl27-p6	4.21	0.113	29.41	52.05	0.663	0.046	0.089	13.09	0.109	99.79	49.82
	FS4-Pl27-p7	4.01	0.11	29.67	51.69	0.664	0.034	0.081	13.48	0.109	99.84	59.82
	FS4-Pl27-p8	1.56	0.102	33.41	46.11	0.576	0.02	0.02	17.75	0.115	99.66	69.81
	FS4-Pl27-p9	1.2	0.087	34.09	45.24	0.539	0.018	0.01	18.37	0.08	99.63	79.82
	FS4-Pl27-p10	1.43	0.087	33.55	46.07	0.586	0.012	0.02	17.96	0.08	99.8	89.82
	FS4-Pl27-p11	1.49	0.091	33.55	45.98	0.62	0.013	0.028	17.86	0.102	99.74	99.81
	FS4-Pl27-p12	1.71	0.097	33.16	46.39	0.64	0.019	0.025	17.43	0.107	99.58	109.8
	FS4-Pl27-p13	1.54	0.086	33.36	46.38	0.636	0.025	0.027	17.66	0.131	99.85	120.4
	FS4-Pl27-p14	1.64	0.083	33.37	46.44	0.634	0.007	0.025	17.65	0.098	99.93	130.4
	FS4-Pl27-p15	1.95	0.105	32.81	46.85	0.635	0.013	0.034	17.12	0.087	99.61	140.4
	FS4-Pl27-p16	1.85	0.096	33.13	46.83	0.644	0.016	0.028	17.3	0.065	99.96	150.4
	FS4-Pl27-p17	1.74	0.09	33.14	46.87	0.641	0.019	0.027	17.42	0.097	100	160.4
	FS4-Pl27-p18	1.76	0.085	33.18	46.82	0.627	0.015	0.035	17.51	0.086	100.1	170.4
	FS4-Pl27-p19	1.69	0.081	33.38	46.61	0.605	0.013	0.025	17.6	0.086	100.1	180.4
	FS4-Pl27-p20	1.58	0.084	33.28	46.41	0.61	0.011	0.026	17.59	0.078	99.66	190.4
	FS4-Pl27-p21	1.72	0.086	33.3	46.48	0.621	0.021	0.028	17.53	0.089	99.87	200.4
	FS4-Pl27-p22	1.71	0.09	33.02	46.86	0.616	0.021	0.028	17.4	0.045	99.8	210.4
	FS4-Pl27-p23	1.75	0.083	33.24	46.67	0.619	0.028	0.028	17.51	0.068	99.99	220.4
	FS4-Pl27-p24	1.71	0.089	33.24	46.62	0.605	0.022	0.031	17.61	0.102	100	230.4

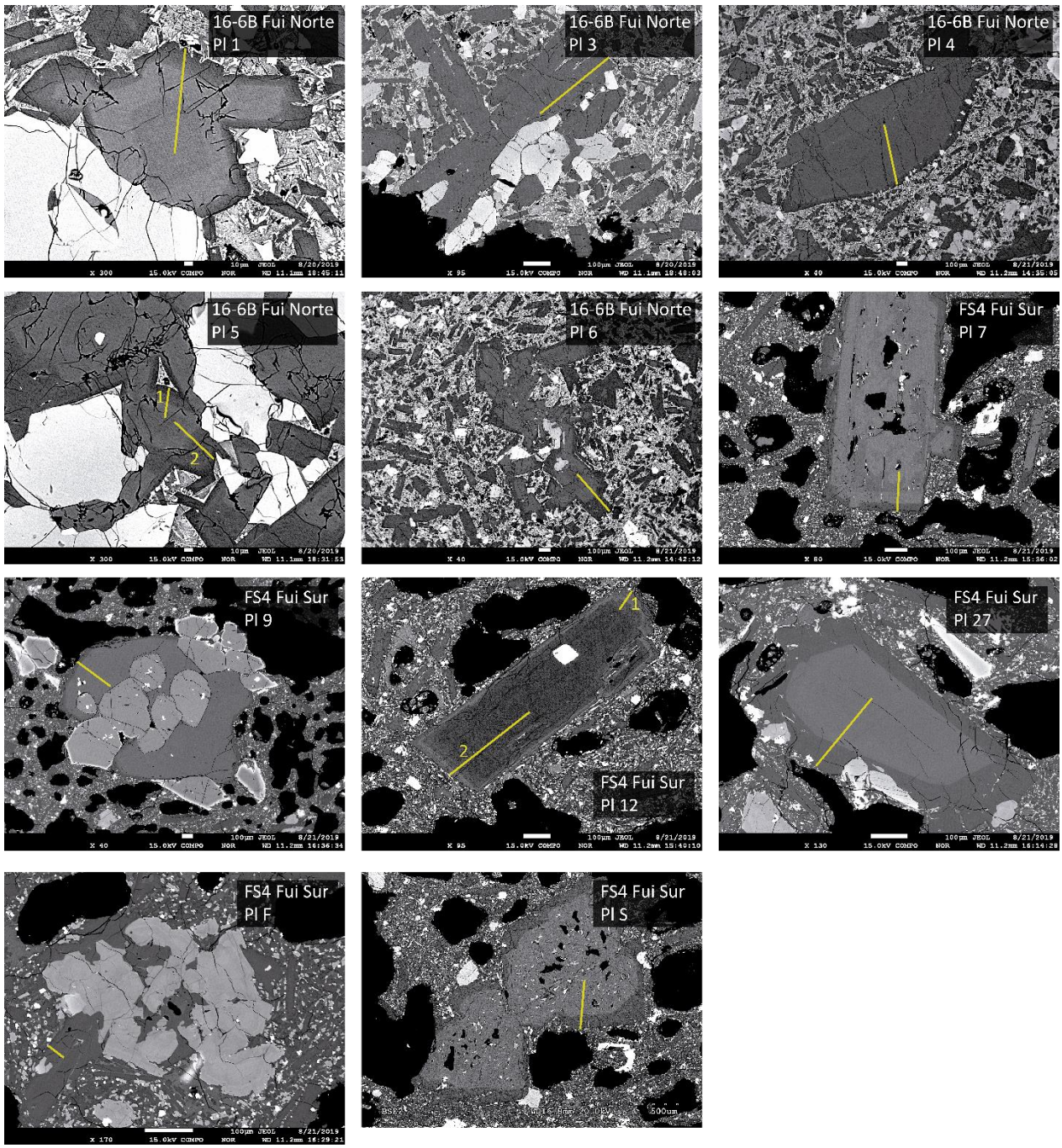

Fig. A.4.2: Ubicación de los perfiles composicionales en cristales de plagioclasa.

Tabla A.4.3: Análisis de química mineral mediante microsonda electrónica (EPMA) de fenocristales (ph) y microlitos (m) de clinopiroxeno.

	LAMARX - Universidad Nacional de Córdoba														
	Point	Type	Na_2O (Wt%)	MgO (Wt%)	Al_2O_3 (Wt%)	SiO_2 (Wt%)	TiO_2 (Wt%)	Cr_2O_3 (Wt%)	MnO (Wt%)	FeO (Wt%)	K_2O (Wt%)	CaO (Wt%)	SrO (Wt%)	NiO (Wt%)	Total (Wt%)
Chanchán	15-3-Px-mf-01	m	0.285	15.25	2.73	51.18	0.873	0.249	0.276	8.52	0.022	20.27	0.015	0.026	99.7
	15-3-Px-mf-02	m	0.286	16.08	1.7263	51.85	0.577	0.051	0.365	9.44	2E-04	20.19	0.016	0	100.6
	15-3-Px-mf-03	m	0.179	16.24	2.82	50.61	0.814	0.127	0.268	8.62	0.005	19.51	0	0	99.19
	15-3-Px-mf-04	m	0.339	13.59	5.58	47.63	1.497	0.192	0.245	8.76	0	21.49	0.035	0.049	99.41
	15-3-Px-mf-05	m	0.276	14.99	3.15	50.5	0.685	0.204	0.245	8.48	0.01	20.81	0	0	99.35
	15-3-Px-mf-06	m	0.329	15.04	3.3	50.49	1.202	0.243	0.338	8.83	0.012	20.77	0.007	0.036	100.6
	15-3-Px-mf-07	m	0.236	16.35	1.6148	51.79	0.764	0.062	0.346	9.81	0.023	18.83	3E-04	0	99.83
	15-3-Px-mf-08	m	0.314	15.44	2.84	51	0.934	0.167	0.307	7.83	0.003	20.95	0.062	0.02	99.87
Fui Norte	166B-pxo-A-2	ph	0.284	15.86	2.15	51.99	0.787	0.235	0.306	8.08	0	21.12	0	0	100.8
	166B-pxo-A-3	ph	0.275	15.68	2.13	51.94	0.716	0.152	0.243	7.91	0.002	21.15	0	0.033	100.2
	166B-pxo-A-4	ph	0.314	14.05	4.86	48.29	1.68	0.385	0.29	9.14	0	20.55	0.008	0	99.57
	166B-pxo-A-5	ph	0.394	12.18	4.79	46.69	2.4	0.006	0.324	13.16	0.022	18.71	0.054	0	98.73
	166B-pxo-A-6	ph	0.362	14.28	4.33	49.34	1.323	0.466	0.192	8.8	0	21.43	0.049	0	100.6
	166B-pxo-B-9	ph	0.353	14.25	4.26	49.53	1.477	0.255	0.271	8.81	0	21.1	0.028	0.056	100.4
	166B-pxo-CP1-13	ph	0.331	14.33	4.34	49.78	1.194	0.37	0.165	8.08	0	21.76	0.072	0.014	100.4
	166B-pxo-8-19	ph	0.32	14.55	5.23	49.43	1.005	0.607	0.146	6.76	0.006	22.05	0.087	0.038	100.2
	166B-pxo-8-20	ph	0.441	14.55	5.01	49.56	1.1	0.857	0.165	6.85	0.01	22.19	0	0	100.7
	166B-pxo-8-21	ph	0.422	14.72	3.51	50.47	1.073	0.132	0.255	8.94	0.015	20.92	0.064	0	100.5
	166B-pxo-8-22	ph	0.438	14.47	4.72	49.56	1.207	0.035	0.205	7.67	0	21.7	0.042	0	100
	166B-pxo-H-27	ph	0.323	14.56	3.86	49.72	1.181	0.324	0.161	8.3	0	21.56	0.186	0	100.2
	166B-pxo-H-28	ph	0.285	15.51	2.39	51.4	0.813	0.121	0.228	7.95	0	21.24	0.071	0	100
	166B-pxo-H-29	ph	0.326	14.23	4.26	49.5	1.239	0.246	0.184	8.75	0.008	21.13	0.025	0	99.9
	166B-pxo-H-30	ph	0.401	13.84	4.45	48.95	1.358	0.172	0.161	8.92	0	21.28	0.049	0.015	99.6
	166B-pxo-H-32	ph	0.392	14.2	4.59	48.93	1.322	0.283	0.275	8.89	0.008	21.02	0.053	0	99.96
	166B-pxo-G-33	ph	0.327	14.5	3.73	50.31	0.99	0.349	0.322	8.21	0	21.58	0	0	100.3
	166B-pxo-CP4-39	ph	0.36	14.19	4.07	49.63	1.416	0.357	0.224	9.06	0.008	21.5	0.039	0.043	100.9
	166B-pxo-CP4-41	ph	0.266	15.69	2.57	51.67	0.86	0.353	0.149	7.69	0.013	21.39	0	0	100.7
	166B-pxo-CP4-42	ph	0.415	13.98	4.59	48.95	1.655	0.237	0.204	8.84	0	21.74	0	0.013	100.6
	166B-pxo-CP4-43	ph	0.295	14.45	4.07	49.65	1.276	0.352	0.224	8.39	0	21.65	0	0.013	100.4
	166B-pxo-17-44	ph	0.306	14.51	4.9	49.69	0.922	0.588	0.165	6.32	0	22.18	0	0.018	99.6
	166B-pxo-9-52	ph	0.342	14.5	3.55	50.47	0.752	0.301	0.259	7.97	0.011	21.8	0.004	0.011	99.97
	166B-pxo-5-56	ph	0.291	15.14	2.74	51	0.873	0.207	0.169	7.75	0	21.73	0	0	99.9
	166B-pxo-5-57	ph	0.379	14.74	3.83	50.25	1.24	0.24	0.173	8.44	0.012	21.47	0	0.013	100.8
	166B-pxo-5-58	ph	0.329	14.55	4.15	49.81	1.194	0.45	0.177	7.86	0	21.97	0.034	0.001	100.5
	166B-pxo-5-63	ph	0.282	14.12	3.87	49.84	1.429	0.212	0.267	8.64	6E-04	21.43	0.021	0	100.1

	LAMARX - Universidad Nacional de Córdoba														
	Point	Type	Na_2O (Wt%)	MgO (Wt%)	Al_2O_3 (Wt%)	SiO_2 (Wt%)	TiO_2 (Wt%)	Cr_2O_3 (Wt%)	MnO (Wt%)	FeO (Wt%)	K_2O (Wt%)	CaO (Wt%)	SrO (Wt%)	NiO (Wt%)	Total (Wt%)
Fui Norte	166B-pxo-5-64	ph	0.259	15.77	2	52.02	0.632	0.154	0.263	8.81	0.006	20.49	0	0.037	100.4
	166B-pxo-c-67	ph	0.353	14.66	3.91	49.69	1.229	0.352	0.196	8.02	0	21.83	0.062	0	100.3
	166B-pxo-3-75	ph	0.296	15.89	2.05	52.07	0.692	0.074	0.283	8.62	0.009	20.78	0	0	100.8
	166B-pxo-3-76	ph	0.298	13.91	4.23	49.9	1.239	0.329	0.216	8.68	0.001	21.8	0.04	0.073	100.7
	166B-pxo-3-77	ph	0.313	14.08	4.18	49.42	1.321	0.314	0.18	8.88	0	21.26	0.085	0.012	100
	166B-Px-D1-93	ph	0.298	15.15	3.2	50.84	0.977	0.206	0.177	8.33	0	21.52	0.038	0.011	100.7
	166B-Px-11-105	ph	0.344	14.47	4.12	49.23	1.534	0.303	0.192	8.87	0.005	20.98	0	0	100
	166B-Px-11-106	ph	0.281	15.66	1.8323	51.68	0.95	0.074	0.317	9.69	0	20.21	0	0	100.7
	166B-Px-16-108	ph	0.31	16.9	2.9	52.32	0.466	0.46	0.224	6.47	0	20.51	0.015	0.033	100.6
	166B-Px-16-109	ph	0.436	15.12	5.18	50.06	1.028	0.659	0.149	6.58	0	21.72	0.053	0.024	101
	166B-Px-16-112	ph	0.333	14.48	4.2	49.63	0.823	0.498	0.118	7.99	0.004	21.88	0	0.036	99.99
	166B-Px-14-113	ph	0.351	15.4	2.92	51.45	0.597	0	0.189	7.96	0.002	21.68	0.009	0	100.6
	166B-Px-E-115	ph	0.301	14.48	3.85	49.8	1.144	0.226	0.165	8.32	0	21.58	0.022	0.024	99.91
	166B-Px-F-119	ph	0.368	14.8	3.8	49.46	1.311	0.335	0.212	8.27	0	21.44	0	0.013	100
	166B-Px-F-123	ph	0.263	15.24	3.67	50.37	1.048	0.3	0.294	8.27	0	21	0.094	0.043	100.6
	166B-Px-MF1-124	m	0.263	15.9	2.32	52.1	0.929	0.126	0.259	8.5	0	20.55	0	0.001	100.9
	166B-Px-MF2-125	m	0.326	16.17	2.07	52.21	0.561	0.261	0.2	7.87	0.003	20.64	0	0	100.3
	166B-Px-MF2-126	m	0.269	13.97	4.4	49.19	1.7	0.214	0.239	8.75	0	21.38	0.008	0	100.1
Fui Sur	FS4-Px-X2-17	ph	0.439	13.97	5.22	48.83	1.43	0.119	0.258	10.87	0.008	19.63	0	0.026	100.8
	FS4-Px-L-21	ph	0.453	13.69	5.2	48.28	1.8	0.054	0.266	10.66	0	19.94	0	0.002	100.3
	FS4-Px-L-22	ph	0.193	16.28	2.14	52.03	0.722	0.023	0.426	10.37	0	18.56	0.046	0.011	100.8
	FS4-Px-L-26	ph	0.436	13.81	4.87	49.12	1.124	0.003	0.305	11.01	0	19.96	0	0.039	100.7
	FS4-Px-29-27	ph	0.325	14.47	4.57	49.74	1.242	0.06	0.262	10.44	0.018	19.57	0.079	0	100.8
	FS4-Px-22-35	ph	0.389	14.25	4.65	49.47	1.492	0.131	0.277	9.93	0	20.1	0.017	0.032	100.7
	FS4-Px-22-36	ph	0.237	17.51	1.93	52.46	0.543	0.057	0.34	11.37	0	16.41	0	0.044	100.9
	FS4-Px-H-51	ph	0.296	14.55	4.06	50.08	1.232	0.19	0.242	9.92	0.004	20.13	0.092	0	100.8
	FS4-Px-H-52	ph	0.327	14.11	4.77	49.32	1.375	0	0.274	9.86	0.004	20.83	0	0	100.9
	FS4-Px-2-56	ph	0.414	13.73	5.35	48.12	1.62	0.156	0.277	10.75	7E-04	19.94	0	0	100.4
	FS4-Px-2-57	ph	0.318	14.62	4.63	49.62	1.324	0.176	0.328	10.85	0	19.28	0	0	101.1
	FS4-Px-A-58	ph	0.283	14.47	4.25	50.06	1.175	0.048	0.297	9.69	0	20.57	0	0	100.8
	FS4-Px-F-63	ph	0.489	13.37	6.18	47.98	1.67	0.097	0.227	10.12	0	20.44	0	0.039	100.6
	FS4-Px-8.2-66	ph	0.354	14.19	5.16	48.95	1.291	0.27	0.258	10.16	0	20.12	0	0.025	100.8
	FS4-Px-15-71	ph	0.363	15.2	2.92	51.5	0.642	0	0.317	9.44	0.006	20.46	0	0	100.8
	FS4-Px-15-72	ph	0.367	14.57	4.66	49.59	1.007	0.136	0.262	10.09	0.004	19.81	0.034	0.021	100.6
	FS4-Px-17-77	ph	0.339	14.89	3.45	50.94	1.01	0.117	0.29	9.41	1E-04	20.45	0.03	0	100.9
	FS4-Px-17-78	ph	0.345	14.59	1.8414	51.87	0.746	0.048	0.543	10.89	0	20.32	9E-04	0	101.2
	FS4-Px-J-86	ph	0.305	15.79	2.54	51.11	1.011	0.076	0.53	12.77	0.021	16.81	0.028	0	101
	FS4-Px-18-87	ph	0.314	13.59	4.75	49.54	1.152	0.068	0.204	9.63	0	21.04	0.001	0	100.3

	LAMARX - Universidad Nacional de Córdoba														
	Point	Type	Na_2O (Wt%)	MgO (Wt%)	Al_2O_3 (Wt%)	SiO_2 (Wt%)	TiO_2 (Wt%)	Cr_2O_3 (Wt%)	MnO (Wt%)	FeO (Wt%)	K_2O (Wt%)	CaO (Wt%)	SrO (Wt%)	NiO (Wt%)	Total (Wt%)
Fui Sur	FS4-Px-3-92	ph	0.394	14.3	4.4	49.33	1.387	0.085	0.289	10.08	0	20.26	0.068	0	100.6
	FS4-Px-4S-105	ph	0.414	13.46	5.86	47.62	1.76	0.116	0.323	11.2	0.009	18.95	0.051	0	99.76
	FS4-Px-mf-100	m	0.134	18.61	1.7602	52.05	0.716	0	0.723	17.94	0.024	8.36	0.048	0	100.4
	FS4-Px-mf-101	m	0.302	16.27	2.49	50.78	0.912	0	0.396	14.14	0.015	14.09	0.004	0.04	99.44
	FS4-Px-mf-102	m	0.246	16.38	1.96	51.34	0.879	0	0.715	17.8	0.036	10.89	0.023	0	100.3
	FS4-Px-mf-103	m	0.153	15.53	1.0477	50.02	0.718	0	0.924	22.8	0.02	8.41	0.035	0.025	99.68
	FS4-Px-mf-104	m	0.213	13.77	1.2512	50.36	1.001	0	0.665	20.4	0.022	12.08	0	0.069	99.83
	FS4-Px-4S-105	ph	0.414	13.46	5.86	47.62	1.76	0.116	0.323	11.2	0.009	18.95	0.051	0	99.76

	University of Bristol (Jeol)													
	Point	Type	Na_2O (Wt%)	MgO (Wt%)	Al_2O_3 (Wt%)	SiO_2 (Wt%)	TiO_2 (Wt%)	Cr_2O_3 (Wt%)	MnO (Wt%)	FeO (Wt%)	K_2O (Wt%)	CaO (Wt%)	NiO (Wt%)	Total (Wt%)
Fui Norte	16-6B-px3-1	ph	0.317	14.62	3.3538	50.01	0.992	0.179	0.217	8.309	0	20.91	0.013	98.93
	16-6B-px8-1	ph	0.353	14.44	5.351	49.38	0.945	0.477	0.144	6.722	0	21.65	0	99.46
	16-6B-px8-2	ph	0.267	15.69	2.9194	51.66	0.62	0.211	0.174	6.353	0	21.54	0.02	99.45
	16-6B-px10-1	ph	0.286	17.86	1.995	52.97	0.34	0.209	0.226	7.139	0.009	18.93	0.019	99.98
	16-6B-px10-2	ph	0.341	15	4.5317	50.4	0.788	0.477	0.145	6.34	0.002	21.57	0.015	99.6
	16-6B-px10-3	ph	0.315	16.73	2.6345	52.48	0.476	0.113	0.201	6.659	0	20.49	0.011	100.1
	16-6B-px16-1	ph	0.305	14.97	4.5463	50.08	0.792	0.697	0.152	6.191	7E-04	21.88	0.021	99.63
	16-6B-px16-2	ph	0.363	15	4.9876	50.25	0.808	0.376	0.174	6.785	0.001	21.09	0.026	99.87
	16-6B-px16-3	ph	0.319	16.23	3.3624	51.63	0.514	0.392	0.157	6.188	0	20.89	0.03	99.71
	16-6B-px-CP1-1	ph	0.325	14.22	4.3299	49.47	1.352	0.341	0.197	8.335	0.003	20.98	0.009	99.56
	16-6B-px-CP1-1r	ph	0.33	14.23	4.4701	49.39	1.217	0.356	0.228	8.077	0	21.11	0.004	99.42
	16-6B-px-CP1-2	ph	0.252	16.08	2.059	52.3	0.686	0.195	0.254	8.199	0	19.98	0.004	100
	16-6B-px-CP1-3	ph	0.318	14.35	4.1	49.78	1.233	0.38	0.224	8.272	0.005	20.95	0	99.6
	16-6B-px-CP1-4	ph	0.334	14.31	4.2081	49.58	1.237	0.304	0.205	8.156	7E-04	21.24	0.005	99.58
	16-6B-px-CP1-5	ph	0.285	15.54	2.5735	51.72	0.716	0.274	0.233	7.64	0.003	20.73	0.007	99.73
	16-6B-px-CP4-1	ph	0.298	15.63	2.6705	51.46	0.773	0.246	0.231	8.093	0.005	20.18	0	99.58
	16-6B-px-CP4-2	ph	0.359	13.5	5.2059	47.77	1.812	0.231	0.25	10.02	0	20.23	0	99.38
	16-6B-px-CP4-3	ph	0.267	16.12	2.2122	51.85	0.738	0.125	0.255	8.279	0	20.03	0.006	99.89
	16-6B-px-E-1	ph	0.263	15.77	2.1389	51.74	0.672	0.165	0.239	7.879	9E-04	20.35	6E-04	99.21
	16-6B-px-E-2	ph	0.325	13.77	4.4429	49.12	1.354	0.105	0.201	8.606	0	21.44	0.006	99.37
	16-6B-px-E-3	ph	0.355	14.11	4.8525	48.35	1.477	0.169	0.233	8.998	0	20.12	0.003	98.66
	16-6B-px-E-4	ph	0.235	16.01	2.2558	51.86	0.627	0.291	0.225	7.286	0	20.5	0.012	99.29
	16-6B-px-F-1	ph	0.332	14.69	3.7608	50.16	1.024	0.236	0.22	7.929	0	21.16	0	99.5
	16-6B-px-F-2	ph	0.288	15.62	2.1917	51.76	0.677	0.156	0.232	7.754	0.001	20.85	0.009	99.53
	16-6B-px-F-3	ph	0.337	14.26	4.4779	49.4	1.304	0.354	0.239	8.364	0.003	20.83	0	99.56

	University of Bristol (Jeol)													
	Point		Na_2O (Wt%)	MgO (Wt%)	Al_2O_3 (Wt%)	SiO_2 (Wt%)	TiO_2 (Wt%)	Cr_2O_3 (Wt%)	MnO (Wt%)	FeO (Wt%)	K_2O (Wt%)	CaO (Wt%)	NiO (Wt%)	Total (Wt%)
Fui Norte	16-6B-px-MF-1	m	0.301	15.49	1.9355	51.5	0.815	0.108	0.291	9.315	0.006	19.26	0.005	99.03
	16-6B-px-MF-2	m	0.336	15.44	2.0454	51.45	0.804	0.091	0.293	9.19	0.016	19.37	0	99.01
	16-6B-px-MF-3	m	0.278	15.9	1.6071	51.83	0.775	0.067	0.347	10.07	0.01	18.32	0.007	99.21
	16-6B-px-MC-1	m	0.247	15.89	2.3449	51.56	0.692	0.197	0.219	7.773	0	20.34	0.01	99.28
	16-6B-px-MC-2	m	0.348	14.31	4.1835	49.81	1.117	0.338	0.204	8.27	0.001	20.88	0.013	99.47
Chanchán	15-3-px-MC6-1	m	0.173	16.61	2.7983	51.62	0.596	0.424	0.234	7.195	6E-04	19.71	0.015	99.38
	15-3-px-MC7-1	m	0.313	15.51	2.7988	51.26	0.787	0.236	0.202	7.732	0	20.65	0.018	99.5
Fui Sur	FS4-px-4s-1	ph	0.376	13.66	5.5028	47.53	1.549	0.147	0.29	10.8	0.007	18.88	0	98.74
	FS4-px-4s-2	ph	0.353	13.16	5.3101	48.3	1.543	0.103	0.292	10.17	0.013	19.72	0.01	98.97
	FS4-px-6-1	ph	0.323	14.54	3.5333	49.61	0.949	0	0.322	9.718	0	19.75	0	98.72
	FS4-px-J-1	ph	0.216	16.27	1.8253	50.92	0.686	0.004	0.523	12.9	0.004	15.38	0.005	98.74
	FS4-px-L-1	ph	0.343	13.51	5.5116	47.28	1.675	0.045	0.278	10.8	0	19.36	0.018	98.83
	FS4-px-H-1	ph	0.287	15.08	3.0894	50.87	0.741	0.059	0.297	9.611	0.001	19.43	0	99.45
	FS4-px-H-2	ph	0.346	13.89	4.3498	49.17	1.022	0.07	0.272	9.475	0.002	20.52	0.01	99.12
	FS4-px-F-1	ph	0.371	13.52	5.8048	47.83	1.517	0.079	0.256	9.862	7E-04	19.6	0.01	98.85
	FS4-px-MC1	ph	0.209	16.43	2.2039	51.82	0.564	0.047	0.361	10.05	0	17.8	0.011	99.48
	FS4-px-MC2	ph	0.367	13.63	4.7482	48.79	1.064	0.185	0.241	9.258	0	20.65	0	98.92
	FS4-px-MC3	ph	0.337	14.11	4.495	49.22	1.261	0.055	0.307	9.963	0	19.83	0.007	99.58
	FS4-px-MC4	ph	0.351	13.83	4.5301	49.17	1.148	0.108	0.25	9.374	0.002	20.37	0.02	99.16
	FS4-px-MC5	ph	0.404	13.23	5.5389	47.85	1.558	0.059	0.26	10.29	0	19.61	0.01	98.81
	FS4-px-MF-1	ph	0.352	14.19	3.98	49.04	1.236	0.024	0.356	10.49	0.018	18.87	0.001	98.55
	FS4-px-MF-2	ph	0.217	17.05	1.9777	51.75	0.672	0	0.523	12.53	0.009	14.23	0	98.94
	FS4-px-MF-3	ph	0.264	15.57	2.5035	51.05	0.946	0	0.513	12.56	0.01	16.06	0	99.46

A.5 Condiciones magmáticas intensivas

A.5.1 Test de equilibrio

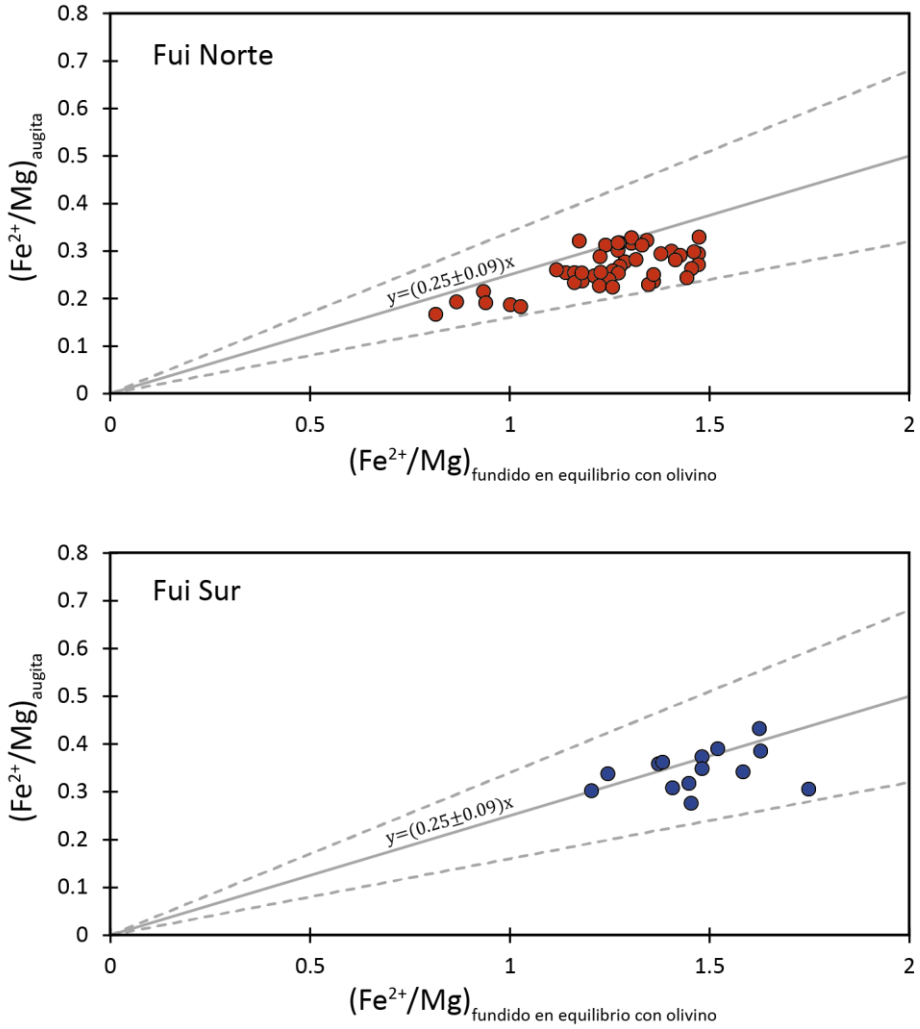

Figura A.5.1.1: Test de equilibrio entre olivino y clinopiroxeno usando las ecuaciones de Grove et al. (1997). En las figuras se muestran las composiciones de Fe^{2+}/Mg de augitas que se encuentran en equilibrio con un fundido determinado a partir de las composiciones de Fe^{2+}/Mg de olivino. Sólo olivinos de composiciones de la Zona 2 se encontraron en equilibrio con clinopiroxenos. La línea continua corresponde al equilibrio entre clinopiroxeno y un fundido básico saturado en H_2O usando $^{cpx\text{-}ol}K_D(Fe^{2+}/Mg)$. Las líneas punteadas corresponden a los errores asociados. Más detalles del método en Morgado et al. (2015). Los datos que pasan este filtro fueron utilizados en geotermobarometría. Variables termodinámicas en la Tabla A.5.2.

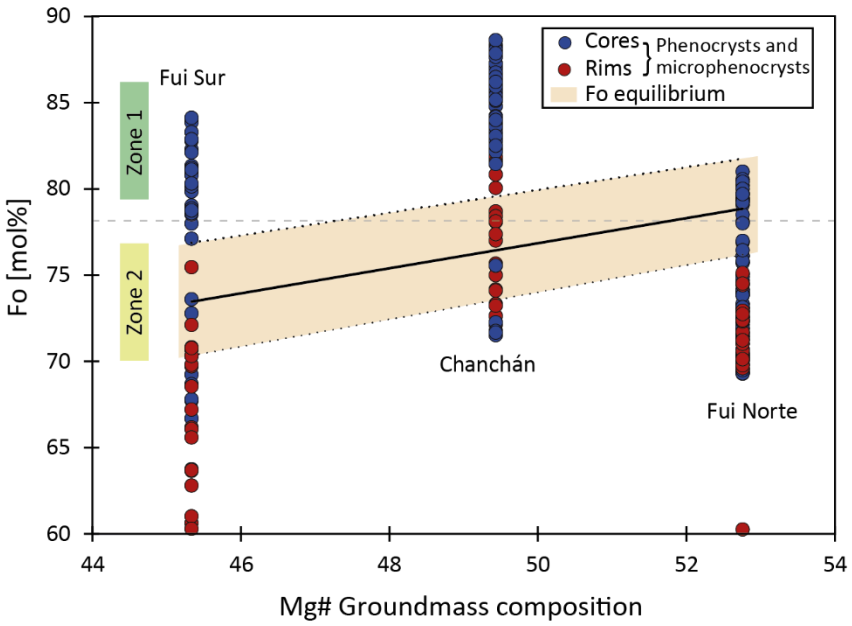

Figura A.5.1.2: Contenido de Fo de olivino vs. #Mg de la composición de masa fundamental para los diferentes CEM (#Mg calculado en moles como $100 \times Mg/(Mg+Fe^{2+})$). Se muestran datos obtenidos a partir de núcleos (azul) y bordes (rojo). Las líneas sólidas y punteadas representan el rango de equilibrio entre olivino y un fundido de composición equivalente a la masa fundamental, usando el coeficiente de partición de Roeder & Emslie (1970) para Fe-Mg entre olivino y fundido (0.3 ± 0.05). La línea gris punteadas representa el límite entras las composiciones de la Zona 1 y Zona 2.

A.5.2 Variables utilizadas en geotermobarómetros

Tabla A.5.2: Detalles de las variables utilizadas en geotermobarómetros para los CEM.

Point	Fe^{2+}	Mg	Ca	K_D Ol/Aug-Fe/Mg	Dca	T (°C) Fe-Mg Ol-Aug	T (°C) Ca in Ol	P (kbar) Ca-exchange Ol-Cpx
Fui Norte								
166B-ol-A-7	0.6000	1.3583	0.0113	1.4995	0.0133	1120	-	-
166B-px-A-6	0.2324	0.7888	0.8480					
166B-ol-B-8	0.5675	1.4082	0.0097	1.2489	0.0116	1163	1144	-
166B-px-B-9	0.2545	0.7889	0.8369					
166B-ol-H-26	0.6035	1.3666	0.0099	1.6263	0.0116	1100	-	-
166B-px-H-27	0.2189	0.8060	0.8553					
166B-ol-H-25	0.5808	1.3782	0.0109	1.4038	0.0130	1135	1159	-
166B-px-H-32	0.2368	0.7889	0.8363					
166B-ol-H-31	0.5520	1.4101	0.0140	1.2361	0.0167	1166	-	-
166B-px-H-29	0.2504	0.7907	0.8414					
166B-ol-H-31	0.5520	1.4101	0.0140	1.1934	0.0165	1174	-	-
166B-px-H-30	0.2534	0.7727	0.8507					
166B-ol-G-34	0.5785	1.3987	0.0083	1.4028	0.0098	1135	-	-
166B-px-G-33	0.2362	0.8012	0.8545					
166B-ol-CP4-36	0.5489	1.4207	0.0096	1.3915	0.0112	1137	1147	-
166B-px-CP4-43	0.2217	0.7984	0.8574					
166B-ol-CP4-37	0.5364	1.4426	0.0076	1.1897	0.0090	1175	1115	1.2
166B-px-CP4-39	0.2445	0.7824	0.8493					
166B-ol-CP4-38	0.5641	1.4125	0.0100	1.2779	0.0118	1158	1151	-
166B-px-CP4-39	0.2445	0.7824	0.8493					
166B-ol-5-60	0.5925	1.3844	0.0088	1.4697	0.0104	1124	1123	-
166B-px-5-57	0.2360	0.8104	0.8455					
166B-ol-5-61	0.5974	1.3684	0.0096	1.6550	0.0111	1096	-	-
166B-px-5-56	0.2209	0.8374	0.8616					
166B-ol-5-62	0.6088	1.3768	0.0104	1.3401	0.0122	1146	-	-
166B-px-5-63	0.2587	0.7840	0.8530					
166B-ol-5-65	0.6036	1.3769	0.0097	1.4670	0.0119	1125	-	-
166B-px-5-64	0.2594	0.8682	0.8088					
166B-ol-1-80	0.5821	1.3722	0.0094	1.5057	0.0115	1119	1133	-
166B-px-3-75	0.2454	0.8712	0.8166					
166B-ol-D1-92	0.5480	1.4323	0.0079	1.4256	0.0093	1132	1117	-
166B-px-D1-93	0.2233	0.8320	0.8471					
166B-ol-11-104	0.5491	1.4404	0.0066	1.2624	0.0079	1161	1089	2.5
166B-px-11-105	0.2425	0.8030	0.8342					
166B-ol-11-103	0.5483	1.4336	0.0063	1.2039	0.0078	1172	1082	4.3
166B-px-11-106	0.2740	0.8626	0.7981					
166B-ol-11-104	0.5491	1.4404	0.0066	1.2000	0.0082	1173	1089	3.2
166B-px-11-106	0.2740	0.8626	0.7981					

Point	Fe^{2+}	Mg	Ca	K_D Ol/Aug-Fe/Mg	Dca	T (°C) Fe-Mg Ol-Aug	T (°C) Ca in Ol	P (kbar) Ca-exchange Ol-Cpx
166B-ol-16-107	0.4338	1.5484	0.0054	1.3044	0.0068	1153	-	5.1
166B-px-16-108	0.1975	0.9194	0.8001					
166B-ol-E-116	0.5615	1.4228	0.0075	1.3982	0.0087	1136	1105	-
166B-px-E-115	0.2267	0.8032	0.8580					
166B-ol-F-117	0.5444	1.4424	0.0078	1.4586	0.0094	1126	1116	-
166B-px-F-123	0.2168	0.8380	0.8279					
166B-ol-F-118	0.5492	1.4396	0.0085	1.5009	0.0100	1119	1129	-
166B-px-F-119	0.2083	0.8195	0.8504					
16-6B-ol3-1	0.5162	1.4567	0.0083	1.4933	0.0099	1121	1133	-
16-6B-px3-1	0.1937	0.8163	0.8390					
16-6B-ol8-3	0.4354	1.5441	0.0068	1.4743	0.0080	1124	1124	-
16-6B-px8-2	0.1654	0.8646	0.8533					
16-6B-ol10-1	0.4569	1.5209	0.0061	1.6007	0.0082	1104	1099	-
16-6B-px10-1	0.1827	0.9737	0.7415					
16-6B-ol10-3	0.4661	1.5133	0.0067	1.6826	0.0083	1092	1112	-
16-6B-px10-3	0.1671	0.9127	0.8037					
16-6B-ol16-2	0.4083	1.5700	0.0062	1.3419	0.0074	1146	-	-
16-6B-px16-2	0.1597	0.8242	0.8329					
16-6B-ol16-3	0.1348	0.5520	0.5630	1.4595	0.6842	1126	-	-
16-6B-px16-3	0.1489	0.8895	0.8229					
16-6B-ol-CP1-1	0.5046	1.4756	0.0089	1.3414	0.0107	1146	1148	-
16-6B-px-CP1-1	0.2014	0.7901	0.8377					
16-6B-ol-CP1-2	0.4949	1.4769	0.0079	1.2845	0.0100	1156	1131	-
16-6B-px-CP1-2	0.2309	0.8850	0.7905					
16-6B-ol-CP1-3	0.5110	1.4661	0.0096	1.3670	0.0115	1142	1159	-
16-6B-px-CP1-3	0.2031	0.7967	0.8360					
16-6B-ol-CP1-4	0.5113	1.4674	0.0084	1.4900	0.0099	1121	1136	-
16-6B-px-CP1-4	0.1857	0.7941	0.8472					
16-6B-ol-CP1-5	0.5382	1.4369	0.0086	1.5581	0.0105	1110	1133	-
16-6B-px-CP1-5	0.2062	0.8579	0.8225					
16-6B-ol-CP4-1	0.5267	1.4496	0.0082	1.4664	0.0102	1125	1128	-
16-6B-px-CP4-1	0.2142	0.8643	0.8018					
16-6B-ol-CP4-2	0.5300	1.4408	0.0079	1.2754	0.0097	1158	1121	-
16-6B-px-CP4-2	0.2179	0.7554	0.8140					
16-6B-ol-CP4-3	0.5718	1.4018	0.0084	1.7232	0.0106	1087	1121	-
16-6B-px-CP4-3	0.2101	0.8878	0.7930					
16-6B-ol-E-1	0.5969	1.3783	0.0096	1.7766	0.0119	1079	1136	-
16-6B-px-E-1	0.2132	0.8746	0.8111					
16-6B-ol-E-2	0.5316	1.4433	0.0093	1.4422	0.0108	1129	1147	-
16-6B-px-E-2	0.1961	0.7678	0.8592					
16-6B-ol-E-3	0.5162	1.4578	0.0107	1.3918	0.0132	1137	1175	-
16-6B-px-E-3	0.2013	0.7912	0.8111					

Point	Fe^{2+}	Mg	Ca	K_D Ol/Aug-Fe/Mg	Dca	T (°C) Fe-Mg Ol-Aug	T (°C) Ca in Ol	P (kbar) Ca-exchange Ol-Cpx
16-6B-ol-E-4	0.5275	1.4365	0.0122	1.6173	0.0149	1102	-	-
16-6B-px-E-4	0.2010	0.8854	0.8149					
16-6B-ol-F-1	0.5389	1.4288	0.0138	1.6792	0.0163	1093	-	-
16-6B-px-F-1	0.1829	0.8143	0.8430					
16-6B-ol-F-2	0.5693	1.4088	0.0084	1.7577	0.0102	1082	1122	-
16-6B-px-F-2	0.1985	0.8635	0.8285					
16-6B-ol-F-3	0.5730	1.4043	0.0107	1.6270	0.0129	1100	1159	-
16-6B-px-F-3	0.1986	0.7920	0.8313					
Fui Sur								
FS4-ol-22-34	0.6088	1.3709	0.0046	1.1897	0.0058	1175	-	-
FS4-px-22-35	0.2940	0.7875	0.0046	1.1897	0.0058			
FS4-ol-22-34	0.6088	1.3709	0.0046	1.2737	0.0071	1158	-	4.7
FS4-px-22-36	0.3342	0.9585	0.0046	1.2737	0.0071			
FS4-ol-H-49	0.5786	1.4062	0.0053	1.1472	0.0066	1184	-	-
FS4-px-H-51	0.2880	0.8030	0.0053	1.1472	0.0066			
FS4-ol-H-50	0.5397	1.4455	0.0051	1.1049	0.0062	1193	-	-
FS4-px-H-52	0.2630	0.7781	0.0051	1.1049	0.0062			
FS4-ol-A-61	0.6433	1.3545	0.0055	1.3892	0.0067	1138	-	3.1
FS4-px-A-58	0.2725	0.7972	0.0055	1.3892	0.0067			
FS4-ol-F-64r	0.6508	1.3333	0.0066	1.2674	0.0081	1160	-	1.5
FS4-px-F-63	0.2854	0.7410	0.0066	1.2674	0.0081			
FS4-ol-4S-108	0.6499	1.3341	0.0074	1.1272	0.0097	1188	-	1.1
FS4-px-4S-105	0.3260	0.7544	0.0074	1.1272	0.0097			
FS4-ol-4s-2	0.5777	1.3929	0.0057	1.1465	0.0074	1184	1060	7.5
FS4-px-4s-2	0.2678	0.7403	0.0057	1.1465	0.0074			
FS4-ol-4s-3	0.5960	1.3726	0.0065	1.3673	0.0082	1141	1076	-
FS4-px-4s-1	0.2442	0.7690	0.0065	1.3673	0.0082			
FS4-ol-J-1	0.6224	1.3653	0.0057	1.1692	0.0091	1179	-	1.5
FS4-px-J-1	0.3570	0.9155	0.0057	1.1692	0.0091			
FS4-ol-L-1	0.6795	1.2959	0.0098	1.7155	0.0126	1088	-	-
FS4-px-L-1	0.2326	0.7609	0.0098	1.7155	0.0126			
FS4-ol-H-1	0.5246	1.4524	0.0072	1.1953	0.0093	1174	1109	0.2
FS4-px-H-1	0.2533	0.8381	0.0072	1.1953	0.0093			
FS4-ol-H-2	0.6025	1.3820	0.0096	1.5805	0.0116	1107	1134	-
FS4-px-H-2	0.2143	0.7767	0.0096	1.5805	0.0116			
FS4-ol-F-1	0.5876	1.3923	0.0072	1.3689	0.0091	1141	1093	-
FS4-px-F-1	0.2339	0.7588	0.0072	1.3689	0.0091			

A.5.3 Cálculo de la composición de masa fundamental

El procedimiento para calcular la composición de la masa fundamental consiste en una resta modal de las composiciones químicas de los fenocristales asociadas a su abundancia, con respecto a la composición geoquímica de roca total. Los detalles de las composiciones de roca total y fenocristales representativos utilizados se encuentran en la Table 5, así como el resultado de la composición calculada de la masa fundamental.

A la muestra de Chanchán (muestra 15-3), que solo presenta fenocristales de olivino, se le restó una composición de la Zona 1 de olivino ($Fo_{86,}$ punto 15-3-Ol-4-30). En Fui Norte (muestra 16-6B), la composición de olivino extraída corresponde a la Zona 2 (Fo_{72}, punto 166B-Ol-CP4-37) debido a que en la muestra, los cristales de olivino con dicha composición son más abundantes (ver histograma de la Fig. 2.7b). Finalmente, en Fui Sur (muestra FS4) se sustrajo una composición de la Zona 1 (Fo_{78}, FS4-Ol-30-79), debido a que corresponde a la composición más abundante de fenocristales de olivino (ver histograma de la Fig. 2.7c). Para los clinopiroxenos, debido a su estrecho campo composicional (Fig. 2.6h, i), los fenocristales de cada muestra fueron aleatoriamente escogidos (166B-pxo-A-6 en Fui Norte y FS4-Px-X2-17 en Fui Sur, ambas corresponden a augitas). En el caso de las composiciones de plagioclasa, se restaron ambas Zonas (1 y 2). Para esto, se escogieron nueve fenocristales de plagioclasa representativas en Fui Norte (Fig. A.5.2.1) y diez en Fui Sur (Fig. A.5.2.2). Las longitudes de los cristales de plagioclasa fueron medidas en sus dos dimensiones, asumiendo que su forma en tres dimensiones es aproximada a un paralelepípedo, con lo cual se aproximó un porcentaje modal de volumen para las composiciones de la Zona 1 y 2.

Una vez escogidas las composiciones y porcentajes de Zona 1 y 2 para plagioclasa (Zona 1 An_{79} 166B-Pl-6-99 y Zona 2 An_{65} 166B-Pl-6-101 en Fui Norte, Zona 1 An_{84} FS4-Pl-27-47 y Zona 2 An_{62} FS4-Pl-27-48 en Fui Sur), el procedimiento fue el siguiente:

Se multiplicó el valor de cada óxido en % peso (C) por el % de la roca total (Vol%), y a este valor se le restó la sumatoria de la multiplicación de todos los óxidos en % peso de cada medida de los minerales, multiplicado por su abundancia (Factor 1, Ec. 1). Luego, se suman todos estos factores que fueron calculados para cada óxido, para de esta forma pasarlos a porcentaje (Factor 2, Ec. 2).

$$Factor\ 1 = (C_i * vol\%)_{RT} - \sum\left(C_i * vol\%_j\right)_{mxl} \qquad (Ec.1)$$

$$Factor\ 2 = \frac{\sum Factor\ 1_i}{Factor\ 1_i * 100} \qquad (Ec.2)$$

$C = \acute{O}x.\ wt\%$

$i = cada\ \acute{o}x.\ wt\%$

$j = cada\ fase\ mineral$

$vol\% = \%\ Volumen$

$RT = Geoquímica\ de\ Roca\ Total$

$Mxl = Química\ Fase\ Mineral$

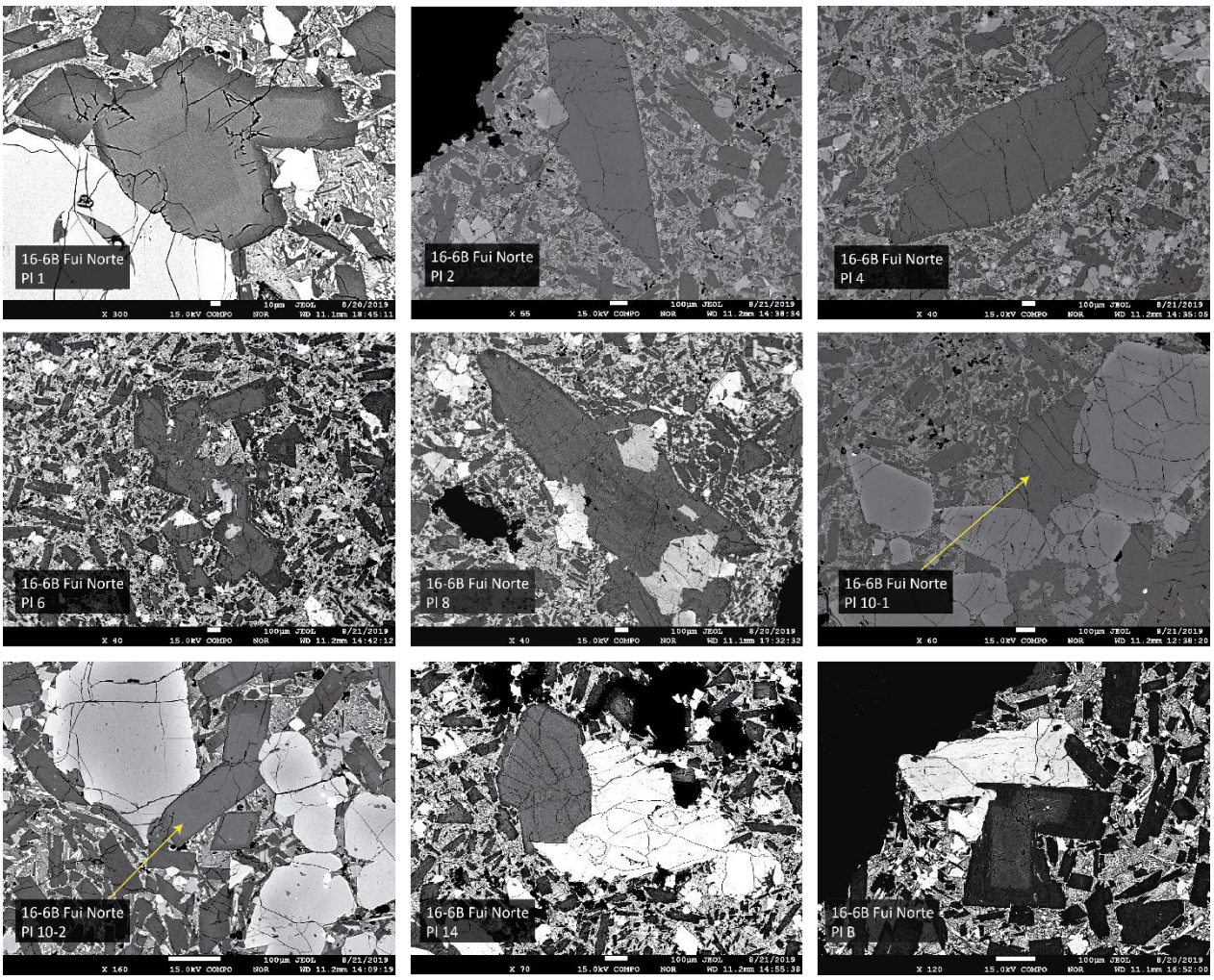

Fig. A.5.3.1: Fenocristales de plagioclasa de la muestra 16-6B utilizadas para medir sus núcleos y bordes.

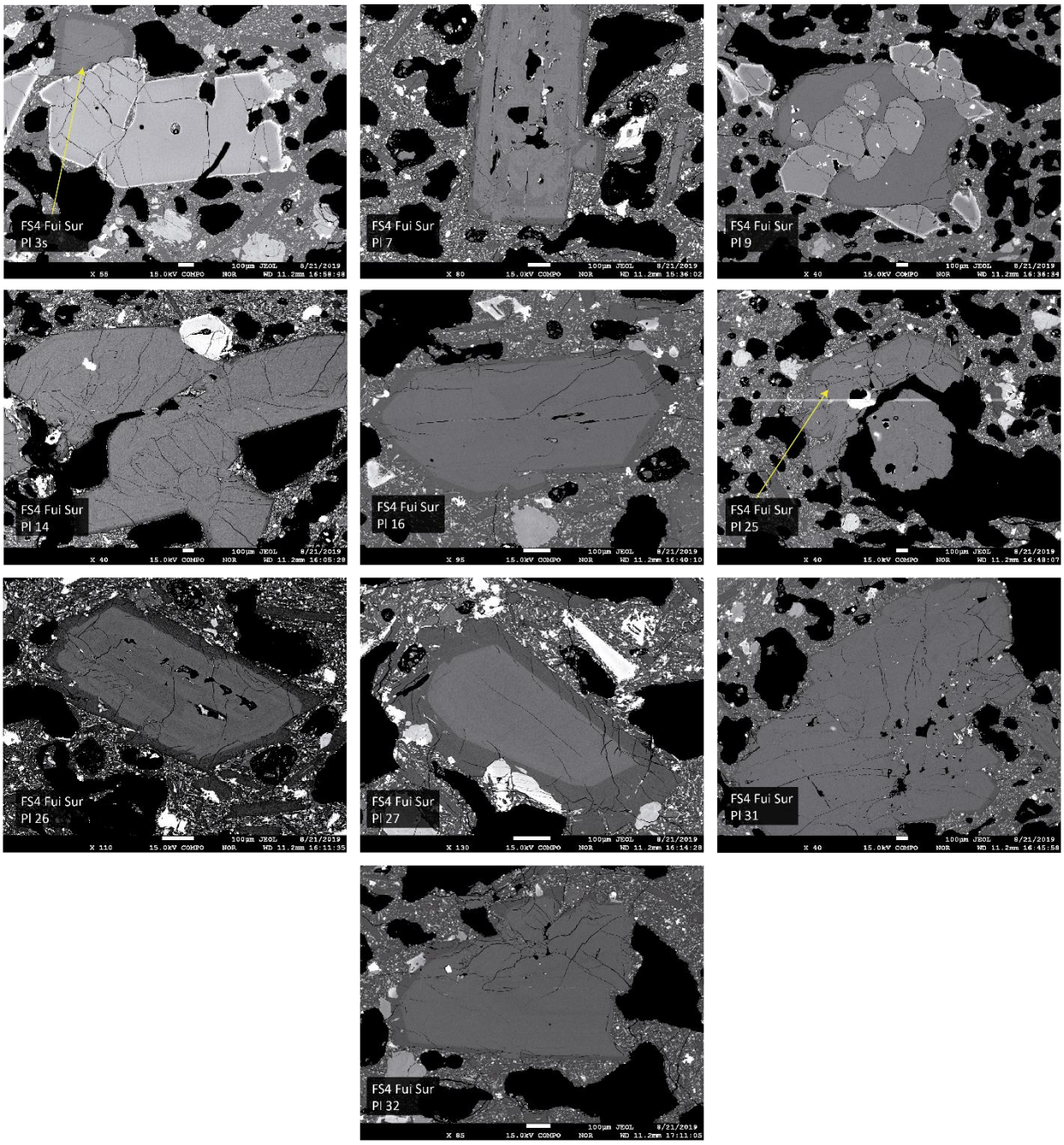

Fig. A.5.3.2: Fenocristales de plagioclasa de la muestra FS4 utilizadas para medir sus núcleos y bordes.

A.5.4 Resultados de la solución numérica para presión y contenido de H_2O

Tabla A.5.4: Resultados de la solución numérica para Presión (kbar) y contenido de agua (wt%), utilizando las ecuaciones de Moore et al. (1998) y Lange et al. (2009).

	Clot	Temperature [°C]	An content [mol %]	P [kbar]	H_2O [wt%]
Fui Norte	3	1118	62	0 - 1.1	0.7 - 1.5
	8	1124	63	0 - 1.2	0.8 - 1.6
	B	1163	64	0 - 0.8	0.4 - 1.2
	CP1	1146	64	0 - 1.0	0.6 - 1.3
	CP4	1125	64	0 - 1.2	0.8 - 1.6
	CP4	1137	64	0 - 1.0	0.6 - 1.3
Fui Sur	F	1141	65	0.2 - 1.5	1.1 - 1.9
	F	1141	62	0.1 - 1.3	0.9 - 1.7
	F	1141	70	0.3 - 2.1	1.5 - 2.3
	F	1160	63	0.0 - 1.1	0.7 - 1.5
	A	1138	63	0.1 - 1.4	1 - 1.8

A.5.5 Resultados del modelamiento en rhyolite-MELTS

Tabla A.5.5.1: Resumen del modelamiento para los CEM Fui Norte.

Ox. Fugacity Buffer	H_2O [wt%]	P [kbar]	T [°C]	Total solids [%]	Mineral composition
QFM-1	1	1	1114	0.86	Pl An70
QFM-1	1	1	1078	19.91	Pl An64
QFM-1	1	1.5	1118	0.85	Pl An69
QFM-1	1	1.5	1082	19.99	Pl An63
QFM-1	1	2	1119	2.85	Pl An67
QFM-1	1	2	1089	18.79	Pl An62
QFM-1	1	2.5	1121	4.73	Pl An66
QFM-1	1	2.5	1094	20.07	Pl An62
QFM-1	1	3	1123	6.59	Pl An65
QFM-1	1	3	1106	16.4	Pl An62
QFM-1	1	4	1128	9.59	Pl An 63
QFM-1	1	1	1120	0.36	Ol Fo72
QFM-1	1	1	1099	8.93	Ol Fo69
QFM-1	1	1.5	1124	0.35	Ol Fo72
QFM-1	1	1.5	1104	8.98	Ol Fo69
QFM-1	1	2	1127	0.34	Ol Fo72
QFM-1	1	2	1108	8.99	Ol Fo69
QFM-1	1	1	1092	12.93	Cpx Wo42.8 En44 Fs13.2
QFM-1	1	1	1078	19.91	Cpx Wo43.3 En42.7 Fs14
QFM-1	1	1.5	1107	7	Cpx Wo41.4 En45.5 Fs13.1
QFM-1	1	1.5	1082	19.99	Cpx Wo42 En43.3 Fs14.7
QFM-1	1	2	1122	1.64	Cpx Wo39.6 En47.2 Fs13.2
QFM-1	1	2	1087	19.98	Cpx Wo40 En44.3 Fs15.7
QFM-1	1	2.5	1094	20.07	Cpx Wo40.5 En44 Fs15.5
QFM	1	0.5	1110	0.46	Pl An70
QFM	1	0.5	1074	19.96	Pl An65
QFM	1	1	1113.5	0.54	Pl An70
QFM	1	1	1082.5	17.3	Pl An64
QFM	1	1.5	1117	1.16	Pl An69
QFM	1	1.5	1087	17.32	Pl An63
QFM	1	1.5	1082	20.13	Pl An62
QFM	1	2	1119	3.04	Pl An67
QFM	1	2	1089	19.54	Pl An62
QFM	1	3	1124	6.61	Pl An65
QFM	1	3	1109	14.73	Pl An62
QFM	1	4	1127	10.11	Pl An62
QFM	1.5	0.5	1085	1.4	Pl An73
QFM	1.5	0.5	1053	19.84	Pl An 68
QFM	1.5	3	1086	12.6	Pl An65
QFM	1.5	3	1073	19.89	Pl An 62

Ox. Fugacity Buffer	H_2O [wt%]	P [kbar]	T [°C]	Total solids [%]	Mineral composition
QFM	2	0.5	1056	7.32	Pl An74
QFM	2	0.5	1037	19.99	Pl An69
QFM	2	1	1055.5	9.82	Pl An72
QFM	2	1	1038	19.16	Pl An69
QFM	2	1	1036.5	19.86	Pl An69
QFM	2	1.5	1054	12.6	Pl An70
QFM	2	1.5	1039	19.97	Pl An68
QFM	2	2	1053	14.86	Pl An68
QFM	2	2	1043	19.83	Pl An66
QFM	2	3	1054	17.87	Pl An65
QFM	2	3	1050	19.89	Pl An64
QFM	1	0.5	1110	0.46	Ol Fo75
QFM	1	0.5	1090	10.49	Ol Fo71
QFM	1	0.5	1074	19.96	Ol Fo69
QFM	1	1	1113	0.54	Ol Fo75
QFM	1	1	1105	4.98	Ol Fo73
QFM	1	1	1082	17.3	Ol Fo69
QFM	1	1.5	1111	4.55	Ol Fo73
QFM	1	1.5	1087	17.32	Ol Fo69
QFM	1	1.5	1082	20.13	Ol Fo68
QFM	2	0.5	1097	0.13	Ol Fo75
QFM	2	0.5	1037	19.99	Ol Fo69
QFM	2	1	1101	0.13	Ol Fo75
QFM	2	1	1036	19.86	Ol Fo69
QFM	2	1.5	1104	0.15	Ol Fo75
QFM	2	1.5	1039	19.97	Ol Fo69
QFM	2	2	1107	0.15	Ol Fo75
QFM	2	2	1057	13.52	Ol Fo70
QFM	1	0.5	1090	10.49	Cpx Wo44.2 En44 Fs11.9
QFM	1	0.5	1074	19.96	Cpx Wo44.3 En42.9 Fs12.8
QFM	1	1	1105	4.98	Cpx Wo43 En45.3 Fs11.7
QFM	1	1	1082	17.3	Cpx Wo43.3 En43.6 Fs13.2
QFM	1	1.5	1119	0.51	Cpx Wo41.9 En46.4 Fs11.7
QFM	1	1.5	1082	20.13	Cpx Wo41.6 En44.2 Fs14.2
QFM	1	2	1127	0.52	Cpx Wo41.2 En46.9 Fs11.9
QFM	1	2	1119	3.04	Cpx Wo41.5 En46.2 Fs12.3
QFM	1	3	1124	6.61	Cpx Wo40.7 En45.8 Fs13.5
QFM	1	3	1109	14.73	Cpx Wo40.6 En44.9 Fs14.5
QFM	2	0.5	1072	2.13	Cpx Wo46.6 En42.8 Fs10.5
QFM	2	0.5	1037	19.99	Cpx Wo46.3 En41.9 Fs11.9
QFM	2	1	1081	1.76	Cpx Wo45.6 En43.7 Fs10.7
QFM	2	1	1036	19.86	Cpx Wo45.7 En42.2 Fs12.2
QFM	2	1.5	1091	1.39	Cpx Wo44.6 En44.6 Fs10.8

Ox. Fugacity Buffer	H_2O [wt%]	P [kbar]	T [°C]	Total solids [%]	Mineral composition
QFM	2	1.5	1039	19.97	Cpx Wo44.8 En42.4 Fs12.8
QFM	2	2	1100	1.04	Cpx Wo43.4 En45.5 Fs11.1
QFM	2	2	1043	19.83	Cpx Wo43.5 En43 Fs13.4
QFM	2	3	1119	0.45	Cpx Wo41.3 En47.3 Fs11.6
QFM	2	3	1050	19.89	Cpx Wo44 En41.9 Fs14.2
NNO	1	0.5	1111	0.09	Pl An71
NNO	1	0.5	1080	19.96	Pl An65
NNO	1	1	1115	0.11	Pl An70
NNO	1	1	1085	19.7	Pl An64
NNO	1	1.5	1118	1.23	Pl An69
NNO	1	1.5	1089	20.06	Pl An63
NNO	1	2	1120	3.02	Pl An68
NNO	1	2	1095	18.87	Pl An62
NNO	1	3	1124	6.91	Pl An65
NNO	1	3	1110	13.85	Pl An62
NNO	1	4	1127	10.24	Pl An62
NNO	1.5	0.5	1083	4.39	Pl An72
NNO	1.5	0.5	1058	19.8	Pl An67
NNO	1.5	3	1088	13.32	Pl An65
NNO	1.5	3	1076	19.97	Pl An62
NNO	2	0.5	1056	10.71	Pl An73
NNO	2	0.5	1041	19.91	Pl An69
NNO	2	1	1057	12.21	Pl An72
NNO	2	1	1040	19.95	Pl An68
NNO	2	1.5	1057	14.02	Pl An70
NNO	2	1.5	1044	20.03	Pl An67
NNO	2	2	1058	15.4	Pl An68
NNO	2	2	1047	20	Pl An66
NNO	2	3	1057	18.37	Pl An65
NNO	2	3	1054	19.86	Pl An64
NNO	1	0.5	1106	1.51	Ol Fo77
NNO	1	0.5	1080	19.96	Ol Fo75
NNO	1	1	1106	4.43	Ol Fo76
NNO	1	1	1085	19.7	Ol Fo74
NNO	2	0.5	1089	0.23	Ol Fo77
NNO	2	0.5	1041	19.91	Ol Fo76
NNO	2	1	1094	0.08	Ol Fo77
NNO	2	1	1075	6.2	Ol Fo76
NNO	2	1.5	1098	0.04	Ol Fo77
NNO	2	1.5	1088	3.2	Ol Fo76
NNO	1	0.5	1101	4.51	Cpx Wo44.5 En45 Fs10.5
NNO	1	0.5	1080	19.96	Cpx Wo43.8 En45.1 Fs11.1
NNO	1	1	1112	0.92	Cpx Wo443.9 En45.5 Fs10.6

Ox. Fugacity Buffer	H_2O [wt%]	P [kbar]	T [°C]	Total solids [%]	Mineral composition
NNO	1	1	1085	19.7	Cpx Wo42.6 En45.6 Fs11.8
NNO	1	1.5	1121	0.05	Cpx Wo43.6 En45.7 Fs10.7
NNO	1	1.5	1089	20.06	Cpx Wo41.5 En46 Fs12.5
NNO	1	2	1130	0.03	Cpx Wo43 En46.1 Fs10.9
NNO	1	2	1093	19.96	Cpx Wo41.4 En45.6 Fs13
NNO	1	3	1146	0.07	Cpx Wo41.5 En47 Fs11.5
NNO	1	3	1102	19.7	Cpx Wo41.5 En44.5 Fs14
NNO	1	4	1162	0.19	Cpx Wo39.9 En48 Fs12.1
NNO	1	4	1109	19.78	Cpx Wo41.5 En43.5 Fs15
NNO	1	5	1129	13.74	Cpx Wo40.6 En44.1 Fs15.3
NNO	1	5	1117	19.92	Cpx Wo41.2 En42.9 Fs15.9
NNO	2	0.5	1079	1.46	Cpx Wo46.6 En43.9 Fs9.5
NNO	2	0.5	1041	19.91	Cpx Wo46 En44 Fs10
NNO	2	1	1087	0.67	Cpx Wo45.9 En44.3 Fs9.8
NNO	2	1	1040	19.95	Cpx Wo45.4 En44.2 Fs10.5
NNO	2	1.5	1096	0.29	Cpx Wo44.9 En45.1 Fs10.1
NNO	2	1.5	1044	20.03	Cpx Wo45.2 En43.8 Fs11
NNO	2	2	1104	0.15	Cpx Wo44.1 En45.6 Fs10.3
NNO	2	2	1047	20	Cpx Wo45.1 En43.4 Fs11.5
NNO	2	3	1121	0.06	Cpx Wo42.7 En46.5 Fs10.8
NNO	2	3	1054	19.86	Cpx Wo44.8 En42.6 Fs12.6
NNO	2	4	1136	0.2	Cpx Wo41.3 En47.4 Fs11.3
NNO	2	4	1062	19.96	Cpx Wo44.2 En42.1 Fs13.8
NNO	2	5	1074	19.97	Cpx Wo43.6 En41.6 Fs14.8

Tabla A.5.5.2: Resumen del modelamiento para los CEM Fui Sur.

Ox. Fugacity Buffer	H_2O [wt%]	P [kbar]	T [°C]	Total solids [%]	Mineral composition
QFM-1	2	1	1056	0.13	Pl An64
QFM-1	2	1	1014	19.91	Pl An59
QFM-1	2	2	1064	0.85	Pl An63
QFM-1	2	2	1023	20.03	Pl An58
QFM-1	2	3	1073	1.46	Pl An61
QFM-1	2	3	1038	17.32	Pl An58
QFM-1	2	3.5	1076	1.97	Pl An61
QFM-1	2	3.5	1049	13.56	Pl An57
QFM-1	2	4	1080	2.38	Pl An60
QFM-1	2	4	1060	10.79	Pl An57
QFM-1	2	5	1082	5.57	Pl An57
QFM-1	2	5	1079	6.92	Pl An57
QFM-1	2.5	1	1034	0.9	Pl An67
QFM-1	2.5	1	994	19.92	Pl An62
QFM-1	2.5	4	1048	6.73	Pl An60
QFM-1	2.5	4	1027	15.99	Pl An57
QFM-1	2.5	5	1050	8.94	Pl An57
QFM-1	3	1.5	1015	4.05	Pl An67
QFM-1	3	1.5	978	20.05	Pl An62
QFM-1	3	2	1016	5.25	Pl An66
QFM-1	3	2	982	20	Pl An61
QFM-1	3	3	1019	7.44	Pl An63
QFM-1	3	3	990	19.9	Pl An59
QFM-1	3	4	1019	10.2	Pl An60
QFM-1	3	4	1002	17.12	Pl An57
QFM-1	2	3.5	1056	10.74	Cpx Wo40.2 En41 Fs18.8
QFM-1	2	3.5	1036	19.9	Cpx Wo41.2 En38.6 Fs20.1
QFM-1	2	4	1076	4.09	Cpx Wo38.2 En43.2 Fs18.6
QFM-1	2	4	1039	19.94	Cpx Wo41.2 En38.3 Fs20.5
QFM-1	2	5	1092	3.44	Cpx Wo39.3 En42.8 Fs17.9
QFM-1	2	5	1079	6.92	Cpx Wo40.4 En41.1 Fs18.6
QFM-1	3	1.5	1022	2.31	Cpx Wo43.2 En41.3 Fs15.4
QFM-1	3	1.5	1015	4.05	Cpx Wo43.5 En40.6 Fs15.9
QFM-1	3	2	1029	2.41	Cpx Wo43.2 En41.2 Fs15.6
QFM-1	3	2	1016	5.25	Cpx Wo43.5 En40 Fs16.4
QFM-1	3	3	1043	2.61	Cpx Wo42.1 En41.8 Fs16.1
QFM-1	3	3	1019	7.44	Cpx Wo43.7 En38.8 Fs17.4
QFM-1	3	4	1057	2.84	Cpx Wo41.6 En42 Fs16.4
QFM	2	1	1058	0.25	Pl An65
QFM	2	1	1017	19.97	Pl An59

Ox. Fugacity Buffer	H_2O [wt%]	P [kbar]	T [°C]	Total solids [%]	Mineral composition
QFM	2	1.5	1061	0.23	Pl An64
QFM	2	1.5	1022	20.1	Pl An59
QFM	2	2	1065	0.17	Pl An62
QFM	2	2	1027	19.82	Pl An57
QFM	2	3	1073	1	Pl An62
QFM	2	3	1042	16.21	Pl An57
QFM	2	4	1077	3.56	Pl An59
QFM	2	4	1062	10.22	Pl An57
QFM	2	4.5	1078	4.92	Pl An58
QFM	2	4.5	1072	7.43	Pl An57
QFM	2.5	1	1036	0.73	Pl An67
QFM	2.5	1	996	19.92	Pl An61
QFM	2.5	4.5	1046	8.63	Pl An57
QFM	2.5	4.5	1043	9.98	Pl An57
QFM	3	1	1058	0.25	Pl An65
QFM	3	1	1017	19.97	Pl An59
QFM	3	1.5	1015	5.28	Pl An66
QFM	3	1.5	980	20.07	Pl An61
QFM	3	2	1016	6.52	Pl An65
QFM	3	2	984	19.93	Pl An60
QFM	3	3	1018	8.58	Pl An62
QFM	3	3	990	19.91	Pl An58
QFM	3	3.5	1018	9.63	Pl An60
QFM	3	3.5	996	18.92	Pl An57
QFM	3	4	1018	10.77	Pl An59
QFM	3	4	1008	15.18	Pl An57
QFM	2	2	1027	19.82	Cpx Wo42.7 En41.2 Fs16.1
QFM	2	3	1065	5.24	Cpx Wo41.7 En42.2 Fs16
QFM	2	3	1034	19.97	Cpx Wo43 En40.1 Fs17
QFM	2	4	1086	1.74	Cpx Wo40.5 En43.3 Fs16.2
QFM	2	4	1041	19.94	Cpx Wo43.3 En38.9 Fs17.8
QFM	2	4.5	1092	2	Cpx Wo40.1 En43.4 Fs16.5
QFM	2	4.5	1072	7.43	Cpx Wo41.7 En40.9 Fs17.4
QFM	2	5	1099	2.15	Cpx Wo39.7 En43.6 Fs16.7
QFM	2	5	1079	19.96	Cpx Wo41.4 En41 Fs17.7
QFM	3	1.5	1030	1.5	Cpx Wo43.4 En42.8 Fs13.8
QFM	3	1.5	1015	5.28	Cpx Wo44 En41.7 Fs14.2
QFM	3	2	1037	1.51	Cpx Wo43.2 En42.6 Fs14.1
QFM	3	2	984	19.93	Cpx Wo44.7 En40.1 Fs15.2
QFM	3	3	1050	1.53	Cpx Wo42.7 En42.6 Fs14.7
QFM	3	3	1018	8.58	Cpx Wo44.4 En39.9 Fs15.7
QFM	3	3.5	1058	1.46	Cpx Wo42.2 En42.8 Fs15
QFM	3	4	1064	1.65	Cpx Wo41.8 En42.9 Fs15.3

Ox. Fugacity Buffer	H_2O [wt%]	P [kbar]	T [°C]	Total solids [%]	Mineral composition
NNO	2	1	1061	1.01	Pl An65
NNO	2	1	1020	19.96	Pl An59
NNO	2	1.5	1064	0.78	Pl An64
NNO	2	1.5	1024	20.1	Pl An58
NNO	2	2	1067	0.72	Pl An63
NNO	2	2	1029	19.9	Pl An57
NNO	2	3	1072	1.76	Pl An61
NNO	2	3	1046	15.29	Pl An57
NNO	2	3.5	1074	2.86	Pl An60
NNO	2	3.5	1055	12.52	Pl An57
NNO	2	2	1056	6.03	Cpx Wo42.1 En43.8 Fs14.1
NNO	2	2	1029	19.9	Cpx Wo43 En42.7 Fs14.3
NNO	2	3	1076	0.61	Cpx Wo41.1 En43.7 Fs14.9
NNO	2	3	1036	19.88	Cpx Wo42.7 En41.7 Fs15.6
NNO	2	3.5	1083	0.83	Cpx Wo41.1 En43.7 Fs15.2
NNO	2	3.5	1039	20.08	Cpx Wo42.8 En41 Fs16.2
NNO	2	4	1089	1.08	Cpx Wo40.7 En43.7 Fs15.5
NNO	2	4	1043	19.94	Cpx Wo42.9 En40.3 Fs16.8
NNO	2	5	1102	1.56	Cpx Wo39.9 En43.9 Fs16.2
NNO	2	5	1048	20.01	Cpx Wo43.2 En38.7 Fs18